Isotopic compositions of fluid inclusions in the Earth crust : determination of fluid sources and palaeoclimatic reconstructions

Thomas Rigaudier

N° d'ordre : 18 - 2010 Année 2010

THESE DE L'UNIVERSITE DE LYON

Délivrée par

L'UNIVERSITE CLAUDE BERNARD LYON 1

ECOLE DOCTORALE

DIPLOME DE DOCTORAT

(arrêté du 7 août 2006)

Présentée et soutenue publiquement le 25 Janvier 2010
par

RIGAUDIER Thomas

TITRE :

Analyse isotopique des inclusions fluides des matériaux de la croûte terrestre : caractérisation des sources des fluides et reconstitutions paléoclimatiques.

Directeur de thèse :

Dr Véronique Gardien

Co-directeur : Prof. Christophe Lécuyer

JURY :

Mme DAUX Valérie	Maître de Conf., LSCE, Université Paris VI	Rapporteur
M. DUBOIS Michel	Professeur, Université Lille 1	Rapporteur
Mme GARDIEN Véronique	Maître de Conf., Université Lyon 1	Directeur
M. LECUYER Christophe	Professeur, Université Lyon 1	Co–Directeur
M. GENTY Dominique	Directeur de Recherche, LSCE, CEA Saclay	Examinateur
M. LOWENSTEIN Tim K.	Professeur, State University of New York, Binghamton	Examinateur
M. PILI Eric	Chercheur au CEA, DAM–Île de France	Examinateur

Résumé

Un des enjeux majeurs en Science de la Terre ces dernières décennies est de comprendre les interactions entre les différentes enveloppes terrestres. Le but poursuivi par ce travail est d'aborder quelques aspects de ces interactions du point de vue des cycles géochimiques des éléments volatils H_2O et CO_2 en se basant sur l'étude des inclusions fluides piégées dans des roches variées de la croûte terrestre, depuis sa surface jusqu'à l'interface croûte–manteau. La première partie de mon travail présente des travaux expérimentaux effectués sur de la halite. L'étude du fractionnement isotopique de l'oxygène et des cinétiques d'équilibration entre H_2O et CO_2 lors de l'évaporation de saumures a montré l'importance des corrections à effectuer sur les mesures isotopiques de l'oxygène pour des solutions de haute salinité. L'élaboration d'un protocole expérimental de précipitation de halite en milieu contrôlé a permis de mettre en évidence le potentiel des inclusions fluides pour les reconstitutions paléoclimatiques. La combinaison des données microthermométriques et des compositions isotopiques de l'hydrogène et de l'oxygène des inclusions aqueuses permet d'estimer les sources et la température de l'eau de formation de la halite ainsi que la vitesse du vent à l'interface eau-air pendant la croissance du cristal. Cette méthode a été ensuite appliquée aux dépôts de halite de Sicile datés du Messinien. La deuxième partie de mon travail est consacrée à l'identification des compositions chimiques et des sources des fluides circulant dans la croûte et à l'interface croûte-manteau à travers l'analyse des compositions isotopiques des inclusions fluides des granites et granulites.

Abstract

One of the major challenges in Earth Sciences during the last decades has been to improve our knowledge of the interaction between the different components of the Earth System. Key aspects to improve the understanding of these processes are the acquisition of new data and the development of models to explain both mass and energy transfer between the deep and superficial components of the Earth system. The goal of this thesis is to study these transfers through the geochemical cycle of volatile elements trapped in fluid inclusions of various materials of the Earth crust. The first part of my work presents experimental study of halite. The study of oxygen isotope fractionation and equilibrium kinetics between H_2O and CO_2 during the evaporation of brines shows that corrections have to be made on the oxygen isotope measurements for high salinity solutions. The elaboration of an experimental protocol to form halite in controlled environment reveals the potential of fluid inclusions for palaeo-climatic reconstructions. Combination of microthermometric data plus hydrogen and oxygen isotopic compositions of aqueous inclusions allows to estimate the sources and the temperature of the parental water of halite as well as the wind speed at the water-air interface during the crystal growth. This method was then applied to the Messinian halite deposits of Sicily. The second part of my work is dedicated to the identification of both the chemical compositions and the sources of fluids circulating in the crust and at the interface crust-mantle through the analysis of isotopic compositions of fluid inclusions in granites and granulites.

REMERCIEMENTS

Ces quatre années (et un peu plus) de thèse n'auraient pu se dérouler dans d'aussi bonnes conditions sans l'aide et le soutien de nombreuses personnes que je tiens à remercier.

Mes remerciements vont tout d'abord aux membres du jury qui ont accepté de juger ce travail, Torsten Vennemann et Michel Dubois mes rapporteurs, Mme Valérie Daux et messieurs Lowenstein, Pili et Genty mes examinateurs.

Un grand merci aux « chefs » sans qui ce travail n'existerait pas. Merci Véronique et Christophe pour la qualité de votre encadrement, votre disponibilité, le soutien et la patience dont vous avez fait preuve durant toutes ces années. C'est aussi grâce à vous que j'ai pu avoir l'opportunité de m'initier à la géochimie expérimentale. J'ai découvert à travers l'expérimentation un monde fascinant dans lequel il faut savoir faire preuve de persévérance car tout ne fonctionne pas au premier essai. Le plus important pour moi demeure néanmoins la confiance que vous m'avez accordée et l'amitié que vous m'avez témoignée.

Véronique, ton immense gentillesse et ton optimisme indestructible m'ont permis de tenir le coup dans les périodes difficiles et je t'en remercie. Grâce à toi j'ai pu aussi découvrir les stages de terrain du côté obscur de la force, j'entends par là l'encadrement et j'en garde d'agréables souvenirs.

Christophe, j'ai encore en tête les longues journées des mois d'été que tu as passé à mes côtés pour me montrer toutes les astuces d'une manip réussie. Travailler à tes côtés a été pour moi un enseignement précieux. Merci également pour ces soirées passées à parler science ou non autour d'un verre avec un air de Mickael Jackson dans les oreilles. Tu m'as aussi fait découvrir les subtils arômes des havanes rappelant l'odeur des chevaux après un galop en plein soleil.

Mille merci à François Martineau pour tout le temps qu'il a consacré à m'apprendre les bases de l'utilisation des lignes d'extraction sous vide et du spectromètre de masse. Merci à François Fourel pour les heures passées devant les spectromètres de masse à acquérir les données.

Une thèse c'est aussi un quotidien, et il est clair que travailler dans un environnement sain est une force de travail supplémentaire. Un grand merci en conséquence à toute la troupe des thésards et autres étudiants/fous furieux qui se sont succédés au fil des années, à savoir par

ordre alphabétique : Baptiste, Bibi, Damien, Dompteur Amiot, « El Fuerbo », Guillaume, Lagoutte, Lorenzo, Mathieu, Maurice, Mélaaaannie, Pompon, Ronan et tous les autres.

Je tiens également à remercier Jean Pierre Suc avec qui j'ai mis un pied dans le Messinien et grâce à qui j'ai pu découvrir les fabuleuses mines de sel de Sicile, Ghislaine qui a passé des heures à me confectionner des lames minces et des lames épaisses, Magali et Sherazade pour leur aide au sein du laboratoire de géochimie, Nathalie qui est toujours disponible et souriante malgré un emploi du temps chargé ; à Philippe pour l'assistance informatique, pour ton intérêt permanent pour mes travaux et pour le réglage de ce joli cadeau avec lequel j'ai pu finir ce travail dans les meilleurs conditions. Je remercie également Laurent pour les discussions, les relectures et ses avis toujours importants. Au moment d'imprimer ce manuscrit, j'ai une pensée particulière pour Dominique.

Je remercie enfin ma famille et tout particulièrement mes parents pour leur aide et leur confiance. Merci de m'avoir constamment soutenu dans mes choix et surtout de m'avoir donné la liberté d'exprimer ma curiosité. Enfin, merci Gab pour ta joie de vivre, ta patience et ton soutien. Merci pour ta compréhension, pour la tolérance dont tu as fais preuve lorsque samedi et dimanche étaient synonymes de lundi. Merci aussi pour avoir su me recueillir et m'accepter alors que j'étais tombé du nid ;)

Table des matières

Chapitre 1

Introduction : Les fluides sur Terre

Chapitre 1

Introduction : Les fluides sur Terre

Certains auteurs utilisent le terme « fluides » pour désigner les gaz et les liquides usuels (comme l'eau, la vapeur d'eau, le dioxyde de carbone, etc.) ; d'autres l'utilisent de manière plus restrictive pour nommer les substances volatiles au dessus de leur température critique. Indifféremment à la terminologie, pour ce travail, nous considérerons les fluides comme un état physique de la matière. Les fluides étudiés dans ce travail (H_2O et CO_2) sont des fluides newtoniens, généralement de faible viscosité à l'état vapeur, liquide ou critique à la surface de la Terre comme la majorité des fluides composés de molécules simples.

1. Distribution des volatils dans les enveloppes terrestres

En considérant les fluides au sens large du terme comme étant des composants volatils des enveloppes terrestres, on peut alors dire que la composition chimique (teneur en volatils) de la Terre n'est encore pas précisément connue. Seule l'atmosphère, qui est l'enveloppe de notre planète directement accessible, est bien caractérisée. Elle est majoritairement composée d'éléments volatils tels que le carbone, l'azote, l'oxygène et l'eau et contient aussi de l'hydrogène, de l'hélium et des gaz rares en moindres quantités. L'origine de l'atmosphère terrestre est encore débattue et l'importance des deux sources majeures (dégazage des silicates et apport tardif par des comètes ou des météorites) n'est toujours pas quantifiée (Voir Chapitre 2.1 pour la discussion).

Les principaux volatils de la lithosphère sont constitués des éléments C, H, O, N, et Ar. Ils se présentent sous des formes peu nombreuses fonctions de l'état d'oxydation de la portion de lithosphère considérée. Ainsi, on retrouve parmi les volatils H_2O, CO_2, CH_4, N_2, CO et H_2 (Watson et al., 1987 ; Brenan et al., 1988 ; Wood et al., 1990 ; Evans, 1996). La

répartition de ces volatils dans les différents réservoirs terrestres est très inégale (Jambon, 1994). Elle dépend de la stabilité des phases hôtes du volatil dans le réservoir considéré, de la quantité initiale sur Terre de ses éléments constitutifs, de la masse du réservoir et des flux entrants et sortants. Les silicates contenant généralement de faibles quantités de volatils et les processus magmatiques fractionnant très fortement les volatils incompatibles, les enveloppes internes sont donc extrêmement hétérogènes du point de vue de leurs compositions chimiques et les valeurs de concentrations en volatils sont sujettes à de grandes incertitudes.

La composition des basaltes non altérés de rides océaniques donne une teneur en eau estimée entre 100 et 1000 ppm (Thompson, 1992 ; Jambon, 1994 ; Sobolev et Chaussidon, 1996). La teneur en carbone du manteau terrestre est quant à elle estimée entre 40 et 400 ppm à partir des calculs de flux actuels de dégazage au niveau des rides (Marty et Tolstikhin, 1998) et de la concentration moyenne en carbone des MORB (Marty et Zimmermann, 1999). Le tableau 1.1 présente la composition en volatils des différentes enveloppes terrestres internes (manteau et croûte continentale) et externes (atmosphère et hydrosphère).

Eléménts	Atmosphère terrestre	Hydrosphère	Croûte continentale	Manteau
H	< 400	11% wt.	100 - 6000	10-100
C	100	26	3000	40-400
O [a]	20.9% wt. O_2	88% wt.	45% wt.	
N	78% wt. N_2	8	60	2

[a] L'oxygène est un volatil dans l'atmosphère (sous forme d'O_2), dans l'hydrosphère (H_2O essentiellement) et même dans le noyau mais c'est un élément très réfractaire dans les silicates (SiO_2).

TAB 1.1 – Composition en volatils des enveloppes terrestres fluides et solides (les concentrations sont en ppm, sauf quand l'unité est précisée).

TAB 1.1 – Amounts of volatiles in both the fluid and solid terrestrial envelopes (concentrations are given in ppm, except with the unit is specified).

2. La lithosphère : zone de transferts de fluides entre les enveloppes internes et externes

L'évolution de la Terre au cours de son histoire est contrôlée par les transferts de matière entre les enveloppes internes et superficielles. Ces interactions existant entre la Terre silicatée (manteau, croûte continentale et croûte océanique) et les enveloppes fluides (hydrosphère, atmosphère) interviennent dans la régulation des compositions océanique et atmosphérique, influent sur les propriétés chimiques, physiques et minéralogiques du manteau et contribuent à l'évolution de la nature de la croûte continentale. Elles ont lieu au cours des phénomènes géodynamiques qui sont la conséquence directe de la tectonique des plaques. Ces interactions sont anciennes comme en témoigne la découverte d'un complexe filonien dans l'Isua Supracrustal Belt (3,8Ga) au sud ouest du Groenland, preuve de l'accrétion d'une croûte océanique à l'Archéen (Furnes et al., 2007). Le volcanisme est le principal responsable des transferts de fluides depuis le manteau vers l'atmosphère alors que le recyclage des fluides dans le manteau se produit au niveau des zones de subduction par l'enfouissement dans le manteau de la croûte océanique hydratée, de matériel sédimentaire et de croûte continentale (figure 1.1).

2.1. Volcanisme et magmatisme : transferts des enveloppes internes vers les enveloppes externes

Les volcans, les rides océaniques et les arcs insulaires sont caractérisés par des transferts de fluides importants faisant suite au dégazage des magmas depuis le manteau vers l'hydrosphère et l'atmosphère. Ces fluides sont essentiellement constitués des phases H_2O et CO_2 (voir par exemple Fischer et al., 1998 ; Marty et Tolstikhin, 1998). Le dioxyde de carbone est le gaz le plus abondamment libéré au niveau des rides océaniques, des points chauds et par le volcanisme d'arc (figure 1.1). De nombreuses techniques ont été utilisées pour estimer le flux de CO_2 libéré au niveau des rides médio–océaniques (MOR). Les rapports $CO_2/^3He$ des fluides hydrothermaux (Des Marais et Moore, 1984 ; Corliss et al., 1979) et des basaltes des

rides médio–océaniques (Marty et Jambon, 1987 ; Sarda et Graham, 1990 ; Graham et Sarda, 1991 ; Marty et Zimmerman, 1999) combinés avec les valeurs des flux d'^{3}He donnent des valeurs de flux de CO_2 de $0{,}1.10^{12}$ à 6.10^{12} mol.an^{-1}. Les estimations de la quantité de CO_2 dans le manteau associé aux taux de production de croûte océanique permettent quant à eux de calculer un flux de CO_2 au niveau des rides médio–océaniques de $0{,}23.10^{12}$ à 18.10^{12} mol.an^{-1} (voir par exemple Gerlach, 1991 ; Javoy et Pineau, 1991 ; Holloway, 1998 ; Cartigny et al., 2001 ; Saal et al., 2002). Le flux de CO_2 provenant des points chauds, calculé à partir des taux de production de magma est inférieur à 3.10^{12} mol.an^{-1} (Marty et Tolstikhin, 1998). Le flux de CO_2 libéré au niveau des arcs volcaniques a été estimé à partir des rapports $CO_2/^3$He des gaz volcaniques d'arcs et du taux de production des magmas, en faisant l'hypothèse que le contenu en ^{3}He du pôle mantellique est le même que pour les MORB. Le flux de CO_2 résultant est d'environ $2{,}5.10^{12}$ mol.an^{-1}, avec environ 80% du carbone provenant de la plaque subductée (Varekamp et al., 1992 ; Sano et Marty, 1995 ; Sano et Williams, 1996 ; Marty et Tolstikhin, 1998).

L'influence des variations de l'intensité du dégazage du CO_2 sur la surface de la Terre est majeure. En effet, le taux de dégazage de CO_2 est considéré comme un facteur majeur contrôlant la pression partielle du CO_2 atmosphérique au cours des temps géologiques (Berner et al., 1983). Des variations de la vitesse d'expansion océanique des dorsales ainsi que des variations dans la fréquence et le volume des émissions de laves provenant du manteau profond (PLUME) peuvent être responsables d'une variation du flux global de CO_2 et d'une modification la pression partielle du CO_2 atmosphérique et par conséquent, de variations climatiques et de modifications de la composition océanique (pH, alcalinité). La nature des gaz volcaniques émis au cours de l'histoire de la Terre a également été invoquée dans le contrôle de l'état redox de l'atmosphère et dans l'apparition d'une atmosphère riche en oxygène il y a environ 2 Ga. Lors des derniers 3,8 Ga, la proportion H_2/H_2O des gaz volcaniques ayant très peu changé et la fraction de CO_2 volcanique réduit en carbone élémentaire étant restée remarquablement constante, une augmentation des rapports CO_2/H2O et SO_2/H_2O des gaz volcaniques serait en majorité responsable de l'augmentation graduelle de l'état d'oxydation de l'atmosphère. (Kasting et al., 1993 ; Holland, 2002 ;

Holland, 2009). La mise en place de cette atmosphère oxydante vers 2 Ga pourrait aussi avoir été enregistrée dans les inclusions fluides des granulites. Ce dernier point est développé dans le chapitre 7.

2.2. Le recyclage des fluides externes dans les enveloppes internes

La subduction de la croûte océanique hydratée et carbonatée dans le manteau est le principal moteur des transferts de fluides depuis la croûte vers le manteau. La croûte océanique est un important réservoir de fluides (CO_2–H_2O) car elle porte des sédiments marins terrigènes et subit altération et hydrothermalisme. Les fluides riches en eau et en dioxyde de carbone sont transportés dans le manteau et leur comportement va alors être contrôlé par les réactions du métamorphisme qui va intervenir à haute pression (Wyllie, 1982). La majorité des fluides de la croûte subductée est retenue dans le prisme d'accrétion ou est libérée entre la surface et 200 km de profondeur (Tatsumi, 1989). La dévolatilisation de la croûte à l'aplomb des zones de subduction lors du métamorphisme HP–BT enrichit en fluides le coin de manteau sus-jacent et participe à la formation de magmas riches en eau. Toutefois, des phases carbonatées (Green et al., 1993) et hydratées (Thompson, 1992) provenant de la plaque plongeante pourraient persister et plonger dans le manteau à de très grandes profondeurs. La relative stabilité de la masse d'eau océanique depuis l'Archéen (Windley, 1977 ; Schubert et Reymer, 1985) est en outre un argument en faveur de l'inefficacité du recyclage de l'eau dans le manteau.

Les transferts de fluides depuis l'atmosphère et l'hydrosphère vers la croûte se font essentiellement par gravité. Ils sont facilités dans les zones de déformation, principalement dans les zones de cisaillement qui présentent une plus forte perméabilité du fait de la présence de failles fragiles ou ductiles. L'eau d'origine météorique ou marine ne peut toutefois pas s'infiltrer à une grande profondeur avec la gravité pour seul moteur. Elle peut être stoppée au niveau de la zone de transition fragile - ductile de la croûte qui s'accompagne d'une chute de perméabilité (Yardley et al., 1994) et peut aussi être consommée plus rapidement qu'elle n'est transportée, par les réactions du métamorphisme du faciès schistes verts (Frost and Bucher, 1994).

Le magmatisme de ride océanique stocke également des fluides dans la croûte océanique néoformée. La déformation ductile cisaillante en extension mise en évidence de part et d'autre des dorsales océaniques est le siège d'une hydratation dynamique profonde de la croûte océanique (Hart, 1973 ; Staudigel et al. 1981, Humphris and Thompson, 1978 ; Mevel, 2003). L'hydratation statique superficielle de la croûte océanique nouvellement formée serait faite via la création d'un important réseau de fissures subverticales engendrées lors du refroidissement (Pili, 1997). Le magmatisme de points chauds et des rifts continentaux injectent également dans la croûte néoformée des fluides recyclés ou mantelliques.

3. Les transferts de fluides entre atmosphère et hydrosphère.

Il est important de noter que la régulation des compositions océanique et atmosphérique n'est pas seulement liée aux interactions existant entre la Terre silicatée (manteau, croûte continentale et croûte océanique) et les enveloppes fluides (hydrosphère, atmosphère). Les cycles atmosphériques constituent les plus grands déplacements de substances chimiques à la surface de la Terre. Ainsi, par les processus d'évaporation et de précipitation et par la circulation océanique, H_2O majoritairement et CO_2 sont échangés entre les enveloppes fluides que sont l'atmosphère et l'hydrosphère (figure 1.1). Ces transferts sont importants puisqu'ils déterminent les modes climatiques de notre planète. L'eau transfère, des tropiques aux pôles, une grande partie de l'énergie calorifique reçue par la Terre et constitue ainsi le régulateur des températures du globe (Miller, 1965). De la même manière, les transferts de CO_2 existent entre l'hydrosphère et l'atmosphère dans le système fermé qu'est le cycle du carbone. Ce point sera développé dans le chapitre 2. Il semble nécessaire de leur accorder de l'importance puisqu'ils participent aussi à la régulation de l'effet de serre (CO_2 et CH_4) et donc à la régulation du climat et ont un impact certain sur la productivité biologique marine.

4. Les inclusions fluides et les cycles géochimiques : problématique

Nous avons vu que les éléments volatils majeurs composent la plus grande partie des enveloppes externes de la Terre. On les retrouve aussi, dans des concentrations variables, dans les différents réservoirs internes et leurs transferts d'une enveloppe à l'autre sous forme de fluides sont illustrés sur la figure (1.1). A l 'échelle globale, la croûte continentale peut être vue comme une interface entre les cycles externes des éléments régis par les interactions entre atmosphère, hydrosphère, biosphère et sédiments et les cycles internes des éléments, qui se déroulent en grande partie dans le manteau. La croute continentale, qui bénéficie d'apports provenant des enveloppes internes et externes est donc une zone privilégiée pour l'étude des transferts de fluides entre les différentes enveloppes terrestres.

La détermination de la composition chimique et des sources des fluides, qu'ils soient impliqués dans les interactions entre atmosphère, biosphère et hydrosphère ou dans les transferts de volatils entre croûte et manteau, se révèle souvent complexe. En effet, ils présentent un défaut majeur qui est leur mobilité. De plus, ils sont rarement conservés au sein des roches. Cependant, il existe un moyen d'accéder à ces fluides : les inclusions fluides. Les inclusions fluides sont des microcavités des cristaux qui contiennent le fluide qui était en contact avec les minéraux de la roche soit lors de leur croissance, soit postérieurement à leur formation. Elles sont donc des témoins privilégiés des circulations fluides et ont la particularité d'être préservées dans tous les matériaux de l'écorce terrestre (sédiments, roches magmatiques et métamorphiques). Au cours de leurs transferts d'une enveloppe à l'autre, des fractionnements isotopiques modifient la composition initiale de ces fluides à travers divers processus. En partant de l'hypothèse que la composition isotopique du fluide n'a pas changé depuis la formation de l'inclusion et le piégeage du contenu, il est alors possible d'accéder à la composition isotopique initiale du fluide. L'analyse des isotopes stables des inclusions fluides apparaît alors comme une méthode permettant de remonter aux conditions de formation des inclusions et par conséquent, permet la détermination des sources des fluides présents dans le milieu lors de leur formation. La démarche de ce travail est d'utiliser les isotopes stables des inclusions fluides de roches diverses de la croûte terrestre, à savoir les évaporites, les granites et les granulites comme traceurs des sources des fluides et des processus physico–chimiques existant dans la croûte continentale, depuis sa surface jusqu'à l'interface croûte–manteau.

Plan du mémoire

Après une présentation des cycles géochimiques importants pour mon étude, à savoir ceux de l'eau et du carbone (Chapitre 2), le chapitre 3 sera consacré aux inclusions fluides. Il me paraissait nécessaire dans ce travail, de m'attarder sur les inclusions fluides. En effet, elles sont le fil directeur de mon travail de thèse puisque c'est à travers elles que j'ai pu suivre les transferts des fluides tels que CO_2 et H_2O entre et à l'intérieur même des enveloppes terrestres, et ce, depuis la base de la croûte jusqu'à la surface de la Terre. Il me semble donc important d'en donner une définition, de présenter les techniques couramment utilisées pour les étudiées et l'évolution de leurs champs d'application. Le chapitre 4 est entièrement consacré à la présentation des techniques expérimentales utilisées lors de ce travail pour l'analyse des inclusions fluides piégées dans les évaporites (halite), les granites et les granulites de la croûte terrestre. Les chapitres suivants montrent les applications de ces études et leurs apports pour la caractérisation des transferts de fluides entre les enveloppes terrestres.

Le chapitre 5 présente une approche expérimentale de formation et d'étude des inclusions fluides des matériaux de surface que sont les évaporites et plus particulièrement la halite. Les importants dépôts salifères présents à la surface du globe terrestre présentent l'inconvénient d'avoir peu de proxys permettant de remonter aux conditions de dépôt. En effet, la reconstruction des modes climatiques est très délicate puisque l'enregistrement sédimentaire ne contient aucun reste de macrofossile ou de squelette carbonaté ou phosphaté. L'absence de préservation de biominéraux empêche donc l'utilisation des isotopes de l'oxygène comme paléothermomètre, outil couramment utilisé en présence de foraminifères, de mollusques ou de dents de poisson. Cette approche expérimentale a donc été réalisée dans le but d'apporter un nouvel outil fiable pour la reconstruction des conditions paléo environnementales amenant aux dépôts de sels massifs. Une première étude a pour objectif de déterminer les corrections isotopiques à effectuer lors de l'analyse des isotopes de l'oxygène de l'eau pour des fortes salinités. Dans un deuxième temps, l'élaboration d'un protocole expérimental visant à faire précipiter de halite en milieu contrôlé (hygrométrie, température de l'eau et vitesse du vent) a permis de mettre en évidence que les compositions isotopiques de l'hydrogène et de l'oxygène des inclusions fluides enregistrent les trajectoires isotopiques d'évaporation de l'eau. Les

pentes de ces trajectoires d'évaporation sont fonction de la température de l'eau et de la vitesse du vent à l'interface eau–air. Ainsi, en combinant les données microthermométriques avec les compositions isotopiques de l'hydrogène et de l'oxygène des inclusions aqueuses, il est possible d'estimer à la fois les sources et la température de l'eau de formation de la halite ainsi que la vitesse du vent à l'interface eau–air pendant la croissance du cristal.

Le chapitre 6 présente une étude des isotopes stables des inclusions fluides piégées dans les granites de Soultz–sous–Forêts. Les sources et les mélanges des fluides présents pendant l'évolution magmatique et post magmatique des granites, dans une croûte en transtension, ont pu être caractérisés grâce à l'étude des compositions isotopiques (H, C et O) du CO_2 et de l'eau des inclusions fluides des quartz et de la roche hôte.

Enfin, le dernier chapitre traite de l'utilisation des compositions isotopiques des inclusions fluides dans les matériaux de la croûte inférieure : les granulites. Une première étude a été effectuée sur des inclusions fluides de granulites du Kenya. Elle permet de retrouver les sources et les mélanges des fluides circulant dans la croûte inférieure pendant le pic de métamorphisme, et dans les niveaux supérieurs de la croûte continentale lors de la remontée des granulites. Une seconde étude a été réalisée sur des inclusions fluides de granulites d'âges variés (du Précambrien au Miocène) et formées dans des contextes différents (subduction ou collision). Elle a permis de définir les sources des quantités importantes de CO_2 présentes en base de croûte lors de la formation des granulites. Cette étude a aussi permis d'appréhender l'analyse des isotopes stables des inclusions fluides comme un nouveau moyen de suivre l'évolution à long terme des isotopes stables des cycles de l'eau et du carbone.

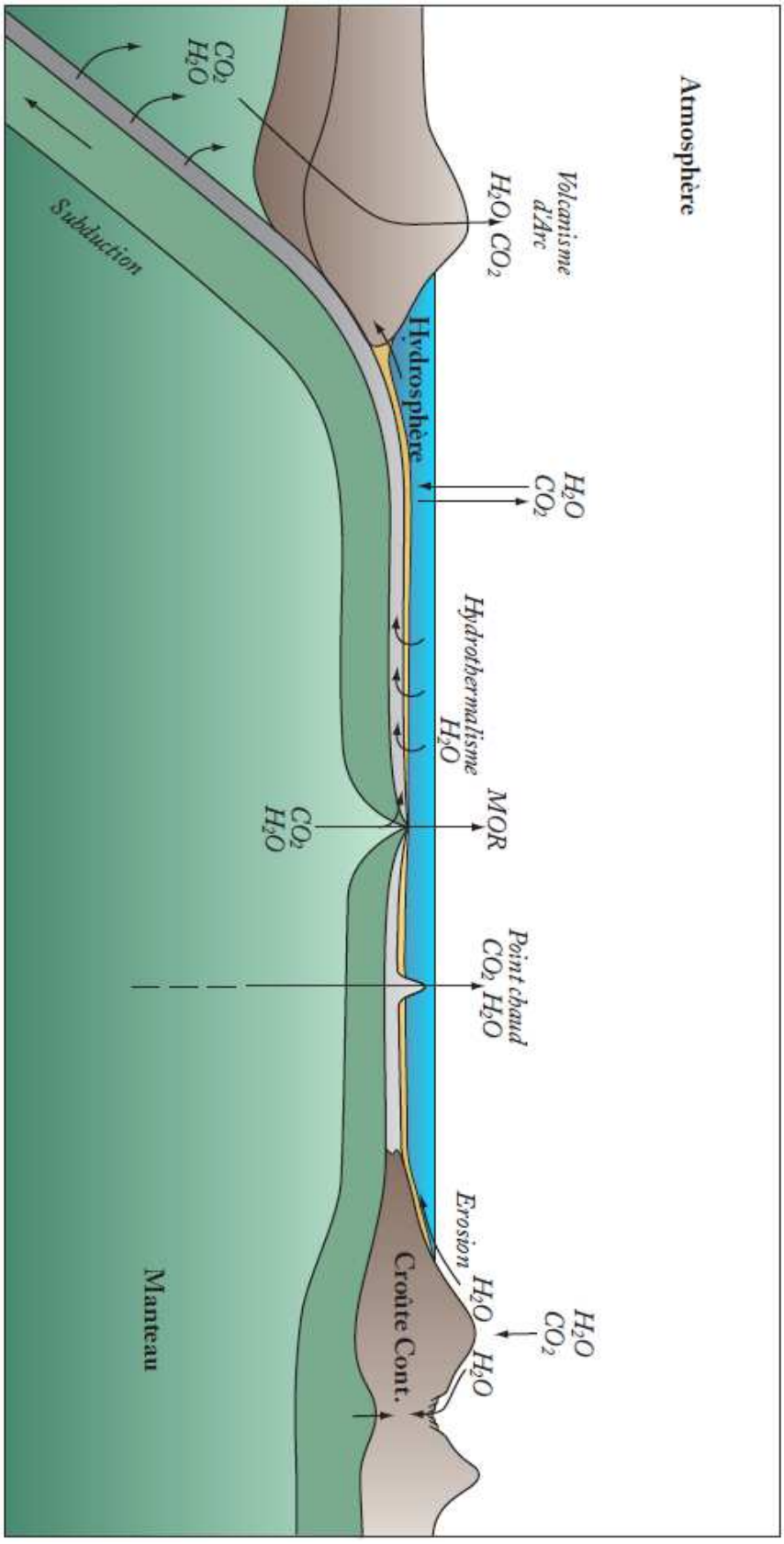

FIG. 1.1 – Les transferts des fluides majeurs au sein de la lithosphère continentale. Pour les valeurs des flux, se référer au texte et aux tables 2.1 et 2.2.

FIG. 1.1 – Water and carbon dioxide transfers within the continental lithosphere

Références

Berner R.A., Lasaga A.C. and Garrels R.M. (1983) The carbonate–silicate geochemical cycle and its effect on atmospheric carbon dioxide over the past 100 million years. *Am. J. Sci.* **283**, 641–683.

Bottinga Y. and Craig H. (1969) Oxygen isotope fractionation between CO_2 and water, and the isotopic composition of marine atmospheric CO_2. *Earth Planet. Sci. Lett.* **5**, 285–295.

Brenan J.M. and Watson E.B. (1988) Fluids in the Litosphere : 2. Experimental constraints on CO_2 transport in dunite and quartzite at elevated P-T conditions with implications for mantle and crustal decarbonation processes. *Earth Planet. Sci. Lett.* **91**, 141–158.

Cartigny P., Jendrzejewski N., Pineau F., Petit F., and Javoy M. (2001) Volatile (C, N, Ar) variability in MORB, and the respective roles of mantle source heterogeneity and degassing: the case of the Southwest Indian Ridge. *Earth Planet. Sci. Lett.* **194**, 241–257.

Chapman S. and Cowling, T. G. (1951) *Mathematical theory of non-uniform gases (2nd ed.)*. Cambridge University Press, **Chapter 10**, 14.

Corliss J.B., Dymond J., Forgon L.I., Edmond J.M., von Herzen R.P., Ballard R.D., Green K., Williams D., Bainbridge A., Crane K. and van Andel T.H. (1979) Submarine thermal springs on the Galápagos Rift. *Science* **203**, 1073–1083.

Des Marais D.J. and Moore J.G. (1984) Carbon and its isotopes in mid-ocean ridge basaltic glasses. *Earth Planet. Sci. Lett.* **69**, 43–57.

Evans W.C. (1996) A gold mine of methane. *Nature* **381**, 114.

Fischer T.P., Giggenbach W.F., Sano Y. and Williams S.N. (1998) Fluxes and sources of volatiles discharged from Kudryavy, a subduction zone volcano, Kurile Islands. *Earth Planet. Sci. Lett.* **160**, 81–96.

Frost B.R. and Bucher K. (1994) Is water responsible for geophysical anomalies in the deep continental crust? A petrological perspective. *Tectonophysics* **231**, 293–309.

Furnes H., De Wit M., Staudigel H., Rosing M. and Muehlenbachs K. (2007) A vestige of Earth's oldest ophiolite. *Science* **315**, 1704–1707.

Gerlach T.M. (1991) Present–day CO_2 emissions from volcanoes. *EOS, Trans., AGU* **72**, 249, 254–255.

Graham D. and Sarda P. (1991) Reply to comment by T.M. Gerlach on "Mid-ocean ridge popping rocks: implications for degassing at ridge crests." *Earth Planet. Sci. Lett.* **105**, 568–573.

Hart R.A. (1973) Geochemical and geophysical implications of the reaction between seawater and the oceanic crust. *Nature* **243**, 76–78.

Holland H.D. (2002) Volcanic gases, black smokers, and the Great Oxidation Event. *Geochim. Cosmochim. Acta* **66**, 3811–3826.

Holloway J.R. (1998) Graphite-melt equilibria during mantle melting: constraints on CO_2 in MORB magmas and the carbon content of the mantle. *Chem. Geol.* **147**, 89–97.

Horita J. and Wesolowski D.J. (1994) Liquid-vapor fractionation of oxygen and hydrogen isotopes of water from the freezing to the critical temperature. *Geochim. Cosmochim. Acta* **58**, 3425–3437.

Humphris S.E. and Thompson G. (1978) Hydrothermal alteration of oceanic basalts by seawater. *Geochim. Cosmochim. Acta* **42**, 107–125.

Jambon A. (1994) Earth degassing and large-scale geochemical cycling of volatile elements. In *Volatiles in magmas* (eds, M.R. Caroll and J.R. Holloway), Reviews in Mineralogy, Mineral Soc. Am., Washington, DC, **30**, 479–517.

Javoy M. and Pineau F. (1991) The volatiles record of a "popping" rock from the Mid-Atlantic Ridge at 14°N: chemical and isotopic composition of gas trapped in the vesicles. *Earth Planet. Sci. Lett.* **107**, 598–611.

Kakuichi M. and Matsuo S. (1985) Fractionation of hydrogen and oxygen isotopes between hydrated and free water molecules in aqueous urea solution. *J. Phys. Chem*. **89**, 4627–4632.

Kasting J.F., Eggler D.H. and Raeburn S.P. (1993) Mantle redox evolution and the oxidation state of Archean atmosphere. *J. Geol.* **101**, 245–257.

Majoube M. (1971) Oxygen-18 and deuterium fractionation between water and steam. *J. Chem. Phys.* **68**, 1423–1436.

Marty B. and Jambon A. (1987) C/3He in volatile fluxes from the solid Earth: Implications for carbon geodynamics. *Earth Planet. Sci. Lett.* **83**, 16–26.

Marty B. and Tolstikhin I.N. (1998) CO_2 fluxes from mid-ocean ridges, arcs and plumes. *Chem. Geol.* **145**, 233–248.

Marty B. and Zimmermann L. (1999) Volatiles (He, C, N, Ar) in mid-ocean ridge basalts : assessment of shallow-level fractionation and characterization of source composition. *Geochim. Cosmochim. Acta* **63**, 3619–3633.

Merlivat L. (1978) Molecular diffusivity of $H_2{}^{16}O$, $HD^{16}O$ and $H_2{}^{18}O$ in gases. *J. Chem. Phys.* **69**, 2864–2871.

Mével C. (2003) Serpentinization of abyssal peridotites at mid-ocean ridges. *C. R. Geoscience* **335**, 825–852.

Miller D.H. (1965) The heat and water budget of the Earth's surface. *Adv. Geophys.* **11**, 175–302.

Pili E. (1997) Distribution et transfert des fluides à l'échelle de la lithosphère continentale. Investigations géochimique et géophysique des granulites de Madagascar. Ph. D. thesis, Université Lyon 1, France.

Saal A.E., Hauri E.H., Langmuir C.H. and Perfit M.R. (2002) Vapour undersaturation in primitive mid-ocean-ridge basalt and the volatile content of Earth's upper mantle. *Nature* **419**, 451-455.

Sano Y. and Marty B. (1995) Origin of carbon in fumarolic gas from island arcs. *Chem. Geol.* **119**, 265–274.

Sano Y. and Williams S.N. (1996) Fluxes of mantle and subducted carbon along convergent plate boundaries. *Geophys. Res. Lett.* **23**, 2749–2752.

Sarda P. and Graham D. (1990) Mid-ocean ridge popping rocks: implications for degassing at ridge crests. *Earth Planet. Sci. Lett.* **97**, 268–289

Schubert G. and Reymer A.P.S. (1985) Continental volume and freeboard through geological time. *Nature* **316**, 336–339.

Sobolev A.V. and Chaussidon M. (1996) H_2O concentrations in primary melts from supra-subduction zones and mid-ocean ridges : Implications for H_2O storage and recycling in the mantle. *Earth Planet. Sci. Lett.* **137**, 45–55.

Staudigel H., Hart S.R and Richardson S.H. (1981) Alteration of the oceanic crust : Processes and timing. *Earth Planet. Sci. Lett.* **52**, 311–327.

Tatsumi Y. (1989) Migration of fluid phases and genesis of basalt magmas in subduction zones. *J. Geophys. Res.* **94**, 4697–4707.

Thompson A.B. (1992) Water in the Earth's upper mantle. *Nature* **358**, 295–302.

Varekamp J.C., Kreulen R., Poorter R.P.E. and Van Bergen M.J. (1992) Carbon source in arc volcanism, with implications for the carbon cycle. *Terra Nova* **4**, 363–373.

Watson E.B. and Brenan J.M. (1987) Fluids in the lithosphere : 1. Experimentally-determined wetting characteristics of CO_2–H_2O fluids and their implications for fluid transport, host-rock physical properties, and fluid inclusion formation. *Earth Planet. Sci. Lett.* **85**, 497–515.

Windley B.F. (1977) Timing of continental growth and emergence. *Nature* **270**, 426–428.

Wood B.J., Brynzia L.T. and Johnson K.E. (1990) Mantle oxidation state and its Relationship to tectonic environment and fluid speciation. *Science* **248**, 337–345.

Wyllie P.J. (1982) Subduction products according to experimental prediction. *Geol. Soc. Am. Bull.* **93**, 468–476.

Yardley B.W.D. and Valley J.W. (1994) How wet is the Earth's crust ? *Nature*, **371**, 205–206.

Chapitre 2

Les Cycles Géochimiques de l'Eau et du Carbone

Chapitre 2

Les Cycles Géochimiques de l'Eau et du Carbone

1. Le cycle de l'eau

1.1. L'origine de l'eau sur Terre.

Bien que la masse de l'océan sur Terre (environ $1{,}4.10^{21}$ kg) ne représente qu'une minuscule fraction (0.02 %) de la masse de la Terre, l'existence de l'océan est suffisante pour la distinguer des autres planètes du Système Solaire. En particulier, l'existence d'eau liquide, essentielle à l'apparition et au développement de la vie. Il y a deux questions fondamentales sur l'origine de l'océan sur la Terre : Quand l'océan s'est-il formé et d'où provient l'eau ? En ce qui concerne la première question, une preuve géologique contraint l'âge de l'océan puisque des roches de l'Isua Supracrustal Belt (3,8 Ga) au sud ouest du Groënland comportent des métasédiments (Appel et al., 1998) ainsi qu'un complexe filonien témoin d'une accrétion océanique (Furnes et al. 2007). L'existence de sédiments implique qu'une quantité substantielle d'eau liquide existait déjà sur Terre il y a 3,8 Ga. Bien qu'il n'y ait pas de réponse directe à la deuxième question, les rapports D/H des océans actuels et les sources possibles de l'eau ont été très discutées.

Trois hypothèses s'affrontent pour expliquer l'origine de l'eau sur Terre :

(1) La formation rapide de l'hydrosphère et de l'atmosphère par l'intermédiaire d'un dégazage intense et rapide du manteau terrestre se serait produite environ 100 à 200 Ma après l'accrétion des planètoïdes (Ozima, 1975 ; Matsui et Abe, 1986 ; Allègre et al., 1986 ; Jambon, 1994)

(2) Les perturbations gravitationnelles engendrées par la présence des planètes géantes auraient permis l'apport de l'eau par des météorites (Morbidelli et al., 2000 ; Raymond et al., 2004 ; Raymond et al., 2005) et des comètes (Gomes et al., 2005) provenant d'au delà de la ceinture d'astéroïdes, 100 Ma après l'accrétion de la Terre (Albarède, 2009).

(3) La présence d'un reste de nébuleuse solaire après la formation de la Terre aurait pu être à l'origine de la formation d'une atmosphère riche en hydrogène. L'hydrogène atmosphérique aurait réagit avec des oxydes (tels que FeO) contenus dans l'océan magmatique terrestre pour produire une quantité suffisante d'eau (Sasaki, 1990 ; Ikoma et Genda, 2006 ; Genda et Ikoma, 2007).

Le but de mon travail est d'aborder les interactions entre les différentes enveloppes terrestres du point de vue des cycles géochimiques. C'est pourquoi, dans ce chapitre, je m'attarderai plus sur les transferts de l'eau d'une enveloppe à une autre plutôt que sur l'origine de l'eau sur Terre.

1.2. Le cycle hydro-tectonique.

La quantité totale d'eau libre (eau de mer, eaux météoriques et glace) de l'exosphère (croûtes, océans et atmosphère) est contrôlée par le dégazage du manteau et par la circulation de l'eau et des groupements OH à la surface de la Terre et dans le réseau cristallin des minéraux. Cette eau structurale ($H2O^{+}$) se forme lors des processus d'altération continentale et pendant l'altération de la croûte océanique. Elle est libérée et redistribuée sous l'effet des processus diagénétiques, métamorphiques et magmatiques au niveau des zones de subduction et dans les autres environnements tectoniques. Wallmann (2001) présente une revue des différents flux régissant le cycle global de l'eau.

1.2.1. Le dégazage du manteau

Le volcanisme sous-marin n'est probablement pas une importante source d'eau libre car la majorité de l'eau libérée par le manteau est dissoute dans la matrice basaltique et seulement une faible fraction est libérée sous forme de gaz ou de liquide (Javoy et Pineau, 1991 ; Le Cloarec and Marty, 1991). Les analyses de basaltes frais des dorsales médio-océaniques suggèrent un contenu moyen en eau de la croûte supérieure proche de 0,2wt% (Moore, 1970 ; Alt et al., 1996 ; Staudigel et al., 1996). Si l'on considère le taux de production total de croûte au niveau des rides médio-océaniques ($5{,}8.10^{22}$ $g.Ma^{-1}$), le flux d'eau provenant du manteau jusqu'à la croûte océanique est alors de 6.10^{18} $mol.Ma^{-1}$. Par contraste, le volcanisme subaérien libère l'eau dans l'atmosphère car seule une petite fraction des volatils est incorporée

dans les solides volcaniques. En faisant l'hypothèse que les magmas mantelliques au niveau des arcs volcaniques et des volcans intra-plaques ont une teneur en eau similaire à celle des rides médio-océaniques (0.2 wt%), un taux de production de magma par le volcanisme subaérien de 10.2 $km^3.an^{-1}$ (Schmincke, 2000) implique une libération d'eau depuis le manteau jusque dans l'atmosphère par le volcanisme subaérien de 3.10^{18} $mol.Ma^{-1}$ (Wallmann, 2001). L'incorporation d'eau au niveau des arcs volcaniques par le recyclage de l'eau subductée est discutée dans un paragraphe ultérieur.

1.2.2. L'altération de la croûte océanique

L'eau peut être trouvée sous trois formes dans la croûte océanique,(i) en remplissage des espaces poreux et dont la quantité peut être estimée par la porosité du milieu (ii) sous la forme (H_2O^-) dans les minéraux hydratés comme les argiles ou les zéolites et extraite à 110°C même si sa libération est assez continue et que quelques fractions sont extraites à des températures supérieures, et (iii) de l'eau de constitution liée aux structures cristallines ou dissoute dans les silicates représentée par le terme H_2O^+. Dans la plupart des études géochimiques, H_2O représente H_2O^+.

Teneur en H_2O^+ de la croûte océanique supérieure basaltique (0-500m):

La teneur en eau de la croûte océanique est régulée par les processus hydrothermaux de hautes et basses températures. La quantité actuelle d'H_2O^+ au niveau des rides océaniques a été estimée grâce aux études effectuées sur les sites de forage DSDP/ODP 896A et 504B au niveau desquels de la jeune croûte océanique a été maintes fois récupérée et analysée au cours des dernières décennies (Alt et al., 1986 ; 1996). Le contenu moyen en H_2O^+ (1,3 ± 0,3wt%) des couches supérieures (0-300 m) correspond à la somme de la teneur en eau initiale des basaltes frais (0,2wt%) et de l'eau absorbée lors de l'altération du plancher océanique au niveau des dorsales océaniques (Alt et al., 1996). L'altération de la croûte supérieure pendant le Crétacé inférieur (120 Ma) a été étudiée de manière approfondie au niveau des sites DSDP

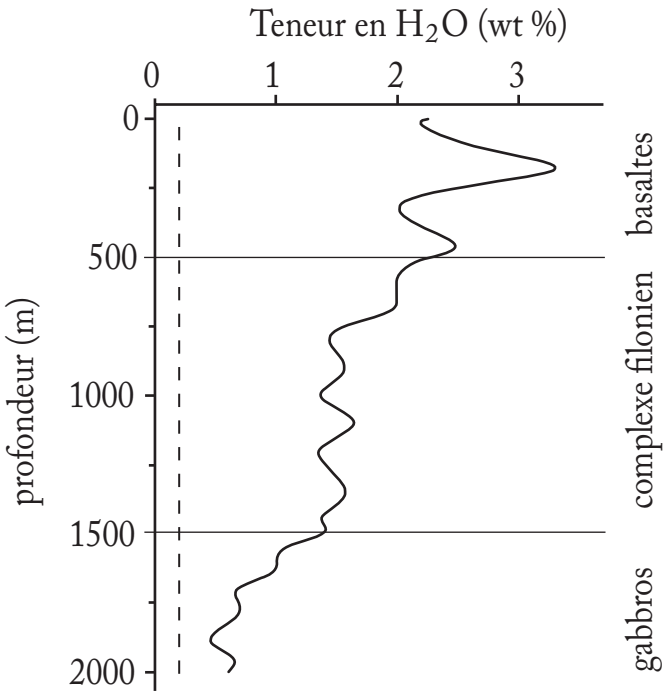

FIG. 2.1 – Représentation schématique de la teneur en H_2O structurelle de la croûte océanique altérée en fonction de la profondeur. Ce profil a été construit avec les données obtenues aux différents sites de forage en haute mer. Voir le texte pour les références. (d'après Wallman, 2001)

FIG. 2.1 – Schematic depht profile of structurally bound water H_2O in altered oceanic crust. The profile is based on data obtained at different deep–sea–drilling sites. See textfor references.

417 et 418 (Fig 2.1). L'importante surface de contact avec l'eau de mer permet aux 500 premiers mètres de croûte supérieure de s'enrichir en eau et de passer de 1,3 ±0,3wt% à 2,8wt% d' H_2O^+ (Staudigel et al., 1996). De la croûte océanique du Jurassique (165 Ma) avec d'importantes teneurs en eau a été échantillonnée au niveau du forage 801 (Alt et al., 1992), confirmant que la croûte océanique vieille (>120 Ma) contient significativement plus d'H_2O que la croûte océanique jeune (6-7 Ma). La forte teneur en eau de la croûte supérieure datée du Crétacé inférieur et du Jurassique peut s'expliquer par la présence d'interactions basses températures continues entre les basaltes et l'eau de mer. On retrouve aussi cette forte teneur en eau de la croûte océanique du Crétacé supérieur dans les schistes métamorphiques de Catalina qui contiennent des schistes bleus d'origine basaltique riches en eau (Bebout, 1996). Wallman (2001) a utilisé les données provenant des sites DSDP 417 et 418 (Staudigel et al., 1990 ; 1995 ; 1996 ; Alt et Teagle, 1999) pour calculer la quantité d'eau absorbée lors de l'altération de la croûte océanique supérieure. En considérant un taux de production de croûte supérieure (0-500 m) égal à $3{,}6.10^{15}$ $g.an^{-1}$ (Staudigel et al., 1996), il a calculé un taux d'absorption de l'eau par les basaltes de la croûte lors de leur altération de $5{,}6.10^{18}$ $mol.Ma^{-1}$. (Table 2.1)

Teneur en H_2O^+ de la croûte océanique inférieure (500-2000m):

Le complexe filonien présent sous la couche supérieure basaltique de la croûte océanique a été intensivement étudié grâce au forage DSDP 504B (Alt et al., 1986 ; 1995 ; Bach et al., 1996). Ces études donnent une teneur en eau moyenne proche de 1,5wt% (Fig 2.1). La couche de gabbros qui s'étend jusqu'à une profondeur de 7 kms n'a jamais été totalement échantillonnée lors des forages. Une section continue de seulement 500m (Hart et al., 1999 ; Stakes et al., 1991 ; Vanko et Stakes, 1991) et quelques échantillons provenant du plancher océanique (Agrinier et al., 1995) ont été analysés. Ces études montrent un faible degré d'altération hydrothermale ainsi qu'une absorption d'eau limitée (Fig 2.1). Peacock (1990) propose une teneur en eau moyenne des gabbros de 1wt%.

En faisant l'hypothèse que la croûte océanique inférieure est composée d'un complexe filonien de 1,5 km d'épaisseur et d'une épaisseur de gabbros de 5 km , et en considérant un

Apports d'eau dans les fosses océaniques	Flux
Eau interstitielle des sédiments	60–100
Eau de constitution des sédiments	5
Eau interstitielle de la croûte océanique supérieure (0–500m)	4
Eau de constitution de la croûte océanique supérieure (0–500m)	6
Eau de constitution de la croûte océanique profonde (0,5–7km) et des péridotites	20–70
Eau d'origine mantellique	6
Sorties d'eau dans l'océan l'atmosphère et le manteau	
Recyclage dans l'océan	60–100
Recyclage par les arcs volcaniques	8–67
Dégazage du manteau	2–3
Subduction dans le manteau (prof. > 250km)	9–23

TAB 2.1 – Flux d'eau actuels (in 10^{18}mole.Ma^{-1}) au niveau des zones de subduction

TAB 2.1 – Current water fluxes (in 10^{18}mole.Ma^{-1}) at subduction zones

taux de production de $5{,}6.10^{22}$ g.Ma^{-1} et des teneurs en eau de 1,5wt% pour les dykes et de 1wt% pour les gabbros, Wallmann (2001) a calculé une absorption d'eau par la croûte inférieure de 28.10^{18} mol.Ma^{-1}. Cette valeur peut être considérée comme une limite supérieure car les couches de gabbros les plus profondes semblent être essentiellement anhydres. Bach et al. (2001) propose d'ailleurs une teneur en H_2O^+ de 0,11wt% pour les gabbros en se basant sur les données provenant du site 735B.

La circulation hydrothermale ne se limite pas seulement à la croûte océanique mais pénètre aussi dans les niveaux péridotitiques du manteau sous-jacent au niveau des rides océaniques, des failles transformantes et des zones de fracture, pour former des serpentinites à des températures de 300°C à 500°C (Seyfried et Dibble Jr., 1980 ; Cannat et al., 1992 ; Agrinier et al., 1995 ; Snow et Dick, 1995 ; Kelley, 1996). Ces processus produisent des panaches de méthane dans la colonne d'eau qui sont observés tout le long de la ride médio-atlantique et dans d'autres régions tectoniquement actives des fonds sous-marins, indiquant une formation de serpentinites dans des zones étendues. (Charou et al., 1998). La quantité totale d'eau piégée dans les péridotites du manteau serpentinisé n'est actuellement pas connue. Schmidt et Poli (1998) proposent que ces interactions de haute température entre les roches et l'eau de mer permettent de fixer plus de 35.10^{18} mol.Ma^{-1} d'eau dans les péridotites. La quantité d'eau totale absorbée par la croûte océanique inférieure (>500 m) et les péridotites lors de leur altération est probablement comprise entre 20 et 70. 10^{18}mol.Ma^{-1} (Table 2.1).

1.2.3. L'altération météorique des silicates

L'altération météorique des roches ignées et de haut grade métamorphique sur les continents produit des minéraux hydratés et d'autres solides contenant de l'H_2O^+. Le taux global de formation de particules au cours de l'altération météorique des silicates peut être estimé à partir de la charge particulaire des cours d'eau avant 1850 et l'industrialisation. En considérant que 75% de ces particules sont des sédiments recyclés (Veizer et Jansen, 1979 ; Holland, 1984 ; Muehlenbachs, 1998), que le flux de particules vers l'océan est de 1.10^{22} g.Ma^{-1} (Berner et Berner, 1996), et que la teneur moyenne en H_2O^+ des produits de

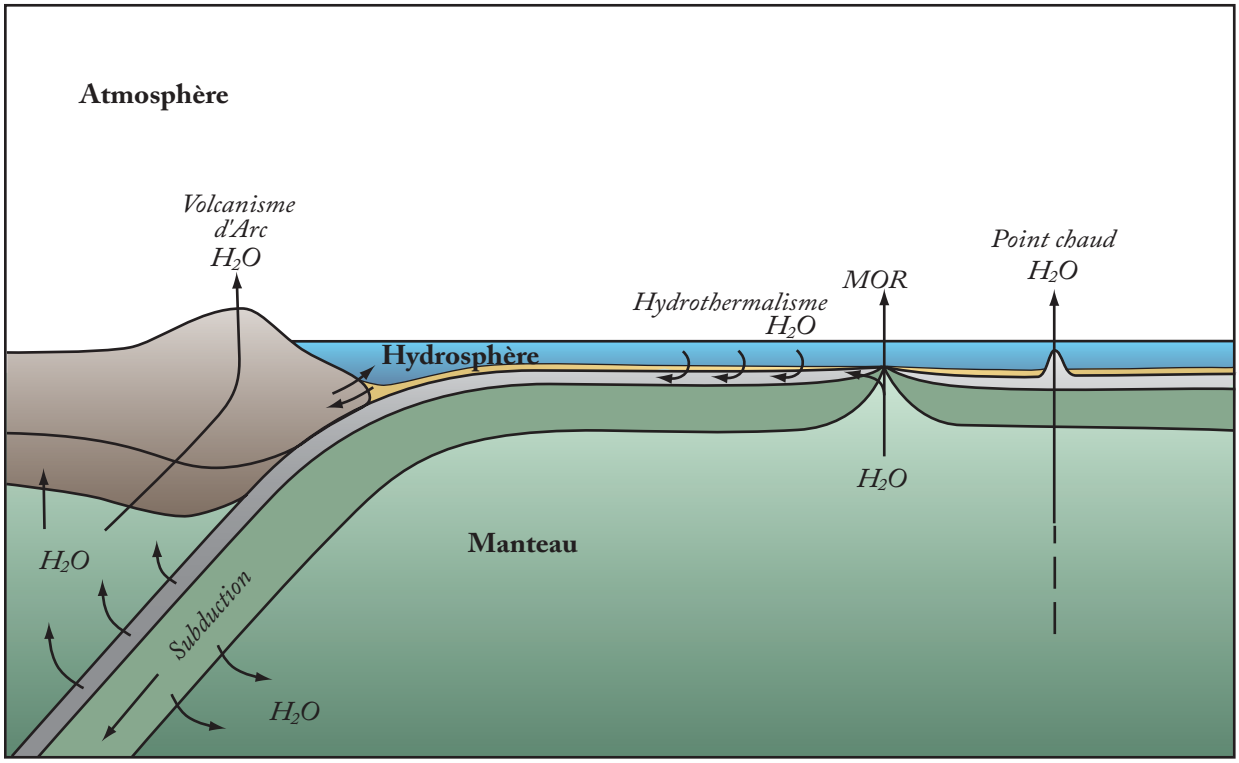

FIG. 2.2 – Représentation schématique des transfers d'eau (essentiellement H_2O^+) dans le cyle de l'eau hydro–tectonique.

FIG. 2.2 – Schematic representation of water transfers (essentially H_2O^+)in the hydro-tectonic water cycle.

l'altération météorique est de 5wt% (Peacock, 1990 ; Bebout, 1996), il en résulte alors un flux de 7.10^{18} mol.Ma^{-1} d'H_2O^+ des continents vers l'océan, généré par l'altération météorique des silicates (Fig. 2.2).

1.2.4. Le recyclage de l'eau au niveau des zones de subduction

Les zones de subduction jouent un rôle majeur dans le cycle géologique (interne) de l'eau. L'eau contenue dans les sédiments et la croûte océanique altérée est soit libérée dans l'exosphère, soit transférée dans le manteau. L'eau entre dans les zones de subduction sous forme d'eau interstitielle piégée dans les espaces poreux, d'eau liée chimiquement aux sédiments, d'eau piégée dans la croûte océanique et dans les péridotites du manteau sous-jacent et est recyclée dans l'océan, dans l'atmosphère par l'émission de fluides sous-marins et au niveau des arcs volcaniques (Table 2.1, Fig. 2.2). En utilisant les données DSDP et les vitesses de convergence des plaques, on estime le volume d'eau interstitielle entrant avec les sédiments au niveau des fosses océaniques entre 1 et 1.8 $km^3.an^{-1}$ (Von Huene et Scholl, 1991 ; Moore et Vrolijk, 1992). L'H_2O^+ sédimentaire est principalement contenue dans les minéraux argileux et les opales biogéniques et entre actuellement dans les fosses océaniques à un taux de 5. $.10^{18}$ mol.Ma^{-1}. (Planck and Langmuir, 1998)

En addition de ces flux, l'eau interstitielle de la croûte supérieure (5% du volume) (Staudigel et al., 1996) peut être considérée comme une source d'eau supplémentaire au niveau des zones de subduction représentant un flux d'environ 4.10^{18} mol.Ma^{-1} (Table 2.1, Fig. 2.2). L'eau interstitielle et l'H_2O^+ sont recyclées dans l'océan par le biais d'écoulements de fluides par diffusion, d'émissions de fluides (vents), de volcans de boue et de diapirs de serpentine. Comme les sédiments sont fortement compactés lors de la subduction, la plupart de l'eau interstitielle est renvoyée dans l'océan au niveau de la zone d'avant-arcs où elle est parfois diluée avec de l'eau « fraîche » libérée pendant la diagénèse des minéraux argileux et des opales biogéniques (Kastner et al., 1990 ; 1993).

Les eaux métamorphiques provenant des couches plus profondes sont libérées à travers le conduit principal des volcans de boues enracinés dans les serpentinites. (Fryer et al., 1990). Des données expérimentales (Schmidt and Poli, 1998) montrent que la quantité d'eau contenue dans la croûte océanique est significativement réduite lors de la subduction et

seulement 25 ± 8.10^{18} mol.Ma^{-1} d'H_2O atteignent la zone source des volcans d'arc à 70-80 km de profondeur. Le reste de l'eau, est expulsé plus superficiellement soit dans l'océan, soit dans la zone froide du coin mantellique sous le slab subducté. Cette eau est soit transportée dans les couches plus profondes par le mouvement de convection descendant où elle contribuera à la formation des magmas du volcanisme d'arc, soit remontera à la surface et nourrira les diapirs de serpentinite. Comme l'eau recyclée est principalement apportée par la compaction des sédiments, le reflux total d'eau vers l'océan est proche du flux entrant (subducté) d'eau interstitielle.

La quantité d'eau libérée dans l'atmosphère par le volcanisme d'arc peut être déduite des analyses des gaz volcaniques (Giggenbach, 1992 ; 1996), des diagrammes de phase (expérimentaux) des basaltes hydratés (Schmidt et Poli, 1998) et des bilans de masse (Ito et al., 1983). Cette quantité d'eau libérée dans l'atmosphère est estimée à 53.10^{18} mol.Ma^{-1} (Wallmann, 2001). Les données expérimentales obtenues à partir de l'étude des eaux métamorphiques libérées indiquent que 33 à 67.10^{18} mol.Ma^{-1} d'H_2O sont disponibles pour le volcanisme d'arc (Schmidt et Poli, 1998) (Table 2.1 ; Fig 2.2). Ces deux évaluations faites de façon indépendantes sont assez proches et significativement plus élevées que les premières estimations faites à partir de l'analyse des bilans de masse (8.10^{18} mol.Ma^{-1} ; Ito et al., 1983 ; Peacock, 1990). Des données supplémentaires sur le contenu en eau de la croûte océanique plongeante et sur l'émission d'eau au niveau des volcans d'arc sont nécessaires pour mieux contraindre le reflux d'eau dans l'atmosphère au niveau des zones de subduction. Une part inconnue de l'eau qui entre en subduction n'est pas recyclée dans l'océan ni dans l'atmosphère mais bien subductée dans le manteau (Schmidt et Poli, 1998). La subduction profonde d'H_2O^+ est favorisée par les faibles températures du slab subducté. (Thompson, 1992) Elle est plus prononcée pour les parties les plus profondes du slab subducté au niveau duquel la saturation en H_2O^+ n'est pas atteinte (Schmidt et Poli, 1998).

1.3. Le cycle externe de l'eau

Le cycle hydro-tectonique décrit dans le paragraphe précédent étant essentiellement contrôlé par la tectonique des plaques, son rôle dans le cycle global de l'eau n'est par conséquent visible que pour des échelles de temps de l'ordre du million d'années et est quantitativement négligeable comparé à la quantité et à la distribution de l'eau dans la circulation hydrologique actuelle à la surface de la Terre et dans la basse atmosphère. Cette différence de dynamique entre le cycle hydrologique et le cycle hydro-tectonique est aussi reflétée par les flux d'énergie impliqués.

Le cycle hydrologique global peut se résumer approximativement de la façon suivante : grâce principalement à l'énergie fournie par le rayonnement solaire, l'eau s'évapore au dessus des surfaces océaniques et terrestres (si de l'eau y est disponible). Cette vapeur d'eau est transportée par les vents et se condense, formant les nuages et produisant des précipitations aussi bien au dessus des continents que des océans. Les précipitations continentales peuvent être stockées provisoirement sous forme de neige et d'humidité dans les sols. Les précipitations non stockées ruissellent et forment les rivières et les fleuves, permettant une décharge d'eau douce dans les océans, bouclant ainsi le cycle global de l'eau (Fig. 2.3). Associés à ce cycle de l'eau, de l'énergie, le sel des océans et les nutriments et minéraux provenant des continents sont transportés et redistribués au sein du système climatique terrestre (Chahine, 1992 ; Schlesinger, 1997). L'eau joue donc un rôle crucial sur l'évolution du climat et du relief terrestres.

La plupart des études réalisées sur le cycle global de l'eau ne portent que sur quelques aspects spécifiques de ce cycle. Il existe relativement peu d'études (e.g., Chahine, 1992 ; Oki, 1999 ; Oki et al., 2006 ; Trenberth et al., 2007) qui ont essayé de fournir une vue synthétique et quantitative du cycle global de l'eau. La plupart du temps, les composants du cycle hydrologique sont étudiés isolément. Ainsi, des efforts importants ont été faits pour rassembler, analyser et évaluer les données mondiales existantes sur la vapeur d'eau (Trenberth et al., 2005), les nuages (Dai et al., 2006), les précipitations (quantité, fréquence, intensité) (Trenberth, 1998 ; Dai, 1999 ; Dai, 2001 ; Trenberth et al., 2003), l'évapotranspiration (Qian et al., 2006), l'humidité des sols, les eaux de ruissellement et la décharge des rivières dans les océans (Dai and Trenberth 2003), les flux d'humidité atmosphériques (Trenberth et Stepaniak 2003), le stockage de l'humidité atmosphérique, et les flux d'eau de ruissellement

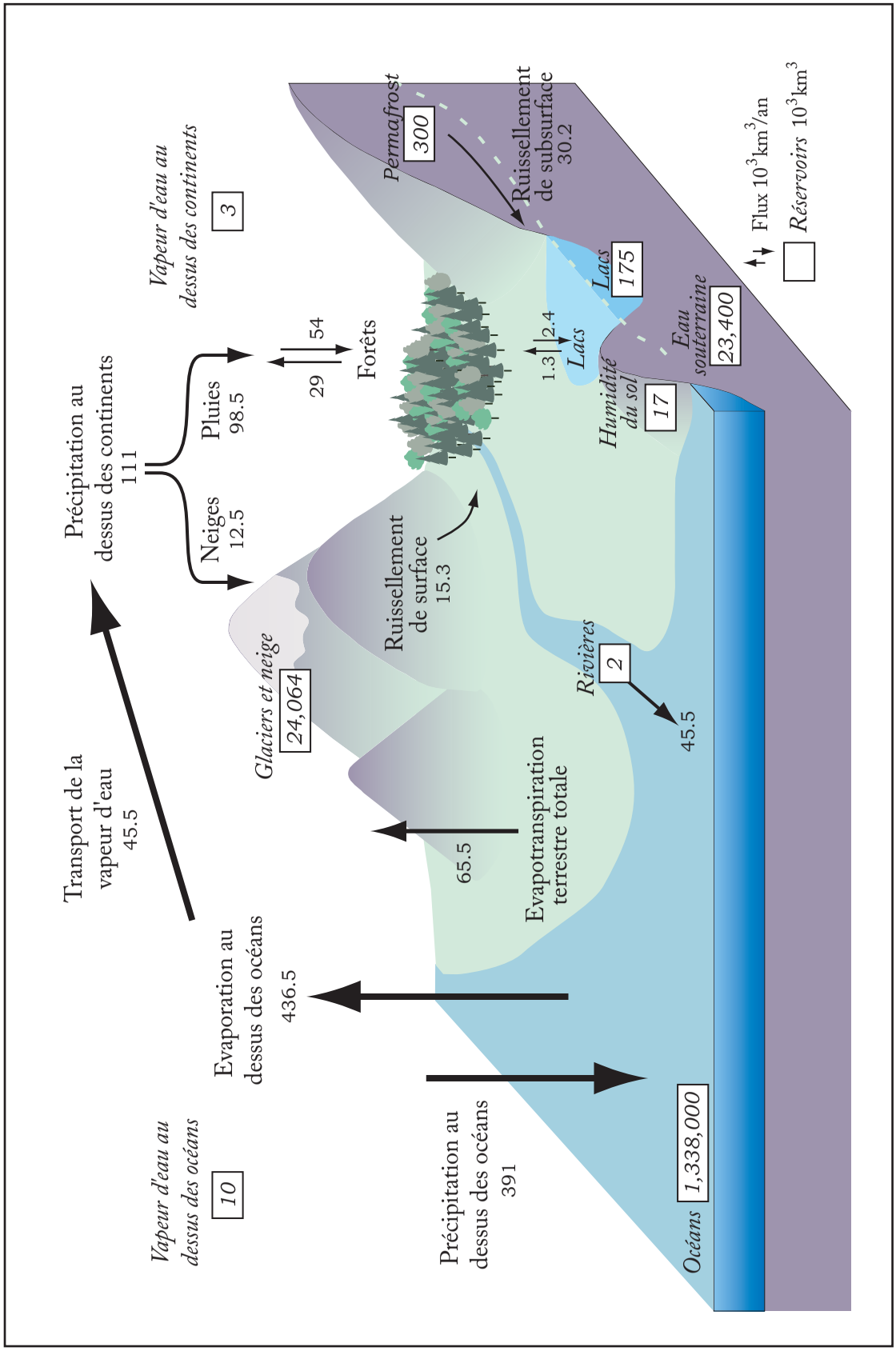

FIG. 2.3 – Flux et réservoirs d'eau dans le cycle externe de l'eau. (d'après Oki et al., 2006)

FIG. 2.3 – Global hydrological water fluxes and storages.

vers l'océan (Dai and Trenberth 2003). Grâce à toutes ces études, il a été clairement établi que l'énergie latente perdue par la surface lors de l'évaporation de l'eau entraîne un refroidissement de la surface terrestre. Cette énergie est restituée dans l'atmosphère lors de la condensation de la vapeur d'eau (formation des nuages) et contribue au réchauffement de l'atmosphère. Il existe donc une relation étroite entre les cycles d'eau et d'énergie dans l'atmosphère. Il est donc clair que le cycle hydrologique et ses modifications jouent un rôle majeur dans le contexte du changement climatique.

Le cycle hydrologique global présenté dans la figure 2.3 est construit à partir des données provenant de l'article de Oki et al., (2006) dans lequel il fait une estimation des principaux flux et réservoirs associés, en compilant les données récentes les plus souvent utilisées. (Korzun, 1978 ; Church, 1996 ; Shiklomanov, 1997 ; Oki, 1999 ; Dirmeyer et al., 2006).

2. Le cycle du carbone

2.1. Les principales formes de carbone sur Terre

Les principales formes de carbone présentes dans l'atmosphère de la Terre depuis sa formation, sont le dioxyde de carbone (CO_2) et le méthane (CH_4). Ces gaz ont joué des rôles cruciaux, mais distincts, dans le développement des différentes formes de vie et dans l'évolution des environnements de surface de la Terre. Le CO_2 est le moteur principal de processus tels que la photosynthèse, le métabolisme et la décomposition organique. Grâce à sa transformation lors de l'altération et grâce à sa précipitation sous forme de carbonate, il fournit en carbone une grande partie des roches sédimentaires de la Terre et contribue au recyclage des matières volatiles à travers la lithosphère. Le méthane représente quant à lui la partie anaérobie du cycle du carbone, de par son importance dans le métabolisme microbien et sa présence dans la matière organique piégée dans les roches et les sédiments.

Ce chapitre portera uniquement sur le cycle du « dioxyde de carbone » avant l'industrialisation. Pour de plus amples informations sur le cycle du méthane, se référer aux travaux de Sundquist et Visser (2003).

2.2. Le cycle du dioxyde de carbone

La figure 2.4 présente les principaux réservoirs de carbone et les flux qui affectent la quantité de CO_2 atmosphérique au cours des temps géologiques. Des estimations ont été effectuées à la fois pour la période glaciaire la plus récente et pour l'holocène supérieur avant l'industrialisation. Les unités utilisées pour quantifier les flux et le stockage du dioxyde de carbone sont celles utilisées le plus souvent dans la littérature : les pétagrammes de carbone ($PgC=10^{15}g$).

Les estimations des principaux flux de carbone de l'Holocène Supérieur présentées dans la figure 2.4 sont dérivées des valeurs données par Houghton (2003) et par Sarmiento et Gruber (2002). La figure 2.4 et la table 2.2 présentent les estimations des composantes géologiques du

Réservoirs	Taille (Pg C)	Références
Atmosphère	590	Oki et al. 2006
Océans	(3,71–3,90).104	Sundquist, 1985, 1993; Houghton, 2003
Surface – inorganique	700–900	Sundquist, 1985; Sarmiento et Gruber, 2002; Houghton, 2003
Profond – inorganique	(3,56–3,80).104	Sundquist, 1993; Sarmiento et Gruber, 2002; Houghton, 2003
Total organique	685–700	Sharp, 1997; Hansell et Carlson, 1998; Doval et Hansell, 2000
Biosphère aquatique	1–3	Falkowski et al., 2000; Sarmiento et Gruber, 2002
Biosphère terrestre et sols	(2,0–2,3).103	Sundquist, 1993; Sarmiento et Gruber, 2002, Houghton, 2003
Végétation	500–600	Sundquist, 1993; Houghton, 2003
Sols	(1,5–1,7).103	Houghton, 2003
Sédiments marins "Reactive"	3000	Sundquist, 1985
Inorganique	2500	
organique	650	
Croûte	(7,78–9,0).107	Holland, 1978; Li, 2000
Carbonates	6,53.107	Li, 2000
Carbone organique	1,25.107	Li, 2000
Manteau	3,24.108	Des Marais, 2001
Réserves fossiles	(4,22–5,68).103	Nakicenovic et al., 1998; Moomaw, 2001
Pétrole	636–842	
Gaz naturel	483–564	
Charbon	(3,10–4,27).103	

Flux	Taille (Pc C an^{-1})	Références
Enfouissement des carbonates	0,13–0,38	Berner et al., 1983, Berner et Berner, 1987; Meybeck, 1987; Drever et al., 1988; Milliman, 1993; Wollast, 1994
Enfouissement du carbone organique	0,05–0,13	Lein, 1984; Berner, 1982; Berner et Raiswell, 1983; Dobrovolsky, 1994; Schlesinger, 1997
Rivières (Carbone inorganique dissous)	0,39–0,44	Berner et al., 1983; Berner et Berner, 1987; Meybeck, 1987; Drever et al., 1988
Rivières (Carbone organique total)	0,30–0,41	Schlesinger et Melack, 1981; Meybeck, 1981; Meybeck, 1988; Degens et al., 1991
Carbone organique dissous	0,21–0,22	Meybeck, 1981; Meybeck, 1988; Spitzy et Leenheer, 1991
Carbone organique particulaire	0,17–0,30	Meybeck, 1981; Milliman et al., 1984; Ittekot, 1988; Meybeck, 1988
Volcanisme	0,04–0,10	Gerlach, 1991; Kerrich et al., 1995; Arthur, 2000; Kerrich, 2001; Morner et Etiope, 2002
Echanges mantelliques	0,022–0,07	Sano et Williams, 1996; Marty et Tolstikhin, 1988; Des Marais, 2001

TAB. 2.2 – Estimations récentes des réservoirs et des flux géologiques de carbone pré–industriels. (d'après Sundquist et Visser, 2003)

TAB. 2.2 – Representative range of recent estimates for pre–industrial reservoirs and geologic fluxes of carbon.

cycle du carbone (altération, transport par les rivières, sédimentation, émissions volcaniques/métamorphiques, réservoirs rocheux et sédimentaires), appelés ainsi parce qu'ils sont généralement plus importants pour de longues échelles de temps. Quelques processus sédimentaires (l'enfouissement et la reminéralisation de la matière organique et des carbonates) peuvent affecter les teneurs en carbone de l'atmosphère sur des échelles de temps de l'ordre de quelques milliers d'années. Ces réservoirs sédimentaires associés à ces échelles de temps sont représentés sur la figure 2.4 et dans la table 2.2 par le terme « reactive sediment » (Sundquist, 1985). Bien que la taille de ces réservoirs ne soit pas connue précisément, ils sont assez importants pour affecter significativement la chimie du système océan-atmosphère à travers des processus tels que la dissolution des carbonates et la diagénèse du carbone organique.

Un autre réservoir de carbone important et potentiellement « reactive sediment » est le pôle des hydrates de méthane. Le méthane est produit le plus souvent par le métabolisme anoxique bactérien du CO_2 ou des substrats organiques dérivés de la photosynthèse du CO_2. En présence d'oxygène ou d'autres accepteurs d'électrons contenant de l'oxygène, le méthane est oxydé en CO_2. C'est la raison pour laquelle le cycle du méthane est présenté sur la figure 4 comme un « sous cycle » du cycle du carbone. La quantité de CO_2 présente dans l'atmosphère pendant les périodes glaciaires peut être précisément calculée à partir de la concentration en CO_2 dans les bulles d'air piégées dans la glace formée pendant ces périodes. Cette concentration est aussi un excellent moyen d'estimer la teneur en carbone inorganique dissous (DIC) dans les océans. Le DIC existe principalement sous quatre formes : le CO_2 dissous, l'acide carbonique (H_2CO_3), les ions bicarbonate (HCO_3^-), et les ions carbonatés (CO_3^{2-}). Les formes ioniques peuvent se combiner avec d'autres ions pour former des ions complexes dans des solutions telles que l'eau de mer. Les réactions chimiques entre les différentes espèces de carbone inorganique dissous sont rapides. L'échange de CO_2 entre l'atmosphère et la surface des océans est tellement rapide que, pour des estimations globales comme celles présentées dans la figure 2.4, la surface des océans peut être considérée comme proche de l'équilibre chimique avec l'atmosphère (Sundquist et Plummer, 1981). L'augmentation de la quantité en DIC entre époques glaciaires et interglaciaires correspondant à l'augmentation en CO_2 atmosphérique (170 PgC) (Fig 2.4) est estimée à environ 30 PgC (Sunquist, 1993).

Les estimations des autres réservoirs de carbone et des flux existant entre ces réservoirs lors de la période glaciaire la plus récente dépendent largement des estimations de la quantité de carbone stockée dans la biosphère terrestre. Puisque le transfert de carbone sur des échelles de temps de l'ordre du millier d'années se limite principalement aux échanges entre l'atmosphère, la biosphère et les océans, une perte ou un gain en carbone dans un de ces réservoirs peut être considéré comme un bon moyen pour faire une estimation des gains et pertes correspondantes dans les autres réservoirs. Les estimations de la masse de la biosphère terrestre glaciaire sont calculées à partir de reconstructions des changements écologiques ou déduites de l'évolution de la composition isotopique du carbone océanique dissous. Il existe un large consensus sur le fait que la quantité de carbone stockée dans la végétation et dans les sols était moins importante pendant la dernière période glaciaire que pendant l'Holocène (Shackelton, 1977 ; Crowley, 1995). Des reconstructions paléo-écologiques, basées sur des données provenant de sols ou de sédiments (Adams et al., 1990 ; Adams et Faure, 1998) ou sur des modèles décrivant les relations climat/végétation pendant les périodes glaciaires (Prentice et al., 1993 ; Otto et al., 2002), montrent que la quantité de carbone stocké dans les sols et la végétation pendant les périodes glaciaires varie de quelques centaines à plus d'un millier de PgC, ce qui est inférieur à la quantité de carbone stockée par le même procédé pendant l'Holocène. Cette large gamme de valeurs reflète plusieurs sources d'incertitude, à savoir sur les limites des modèles paléoclimatiques et paléo-écologiques, sur les modèles climatiques et les hypothèses des effets du CO_2 dans l'atmosphère, sur les interactions entre le climat et la végétation, et sur les quantités de carbone stockées dans les différents biotopes et milieux côtiers (Prentice et Fung, 1990 ; Van Campo et al., 1993 ; François et al., 1999).

L'enregistrement isotopique du carbone des sédiments marins donne des renseignements importants sur les changements glaciaires/interglaciaires dans le stockage du carbone par la biosphère terrestre. Pendant la photosynthèse, les plantes assimilent préférentiellement le $^{12}CO_2$, produisant une atmosphère relativement enrichie en $^{13}CO_2$. Le carbone assimilé par les plantes terrestres pendant la photosynthèse peut être appauvri en ^{13}C de 3‰ à 25‰ par rapport à la source de carbone inorganique. L'importance de cet appauvrissement varie principalement parce que les plantes peuvent utiliser plusieurs voies biochimiques pour assimiler le carbone. La voie la plus commune est la carboxylation du ribulose. Cette réaction,

qui est catalysée chez les plantes en C3 par la Ribulose-1,5-bisphosphate carboxylase oxygénase (RUBISCO), enzyme du cycle de Calvin, est à l'origine d'une baisse du $\delta^{13}C$ de 15 à 25‰ (O'Leary, 1998). La carboxylation du phosphoenol pyruvate (PEP) ou « voie en C4 », est plus couramment observée pour le maïs et les autres graminées. Bien que la voie en C4 fonctionne en association étroite avec la carboxylation du ribulose, la baisse résultante du $\delta^{13}C$ n'est que de 3 à 8‰ (Deleens et al., 1983). Parce que la voie en C3 est la plus commune pour la photosynthèse chez les pantes terrestres, cette voie détermine probablement le $\delta^{13}C$ moyen du CO_2 atmosphérique transféré entre la végétation et les sols pendant les transitions glaciaires/interglaciaires.

L'échange du CO_2 entre l'atmosphère et les océans étend l'effet du fractionnement isotopique des plantes terrestres au réservoir océanique qu'est le DIC. Un changement global significatif au niveau de la quantité de carbone photosynthétisé stocké dans les plantes et les sols pourrait changer la composition isotopique du carbone du CO_2 atmosphérique et du DIC océanique. Les compositions isotopiques du carbone du CO_2 atmosphérique et du DIC océanique sont aussi affectées par d'autres facteurs, notamment l'échange de gaz à la surface des mers, les réactions chimiques entre les différentes espèces de DIC, et la photosynthèse réalisée par les organismes marins. Par exemple, la photosynthèse des organismes marins produit du carbone appauvri de 10 à 30‰ par rapport à la source (Deines, 1980). Il est admis que la photosynthèse des organismes marins se produit principalement par la voie biochimique C3, mais les effets de la photosynthèse en C4 des diatomées peuvent jouer un rôle dans la large gamme des isotopes du carbone observés pour les écosystèmes planctoniques (Reinfelder et al., 2000). Les changements dans ces facteurs jouant un rôle dans le fractionnement isotopique des océans lors des transitions entre les périodes glaciaires et interglaciaires doivent être quantifiés pour déterminer la signature isotopique des changements dans la biosphère terrestre (Hofmann et al., 1999).

Les effets du fractionnement isotopique dû à la photosynthèse des organismes marins, aux échanges gazeux et aux réactions chimiques entre les espèces de DIC sont plus prononcés pour le CO_2 atmosphérique et le DIC de la surface des océans. Le DIC des océans profonds n'est pas significativement affecté par ces facteurs. Les variations isotopiques du DIC

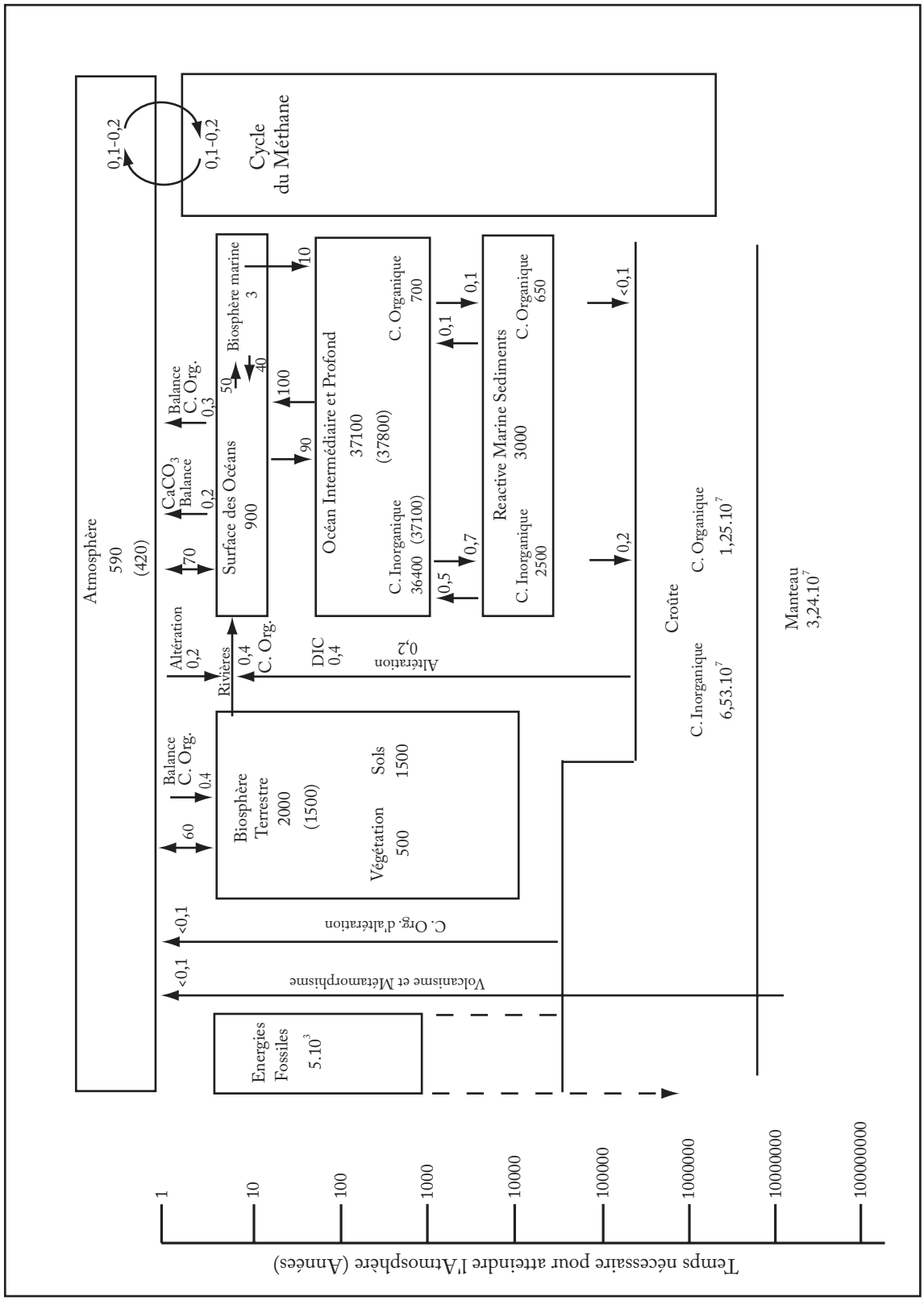

FIG. 2.4 – Flux et réservoirs de carbone dans le cycle global du carbone. Les valeurs calculées pour les périodes glacaires sont entre parenthèses. La barre verticale sur la gauche de la figure donne le temps approximatif (en années) nécessaire pour que le carbone des différents réservoirs atteigne l'atmosphère. (d'après Oki et al. 2006)

FIG. 2.4 – Reservoirs and fluxes of the global carbon cycle. Values for glacial periodsare shown in parentheses. The vertical bar on the left shows approximate time (in years) necessary for the different reservoirs to affect the atmosphere.

océanique lors des transitions glaciaire/interglaciaire sont donc enregistrées dans les coquilles calcaires des organismes présents dans les sédiments, et les variations isotopiques du CO_2 atmosphérique sont enregistrées dans les glaces. Ces enregistrements indiquent une augmentation du $\delta^{13}C$ du DIC océanique de l'ordre de 0,3 à 0,5‰ lors d'une transition glaciaire/interglaciaire (Sarnthein et al., 1988 ; Curry et al., 1988 ; Duplessy et al., 1988 ; Ku et Luo, 1992 ; Crowley, 1995), et correspond à une augmentation du $\delta^{13}C$ du CO_2 atmosphérique de 0,1 à 0,5‰ (Leuenberger et al., 1992 ; Smith et al., 1999). Des calculs de bilan de masse basés sur ces variations isotopiques permettent de retrouver la quantité de carbone organique stocké dans les sols et les plantes (Sundquist, 1993 ; Bird et al., 1996). Sundquist (1993) suggère une gamme variant de 450 à 750 PgC, alors que Bird et al. (1996) suggèrent une gamme de 300 à 700 PgC. En appliquant les équations de bilan de masse de Bird et al. (1996), Sundquist et Visser (2007) trouvent une gamme de l'ordre de 400 à 800 PgC à partir des variations de la composition isotopique du carbone atmosphérique et océanique donnés dans le texte, et une valeur de -22 à -25‰ (vs PDB) pour le carbone piégé par la biosphère pendant la déglaciation. Ces calculs ne prennent pas en compte les effets possibles de l'augmentation de production de méthane et l'oxydation pendant les périodes de déglaciation (Maslin et Thomas, 2003).

Les procédures décrites ci-dessus fournissent une base de données raisonnable pour estimer la redistribution du stockage du carbone entre l'atmosphère, la biosphère terrestre et les océans au cours de la dernière période glaciaire. Les estimations des réservoirs de carbone pendant la dernière période glaciaire présentés dans la figure 2.4 sont dérivées des calculs de bilan de masse décrits ci-dessus. Les estimations des flux de carbone existant pendant cette période étant beaucoup moins certains, ils ne sont pas présentés.

Conclusion

Les fluides comme aqueux et carboniques sont donc présents dans toutes les enveloppes terrestres. Leurs transferts d'un réservoir à l'autre se fait à travers des cycles géochimiques. Vecteurs d'éléments chimiques et de chaleur, leur présence va affecter les propriétés physico-chimiques des enveloppes qui les contiennent. La caractérisation des fluides tels qu'H_2O et CO_2 est donc un défi intéressant pour comprendre quels rôles ils jouent dans l'évolution de la composition chimique de la Terre et dans les interactions entre les différentes enveloppes, ou pour comprendre quelle a été leur implication dans l'apparition de la vie. Cependant, qu'ils soient impliqués dans les interactions entre atmosphère, biosphère et hydrosphère ou dans les transferts de volatils entre croûte et manteau, la caractérisation de ces fluides se révèle souvent complexe du fait de leur mobilité. C'est à travers l'étude des inclusions fluides que je tenterai de répondre aux questions posées.

Références

Adams J.M., Faure H., Faure–Denard L., McGlade J. and Woodward F.I. (1990) Increases in terrestrial carbon storage from the last glacial maximum to the present. *Nature* **348**, 711–714.

Adams J.M. and Faure H. (1998) A new estimate of changing carbon storage on land since the last glacial maximum, based on global land ecosystem reconstruction. *Global Planet. Change* **16–17**, 3–24.

Agrinier P., Hékinian R., Bideau D. and Javoy M. (1995) O and H stable isotope compositions of oceanic crust and upper mantle rocks expose in the Hess Deep near the Galapagos Triple Junction. *Earth Planet. Sci. Lett.* **136**, 183-196.

Albarède F. (2009) Volatile accretion history of the terrestrial planets and dynamic implications. *Nature* **461**, 1227–1233.

Allègre C.J., Staydacher T. and Sarda P. (1986) Rare gaz systematics : formation of atmosphere, evolution and structure of the Earth's mantle. *Earth Planet. Sci. Lett.* **81**, 127-150.

Alt J.C. and Teagle D.A.H. (1999) The uptake of carbon during alteration of oceanic crust. *Geochim. Cosmochim. Acta* **63**, 1527-1536.

Alt J.C., Honnorez J., Laverne C. and Emmemermann R. (1986) Hydrothermal alteration of a 1 km section through the upper oceanic crust, Deep Sea Drilling Project Hole 504B : Mineralogy, chemistry, and evolution of seawater-basalt interactions. *J. Geophys. Res.* **91**, 10309-10335.

Alt J.C., France-Lanord C., Castillo P. and Galy A. (1992) Low-temperature hydrothermal alteration of Jurassic ocean crust, Site 801. *Proc. O.D.P., Sci. Res.* **129**, 415-427.

Alt J.C., Zuleger E. and Erzinger J. (1995) Mineralogy and stable isotopic composition of the hydrothermally altered lower sheeted dike complex, Hole 504B, Leg 140. *Proc. O.D.P., Sci. Res.* **137**, 155-166.

Alt J.C., Teagle D.A.H., Laverne C., Vanko D.A., Bach W., Honnorez J., Becker K., Ayadi M. and Pezard P.A. (1996) Ridge flank alteration of upper ocen crust in the eastern Pacific: Synthesis of results for volcanic rocks of Holes 504B and 896A. *Proc. O.D.P., Sci. Res.* **148**, 435-450.

Appel P.W.U., Fedo C.M., Moorbath S. and Myers J.S. (1998) Recognizable primary volcanic and sedimentary features in a low-strain domain of the highly deformed, oldest known (3.7–3.8 Gyr) Greenstone Belt, Isua, West Greenland. *Terra Nova* **10**, 57–62.

Arthur M.A. (2000) Volcanic contributions to the carbon and sulfur geochemical cycles and global change. In *Encyclopedia of Volcanoes* (eds. H. Sigurdsson, B.F. Houghton, S.R. McNutt, H. Rymer and J. Stix), Academic Press, San Diego, 1045–1056.

Bach W., Erzinger J., Alt J.C. and Teagle D.A.H. (1996) Chemistry of the lower sheeted dike complex, Hole 504B (Leg 148): Influence of magmatic differentiation and hydrothermal alteration. *Proc. O.D.P., Sci. Res.* **148**, 39-55.

Bach W., Alt J.C., Niu Y., Humphris S.E., Erzinger J., and Dick H.J.B. (2001) The geochemical consequences of late–stage low–grade alteration of lower ocean crust at the SW Indian Ridge: Results from ODP Hole 735B (Leg 176). *Geochim. Cosmochim. Acta* **65**, 3267–3287.

Bebout G.E. (1996) Volatile Transfer and Recycling at Convergent Margins: Mass-Balance and Insights from High-P/T Metamorphic Rocks In *Subduction, Top to Bottom* (eds G.E. Bebout, DW Scholl, S.H. Kirby, and J.P. Platt), American Geophysical Union **96**, 179-193.

Berner R.A. (1982) Burial of organic carbon and pyrite sulfur in the modern ocean: its geochemical and environmental significance. *Am. J. Sci.* **282**, 451–473.

Berner R.A. and Raiswell R. (1983) Burial of organic carbon and pyrite sulfur in sediments over Phanerozoic time: a new theory. *Geochim. Cosmochim. Acta* **47**, 855–862.

Berner R.A., Lasaga A.C. and Garrels R.M. (1983) The carbonate–silicate geochemical cycle and its effect on atmospheric carbon dioxide over the past 100 million years. *Am. J. Sci.* **283**, 641–683.

Berner E.K. and Berner R.A. (1987) *The Global Water Cycle.* Prentice–Hall, Englewood Cliffs.

Bird M.I., Lloyd J. and Farquhar G.D. (1996) Terrestrial carbon–storage from the last glacial maximum to the present. *Chemosphere* **33**, 1675–1685.

Cannat M., Bideau D. and Bougault H. (1992) Serpentinized peridotites and gabbros in the Mid-Atlantic ridge axial valley at 15°37'N and 16°52'N. *Earth Planet. Sci. Lett.* **109**, 87-106.

Chahine M.T. (1992) The hydrological cycle and its influence on climate. *Nature* **359**, 373-380.

Charou J.L., Fouquet Y., Bougault H., Donval J.P., Etoubleau J., Jean-Baptiste P., Dapoigny A., Appriou P. and Rona P.A. (1998) Intense CH_4 plumes generated by serpentinization of ultramaficrocks at the intersection of the 15°20'N Fracture Zone and the Mid-Atlantic Ridge. *Geochim. Cosmochim. Acta* **62**, 2323-2333.

Church T.M. (1996) An underground route for the water cycle. *Nature* **380**, 579–580.

Crowley T.J. (1995) Ice age terrestrial carbon changes revisited. *Global Biogeochem. Cycles* **9**, 377–389.

Curry W.B., Duplessy J.C., Labeyrie L.D. and Shackleton N.J. (1988) Changes in the distribution of $\delta^{13}C$ of deep water Σ CO_2 between the last glaciation and the Holocene. *Paleoceanography* **3**, 317–341.

Dai A. (2001) Global precipitation and thunderstorm frequencies. Part I: Seasonal and interannual variations. *Journal of Climate* **14**, 1092-1111.

Dai A. and Trenberth K.E. (2003) New estimates of continental discharge and oceanic freshwater transport. *Proc. Symp. on Observing and Understanding the Variability of Water in Weather and Climate*, CA, Amer. Meteor. Soc. CD–ROM, JP1.11.

Dai, A., Giorgi F. and Trenberth K.E. (1999) Observed and model-simulated diurnal cycles of precipitation over the contiguous United States. *J. Geophys. Res.* **104**, 6377-6402.

Dai A. Karl T.R., Sun B. Trenbreth K.E. (2006) Recent trends in cludiness over the United States: A tale of monitoring inadequacies. *Bull.Amer. Meteor. Soc.* **87***, 597-606.*

Deines P. (1980) The isotopic composition of reduced organic carbon. In *Handbook of Environmental Isotope Geochemistry* (eds. P. Fritz and J.C. Fontes), Elsevier, New York, 329–406.

Deleens E., Ferhi A. and Querioz O. (1983) Carbon isotope fractionation by plants using the C4 pathway. *Physiol. Veg.* **21**, 897–905.

Des Marais D.J. (2001) Isotopic evolution of the biogeochemical carbon cycle during the Precambrian. *Rev. Mineral. Geochem.* **43**, 555–578.

Dirmeyer, P. A., Gao X., Zhao M., Guo Z., Oki T. and Hanasaki N. (2006) The Second Global Soil Wetness Project (GSWP-2): Multi-model analysis and implications for our perception of the land surface. *Bull. Amer. Meteor. Soc.* **87**, 1381-1397.

Dobrovolsky V.V. (1994) *Biogeochemistry of the World's Land.* CRC Press, Boca Raton, Florida.

Doval M.D. and Hansell D.A. (2000) Organic carbon and apparent oxygen utilization in the Western South Pacific and the central Indian Oceans. *Mar. Chem.* **68**, 249–264.

Drever J.L., Li Y.H. and Maynard J.B. (1988) Geochemical cycles: the continental crust and the oceans. In *Chemical Cycles in the Evolution of the Earth* (eds. C.B. Gregor, R.M. Garrels, F.T. Mackenzie and J.B. Maynard), Wiley, New York, 17–53.

Duplessy J.C., Shackleton N.J., Fairbanks R.G., Labeyrie L., Oppo D. and Kallel N. (1988) Deepwater source variations during the last climatic cycle and their impact on the global deepwater circulation. *Paleoceanography* **3**, 343–360.

Falkowski P., Scholes R.J., Boyle E., Canadell J., Canfield D., Elser J., Gruber N., Hibbard K., Hogberg P., Linder S., Mackenzie F.T., Moore I.B., Pedersen T., Rosenthal Y., Seitzinger S., Smetacek V. and Steffen W. (2000) The global carbon cycle: a test of our knowledge of Earth as a system. *Science* **290**, 291–296.

Francois L.M., Godderis Y., Wamant P., Ramstein G., de Noblet N. and Lorenz S. (1999) Carbon stocks and isotopic budgets of the terrestrial biosphere at mid–Holocene and last glacial maximum times. *Chem. Geol.* **159**, 163–189.

Fryer P., Pearce J.A. and Stokking L.B (1990) *Proceedings of the Ocean Drilling Program, Initial Reports, Leg 125*. Ocean Drilling Program.

Furnes H., De Wit M., Staudigel H., Rosing M. and Muehlenbachs K. (2007) A vestige of Earth's oldest ophiolite. *Science* **315**, 1704–1707.

Genda H. and Ikoma M. (2007) Origin of the ocean on the Earth: Early evolution of water D/H in a hydrogen–rich atmosphere. *Icarus* **194**, 42–52.

Gerlach T.M. (1991) Present–day CO_2 emissions from volcanoes. *EOS, Trans., AGU* **72**, 249, 254–255.

Giggenbach W.F. (1992) Isotopic shifts in waters from geothermal and volcanic systems along convergent plate boundaries and their origin. *Earth Planet. Sci. Lett.* **113**, 495–510.

Giggenbach W.F. (1996) Chemical composition of Volcanic Gases. In *Monitoring and Mitigation of Volcanic Hazards* (eds. R. Scosper and R.I. Tilling), Springer-Verlag, 221-256.

Gomes R., Levison H.F., Tsiganis K. and Morbidelli M. (2005) Origin of the cataclysmic late heavy bombardment period of the terrestrial planets. *Nature* **435**, 466–469.

Hansell D.A. and Carlson C.A. (1998) Deep–ocean gradients in the concentration of dissolved organic carbon. *Nature* **395**, 263–266.

Hart S.R., Blusztajn J., Dick H.J.B., Meyer P.S. and Muehlenbachs K. (1999) The fingerprint of seawater circulation in a 500-meter section of ocean crust gabbros. *Geochim. Cosmochim. Acta* **63**, 4059-4080.

Hofmann M., Broecker W.S. and Lynch–Stieglitz J. (1999) Influence of a [$CO_{2(aq)}$] dependent biological C–isotope fractionation on glacial C13/C12 ratios in the ocean. *Global Biogeochem. Cycles* **13**, 873–883.

Holland H.D. (1978) *Chemistry of the Atmosphere and Oceans.* Wiley, New York.

Holland H.D. (1984) *The Chemical evolution of the Atmosphere and Oceans.* Princeton University Press.

Houghton R.A (2003) The Contemporary Carbon Cycle. In *Treatise on Geochemistry, Volume 8* (eds. H.D. Holland and K.K. Turekian), Elsevier, New York, 473–513.

Ikoma M. and Genda H. (2006) Constraints on the mass of a habitable planet with water of nebular origin. *Astrophys. J.* **648**, 696–706.

Ito E., Harris D.M. and Anderson A.T. (1983) Alteration of oceanic crust and geologic cycling of chlorine and water. *Geochim. and Cosmochim. Acta* **47**, 1613-1624.

Ittekot V. (1988) Global trends in the nature of organic matter in river suspensions. *Nature* **332**, 436–438.

Jambon A. (1994) Earth degassing and large-scale geochemical cycling of volatile elements. In *Volatiles in magmas* (eds, M.R. Caroll and J.R. Holloway), Reviews in Mineralogy, Mineral Soc. Am., Washington, DC, **30**, 479–517.

Javoy M. and Pineau F., 1991. The volatiles record of a "popping" rock from the Mid-Atlantic Ridge at 14°N: chemical and isotopic composition of gas trapped in the vesicles. *Earth Planet. Sci. Lett.* **107**, 598–611.

Kastner M., Elderfield H., Martin J.B., Suess E., Kvenvolden K.A. and Garrison R.E. (1990) Diagenesis and interstitial-water chemistry at the Peruvian continental margin-Major constituents and strontium isotopes. *Proc. O.D.P., Sci. Res.* **112**, 413-440.

Kastner M., Elderfield H., Jenkins W.J., Gieskes J.M. and Gamo T. (1993) Geochemical and isotopic evidence for fluid flow in the Western Nankai Subduction Zone, Japan. *Proc. O.D.P., Sci. Res*. **131**, 397-413.

Kelley D.S. (1996) Methane-rich fluids in the oceanic crust. *J. Geophys. Res.* **101**, 2943-2962.

Kerrick D.M. (2001) Present and past nonanthropogenic CO_2 degassing from the solid earth. *Rev. Geophys.* **39**, 565–585.

Kerrick D.M., McKibben M.A., Seward T.M. and Caldeira K. (1995) Convective hydrothermal CO_2 emission from high heat flow regions. *Chem. Geol.* **121**, 285–293.

Korzun V.I. (1978) *World Water Balance and Water Resources of the Earth. Studies and Reports in Hydrology*, Vol 25, UNESCO, 587 pp.

Ku T.L. and Luo S. (1992) Carbon isotopic variations on glacial–to–interglacial time scales in the ocean: modeling and implications. *Paleoceanography* **7**, 543–562.

Le Cloarec M.F. and Marty B. (1991) Volatile fluxes from volcanoes. *Terra Nova* **3**, 17-27.

Lein A.Y. (1984) Anaerobic consumption of organic matter in modern marine sediments. *Nature* **312**, 148–150.

Leuenberger M., Siegenthaler U. and Langway C.C. (1992) Carbon isotope composition of atmospheric CO_2 during the last ice age from an Antarctic ice core. *Nature* **357**, 450–488.

Li Y.H. (2000) *A compendium of geochemistry: from solar nebula to the human brain.* Princeton University Press, Princeton.

Marty B. and Tolstikhin I.N. (1998) CO_2 fluxes from mid–ocean ridges, arcs, and plumes. *Chem. Geol.* **145**, 233–248.

Maslin M.A. and Thomas E. (2003) Balancing the deglacial global carbon budget: the hydrate factor. *Quat. Sci. Rev.* **22**, 1729–1736.

Meybeck M. (1981) River transport of organic carbon to the ocean. In *Flux of Organic Carbon by Rivers to the Oceans.* Carbon Dioxide Effects Research and Assessment Program (eds. G.E. Likens and F.T. Mackenzie), US DOE, Washington, DC, 219–269.

Meybeck M. (1987) Global chemical weathering of surficial rocks estimated from river dissolved loads. *Am. J. Sci.* **288**, 401–428.

Meybeck M. (1988) How to establish and use world budgets of riverine materials. In *Physical and Chemical Weathering in Geochemical Cycles* (eds. A. Leman and M. Meybeck), Kluwer Academic, Dordrecht, 247–272.

Milliman J.D. (1993) Production and accumulation of calcium carbonate in the ocean: budget of a nonsteady state. *Global Biogeochem. Cycles* **7**, 927–957.

Milliman J.D., Quinchun X. and Zuosheng Y. (1984) Transfer of particulate organic carbon and nitrogen from the Changjiang River to the ocean. *Am. J. Sci.* **284**, 824–834.

Moomaw W.R., Moreira J.R., Blok K., Greene D.L., Gregory K., Jaszay T., Kashiwagi T., Levine M., McFarland M., Prasad N.S., Price L., Rogner H.H., Sims R., Zhou F. and Zhou P. (2001) Technological and economic potential of greenhouse gas emissions reduction. In *Climate Change 2001: Mitigation. Contribution of Working Group III to the Third Assessment Report of the Intergovernmental Panel on Climate Change* (eds. B. Metz, O. Davidson, R. Swart and J. Pan), Cambridge University Press, New York, 171–299.

Moore J.G. (1970) Water content of basalt erupted on the ocean floor. *Contrib. Miner. Petrol.* **28**, 272-279.

Moore J.C. and Vrolijk P. (1992) Fluids in accretionary prisms. *Rev. Geophys.* **30**, 113-135.

Morbidelli A., Chambers J., Lunine J.I., Petit J.M., Robert F., Valsecchi G.B. and Cyr K.E. (2000) Source regions and time scales for the delivery of water to Earth. *Meteorit. Planet. Sci.* **35**, 1309–1320.

Morner N.A. and Etiope G. (2002) Carbon degassing from the lithosphere. *Global Planet. Change* **33**, 185–203.

Muehlenbachs K. (1998) The oxygen isotope composition of the oceans, sediments and the seafloor. *Chem. Geol.* **145**, 263-273.

Nakicenovic N., Grubler A. and McDona A. (1998) *Global Energy Perspectives.* Cambridge University Press, New York.

Oki T. (1999) The global water cycle. In *Global Energy and Water Cycles* (eds. K.A. Brownig and R.J. Gurney), Cambridge University Press, 10-29.

Oki T. and Kanae S. (2006) Global hydrological cycles and world water resources. *Science* **313**, 1068-1072.

O'Leary M.H. (1988) Carbon isotopes in photosynthesis. *BioScience* **38**, 328–335.

Otto D., Rasse D., Kaplan J., Wamant P. and Francois L. (2002) Biospheric carbon stocks reconstructed at the last glacial maximum: comparison between general circulation models using prescribed and computed sea surface temperatures. *Global Planet. Change* **33**, 117–138.

Ozima M. (1975) Ar isotopes and Earth-atmosphere evolution models. *Geochim. Cosmochim. Acta* **39**, 1127-1140.

Peacock M. (1990) Fluid processes in subduction zones. *Science* **248**, 329-337.

Planck T. and Langmuir C.H. (1998) The chemical composition of subducting sediment and its consequences for the crust and mantle. *Chem. Geol.* **145**, 325-394.

Prentice K.C. and Fung I.Y. (1990) The sensitivity of terrestrial carbon storage to climate change. *Nature* **346**, 48–51.

Prentice K.C., Sykes M., Lautenschlager M., Harrison S., Denissenko O. and Bartlein P. (1993) Modelling global vegetation patterns and terrestrial carbon storage at the last glacial maximum. *Global Ecol. Biogeogr. Lett.* **3**, 67–76.

Qian T., Dai A., Trenberth K.E. and Oleson K.W. (2006) Simulation of global land surface conditions from 1948 to 2004: Part I: Forcing data and evaluations. *J. Hydrometeo.* **7**, 953-975.

Raymond S.N., Quinn T. and Lunine J.I. (2004) Making other Earths: Dynamical simulations of terrestrial planet formation and water delivery. *Icarus* **168**, 1–17.

Raymond S.N., Quinn T. and Lunine J.I. (2005) Terrestrial planet formation in disks with varying surface density profiles. *Astrophys. J.* **632**, 670–676.

Reinfelder J.R., Kraepiel A.M. and Morel F.M.M. (2000) Unicellular C_4 photosynthesis in marine diatom. *Nature* **407**, 996–999.

Robinson P.T., Dick H.J.B. and Von Herzen R. (1991) Metamorphism and alteration in oceanic layer 3: Hole 735B. *Proc. O.D.P., Sci. Res.* **118**, 541-549.

Sano Y. and Williams S.N. (1996) Fluxes of mantle and subducted carbon along convergent plate boundaries. *Geophys. Res. Lett.* **23**, 2749–2752.

Sarmiento J.L. and Gruber N. (2002) Sinks for anthropogenic carbon. *Phys. Today* **5**, 30–36.

Sarnthein M., Winn K., Duplessy J.C. and Fontugne M.R. (1988) Global variations of surface ocean productivity in low and mid latitudes: influence on CO_2 reservoirs of the deep ocean and atmosphere during the last 21,000 years. *Paleoceanography* **3**, 361–399.

Sasaki S. (1990) The primary solar-type atmosphere surrounding the accreting Earth: H2O-induced high surface temperature. In *Origin of the Earth* (eds. H.E. Newsom and J.H. Jones), Oxford Univ. Press, New York, 195–209.

Schlesinger W.H. (1997) *Biogeochemistry: An Analysis of Global Change*. Academic Press, New York.

Schlesinger W.H. and Melack J.M. (1981) Transport of organic carbon in the world's rivers. *Tellus* **33B**, 172–187.

Schmidt M.W. and Poli S. (1998) Experimentally based water budgets for dehydrating slabs and consequences for arc magma generation. *Earth Planet. Sci. Lett.* **163**, 361–379.

Schmincke H.U. (2000) *Vulkanismus*. Wissenschaftliche Buchgesellschaft.

Seyfried W.F. and Dibble W.E.Jr. (1980) Seawater-peridotite interaction at 300°C and 500 bars: implications for the origin of oceanic serpentinites. *Geochim. Cosmochim. Acta* **44**, 309–321.

Shakleton N.J. (1977) Carbon–13 in Uvigerina: tropical rainforest history and the equatorial Pacific carbonate dissolution cycles. In *The Fate of Fossil Fuel CO_2 in the Oceans*. (eds. N.R. Andersen and A. Malahoff), Plenum, New York, 401–427.

Sharp J.H. (1997) Marine dissolved organic carbon: are the older values correct? *Mar. Chem.* **56**, 265–277.

Shiklomanov I.A. (Ed.) (1997) *Assessment of water resource and water availability in the world*, World Meteorological organization, Stockholm Environment Institute, Geneva, Switzerland.

Smith H.J., Fischer H., Wahlen M., Mastroianni D. ad Deck B. (1999) Dual modes of the carbon cycle since the last glacial maximum. *Nature* **400**, 248–250.

Snow J.E. and Dick H.J.B. (1995) Pervasive magnesium loss by marine weathering of peridotite. *Geochim. Cosmochim. Acta* **59**, 4219–4235.

Spitzy A. and Leenheer J. (1991) Dissolved organic carbon in rivers. In *SCOPE 42: Biogeochemistry of Major World Rivers* (eds. E.T. Degens, S. Kempe and J.E. Richey), Wiley, New York, 213–232.

Stakes D., Mével C., Cannat M. and Chaput T. (1991) Metamorphic stratigraphy of hole 735B. *Proc. O.D.P., Sci. Res.* **118**, 153-180.

Staudigel H.R., Hart S., Schmincke H.U. and Smith B.M. (1990) Cretaceous ocean crust at DSDP Sites 417 and 418: Carbon uptake from weathering versus loss by magmatic outgassing. *Geochim. Cosmochim. Acta* **53**, 3091–3094.

Staudigel H., Davies G.R., Hart S.R., Marchant K.M. and Smith B.M. (1995) Large scale isotopic Sr, Nd and O isotopic Anatomy of altered oceanic crust: DSDP/ODP sites 417/418. *Earth Planet. Sci. Lett.* **130**, 169–180.

Staudigel H., Plank T., White B. and Schmincke H.U. (1996) Geochemical Fluxes During Seafloor Alteration of the Basaltic Upper Oceanic Crust: DSDP sites 417 and 418. In *Subduction Top to Bottom* (eds. G.E. Bebout, D.W. Scholl, S.H. Kirby, and J.P. Platt), Vol. 96, AGU, pp 19-38.

Sundquist E.T. (1985) Geological perspectives on carbon dioxide and the carbon cycle. In *The Carbon Cycle and Atmospheric CO_2: Natural Variations Archean to Present: Geophysical Monograph 32* (eds. E.T. Sundquist and W.S. Broecker), American Geophysical Union, Washington, DC, 5–60.

Sundquist E.T. (1993) The global carbon dioxide budget. *Science* **259**, 934–941.

Sundquist E.T. and Plummer L.N. (1981) Carbon dioxide in the ocean surface layer: some modeling considerations. In *Carbon Cycle Modelling* (ed. B. Bolin), Wiley, New York, 259–270.

Sundquist E.T. and Visser K. (2003) The Geologic History of the Carbon Cycle. In *Treatise on Geochemistry, Volume 8* (eds. H.D. Holland and K.K. Turekian), Elsevier, New York, 425–472.

Thompson A.B (1992) Water in the earth's upper mantle. *Nature* **358**, 295-302.

Trenberth K.E. (1998) Atmospheric moisture residence times and cycling Implications for rainfall rates with climate change. *Climatic Change* **39**, 667-694

Trenberth K.E. and Stepaniak D.P. (2003) Co-variability of components of poleward atmospheric energy transports on seasonal and interannual timescales. *J. Climate* **16**, 3691-3705.

Trenberth K.E, Dai A., Rasmussen R.M. and Parsons D.B. (2003) The changing character of precipitation. *Bull. Amer. Meteor. Soc.* **84**, 1205-1217.

Trenberth K.E, Fasullo J. and Smith L. (2005) Trends and variability in column integrated atmospheric water vapor. *Climate Dynamics*, **24**, 741-758.

Trenberth K.E, Smith L., Qian T., Dai A. and Fasullo J. (2007) Estimates of the Global Water Budget and its Annual Cycle Using Observational and Model Data. *J. Hydrometeo. Special Section* **8**, 758–769.

Van Campo E., Guiot J. and Peng C. (1993) A data–based reappraisal of the terretrial carbon budget at the last glacial maximum. *Global Planet. Change* **8**, 189–201.

Vanko D.A. and Stakes D.S. (1991) Fluids in oceanic layer 3: Evidence from veined rocks; Hole 735B, southwest Indian Ridge. *Proc. O.D.P., Sci. Res.* **118**, 181-215.

Veizer J. and Jansen S.L. (1979) Basement and sedimentary recycling and continental evolution. *J. Geology* **87**, 341-370.

Von Huene R. and Scholl D.W. (1991) Observations at convergent margins concerning sediment subduction, subduction erosion, and the growth of continental crust. *Rev. Geophys.* **29**, 279-316.

Wallmann K. (2001) The geological water cycle and the evolution of marine $\delta^{18}O$ values. *Geochim. Cosmochim. Acta*, **65**, 2469-2485.

Wollast R. (1994) The relative importance of biomineralization and dissolution of $CaCO_3$ in the global carbon cycle. In *Past and Present Biomineralization Processes* (ed. F. Doumenge). Musée Océanographie, Monaco, 13–35.

Chapitre 3

Les Inclusions Fluides :
Définitions et Champs d'Application

Chapitre 3

Les Inclusions Fluides : Définitions et Champs d'Application

Nous avons vu que les fluides sont présents et circulent dans toutes les enveloppes terrestres. A l'échelle de la Terre, la lithosphère apparaît comme l'interface entre les enveloppes internes et externes. Cette lithosphère est hétérogène et polyphasée et subit une dynamique forte qui résulte d'importants déséquilibres thermodynamiques et mécaniques. Ce sont ces déséquilibres thermodynamiques qui sont le moteur des transferts de fluides tels que CO_2 et H_2O entre les différentes enveloppes terrestres. Compte tenu de leur mobilité, la caractérisation de ces fluides se révèle souvent complexe et l'échantillonnage direct étant limité, ce sont avant tout les méthodes indirectes qui vont apporter des informations sur la nature de ces fluides. Les témoins de ces circulations de fluides qu'elles soient anciennes ou actuelles, sont les inclusions fluides.

L'objectif de ce chapitre n'est pas de présenter l'ensemble des connaissances apportées aux Sciences de la Terre grâce à l'étude des inclusions fluides. Il existe en effet des ouvrages assez complets présentant l'avancée de la recherche dans ce domaine comme celui de Roedder (1984). Il me paraissait cependant nécessaire dans ce travail, de s'attarder sur les inclusions fluides. En effet, ces inclusions fluides sont le fil directeur de mon travail de thèse puisque c'est à travers elles que j'ai pu suivre les transferts des fluides tels que CO_2 et H_2O entre et à l'intérieur même des enveloppes terrestres, et ce, depuis la base de la croûte jusqu'à la surface de la Terre. Il me semble donc important de donner une définition des inclusions fluides, de présenter les techniques couramment utilisées pour les étudiées et l'évolution de leurs champs d'application.

A

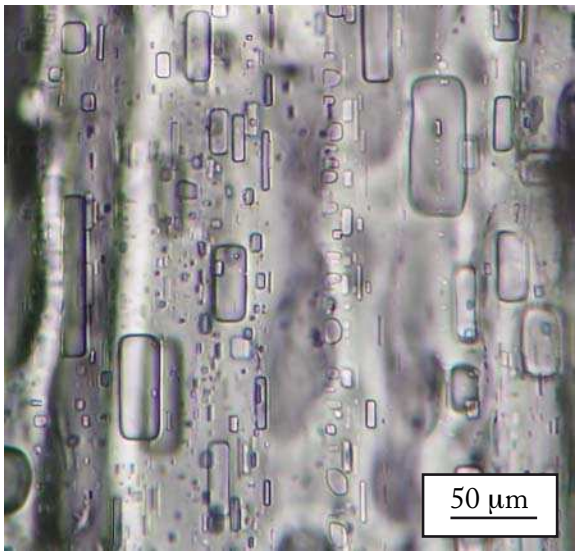

B

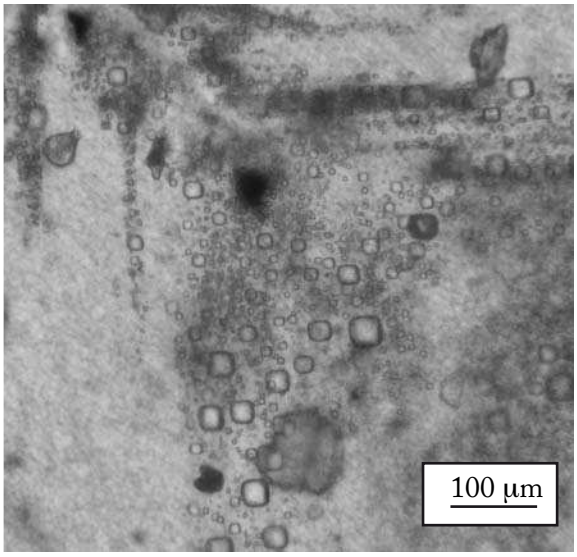

C

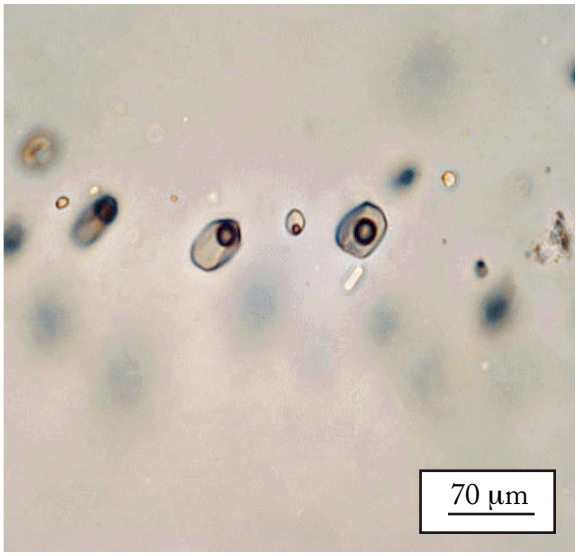

FIG. 3.1 – Photographies d'inclusions fluides. A – Bande d'inclusions fluides en grande densité soulignant les stades de croissance d'un cristal de halite synthétique. B – Relique d'un chevron de halite souligné par des inclusions fluides monophasées. C – Inclusions fluides primaires avec une bulle de vapeur, isolées dans un quartz.

FIG. 3.1 – Photomicrographs of fluid inclusions. A – Densely packed band of primary fluid inclusions outlying the growth stages of a synthetic halite crystal. B – Relic of chevron structure in natural halite with single-phase fluid inclusions. C – Isolated primary fluid inclusions in quartz with vapour bubble.

1. Qu'est-ce qu'une inclusion fluide ?

Les inclusions fluides sont de petites cavités à l'intérieur des minéraux. Leur taille peut varier du micron à plusieurs centaines de microns mais les tailles moyennes sont généralement comprises entre 5 et 50 μm (figure 3.1). Elles contiennent des microvolumes du fluide qui a été en contact avec les minéraux de la roche, soit lors de leur croissance, soit postérieurement à leur formation. D'un point de vue thermodynamique, l'inclusion fluide peut être considérée comme un système fermé, ce qui implique que la composition chimique du fluide préservé à l'intérieur de l'inclusion est la même que lors de la formation de l'inclusion et du piégeage du fluide. Il est donc possible, par le biais des inclusions fluides, d'accéder à la composition initiale du fluide présent dans le milieu lors de la formation des minéraux. Des expériences de synthèse d'inclusions fluides dans divers minéraux (quartz, sels…) montrent que leur formation est très rapide (quelques jours à quelques mois) et qu'elle dépend de la vitesse de croissance des minéraux. Compte tenu de la rapidité de piégeage, les inclusions enregistrent les changements du milieu extérieur. En d'autres termes, l'étude des inclusions fluides permet de préciser les conditions « paléo environnementales, P-T » de formation des roches endogènes et exogènes c'est-à-dire depuis le manteau profond jusqu'aux formations de surface telles que les évaporites ou les karsts (Dubois, 2000).

2. Représentativité des inclusions fluides.

La représentativité des inclusions fluides est une question qui est toujours plus ou moins sujette à débats, notamment pour les données provenant d'inclusions fluides d'évaporites (voir par exemple Roedder et Skinner, 1968 ; Wilcox, 1968 ; Kovalevich, 1975, 1976 ; Roedder, 1984). En effet, l'étude des inclusions fluides n'est pas sans complexité et la validité des données obtenues est dépendante d'un certain nombre de postulats (Dubois, 2000). Ces postulats sont au nombre de trois :

2.1. Principe de conservation de la composition

La composition du fluide piégé dans l'inclusion n'a pas changé depuis le piégeage. En d'autres termes, l'inclusion fluide se comporte comme un système fermé dit « isoplèthe ». Il existe toutefois des phénomènes qui peuvent affecter la composition initiale du fluide :

(1) La diffusion différentielle d'un constituant. Même si H_2 n'est pas commun dans la plupart des systèmes sédimentaires, l'hydrogène est potentiellement un élément capable de diffuser à travers le minéral hôte (Hall et al., 1989 ; Morgan et al., 1993), entrainant alors une modification de la composition isotopique (δD de H_2 et H_2O) de l'inclusion. Des travaux expérimentaux ont aussi montré que dans certains cas l'eau pouvait diffuser préférentiellement par rapport à CO_2 et être à l'origine d'inclusions uniquement carboniques ou à rapport CO_2/H_2O variables (Bakker et Jansen, 1990, 1994).

(2) La recristallisation du minéral hôte (précipitation/dissolution). Ce phénomène est particulièrement important dans les systèmes sédimentaires et dans le manteau dans lesquels les minéraux sont très solubles. Les minéraux recristallisés referment alors des inclusions fluides qui ressemblent à des inclusions fluides primaires mais qui contiennent les fluides présents pendant la recristallisation de la phase minérale et non lors de la précipitation initiale du minéral (Goldstein, 1986).

(3) Une déformation intense du minéral hôte peut ouvrir les inclusions qui peuvent être ensuite remplies par d'autres fluides ayant circulé ultérieurement dans la roche (Goldstein, 1986). Ce phénomène est appelé « re-filling ».

2.2. Principe de conservation du volume

Le volume de l'inclusion fluide n'a pas changé depuis le piégeage. Cela signifie que le système évolue à volume constant et donc à densité constante (premier postulat). D'un point de vue thermodynamique, le système est considéré comme isochore. Plusieurs processus peuvent modifier le volume de l'inclusion :

(1) La recristallisation du minéral hôte (précipitation/dissolution). Les phénomènes de précipitation ou de dissolution sur les parois de l'inclusion peuvent modifier son volume.

(2) L'étranglement ou « necking-down ». Dans de nombreux minéraux, le changement de forme par étranglement d'une inclusion hétérogène (plusieurs phases) peut être à l'origine de la formation d'inclusions plus petites. La répartition des phases n'étant pas homogène dans les inclusions générées, les propriétés de l'inclusion initiale et donc du fluide piégé, ne sont pas conservées. Il a été mis en évidence que ces processus d'étranglement apparaissent plus rapidement pour des températures élevées (Bodnar et al., 1985 ; Brantley, 1992).

(3) Le rééquilibrage thermique. Le rééquilibrage de l'inclusion provoqué par un réchauffement de l'échantillon, qu'il soit naturel ou qu'il intervienne en laboratoire, est peut-être le plus grand problème pour la préservation des inclusions fluides dans les minéraux diagénétiques. La surpression générée à l'intérieur de l'inclusion par le réchauffement de l'inclusion peut être responsable d'une décrépitation ou d'un étirment de l'inclusion (Bodnar et Bethke, 1984 ; Commings et Cerconne, 1986 ; McLimans, 1987 ; Prezbindowski et Tapp, 1991). La décrépitation intervient si la pression interne de l'inclusion dépasse le point de rupture du minéral hôte.

2.3. Homogénéité du fluide au moment du piégeage

Pour que la densité et la composition de l'inclusion fluide soient représentatives des conditions de piégeage, il est nécessaire que le fluide piégé dans l'inclusion soit homogène, c'est à dire qu'il ne comporte qu'une seule phase. Le fluide présent dans la roche au moment de la formation des inclusions peut quant à lui, être hétérogène (Cas des fluides à eau–gaz à basse température). Cependant, les inclusions formées à partir de ce fluide doivent être formées à partir de chacune des phases en équilibre pour respecter ce troisième postulat.

3. Les principales techniques d'étude des inclusions fluides

Classiquement l'étude des inclusions fluides combine l'analyse pétrologique, microthermométrique et la spectroscopie Raman. Ces 20 dernières années, de nouvelles techniques d'analyse quantitative ont été appliquées aux inclusions fluides. Elles sont basées sur l'analyse des radiations electromagnétiques produites par l'excitation du contenu des inclusions par des flux de particules accélérées ou des électrons.

3.1. L'analyse pétrologique et microstructurale

Cette analyse consiste en la description des inclusions à température ambiante (taille, forme, disposition des cristaux, nombre de phases dans l'inclusion...). Elle est primordiale avant toute étude d'inclusions fluides. En effet, elle permet de contraindre la part des processus secondaires (diagenèse, altération, déformation) susceptibles d'affecter les minéraux. En effet certaines caractéristiques des minéraux, comme par exemple leur solubilité ou leur aptitude à se déformer laissent les géologues assez septiques quant à la préservation des inclusions fluides. Il est donc nécessaire, avant chaque étude d'inclusions fluides, de vérifier si les postulats de base sont respectés. Ces postulats, présentés précédemment (Chapitre 3.2), sont au nombre de trois : (1) conservation de la composition de l'inclusion, (2) conservation du volume de l'inclusion et (3) le fluide doit être monophasé au moment du piégeage. En

conséquence, si une étude pétro-structurale fine est menée permettant d'évaluer les processus secondaires d'altération, les inclusions fluides contenues dans tous types de minéraux même très fragiles peuvent être considérées comme représentatives de la nature des fluides parents.

3.2. La spectroscopie Raman

La spectroscopie Raman permet de déterminer la composition et la concentration de certains constituants par le phénomène de changement de longueur d'onde caractéristique d'un milieu matériel qui accompagne la diffusion de la lumière. C'est une méthode non destructive et ponctuelle qui permet de connaître la composition de la phase volatile (CH_4, CO_2, N_2, H_2S) contenues dans les inclusions fluides.

3.3. Les analyses PIXE, PIGE LA-AOS et LA-ICP-MS

Ces 20 dernières années différentes techniques ont été mises au point afin de déterminer les teneurs en ions d'inclusions individuelles. Ces méthodes modernes sont basées sur l'analyse électromagnétique de radiations produites par l'excitation de particules ou d'électrons accélérés comme par exemple les microanalyses d'inclusions congelées par X-ray (Ayora et al., 1994) ; la spectroscopie par émission de rayons X (PIXE) ou de rayons gamma (PIGE) (Anderson et al., 1989 ; Volfinger et al., 1997), la spectroscopie par fluorescence X au synchrotron (Frantz et al., 1988 ; Nagaseki et al., 2006). Ces méthodes non destructives mais lourdes d'utilisation permettent d'obtenir les teneurs en éléments traces (Cl, Za, Br) et majeurs (Na, Ca, Fe, Mn, K,) d'inclusions individuelles. Cependant les résultats sont aléatoires car limités par la forme et la profondeur des inclusions dans le minéral hôte. Des méthodes destructives à l'échelle du faisceau laser et basées sur l'analyse par ICP-MS (Shepherd et Chenery, 1995 ; Moissette et al., 1996 ; Graupner et al., 2005) ou sur la spectroscopie optique d'émission (EOS) (Boiron et al., 1997 ; Fabre et al., 1999) couplées à l'ablation laser permettent d'analyser le liquide des inclusions fluides et donnent de meilleurs limites de détection pour les éléments traces et majeurs.

3.4. La microthermométrie

L'analyse microthermométrique est une technique non destructive qui consiste en une observation minutieuse des changements de phase d'une inclusion individuelle qui surviennent lorsqu'elle est soumise à des cycles de chauffage et de refroidissement, dans une gamme de températures comprises entre -180°C et +600°C. Cette analyse est réalisée à l'aide d'une platine chauffante/réfrigérante couplée à un microscope optique. Les mesures de ces changements de phase permettent d'estimer les conditions de piégeage des fluides à condition que les postulats de base de l'étude des inclusions fluides soient respectés. Les températures habituellement mesurées sont la température d'homogénéisation, la température de l'eutectique (début de la fusion) et la température de dernière fusion (ou température de dissolution). Après congélation totale (solidification) l'inclusion est lentement réchauffée jusqu'à homogénéisation totale (état à une phase). Le début de la fusion de l'inclusion solidifiée permet l'identification de la phase liquide et du système gazeux associé (H_2O–NaCl, H_2O–CO_2, CO_2–CH_4, etc.). La température finale de fusion (ou température de dissolution) donne la concentration des composants dans le système correspondant. La température d'homogénéisation de l'inclusion (lorsqu'il ne reste plus qu'une seule phase dans l'inclusion) indique la température minimum de formation de l'inclusion.

Les analyses microthermométriques peuvent être effectuées aussi bien pour des températures élevées (roches magmatiques ou métamorphiques) que pour des températures basses (roches exogènes). Dans le cadre de ma thèse, des mesures microthermométriques ont été effectuées sur des halites de Sicile (Chapitre 5.2) et sur des granulites de Tanzanie (Chapitre 7.2). Les protocoles utilisés pour ces études seront présentés dans le chapitre suivant (Chapitre 4.3).

3.5. L'analyse des isotopes stables des inclusions fluides

Les méthodes d'études précédemment décrites donnent accès et cela avec de plus en plus de précision, à la nature des fluides et aux propriétés du milieu (pression, température, composition) lors de leur piégeage. Bien que primordiales dans la compréhension des interactions fluides-roches, ces méthodes ne permettent cependant pas la caractérisation des sources (réservoirs) de ces fluides. L'analyse des isotopes stables des inclusions fluides, en particulier de l'hydrogène, de l'oxygène et du carbone, est un outil indispensable pour définir

l'origine des fluides présents dans les inclusions et caractériser leurs mélanges quand ces fluides sont issus de deux ou plusieurs sources différentes. Cette méthode présente l'inconvénient d'être destructrice pour l'échantillon puisqu'elle nécessite la récupération des fluides soit par décrépitation, soit par broyage de l'échantillon mais elle a cependant l'avantage de ne pas être conditionnée par le principe de conservation du volume de l'inclusion. En effet, seule la composition chimique de l'inclusion ne doit pas avoir changé depuis le piégeage du fluide. Un changement de volume d'inclusion n'entrainera pas de modification de l'information isotopique enregistrée dans l'inclusion. L'essentiel de mon travail de thèse est fondé sur l'analyse des compositions isotopiques (H, C et O) des inclusions fluides. Les techniques utilisées au cours de ce travail seront décrites dans le chapitre suivant (Chapitres 4.1 et 4.2).

4. Evolution des champs d'application

Dubois (2000) a montré, en faisant l'historique de la discipline, que bien que cette discipline soit jeune (50 ans), l'intérêt pour les inclusions fluides est déjà ancien. Même si les premières observations ponctuelles d'inclusions fluides sont reportées dès le XVIII^{e} (Dolomieu, 1792), le texte servant encore de référence est celui de Sorby (1958).

Dès l'origine, les champs d'application des inclusions ont été larges. L'étude des inclusions fluides a ensuite été intimement liée à l'évolution des idées sur le métamorphisme (Spear, 1993), sur la tectonique et sur l'origine des granites et des filons associés. D'autres champs d'application comme la métallogénie (Roedder, 1962 ; Roedder, 1963 ; Poty et Weisbord, 1976) et l'étude des fluides à la base de la croûte (voir par exemple Touret, 1971 ; Touret, 1977 ; Touret, 1981 ; Newton, 1986) et dans le manteau (Roedder, 1965 ; Pasteris, 1987 ; Roedder, 1994 ; Szabo et Bodnar, 1995) se sont ouverts à cette discipline par la suite.

L'utilisation de cette technique dans l'étude des bassins sédimentaires a ensuite ouvert à la discipline un nouveau champ d'application. En effet, l'étude des inclusions fluides s'est révélée d'un intérêt crucial pour comprendre l'évolution des systèmes diagénétiques (Goldstein et Reynolds, 1994) et sédimentaires (Goldstein, 2001). L'application des études d'inclusions fluides aux systèmes diagénétiques a été très bénéfique à l'exploration pétrolière, pour la compréhension de la systématique des réservoirs (Pottorf et al., 1997 ; Brennan et Goldstein,

1998), pour la détermination de la composition des hydrocarbures et pour l'étude de leur migrations (Burruss, 1987 ; Karlsen et al., 1993 ; Hall, 1996 ; Smith, 1997).

Au cours des dernières décennies durant lesquelles la paléoclimatologie a connu un intérêt grandissant au sein de la communauté scientifique, l'application des études d'inclusions fluides aux systèmes sédimentaires a permis une avancée importante dans la reconstruction des paléoenvironnements. Les inclusions aqueuses piégées dans la calcite précipitée sous la forme de spéléothèmes dans des grottes, ont par exemple été utilisées pour la reconstruction des paléo–températures moyennes de l'air (Schwarz et al., 1976 ; Matthews et al., 2000). L'étude des inclusions fluides d'eau de mer à l'intérieur de carbonates marins a fourni un enregistrement des variations de la composition du système océan–atmosphère dans le passé (Johnson et Goldstein, 1993). De même, l'étude des inclusions de gaz piégées dans la glace des glaciers a fourni un enregistrement de la chimie des atmosphères anciennes pour un passé géologique récent (Raynaud et al, 1993).

Enfin, de nombreuses études effectuées sur des inclusions fluides préservées dans des cristaux de halite ont permis de donner des informations détaillées sur les variations de la chimie des eaux de mer anciennes du Protérozoïque (Kovalevich, 2006), du Phanérozoïque (Kovalevich et al., 1998 ; Lowenstein et al., 2001 ; Horita et al., 2002 ; Brennan et Lowenstein, 2002 ; Petrychenko et al., 2005) sur la chimie des eaux de mer actuelles (Timofeeff et al., 2001). Les inclusions fluides préservées dans la halite ont aussi été utilisées pour la reconstruction détaillée des températures minimales de l'eau de surface par l'application des techniques de microthermométrie (Roberts et Spencer, 1995 ; Lowenstein et al., 1988 ; Benison et Goldstein, 1999 ; Satterfield et al., 2005).

Références

Anderson A.J., Clark A.H., Ma X.P., Palmer G.R., MacArthur J.D. and Roedder E. (1989) Proton–induced X–ray and gamma–ray emission analysis of unopened fluid inclusions. *Econ. Geol.* **84**, 924–939.

Ayora C., Garcia–Veigas J. and Pueyo J.J. (1994) The chemical and hydrological evolution of an ancient potash–forming evaporite basin as constrained by mineral sequence, fluid inclusion composition, and numerical simulation. *Geochim. Cosmochim. Acta* **58**, 3379–3394.

Bakker R.J. and Jansen J.B.H. (1990) Preferential water leakage from fluid inclusions by means of mobile dislocations. *Nature* **345**, 58–60.

Bakker R.J. and Jansen J.B.H. (1994) A mechanism for preferential H_2O leakage from fluid inclusions in quartz based on TEM observations. *Contrib. Mineral. Petrol.* **116**, 7–20.

Benison K.C. and Goldstein R.H. (1999) Permian paleoclimate data from fluid inclusions in halite. *Chem. Geol.* **154**, 113–132.

Bodnar R.J. and Bethke P.M. (1984) Systematics of stretching of fluid inclusions 1 : Fluorite and sphalerite at 1 atmosphere confining pressure. *Econ. Geol.* **79**, 141–161.

Bodnar R.J., Reynolds T.J. and Kuehn C.A. (1985) Fluid–inclusion systematics in epithermal systems. In *Society of Economic Geologists, Reviews in Economic Geology, **2**, Geology and Geochemistry of Epithermal Systems.* (eds. Berger B. and Bethke R.), 73–97.

Boiron M.C., Moisette A., Fabre C., Dubessy J., Banks D and Yardley B. (1997) Ion analysis in individual fluid inclusions by laser ablation-optical emisson spectroscopy : Application to natural inclusions. *ECROFI XIV Abstracts, Nancy,* 44–45.

Brantley S.L. (1992) The effect of fluid chemistry on quartz microcrack lifetimes. *Earth Planet. Sci. Lett.* **113**, 145–156.

Brennan S.T. and Goldstein R.H. (1998) Fluid and thermal history of an exhumed petroleum reservoir. *PACROFI program and abstracts, Las Vegas* (unpaginated).

Brennan S.T. and Lowenstein T.K. (2002) The major–ion composition of Silurian seawater. *Geochim. Cosmochim. Acta* **66**, 2683–2700.

Burruss R.C. (1987) Crushing–cell, capillary column gas chromatography of petroleum fluid inclusions : Method and application to petroleum source rocks, reservoirs, and low temperature hydrothermal ores. *American Current Research on Fluid Inclusions, Socorro, NM, Abstracts* (unpaginated).

Comings B.D. and Cercone K.R. (1986) Experimental contamination of fluid inclusions in calcite. *Soc. Econ. Paleonto. Mineral. Abstr.* **3**, 24.

Dolomieu C.D. (1792) Sur de l'huile de pétrole dans le cristal de roche et les fluides élastiques tirés du quartz. *Observations sur la physique, l'histoire naturelle et les arts* **42**, 318–319.

Dubois M. (2000) Inclusions fluides : Approche expérimentale, thermodynamique et applications aux phénomènes hydrothermaux et diagénétiques. *Mémoire d'H.D.R.*, Université des Sciences et Technologies de Lille, 234 pp.

Fabre C., Boiron M.C., Dubessy J., Cathelineau M. and Banks D. (1999) Analysis of fluid inclusions by laser ablation–optical emission spectroscopy, microthermometry and Raman spectroscopy : a reconstitution of the composition and temperature of trapped fluids. *ECROFI XV Abstracts, Potsdam,* 97–99.

Frantz J.D., Mao H.K., Zhang Y., Wu Y., Thompson A.C., Underwood J.H., Glauque R.D. Jones K.W. and Rivers M.L. (1988) Analysis of fluid inclusions by X–ray fluorescence using synchrotron radiation. *Chem. Geol.* **69**, 235–244.

Goldstein R.H. (1986) Reequilibration of fluid inclusions in low–temperature calcium–carbonate cement. *Geology* **14**, 792–795.

Goldstein R.H. (2001) Fluid inclusions in sedimentary and diagenetic systems. *Lithos* **55**, 159–193.

Goldstein R.H. and Reynolds T.J. (1994) Systematics of fluid inclusions in diagenetic minerals. *SEPM (Society for Sedimentary Geology), Short Course Notes* **31**, 199 pp.

Graupner T., Brätz H. and Klemd R. (2005) LA–ICP–MS micro–analysis of fluid inclusions in quartz using a commercial Merchantek 266 nm Nd:YAG laser : a pilot study. *Eur. J. Mineral.* **17**, 93–102.

Hall D.L. (1996) Application of fluid inclusions to petroleum exploration : Some recent advances and case studies. *PACOFRI VI Abstracts, Madison*, 59–60.

Hall D.L., Sterner S.M. and Bodnar R.J. (1989) Experimental evidence for hydrogen diffusion into fluid inclusions in quartz. *Geol. Soc. Am. Abstr.* **21**, A358.

Horita J., Zimmermann H. and Holland H.D. (2002) Chemical evolution of seawter during the Phanerozoic : Implications from the record of marine evaporites. *Geochim. Cosmochim. Acta* **66**, 3733–3756.

Johnson W.J. and Goldstein R.H. (1993) Cambrian seawater preserved as inclusions in marine low–magnesium calcite cement. *Nature* **362**, 335–337.

Karlsen D.G., Nedkvitne T. and Larter S.R. (1993) Hydrocarbon composition of authigenic inclusions : Application to elucidation of petroleum reservoir filling history. *Geochim. Cosmochim. Acta* **57**, 3641–3659.

Kovalevich V.M. (1975) Thermometric studies of inclusions in artificial crystals of halite. *Fluid Inclusion Res.* **8**, 96.

Kovalevich V.M. (1976) Halite of the salt deposits of Miocene age from the Forecarpathians. *Fluid Inclusion Res.* **9**, 72.

Kovalevich V.M., Peryt T.M. and Petrichenko O.I. (1998) Secular variation in seawater chemistry during the Phanerozoic as indicated by brine inclusions in halite. *J. Geol.* **106**, 695–712.

Kovalevych V.M., Marshall T., Peryt T.M., Petrychenko O.Y. and Zhukova S.A. (2006) Chemical composition of seawater in Neoproterozoic: Results of fluid inclusion study of halite from Salt Range (Pakistan) and Amadeus Basin (Australia). *Precamb. Res.* **144**, 39–51.

Lowenstein T.K., Li J. and Brown C.N. (1998) Paleotemperatures from fluid inclusions in halite : method verification and a 100,00 year paleotemperature record, Death Valley, CA. *Chem. Geol.* **150**, 223–245.

Lowenstein T.K., Timofeeff M.N., Brennan S.T., Hardie L.A. and Demicco R.V. (2001) Oscillations in Phanerozoic Seawater Chemistry : Evidence from Fluid Inclusions. *Science* **294**, 1086–1088.

Matthews A., Ayalon A and Bar-Matthews M. (2000). D/H ratios of fluid inclusions of Soreq cave (Israel) speleothems as a guide to the Eastern Mediterranean Meteoric Line relationships in the last 120 ky. *Chem. Geol.* **166**, 183–191.

McLimans R.K. (1987) The application of fluid inclusions to migration of oil and diagenesis in petroleum reservoirs. *Appl. Geochem.* **2**, 585–603.

Moissette A., Shepherd T.J. and Chenery S.R. (1996) Calibration strategies for the elemental analysis of individual aqueous fluid inclusions by laser ablation–ICP–MS. *J. Anal. Atom. Spec.* **11**, 177–186.

Morgan G.B., Chou I.M., Pasteris J.D. and Olsen S.N. (1993) Re–equilibration of CO_2 fluid inclusions at controlled hydrogen fugacities. *J. Metam. Geol.* **11**, 155–164.

Nagaseki H., Hayashi K. and Iida A. (2006) Quantitative analysis of fluid inclusions by synchrotron X–ray fluorecence. *Eur. J. Mineral.* **18**, 309–318.

Newton R.C. (1986) Fluids of granulite facies metamorphism. In *Fluid–rock interactions during metamorphism* (eds. J.V. Walther and B.J. Wood). Springer–Verlag, New–York, 36–59.

Pasteris J.D. (1987) Fluid inclusions in mantle xenoliths. In *Mantle Xenoliths* (ed. P.H. Nixon). Wiley, Chichester, 691–707.

Petrychenko O.Y., Peryt T.M. and Chechel E.I. (2005) Early Cambrian seawater chemistry from fluid inclusion in halite from Siberian evaporites. *Chem. Geol.* **219**, 149–161.

Pottorf R.J., Gray G.G., Kozar M.G., Flitchen W.M. and Richardson M. (1997) Paleothermometry techniques applied to burial history and hydrocarbon migration analyses, Tampico–Misantla Basin, Mexico. *American Association of Petroleum Geologists Abstracts with Programs,* p. A94.

Poty B. and Weisbrod A. (1976) Les inclusions fluides comme guide pour la prospection des gîtes métallifères. *Ann. Mines,* 1–6.

Prezbindowski D.R. and Tapp J.B. (1991) Dynamics of fluid inclusion alteration in sedimentary rocks : a review and discussion. *Org. Geochem.* **17**, 131–142.

Raynaud D., Jouzel J., Barnola J.M., Chappellaz J., Delmas R.J. and Lorius C. (1993) The ice record of greenhouse gases. *Science* **259**, 926–934.

Roberts S.M. and Spencer R.J. (1995) Paleotemperatures preserved in fluid inclusions in halite. *Geochim. Cosmochim. Acta* **59**, 3929–3942.

Roedder E. (1962) Studies of fluid inclusion I : Low temperature application of a dual–purpose freezing and heating stage. *Econ. Geol.* **57**, 1045–1061.

Roedder E. (1963) Studies of fluid inclusion II : Freezing data and their interpretation. *Econ. Geol.* **58**, 167–211.

Roedder E. (1965) Liquid CO_2 inclusions in olivine–bearing nodules and phenocrysts from basalts. *Am. Mineral.* **50**, 1746–1782.

Roedder E. (1984) Fluid Inclusions. *Mineralogical Society of America, Reviews in Mineralogy* **12**, Washington D.C., 644 pp.

Roedder E. (1994) Fluid inclusion evidence of mantle fluids. In *Minerals: Methods and Applications* (eds. B. DeVivo and M.L. Frezzotti). Virginia Polytechnic Institute and State University, Blacksburg, 283–296.

Roedder E. and Skinner B.J. (1968) Experimental evidence that fluid inclusions do not leak. *Econ. Geol.* **63**, 715–730.

Satterfield C.L., Lowenstein T.K., Vreeland R.H. and Rosenzweig W.D. (2005) Paleobrine temperatures, chemistries, and paleoenvironments of Silurian salina formation F–1 Salt,

Michigan Basin, U.S.A., from petrography and fluid inclusions in halite. *J. Sedim. Res.* **75**, 534–546.

Schwarcz H.P., Harmon R.S., Thompson P. and Ford D.C. (1976) Stable isotope studies of fluid inclusions in speleothems and their paleoclimatic significance. *Geochim. Cosmochim. Acta* **40**, 657-665.

Shepherd T.J. and Chenery S.R. (1995) Laser ablation ICP–MS elemental analysis of individual fluid inclusions : An evaluation study. *Geochim. Cosmochim. Acta* **59**, 3997–4007.

Smith M.P. (1997) Fluid inclusion well logs : Petroleum migration, seals, and proximity to pay. *ECROFI XIV Abstracts, Nancy*, p. 310.

Sorby H.C. (1858) On the microscopical structure of crystals indicating the origin of rocks and minerals. *Quater. J. Geol. Soc. London* **14**, 453–500.

Spear F.S. (1993) Metamorphic phase equilibria and pressure–temperature–time paths. *Mineral. Soc. Am. Monograph*, 799 pp.

Szabo C. and Bodnar R.J. (1995) Chemistry and origin of mantle sulfides in spinel peridotite xenoliths from alkaline basaltic lavas, Norgrad–Gömör Volcanic Field, northern Hungary and southern Slovakia. *Geochim. Cosmochim. Acta* **59**, 3917–3927.

Timofeeff M.N., Lowenstein T.K., Brennan S.T., Demicco R.V., Zimmermann H., Horita J. and Von Borstel L.E. (2001) Evaluating seawater chemistry from fluid inclusions in halite : Examples from modern marine and nonmarine environments. *Geochim. Cosmochim. Acta* **65**, 2293–2300.

Touret J. (1971) Le faciès granulitique en Norvège Méridionale II : Les inclusions fluides. *Lithos* **4**, 423–436.

Touret J. (1977) The significance of fluid inclusions in metamorphic rocks. In *Thermodynamics in Geology* (ed. D.G. Fraser). NATO ASI Series, C. 35, Reidell Pub., Dordrecht, 113–168.

Touret J. (1981) Fluid inclusions in high grade metamorphic rocks. In *Short Course in Fluid Inlusions: Application to Petrology* (eds. L.S. Hollister and M.L. Craford). Min. Assoc. Canada, Calgary, 182–308.

Volfinger M., Ramboz C., Aissa M. and Choï C.G. (1997) Some practical aspects of the quantitative analysis of fluid inclusions by the PIXE method. *ECROFI XIV Abstracts, Nancy*, 344–345.

Wilcox W.R. (1968) Removing inclusions from crystals by gradient techniques. *Industr. Engin. Chemistry* **60**, 12–23.

Chapitre 4

Techniques Analytiques

Chapitre 4

Techniques Analytiques

1. Mesures des compositions isotopiques (H et O) de l'eau des inclusions fluides dans la halite et des eaux résiduelles au cours de l'évaporation d'un volume d'eau.

1.1. Rapports D/H et $^{18}O/^{16}O$ de l'eau des inclusions fluides.

L'eau piégée dans la halite est extraite par décrépitation thermique. Une quantité de 50 à 150 mg de halite sous forme de grains de taille millimétrique est étuvée pendant une nuit à 110°C puis placée dans un tube en quartz, surmontée de laine de silice afin d'éviter la contamination de la ligne d'extraction purifiée (Fig. 4.1) par des particules fines de halite générées lors de la décrépitation. Les échantillons sont mis à dégazer sous vide à 80°C pendant au moins 90 min. Ils sont ensuite portés par chauffage résistif à une température d'au moins 800°C pendant 15 min permettant l'extraction complète de l'eau des inclusions. Les valeurs des blancs pour les analyses d'eau étaient très faibles pour l'ensemble de la série d'expériences, ne contribuant pas à plus de 1% de la quantité totale d'eau extraite des inclusions fluides.L'eau collectée par la décrépitation des inclusions fluides, de l'ordre 50 à 200 μmoles, est ensuite transférée sous vide dans un réacteur de micro–équilibration (Fig. 4.1) dans lequel sont ajoutées 5 à 10 μmoles de CO_2 de composition isotopique connue. Le réacteur de micro–équilibration est finalement immergé dans un Bain–Marie thermostaté à 25°C pendant 48h. L'eau et le CO_2 de quantités et de compositions isotopiques connues sont donc capables d'échanger leurs isotopes de l'oxygène. Les compositions isotopiques des deux fluides en contact dans le réacteur sont à l'équilibre après 48h de réaction. Après ce temps, les échantillons d'eau et de CO_2 équilibrés sont séparés par cryogénie sous vide. Les valeurs de $\delta^{18}O$ de l'eau peuvent être calculées à partir des mesures de $\delta^{18}O$ du CO_2 en utilisant

l'équation de bilan de masse (1) de Kishima et Sakai (1980). Les précisions obtenues pour les valeurs de $\delta^{18}O$ de l'eau des halites déterminées par équilibration sont proches de 0,5‰ et dépendent du rapport molaire $[CO_2]/ [H_2O]$ pendant la procédure d'équilibration (Fig. 4.2).

$$(1) \quad \delta^{18}O\,H_2O = \left(\delta^{18}O\,CO_2(f) - \delta^{18}O\,CO_2(i)\right)\left(2\frac{[CO_2]}{[H_2O]}\right) + \left(1 + \frac{\delta^{18}O\,CO_2(f)}{1000}\right)\frac{1000}{\alpha_{CO_2\text{-}H_2O}} - 1000$$

avec $\alpha\ CO_2–H_2O$ = 1.0412 à T= 25°C (O'Neil and Adami, 1969)

$\delta^{18}O\ CO_2$ (f) = $\delta^{18}O$ du CO_2 équilibré avec H_2O après 48h

$\delta^{18}O\ CO_2$ (i) = $\delta^{18}O$ du CO_2 avant l'équilibration avec H_2O = 15.3±0.1‰ (SMOW)

$[CO_2]$ et $[H_2O]$ sont les quantités des deux fluides en μmoles

Après l'équilibration et la collecte du CO_2 dans un porte–échantillon pour l'analyse du $\delta^{18}O$ de l'eau, l'eau est transférée puis emprisonnée sous vide dans un tube en silice contenant environ 500 mg de poudre fine de chrome métal (Fig. 4.1). Cette eau est ensuite réduite par le chrome à 1000°C pendant 5 minutes pour produire du H_2 moléculaire dont les rapports D/H sont déterminés avec un spectromètre de masse GV Prism™ en Dual–Inlet (Fig 4.5). Ce protocole est adapté des méthodes de réduction de l'eau par le zinc (Vennemann et O'Neil, 1993) et par le chrome (Morrison et al., 2001) de façon à obtenir une bonne reproductibilité analytique et surmonter les problèmes de fractionnement engendrés par les réactions entre le zinc et l'hydrogène (Demény, 1995). La reproductibilité externe des mesures des rapports D/H a été établie à environ ±3‰ en normalisant les données brutes par rapport à l'échelle SMOW/SLAP. Les quantités d'eau des échantillons, indispensables pour résoudre l'équation (1), sont les variables les plus délicates à quantifier. Elles ont été déterminées par comparaison avec des séries d'analyse d'échantillons d'eau de poids connus compris entre 0,5 et 3,5 μL. Après détente du gaz H_2 dans un volume constant du système d'introduction des échantillons du spectromètre de masse, la quantité de gaz est estimée à partir de la valeur de l'intensité du signal sur le collecteur de la masse 2. L'incertitude associée à la détermination des quantités d'eau des échantillons est proche de ±0.05 μL. La reproductibilité interne des analyses D/H des eaux de référence est de l'ordre de 1,5‰.

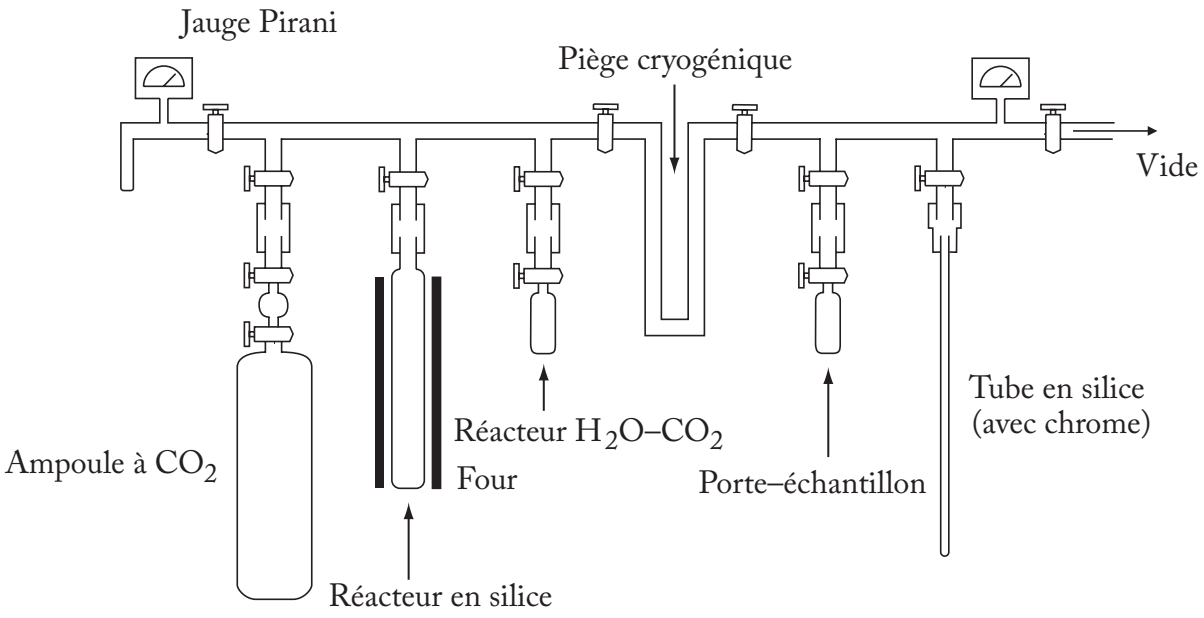

FIG. 4.1 – Schéma de la ligne d'extraction purifiée sous vide utilisée pour l'analyse des rapports D/H et $^{18}O/^{16}O$ de l'eau des inclusions fluides.

FIG. 4.1 – Schematic representation of the water extraction line under vacuum used for analysis of D/H and $^{18}O/^{16}O$ ratios of water in fluid inclusions.

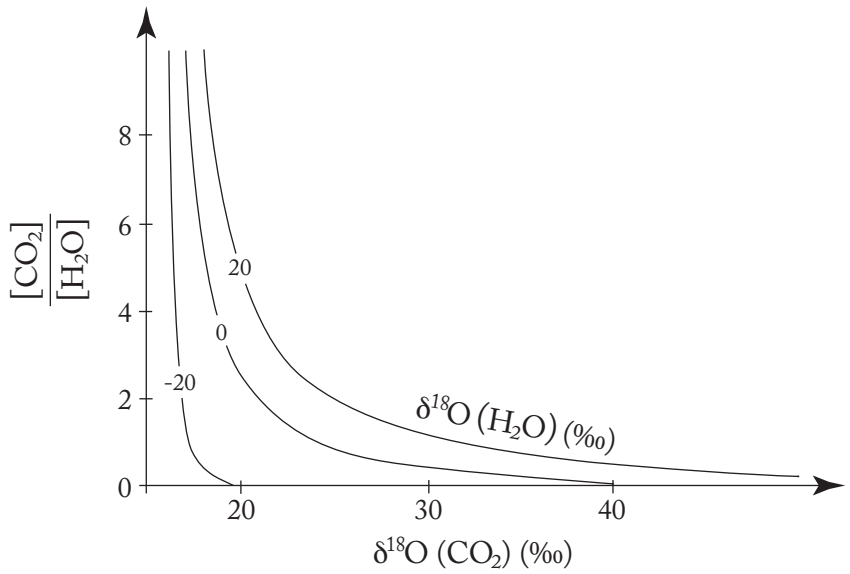

FIG. 4.2 – Valeurs de $\delta^{18}O$ de l'eau calculées à partir des mesures de $\delta^{18}O$ du CO2 par application de l'équation de bilan de masse (1) de Kishima et Sakai (1980). La précision de la mesure dépend du rapport molaire [CO2]/ [H2O]. (d'après Lécuyer et al. 1999)

FIG. 4.2 – $\delta^{18}O$ values of water calculated from measurements of $\delta^{18}O$ values of CO2 following the mass balance equation (1) of Kishima et Sakai (1980). Accuracy of measures depends on [CO2]/ [H2O] molar ratio. (after Lecuyer et al., 1999)

1.2. Rapports D/H et $^{18}O/^{16}O$ des eaux libres.

Des aliquots de 200 µL d'eau ont été mis à réagir de façon automatisée à 313 K avec CO_2 et H_2 en présence d'un catalyseur en Platine, et analysés grâce à un système MultiPrep™ couplé à un spectromètre de masse GVI IsoPrime™ dual inlet (Fig 4.6). La reproductibilité des mesures des rapports D/H et $^{18}O/^{16}O$ a été établie respectivement à environ ±1‰ et ±0.1‰, en normalisant les données brutes par rapport aux standards internationaux SMOW, SLAP et GISP. Les coefficients de fractionnement entre CO_2 et H_2O, et H_2O et H_2 étant halo–dépendant, des corrections ont dû être effectuées sur les valeurs des rapports isotopiques de l'hydrogène et de l'oxygène de l'eau en fonction de la salinité suivant Lécuyer et al. (2009).

2. Mesures des compositions isotopiques (H et C) de l'eau et du CO_2 des inclusions fluides des granites et des granulites et mesures des rapports D/H de leur eau de constitution.

2.1. Extraction des fluides (H_2O et CO_2) des différentes générations d'inclusions fluides.

Les fluides piégés dans les granites et les granulites ont été extraits par décrépitation thermique. Environ 1g de minéraux (quartz pour les granites et quartz, plagioclase, pyroxène et grenat pour les granulites) sous forme de grains de taille millimétrique sont lavés à l'acide nitrique dilué et rincés à l'eau doublement déionisée avant d'être étuvés pendant toute une nuit à 110°C. Les échantillons sont ensuite placés dans un tube en quartz et mis à dégazer sur une ligne d'extraction purifiée sous vide (Fig. 4.3) à 110°C pendant au moins 2h. Après une détermination préalable des températures d'homogénéisation des inclusions fluides par microthermométrie, il apparaît que le chauffage par paliers des échantillons peut être considéré comme le meilleur protocole pour séparer les fluides des inclusions primaires et secondaires. Idéalement, il est prévu que les fluides des inclusions secondaires, se formant

dans les microfissures des minéraux, soient libérés à des températures de 300–350°C alors que la majorité des fluides des inclusions primaires sont collectés à des températures de 700–800°C. Pour chaque étape de température, les fluides libérés lors de la décrépitation des inclusions sont collectés pendant au moins 20 minutes. Cette méthode ne garantit cependant pas la séparation des fluides des deux générations d'inclusions sans une contamination de la génération de haute température par les fluides secondaires. En effet, si la température de décrépitation des inclusions dépend de la pression interne du fluide dans les inclusions, elle dépend aussi de leur taille ainsi que de la force du réseau cristallin. Par conséquent, les inclusions fluides secondaires de petite taille ont tendance à décrépiter pour des températures plus élevées que prévu et proches des températures de décrépitation des inclusions fluides primaires. De même, les inclusions primaires les plus petites peuvent échapper à la décrépitation effectuée à 700°C, même si aucune quantité non négligeable d'eau est extraite pour des températures supérieures à 800°C. Finalement, CO_2 et H_2O sont séparés cryogéniquement et les gaz non condensables sont purgés. H_2O est ensuite transférée dans un tube en verre de silice contenant 300 mg de chrome métallique et CO_2 est collecté dans un porte–échantillon.

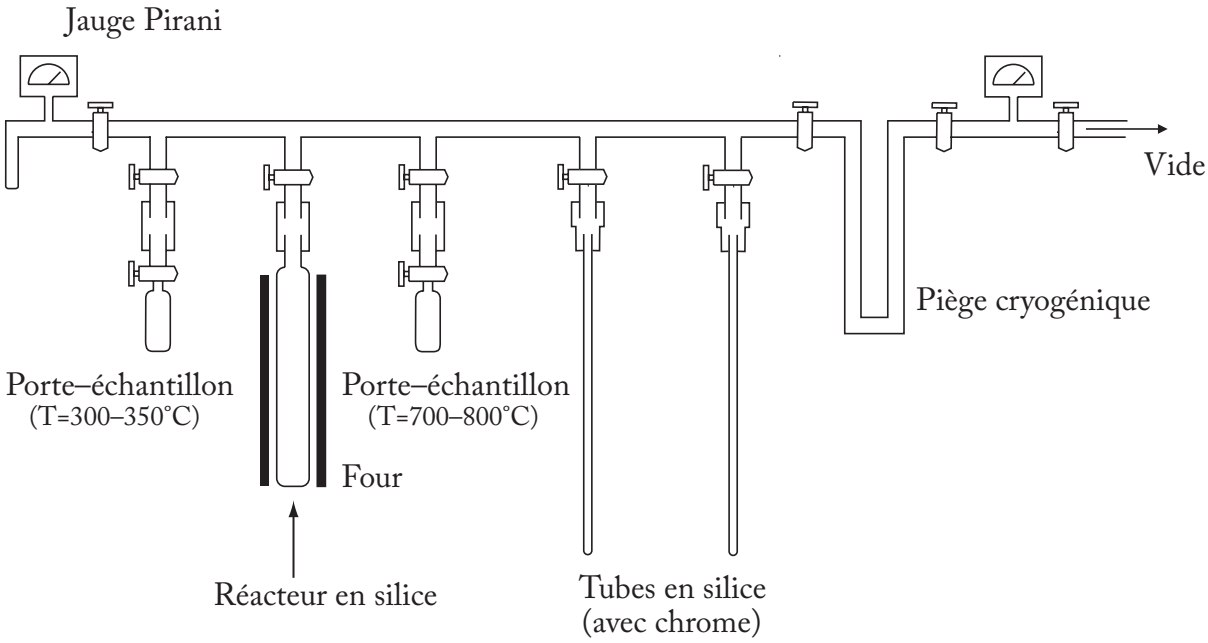

FIG. 4.3 – Schéma de la ligne d'extraction purifiée sous vide utilisée pour l'analyse des rapports D/H de l'eau et $^{13}C/^{12}C$ du dioxyde de carbone des deux générations d'inclusions fluides.

FIG. 4.3 – Purified extraction line used for analysis of D/H ratios af water and $^{13}C/^{12}C$ ratios of carbon dioxide of two generations of fluid inclusions.

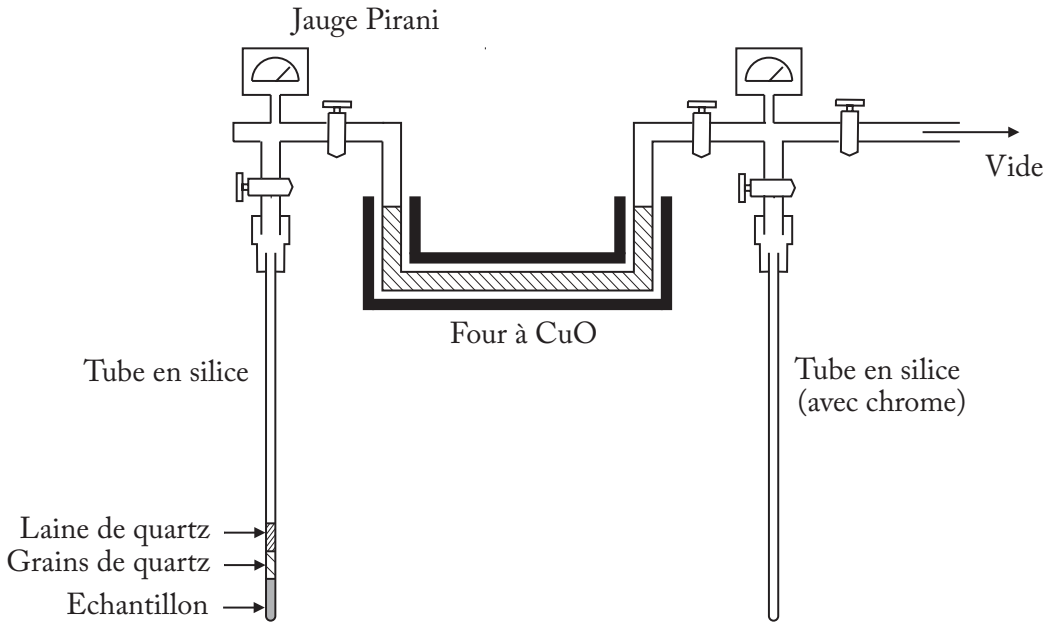

FIG. 4.4 – Schéma de la ligne d'extraction utilisée pour l'analyse du rapport D/H de roches totales

FIG. 4.4 – Purified extraction line used for analysis of bulk rocks D/H ratios.

2.2. Extraction de l'eau de constitution des échantillons de roche totale.

Les échantillons de granite et de granulite sont broyés en une poudre très fine, impliquant l'ouverture des inclusions fluides piégées dans la roche. Une quantité de 150 à 200 mg de cette poudre est placée dans un tube en silice et surmontée de grains de quartz et de laine de silice afin d'éviter que le tube ne s'écrase sous l'effet du chauffage. L'échantillon est chauffé sous vide à une température de 150°C pendant 1 heure pour supprimer toute trace d'eau atmosphérique qui aurait pu être adsorbée. Il est ensuite chauffé au chalumeau sous vide pendant plusieurs minutes à une température avoisinant les 1200°C jusqu'à fusion complète, entrainant la libération de l'eau des minéraux hydratés. La ligne d'extraction en pyrex™ sous vide (Fig. 4.4) est maintenue à une température de 80°C pendant toute la manipulation pour empêcher la condensation de l'eau sur les parties intérieures de l'appareillage expérimental. L'eau est collectée par cryogénie dans l'azote liquide, dans un tube en silice contenant environ 300 mg de chrome métal, après une transformation préalable de la fraction d'hydrogène dégagée en eau par passage dans un four à CuO à 500°C (Fig. 4.4). L'oxydation de l'hydrogène en eau est une étape nécessaire pour éviter l'acquisition de rapports D/H surestimés pour une gamme de température comprise entre 600°C et 1200°C (Cerrai et al., 1954 ; Simon, 2003).

2.3. Mesures des rapports isotopiques du dioxyde de carbone et de l'eau.

La composition isotopique du carbone du CO_2 des inclusions primaires et secondaires a été mesurée avec un spectromètre de masse GV Prism™ en Dual–Inlet. La reproductibilité interne est de ±0,5‰ pour les échantillons de taille inférieure à 10 μmoles et de ±0,3‰ pour les échantillons de taille supérieure. La quantité de CO_2 récolté a été mesurée avec une incertitude proche de ±2 μmoles en utilisant une gauge de pression calibrée Keller. Les rapports D/H de l'eau contenue dans les tubes scellés sous vide ont été analysés suivant la méthode de réduction par le chrome à 1000°C décrite précédemment dans ce chapitre (Chapitre 4.1).

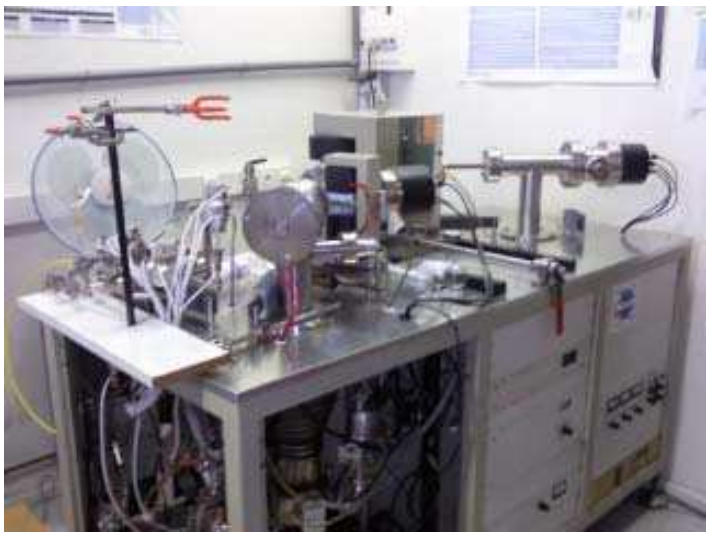

FIG. 4.5 – Spectromètre de masse GV Prism™ de l'UMR 5125 (Université Lyon 1)
FIG. 4.5 – GV Prism™ Mass spectrometer (UMR 5125, Université Lyon 1)

FIG. 4.6 – Spectromètre de masse GVI IsoPrime™ couplé à un système MultiPrep™
FIG. 4.6 – GVI IsoPrime™ mass spectrometer with a MultiPrep™ system

3. Microthermométrie des inclusions fluides

3.1. Microthermométrie des inclusions fluides dans la halite naturelle

Les échantillons de halite sont préparés en suivant les méthodes de Roberts and Spencer (1995) et Lowenstein et al. (1998). Ils sont coupés en lamelles de 5 mm de largeur et de 500 μm à 200 μm d'épaisseur puis collés sur des lames en verre avec de la résine époxy (Araldite). Les inclusions fluides à analyser sont ensuite sélectionnées par le biais d'une étude pétrographique au microscope optique. Les inclusions fluides renfermant une bulle de vapeur à température ambiante (25°C) sont écartées pour éviter de biaiser les mesures en incluant des valeurs de température d'homogénéisation trop élevées ne reflétant pas les températures réelles de formation de la halite (Roberts and Spencer, 1995). Les échantillons de halite sélectionnés contiennent des inclusions fluides monophasées, de taille comprise entre 10 et 50 μm soulignant les structures en chevrons (Fig. 4.7). Ils sont placés dans des petits conteneurs en présence de dessiccant pour empêcher la condensation de la vapeur d'eau sur la surface des échantillons. Ils sont ensuite refroidis à -20°C dans un congélateur pendant trois jours afin de nucléer les bulles de vapeur à l'intérieur des inclusions.

Les mesures microthermométriques sont réalisées avec une platine chauffante/réfrigérante Linkam Inc. THM 600 couplée à un microscope optique (Fig. 4.8) et calibrée avec des inclusions fluides synthétiques (eau pure : température de fusion de la glace = 0.0°C ; CO_2 pur : température de fusion = -56.6°C ; clathrate : température de fusion = 10.0°C). La température critique d'homogénéisation de l'eau pure à 374.1°C na pas été utilisée pour la calibration puisqu'elle est très élevée par rapport à la gamme de températures d'homogénéisations (Th°C) attendues pour les inclusions fluides dans la halite (15°C < Th < 45°C). La condensation de la vapeur d'eau à la surface des échantillons est limitée par l'ajout de dessiccant dans la chambre de la platine. Les échantillons sont transférés le plus rapidement possible du congélateur à la platine chauffante/réfrigérante Linkam Inc. préalablement refroidie pour éviter un réchauffement incontrôlé des inclusions. Les échantillons sont ensuite réchauffés avec un taux de 5°C par minute de -10°C à 15°C et à raison de 1°C par minute de 15°C à 50°C. Les températures d'homogénéisation des inclusions fluides sont déterminées avec une précision de ±0.5 °C.

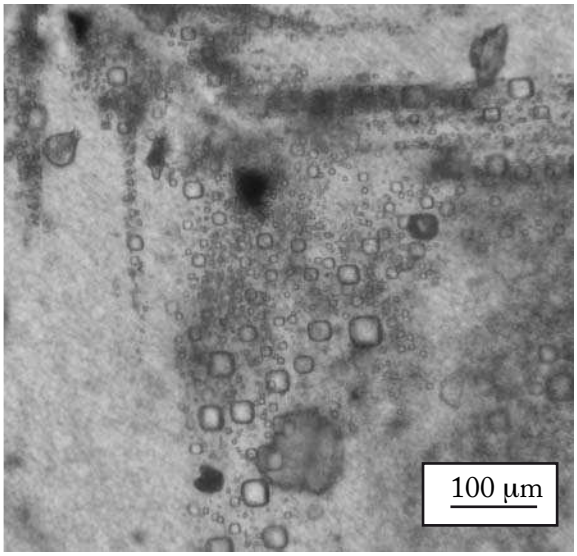

FIG. 4.7 – Relique d'un chevron de halite souligné par des inclusions fluides monophasées. Les inclusions monophasées sont sélectionnées pour l'étude microthermométrique.

FIG. 4.7 – Relic of chevron structure in natural halite with single-phase fluid inclusions. Single–phase fluid inclusions are selected for microthermometric study.

FIG. 4.8 – Installation microthermométrique de l'UMR 5125 (Université Lyon 1). Platine chauffante/réfrigérante Linkam Inc. THM 600 couplée à un microscope optique.

FIG. 4.8 – Apparatus for microthermometric studies (UMR 5125, Université Lyon 1). Linkam Inc. THM 600 Heating/freezing stage.

3.2. Microthermométrie des inclusions fluides dans les granulites.

Des lames épaisses de granulite d'une épaisseur de 200 μm ont été confectionnées au sein du laboratoire « PaléoEnvironnements et PaléobioSphère ». Une étude pétrographique et une analyse Raman des échantillons sont réalisées au préalable pour déterminer le caractère primaire ou secondaire et la composition chimique des inclusions fluides. Les mesures microthermométriques sont effectuées avec la platine chauffante/réfrigérante Linkam Inc. THM 600 couplée à un microscope optique (Fig. 4.7) et calibrée avec des inclusions fluides synthétiques (eau pure : température de fusion de la glace = 0.0°C ; température critique d'homogénéisation = 374.1°C ; CO_2 pur : température de fusion = -56.6°C ; clathrate : température de fusion = 10.0°C). Les échantillons sont d'abord portés à une température de -196°C avec de l'azote liquide, entrainant le gel des inclusions fluides. Ils sont ensuite réchauffés lentement jusqu'à 380°C. Les températures de fusion (de H_2O et CO_2) et la température d'homogénéisation totale des inclusions sont déterminées avec une précision respectivement de ±0.5 °C et de ±1°C. Les volumes molaires des inclusions de CO_2 sont également calculés à partir de la valeur de la température d'homogénéisation totale des inclusions en utilisant le logiciel MacFlincor™. Ce logiciel a été développé pour traiter les données de laboratoire obtenues sur les inclusions fluides et pour calculer les isochores P–T des fluides composés de H_2O, CO_2, N_2, CH_4 et NaCl (Brown et Hagemann, 1994).

Références

Brown P.E. and Hagemann S.G. (1994) MacFlinCor: a computer program for fluid inclusion data reduction and manipulation. In *Fluid Inclusions in Minerals: Method and Applications* (eds, B. De Vivo and J.M. Frezzotti), Virginia Tech Press, USA, 231-250.

Cerrai E., Marchetti R., Renzoni R., Roseo L., Silvestri M. and Villani S. (1954) A thermal method for concentrating heavy water. *Chem. Eng. Prog. Symp.*, **50**, 271-280.

Demeny (1995) H isotope fractionation due to hydrogen–zinc reactions and its implications on D/H analysis of water samples. *Chem. Geol.*, **121**, 19–25.

Kishima N. and Sakai H. (1980) O-18 and deuterium determination on a single water sample of a few milligrams. *Anal. Chem.* **52**, 356–358.

Lécuyer C., Dubois M., Marignac Ch., Gruau G., Fouquet, Y. and Ramboz C. (1999) Phase separation and fluid mixing in subseafloor back arc hydrothermal systems : A microthermometric and oxygen isotope study of fluid inclusions in the barite-sulfide chimneys of the Lau basin. *J. Geophys. Res.* **104**, 17911-17927.

Lécuyer C., Gardien V., Rigaudier T., Martineau F., Fourel F. and Cros A. (2009) Oxygen isotope fractionation and equilibration kinetics between CO_2 and H_2O as a function of salinity of aqueous solutions. *Chem. Geol.*, **264**, 221–233.

Lowenstein T.K., Li J. and Brown C.N. (1998) Paleotemperatures from fluid inclusions in halite : method verification and a 100,00 year paleotemperature record, Death Valley, CA. *Chem. Geol.*, **150**, 223–245.

Morrison J., Brockwell T., Merren T., Fourel F. and Phillips A.M. (2001) Online high–precision stable hydrogen isotopic analysis on nanoliter water samples. *Anal. Chem.*, **73**, 3570–3575.

O'Neil J.R. and Adami L.H. (1969) The oxygen isotope partition function ratio of water and the structure of liquid water. *J. Phys. Chem.* **73**, 1553–1558.

Roberts S.M. and Spencer R.J. (1995) Paleotemperatures preserved in fluid inclusions in halite. *Geochim. Cosmochim. Acta* **59**, 3929-3942.

Simon L. (2003) Quelques exemples de modélisations géochimiques des interactions entre les enveloppes terrestres. Ph. D. thesis, Ecole Normale Supérieure de Lyon.

Vennemann T.W. and O'Neil J.R. (1993) A simple inexpensive method of hydrogen isotope and water analysis of minerals and rocks based on zinc reagent. *Chem. Geol.*, **103**, 227–234.

Chapitre 5

Les isotopes stables des inclusions fluides de la halite : un nouveau proxy pour les reconstructions paléoclimatiques

5.1.

Oxygen isotope fractionation and equilibration kinetics between CO_2 and H_2O as a function of salinity of aqueous solutions.

Fractionnement isotopique de l'oxygène et cinétiques d'équilibration entre CO_2 et H_2O en fonction de la salinité des solutions aqueuses.

Résumé

Le fractionnement isotopique de l'oxygène et les cinétiques d'équilibration entre CO_2 et H_2O ont été étudiés à 313 K pour des salinités comprises entre 0 et 250 $g.L^{-1}$. Dans cette gamme de salinité, les temps de réaction nécessaires pour atteindre l'équilibre isotopique entre CO_2 et H_2O passent de 4h à 12h. Les échanges isotopiques sont comparables pour les solutions salines élaborées avec KCl et celles fabriquées avec NaCl, et sont décrits par des réactions cinétiques de premier ordre par $\ln(k) = -8{,}1485\ (\pm 0{,}0057) - 0{,}00474\ (\pm 3{,}87.10^{-5}) \times S$. Le coefficient de fractionnement de l'oxygène entre CO_2 et H_2O augmente avec la salinité pour les deux types de solutions (NaCl et KCl) pour une gamme de concentrations comprise entre 0 et 250 $g.L^{-1}$ suivant l'équation suivante : $1000\ln(\alpha_{CO_2\text{-}H_2O}) = 37{,}02\ (\pm 5.10^{-3}) + 3{,}96.10^{-3}\ (\pm 1{,}1.10^{-4}) \times S - 6{,}38.10\text{-}6\ (\ 4{,}5.10^{-7}) \times S^2$ ($R^2 = 0{,}998$). Les analyses des compositions isotopiques d'échantillons d'eau de mer de salinité 35 $g.L^{-1}$ nécessitent des corrections mineures de -0,15‰. Cependant, les rapports isotopiques de l'oxygène sont surestimés de 0,4‰ à 0,6‰ pour les eaux naturelles fortement salées ($100 < S < 250\ g.L^{-1}$). Les rapports isotopiques de l'oxygène doivent donc être corrigés lors de l'étude de saumures hydrothermales ou d'eaux salées échantillonnées dans les lacs hyper salins et les lagons, à cause des variations du coefficient de fractionnement de l'oxygène entre CO_2 et H_2O en fonction de la salinité.

Chemical Geology 264 (2009) 122–126

Contents lists available at ScienceDirect

Chemical Geology

journal homepage: www.elsevier.com/locate/chemgeo

Oxygen isotope fractionation and equilibration kinetics between CO_2 and H_2O as a function of salinity of aqueous solutions

Christophe Lécuyer [a,b,*], Véronique Gardien [a], Thomas Rigaudier [a], François Fourel [a], François Martineau [a], Alexandre Cros [a]

[a] Laboratoire UMR CNRS 5125, 'Paléoenvironnements et Paléobiosphère', Université Lyon 1, Lyon 69003, France
[b] Institut Universitaire de France, 103, bd Saint-Michel, 75005 Paris, France

ARTICLE INFO

Article history:
Received 26 November 2008
Received in revised form 24 February 2009
Accepted 25 February 2009

Editor: D. Rickard

Keywords:
Oxygen isotope
Fractionation
Kinetics
Salinity
Equilibration technique
Aqueous solutions

ABSTRACT

Oxygen isotope fractionation and equilibration kinetics between CO_2 and H_2O have been investigated at 313 K for salinities (S) ranging from 0 to 250 g L^{-1}. In this range of salinity, times needed to reach oxygen isotope equilibrium between CO_2 and H_2O increase from 4 h to 12 h. Isotopic exchanges are comparable for KCl and NaCl-like (sea salt) solutions and are described by first-order kinetic reactions with $\ln(k) = -8.1485(\pm 0.0057) - 0.00474(\pm 3.87\times10^{-5})S$. The oxygen isotope fractionation factor between CO_2 and H_2O increases with salinity for both sea salt and KCl solutions with concentrations ranging from 0 to 250 g L^{-1} according to the following equation: $1000\ \ln(\alpha_{CO2-H2O})\text{sea salt} = 37.02(\pm 5\times10^{-3}) + 3.96\times10^{-3}(\pm 1.1\times10^{-4})S - 6.38\times10^{-6}(\pm 4.5\times10^{-7})S^2$ ($R^2 = 0.998$). The oxygen isotope analysis of seawater samples with a salinity of 35 g L^{-1} requires minor corrections of −0.15‰ (V–SMOW). However, oxygen isotope ratios are overestimated by 0.4‰ to 0.6‰ in the case of highly saline natural waters ($100 < S < 250$ g L^{-1}). Corrections of the oxygen isotope ratios due to changes in the salinity-dependent fractionation factors between CO_2 and H_2O must be taken into account during the study of waters sampled from salt marshes, hypersaline lakes and lagoons, or hydrothermal brines.

1. Introduction

Determination of oxygen isotope ratios of natural waters is commonly obtained by equilibration with carbon dioxide according to Epstein and Mayeda's (1953) fundamental study. Since the recent development of automated preparation systems for the measurement of stable oxygen and hydrogen isotope ratios of waters, analytical precisions of ±0.05‰ and ±0.5‰ can be reached routinely with samples of about 200 µL by using isotopic equilibration techniques between CO_2 and H_2O (e.g. Horita et al., 1989; McCarthy et al., 2005). These high-precision isotopic measurements allow an increase in resolution of source water identification, and mixing or evaporation–condensation processes that can affect them in the hydrosphere or during interactions with the atmosphere or the Earth's crust. These physical and chemical processes are able to change the ionic concentration of aqueous solutions from highly diluted to over-saturated solutions. For example, rainfall located in the central parts of continents have a salinity (S) ≈ 0 g L^{-1} whereas highly evaporated waters of the Dead Sea or hydrothermal brines of the Red Sea have S = 250–300 g L^{-1} eq. NaCl.

It is known since the studies pioneered by Taube (1954), Craig and Gordon (1965), O'Neil and Adami (1969) and Truesdell (1974) that oxygen isotope fractionation between CO_2–H_2O depends on both the chemical composition and the ionic strength of aqueous salt solutions. Other studies have confirmed that the resulting oxygen isotopic offsets relative to the fractionation factor determined for pure water are much higher than analytical precisions (Sofer and Gat, 1972; Kazahaya, 1986; O'Neil and Truesdell, 1991; Fortier, 1994) even though

Table 1
X-ray-fluorescence chemical analysis of a natural sea salt from the salt marsh of Guérande, France.

Element wt.%	Sea salt "Guérande"
SiO_2	0.06
MgO	0.32
CaO	0.2
Na_2O	88
K_2O	0.06
H_2O^+	4.04
H_2O^-	7.29
Sum	99.97
Ppm	
Sr	62
Rb	7
S	21200

* Corresponding author. Laboratoire UMR CNRS 5125, 'Paléoenvironnements et Paléobiosphère', Université Lyon 1, Lyon 69003, France.
E-mail address: clecuyer@univ-lyon1.fr (C. Lécuyer).

0009-2541/$ – see front matter © 2009 Elsevier B.V. All rights reserved.
doi:10.1016/j.chemgeo.2009.02.017

Table 2
Comparison of the $\delta^{18}O$ of an aqueous solution of $S = 150$ g L^{-1} obtained by dissolution of the non-dried sea salt (TES150-1 and TES150-2 samples) with double-deionized water ($\delta^{18}O = -10.38$‰ V–SMOW) with a third one (TES150-D) obtained with the same salt dried at 110 °C overnight before being dissolved.

Aqueous solution	Salinity (g L^{-1})	H_2O in salt wt.%	$\delta^{18}O$ (‰ V–SMOW)
TES150-1	150	7	−10.35
TES150-2	150	7	−10.38
TES150-D	150	0	−10.37

Horita et al. (1995) concluded that NaCl has little effect (within analytical uncertainties) on the oxygen isotope fractionation factor at temperatures below 200 °C. Precise knowledge of the relationship that linked fractionation factors to the salt content is a prerequisite to the oxygen isotope analysis of waters from salt marshes, hypersaline lagoons, and hydrothermal brines (e.g. Chiodini et al., 2001; Pierret et al., 2001; Kloppmann et al., 2002; Risacher et al., 2003; Ladouche and Weng, 2005; Alexeev et al., 2007). Mixing of water end-members is also commonly performed by using both D/H and $^{18}O/^{16}O$ as natural tracers. This quantification can be weakened without applying the adequate salinity-dependent fractionation factors during the case study of water reservoirs with highly contrasted salinities. Approximations on the knowledge of these isotopic fractionation factors would also generate errors on the determination of the source of rainfall that are based on the slopes and intercepts of evaporation trajectories relative to the meteoric water line.

However, a systematic approach to calculate oxygen isotope fractionation factors and exchange kinetics for the CO_2–H_2O system as a function of salinity is still lacking. Therefore we have determined oxygen isotope fractionation factors and exchange kinetics between CO_2 and H_2O in NaCl (sea salt) and KCl aqueous solutions with salinities ranging from 0 to 250 g L^{-1}.

2. Analytical techniques

Two hundred and ninety-nine oxygen isotope measurements of water have been performed to determine kinetics and oxygen isotope fractionation between CO_2 and H_2O at 313 K for salinities ranging from 0 to 250 g L^{-1}. Two salts have been used for the experiments, a synthetic sylvite (99.9% KCl) and a natural sea salt mainly made of NaCl (Table 1) that was sampled in the Guérande salt marsh along the Northern Atlantic seaside in North-western France. Aqueous solutions of salinity ranging from 15 to 250 g L^{-1} have been prepared by dissolving from 1.9 to 31.5 g of KCl and a natural sea salt from the salt marsh of Guérande, France, in 125 mL of double-distilled water (DDW) which has a $\delta^{18}O$ value of -10.38 ± 0.05‰ (V–SMOW). A 3 L aliquot of this doubly distilled water was stored in a glass bottle. The natural sea salt is mainly NaCl with a minor sulfate content and 7 wt.% of adsorbed H_2O (Table 1) according to XRF analysis performed at the University Claude Bernard Lyon 1 (LST UMR 5570). This salt was therefore dried at 110 °C overnight before to be dissolved in double-distilled water (DDW). It is however noteworthy that the $\delta^{18}O$ of DDW and of the same water of $S = 150$ g L^{-1} obtained by dissolution of the non-dried sea salt are similar within analytical uncertainties (Table 2).

It was calibrated versus SMOW GISP and SLAP to determine its $\delta^{18}O$ value and it was used for all the salt solutions. Prior to equilibration analyses of salty solutions, we investigated the variations of the equilibration time as a function of the salinities of the solutions. For $S = 0$; 35; 150 and 250 g L^{-1}, the rate of oxygen isotope exchange with time between CO_2 and H_2O is reported as '$\delta^{18}O$ offset' where $\delta^{18}O\ \text{offset} = ((^{18}O/^{16}O_{SAM} - {}^{18}O/^{16}O_{DDW})/{}^{18}O/^{16}O_{DDW} - 1) \times 10^3$ (SAM = sample; DDW = doubly distilled water).

Aliquots of 200 µL of water were automatically reacted at 313 K with CO_2 and analyzed using a MultiPrep™ system on line with an Elementar IsoPrime™ dual inlet IRMS. Internal and external $\delta^{18}O$ reproducibilities were ±0.03‰ and ±0.1‰, respectively. Oxygen isotope ratios are reported relative to V–SMOW in the ‰ δ unit after scaling the raw data to the "true" isotopic ratios of SMOW, SLAP and GISP international standards. Kinetics experiments were performed analyzing water samples immediately after the autofill sequence was completed. The autofilling time was taken into account to determine the total equilibration time. All the experiments have been performed at 313 K, a temperature routinely used by some of the automated preparation systems dealing with the stable isotope analysis of large series of water samples.

3. Results

The Doubly Distilled Water (DDW) has a $\delta^{18}O$ value of −10.38‰ (V–SMOW). For each sea salt solution, steady-state isotopic

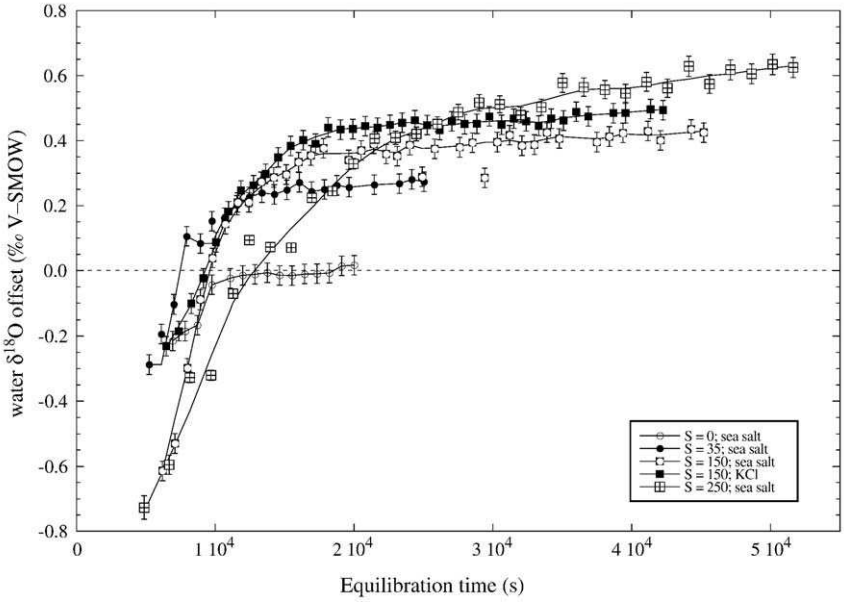

Fig. 1. Variations with equilibration time of the oxygen isotope offset (defined as the difference between measured water $\delta^{18}O$ at any time *t* and the composition of pure water with a $\delta^{18}O$ of −10.38‰ V–SMOW) of sea salt (NaCl-like) and KCl aqueous solutions at 313 K. Note that for the five experiments, oxygen isotope compositions of waters reach steady-state values for equilibration times depending on salinities and not on salt composition.

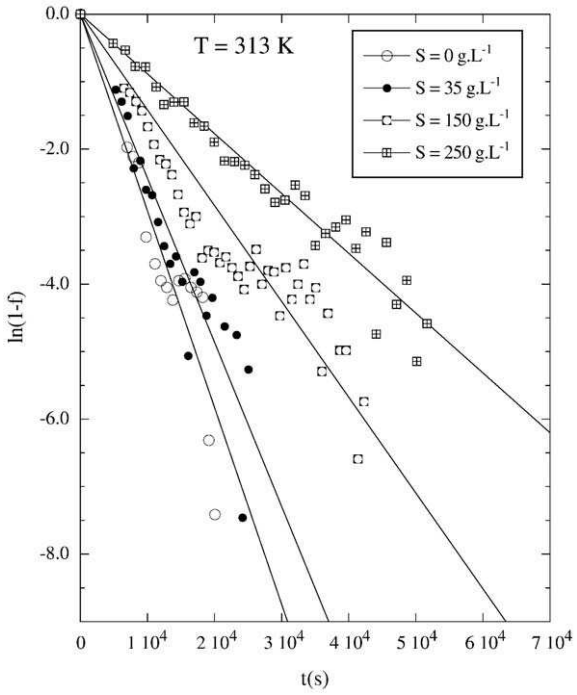

Fig. 2. Progress with time of the fraction of oxygen isotopes exchanged between carbon dioxide and water at 313 K. The absolute values of the slopes of the straight lines are the rate constants k of the reaction for salinities of 0, 35, 150, and 250 g L^{-1}, respectively. For $S=0$: $\ln(1-f)=-2.91\times10^{-4}(\pm1.29\times10^{-5})$ with $R^2=0.835$; for $S=35$: $\ln(1-f)=-2.43\times10^{-4}(\pm8.27\times10^{-6})$ with $R^2=0.877$; for $S=150$: $\ln(1-f)=-1.42\times10^{-4}(\pm3.49\times10^{-6})$ with $R^2=0.831$ and for $S=250$: $\ln(1-f)=-8.85\times10^{-5}(\pm1.72\times10^{-6})$ with $R^2=0.946$.

compositions are observed and are considered to represent isotopic equilibrium values between CO_2 and H_2O (Fig. 1; data are available as electronic supplement).

The order of the reaction was tested by a best fit of the data with a first-order law:

$$f = 1 - exp(-kt) = \frac{\delta^{18}O_i - \delta^{18}O_t}{\delta^{18}O_i - \delta^{18}O_e} \text{ with } k = Ae^{-\frac{E_a}{RT}} \quad (1)$$

where f is the fraction of isotopic exchange between carbon dioxide and water, $\delta^{18}O_i$ is the initial oxygen isotope composition of CO_2 (at

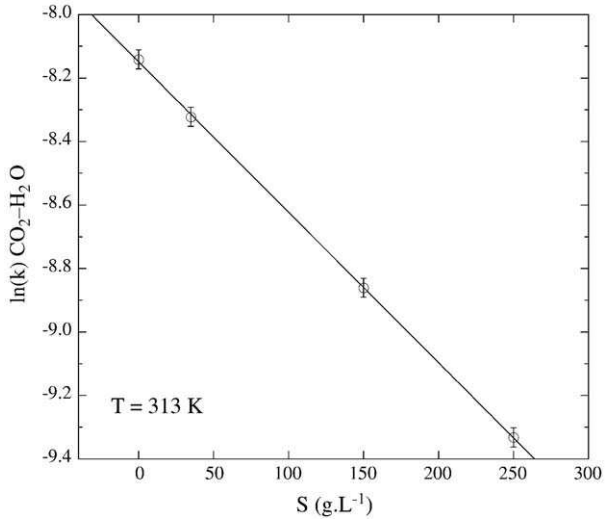

Fig. 3. Linear variations of $\ln(k)$ with the salinity of a sea salt solution at 313 K. k is the rate constant (s^{-1}) of the reaction of oxygen isotope exchange between CO_2 and H_2O. $\ln(k)$ sea salt $=-8.1485(\pm0.0057)-0.00474(\pm3.87\times10^{-5})S$ with $R^2=0.999$.

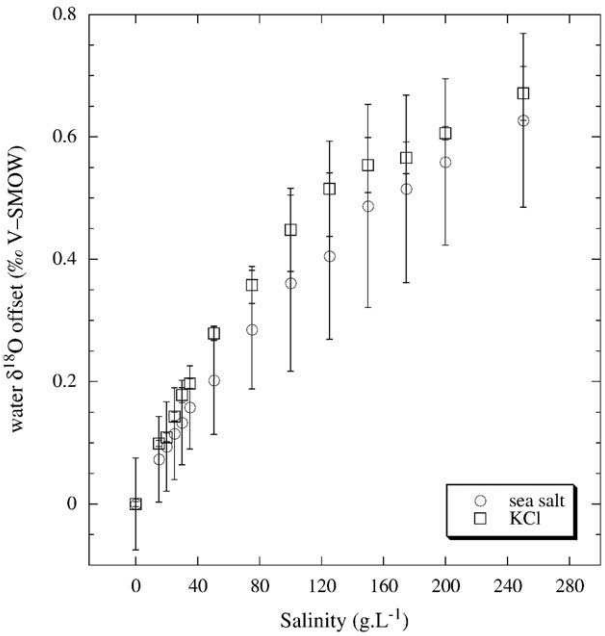

Fig. 4. Variations of water $\delta^{18}O$ offsets (defined as the difference between measured water $\delta^{18}O$ at equilibrium and the composition of pure water with a $\delta^{18}O$ of −10.38‰ V–SMOW) as a function of salinity for a sea salt and a KCl solution at 313 K. Note that both curves are similar to each other taking into account analytical uncertainties.

$t=0$; $\delta^{18}O=25.23\pm0.02$‰; $n=5$), $\delta^{18}O_t$ is the composition of CO_2 measured at any time t, $\delta^{18}O_e$ is its composition at equilibrium (deduced from observed steady-state values), and k (s^{-1}) is the rate constant of the reaction. Using Eq. (1), for each set of $\delta^{18}O_t$ obtained for a given salinity, the linear regression of data yield the rate constant k (Fig. 2) which is related to the salinity (Fig. 3) according to the following equation:

$$\ln(k)\text{ sea salt} = -8.1485(\pm0.0057) - 0.00474\left(\pm3.87.10^{-5}\right)S \quad (2)$$
$$\left(R^2 = 0.999\right).$$

In this range of salinity, times needed to reach oxygen isotope equilibrium between CO_2 and H_2O increase from 4 h to 12 h. These values are considered to be minimal reaction times required to accurately determine the oxygen isotope ratios of aqueous salt solutions by fluid equilibration techniques. It is noteworthy that "equilibration curves" for sea salt and KCl solutions of $S=150$ g L^{-1} are close each other (Fig. 4), showing that the nature of the cation does not influence the kinetics of isotopic exchange between CO_2 and H_2O.

Steady-state values of isotopic offsets have also been obtained for 14 sea salt and KCl solutions of salinity ranging from 0 to 250 g L^{-1} (Tables 3 and 4). The oxygen isotope offsets increase similarly with increasing salinity for both KCl and sea salt solutions (Fig. 4). Assuming that they represent equilibrium isotopic values between CO_2 and H_2O, oxygen isotope fractionation factors α are fitted as a function of salinity at a constant temperature of 313 K for sea salt (NaCl-like) and KCl solutions (Tables 3 and 4). These fractionation factors are linearly correlated to the salt content when $S\leq35$ g L^{-1}, above this value the experimental data deviate from the straight line (Fig. 5). The whole data set can be empirically described by the following equation:

$$1000\ln\left(\alpha_{CO_2-H_2O}\right)\text{sea salt} = 37.02\left(\pm5.10^{-3}\right) + 3.96.10^{-3} \quad (3)$$
$$\left(\pm1.05.10^{-4}\right)S - 6.38.10^{-6}$$
$$\left(\pm4.5.10^{-7}\right)S^2\ \left(R^2 = 0.998\right).$$

Table 3
Variations of the oxygen isotope offset (defined as the difference between measured water $\delta^{18}O$ at equilibrium between CO_2 and H_2O and the composition of pure water with a $\delta^{18}O$ of −10.38‰ V–SMOW) with the salinity of sea salt (NaCl-like) aqueous solutions.

Salinity	$\delta^{18}O$ offset	$\delta^{18}O$ offset	$\delta^{18}O$ offset	$\delta^{18}O$ offset	$\delta^{18}O$ offset	$\delta^{18}O$ offset	$\delta^{18}O$ offset	$\delta^{18}O$ offset	$\delta^{18}O$ offset	$\delta^{18}O$ offset	SD	$\alpha(CO_2–H_2O)$
g L^{-1} Sea salt	Exp. 1	Exp. 2	Exp. 3	Exp. 4	Exp. 5	Exp. 6	Exp. 7	Exp. 8	Exp. 9	Mean		
0	0.00	0.00	0.00	0.00	0.00	0.00	0.00	0.00	0.00	0.00	0.075	1.037700
15.02	0.00	−0.02	0.15	0.08	0.05	0.09	0.20	0.05	0.04	0.07	0.070	1.037774
20.06	0.01	−0.03	0.16	0.09	0.14	0.14	0.19	0.07	0.07	0.09	0.073	1.037794
25.00	0.02	0.02	0.19	0.12	0.12	0.21	0.21	0.06	0.09	0.11	0.075	1.037816
29.92	0.03	0.03	0.19	0.15	0.15	0.20	0.23	0.11	0.11	0.13	0.069	1.037834
35.04	0.09	0.03	0.20	0.13	0.20	0.21	0.25	0.16	0.14	0.16	0.068	1.037859
50.54	0.12	0.04	0.22	0.15	0.23	0.32	0.31	0.19	0.22	0.20	0.088	1.037904
75.02	0.20	0.10	0.29	0.22	0.35	0.41	0.40	0.30	0.29	0.28	0.097	1.037988
100.09	0.20	0.14	0.32	0.28	0.47	0.53	0.56	0.36	0.40	0.36	0.144	1.038064
125.12	0.25	0.18	0.38	0.34	0.50	0.58	0.57	0.42	0.43	0.40	0.136	1.038109
150.00	0.29	0.24	0.46	0.40	0.69	0.71	0.63	0.46	0.49	0.49	0.166	1.038192
174.65	0.35	0.29	0.44	0.43	0.68	0.70	0.70	0.52	0.53	0.51	0.153	1.038220
199.81	0.41	0.37	0.50	0.48	0.75	0.69	0.72	0.56	0.56	0.56	0.136	1.038264
250.12	0.46	0.42	n.d.	0.56	0.78	0.80	0.74	0.63	0.63	0.63	0.142	1.038333

Mean values and standard deviations (SD) have been obtained with nine experiments (exp.).

Eq. (3) provides solutions to correct isotopic biases resulting from the "salt effect" when measuring oxygen isotope compositions of natural saline waters. In the case of seawater-like samples with a salinity of 35 g L^{-1}, the $\delta^{18}O$ offset of 0.15‰ is rather small but significant relative to analytical uncertainties. For hypersaline solutions with $S \geq 200$ g L^{-1}, the large $\delta^{18}O$ offsets of 0.6–0.7‰ can induce large analytical errors and misinterpretations if not corrected from raw data.

4. Discussion

Quality of the data fit computed and illustrated in Fig. 2 suggests that oxygen isotope exchange between CO_2 and H_2O obeys a first-order reaction, a conclusion previously reached by Fortier (1994) for calcium chloride solutions from 0 to 4.0 M between 25 °C and 50 °C. However, at 313 K and 2.5 M, the rate constant for a $CaCl_2$ solution ($\ln(k) = -7.83$) is about one order higher than the one inferred from this study for a NaCl solution ($\ln(k) = -8.86$). Time needed to reach oxygen isotope equilibrium between CO_2 and H_2O increases with the increasing salinity of aqueous solutions. Our recommended values ranging from 4 h to 12 h for salinities ranging from 0 to 250 g L^{-1} need to be compared to those recommended for the use of automated preparation systems: "typical equilibration times are 4.5 h for CO_2" (System Description, p.12, in MultiPrep™ User's Guide, Micromass UK).

Table 4
Variations of the oxygen isotope offset (defined as the difference between measured water $\delta^{18}O$ at equilibrium between CO_2 and H_2O and the composition of pure water with a $\delta^{18}O$ of −10.38‰ V–SMOW) with the salinity of KCl aqueous solutions.

Salinity	$\delta^{18}O$ offset	$\delta^{18}O$ offset	$\delta^{18}O$ offset	SD	$\alpha(CO_2–H_2O)$
g L^{-1} KCl	Exp. 1	Exp. 2	Mean		
0	0.00	0.00	0.00	0.004	1.037700
15.02	0.10	0.10	0.10	0.005	1.037800
20.04	0.10	0.11	0.11	0.007	1.037810
24.96	0.14	0.15	0.14	0.007	1.037845
30.05	0.17	0.19	0.18	0.012	1.037880
35.04	0.19	0.20	0.20	0.008	1.037899
50.54	0.29	0.27	0.28	0.012	1.037982
75.06	0.38	0.34	0.36	0.030	1.038062
99.87	0.50	0.40	0.45	0.068	1.038153
124.98	0.57	0.46	0.51	0.078	1.038220
150.05	0.59	0.52	0.55	0.045	1.038260
174.93	0.58	0.55	0.57	0.026	1.038272
200.32	0.61	0.60	0.61	0.011	1.038311
250.14	0.64	0.70	0.67	0.044	1.038377

Mean values and standard deviations (SD) have been obtained with two experiments (exp.).

For salinities higher than 35 g L^{-1}, values of $1000\ln\alpha$ deviate from a straight line when reported against solution salinities. This result differs from what was described by Bourg et al. (2001) who concluded that there is no significant oxygen-18 salt effect in a range of concentrations from 0.5 to 2 times that of seawater. The observed complex relationship between these two parameters could result from changes in carbon speciation with increasing solute concentration. Indeed, Millero et al. (2007) have studied the dependence of dissociation constants of carbonic acid on both molality (0–6 M) and temperature (0–50 °C) of NaCl solutions. One of the main conclusions of their study is that both activity coefficients of HCO_3^- and CO_3^{2-} are very sensitive to molality at a given temperature and that this dependence must be taken into account during studies of the carbonate system in hydrothermal brines. From our data, a simple second-order polynomial equation allows to calculate values of $1000\ln\alpha(CO_2–H_2O)$ for NaCl or KCl solutions with any salinity lower or equal to 250 g L^{-1}.

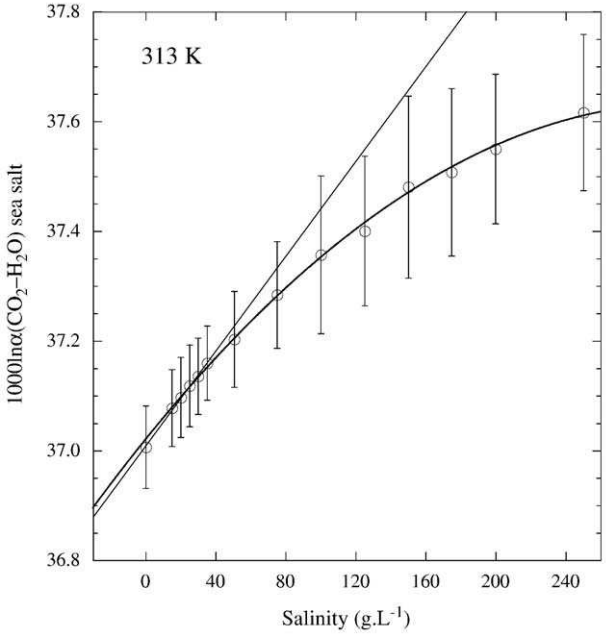

Fig. 5. Variations of $1000\ln\alpha(CO_2–H_2O)$ as function of salinity for a sea salt solution at 313 K. Experimental data follow empirically a second-order polynomial law, they deviate from a straight line which relates $1000\ln\alpha(CO_2–H_2O)$ to salinity for sea salt solutions of $S \leq 35$ g L^{-1}. Equation of the straight line is: $1000\ln\alpha(CO_2–H_2O) = 4.32 \times 10^{-3}(\pm 1.02 \times 10^{-4})S + 37.009(\pm 2.41 \times 10^{-3})$ with $R^2 = 0.998$.

Fitted fractionation factors for oxygen isotopes increase with increasing solute concentrations (Fig. 5). These results mean that values of $1000\ln\alpha$ between pure water and water bound to ions are negative (O'Neil and Truesdell, 1991), and more and more negative with the increasing solute concentration. O'Neil and Truesdell (1991) proposed that these salts act as breakers of the water structure. The solute alters the water structure with cation–H_2O bonds that are weaker than the co-existing H_2O–H_2O bonds, resulting in modified vibrational frequencies of the water molecules (Feder and Taube, 1952; O'Neil and Adami, 1969). For example, fractionations of both hydrogen and oxygen isotopes have been documented between hydrated and free water molecules in aqueous urea solution (Kakiuchi and Matsuo, 1985). Oxygen isotope fractionation factors between CO_2–H_2O are then strongly correlated to the concentration of the solute.

O'Neil and Truesdell (1991) made oxygen isotope equilibrations with alkali chloride solutions and their results revealed that K^+ is a stronger water structure breaker than Na^+. Moreover, these authors consider that NaCl constitutes a unique salt that fails to produce a sizable oxygen isotope fractionation between carbon dioxide and water as previously observed by Taube (1954) and Sofer and Gat (1972). Cole and Wesolowski (1989) have shown the influence of NaCl aqueous solutions on both equilibrium constants and rates of isotopic exchange in mineral–fluid systems. Results obtained from this study are at variance with the conclusions inferred from these pioneering studies. Direction and amplitude of oxygen isotope fractionation between CO_2–H_2O as a function of salinity are similar when using either KCl or NaCl solutions taking into account analytical uncertainties (Fig. 4). In addition, for salinities equal or above those of seawater-like solutions, changes in the fractionation factor values are large enough (Fig. 5) to cause errors much larger than those resulting from the chemical procedures and isotopic ratio mass spectrometer measurements.

5. Conclusions

Direction and relative amplitudes of the measured $^{18}O/^{16}O$ fractionations at 313 K between CO_2 and H_2O are well correlated to the water structure-breaking capacity of the NaCl and KCl solutes. Kinetics of reaction lead to propose minimal times needed to reach equilibrium depending on the solute content of analyzed waters. Oxygen isotope fractionations between CO_2 and H_2O increase with salinity for both NaCl and KCl solutions, therefore allowing the correction of fractionation factors for any salinity comprised between 0 and 250 g L^{-1}. Isotopic fractionations known between CO_2 and pure H_2O must be corrected from such a "salinity" effect for aqueous solutions whose salinity is equal or higher to that of marine waters.

Acknowledgements

This study has been supported by funds provided by French CNRS and IUF. The authors thank the two anonymous reviewers who contributed to improve the quality of this work.

Appendix A. Supplementary data

Supplementary data associated with this article can be found, in the online version, at doi:10.1016/j.chemgeo.2009.02.017.

References

Alexeev, S.V., Alexeeva, L.P., Borisov, V.N., Shouakar-Stash, O., Frape, S.K., Chabaux, F., Kononov, A.M., 2007. Isotopic composition (H, O, Cl, Sr) of ground brines of the Siberian Platform. Russ. Geol. Geophys. 48, 225–236.

Bourg, C., Stievenard, M., Jouzel, J., 2001. Hydrogen and oxygen isotopic composition of aqueous salt solutions by gas–water equilibration method. Chem. Geol. 173, 331–337.

Chiodini, G., Marini, L., Russo, M., 2001. Geochemical evidence for the existence of high-temperature hydrothermal brines at Vesuvio volcano, Italy. Geochim. Cosmochim. Acta 65, 2129–2147.

Cole, D.R., Wesolowski, D.J., 1989. Influence of NaCl aqueous solutions on isotopic equilibria and rates of exchange in mineral–fluid systems. Trans. Geotherm. Res. Council 13, 227–234.

Craig, H., Gordon, L.I., 1965. Deuterium and oxygen-18 variations in the ocean and the marine atmosphere. In: Tongiorgi, E. (Ed.), Stable Isotopes in Oceanographic Studies and Paleotemperatures. Lab. Geol. Nucl., pp. 9–130.

Epstein, S., Mayeda, T.K., 1953. Variation in O^{18} content of waters from natural sources. Geochim. Cosmochim. Acta 4, 213–224.

Feder, H.M., Taube, H., 1952. Ionic hydration: an isotopic fractionation technique. J. Chem. Phys. 20, 1335–1336.

Fortier, S.M., 1994. An on-line experimental/analytical method for measuring the kinetics of oxygen isotope exchange between CO_2 and saline/hypersaline salt solutions at low (25–50 °C) temperatures. Chem. Geol. 116, 155–162.

Horita, J., Ueda, A., Mizukami, K., Takatori, I., 1989. Automatic δD and $\delta^{18}O$ analyses of multi-water samples using H_2– and CO_2–water equilibration methods with a common equilibration set-up. Appl. Radiat. Isotopes 40, 801–805.

Horita, J., Cole, D.R., Wesolowski, D.J., 1995. The activity–composition relationship of oxygen and hydrogen isotopes in aqueous salt solutions: III. Vapor–liquid water equilibration of NaCl solutions to 350 °C. Geochim. Cosmochim. Acta 59, 1139–1151.

Kakiuchi, M., Matsuo, S., 1985. Fractionation of hydrogen and oxygen isotopes between hydrated and free water molecules in aqueous urea solution. J. Phys. Chem. 89, 4627–4632.

Kazahaya, K. (1986) Chemical and isotopic studies on hydrothermal solutions. Ph. D. dissertation, Tokyo Inst. Techn., pp. 185.

Kloppmann, W., Girard, J.-P., Négrel, Ph., 2002. Exotic stable isotope compositions of saline waters and brines from the crystalline basement. Chem. Geol. 184, 49–70.

Ladouche, B., Weng, Ph., 2005. Hydrochemical assessment of the Rochefort marsh: role of surface and groundwater in the hydrological functioning of the wetland. J. Hydrol. 314, 22–42.

McCarthy, K.T., Pichler, T., Price, R.E., 2005. Geochemistry of Champagne Hot Springs shallow hydrothermal vent field and associated sediments, Dominica, Lesser Antilles. Chem. Geol. 224, 55–68.

Millero, F., Huang, F., Graham, T., Pierrot, D., 2007. The dissociation of carbonic acid in NaCl solutions as a function of concentration and temperature. Geochim. Cosmochim. Acta 71, 46–55.

O'Neil, J.R., Adami, L.H., 1969. The oxygen isotope partition function ratio of water and the structure of liquid water. J. Phys. Chem. 73, 1553–1558.

O'Neil, J.R., Truesdell, A.H., 1991. Oxygen isotope fractionation studies of solute–water interactions. In: Taylor, H.P., O'Neil, J.R., Kaplan, I.R. (Eds.), Stable Isotope Geochemistry: A Tribute to Samuel Epstein. The Geochemical Society, Special Publication n°, vol. 3, pp. 17–25.

Pierret, M.C., Clauer, N., Bosch, D., Blanc, G., France-Lanord, C., 2001. Chemical and isotopic ($^{87}Sr/^{86}Sr$, $\delta^{18}O$, δD) constraints to the formation processes of Red-Sea brines. Geochim. Cosmochim. Acta 65, 1259–1275.

Risacher, F., Alonso, H., Salazar, C., 2003. The origin of brines and salts in Chilean salars: a hydrochemical review. Earth Sci. Rev. 63, 249–293.

Sofer, Z., Gat, J.R., 1972. Activities and concentrations of oxygen-18 in concentrated aqueous salt solutions: analytical and geophysical implications. Earth Planet. Sci. Lett. 15, 232–238.

Taube, H., 1954. Use of oxygen isotope effects in the study of hydrated ions. J. Chem. Phys. 58, 523–528.

Truesdell, A.H., 1974. Oxygen isotope activities and concentrations in aqueous salt solutions at elevated temperatures: consequences for isotope geochemistry. Earth Planet. Sci. Lett. 23, 387–396.

5.2.

Experimental determination of δD–δ18O trajectories during water evaporation: The record of temperatures and wind velocities in water inclusions of synthetic and natural halites.

Détermination expérimentale des trajectoires δD–δ18O au cours de l'évaporation d'une eau: enregistrement potentiel des températures et des vitesses de vent dans les inclusions aqueuses de halites synthétiques et naturelles.

Résumé

Les fractionnements isotopiques de l'hydrogène et de l'oxygène entre l'eau liquide et sa vapeur ont été déterminés expérimentalement en fonction de la température de l'eau et de la vitesse du vent lors de l'évaporation d'une solution de NaCl (35 g.L-1). Pour une vitesse de vent nulle, les pentes "a" des trajectoires δD–δ^{18}O d'évaporation des eaux résiduelles diminuent avec l'augmentation de la température en suivant une loi hyperbolique. A une température donnée, les pentes des trajectoires δD–δ^{18}O d'évaporation augmentent linéairement avec l'augmentation de la vitesse du vent. Ces résultats expérimentaux peuvent être modélisés en utilisant les équations de distillation de Rayleigh et en tenant compte des effets cinétiques liés à la présence de vent. Les compositions isotopiques de l'hydrogène et de l'oxygène des inclusions aqueuses piégés dans les cristaux de halite précipités ont été déterminées par des techniques de micro–équilibration. Ces compositions isotopiques reflètent précisément celles des eaux résiduelles environnantes présentes dans le milieu lors de la croissance des cristaux de halite. Les compositions isotopiques des inclusions aqueuses piégées dans de la halite naturelle provenant des dépôts salifères du Messinien de Sicile suggèrent que la halite a précipité dans des eaux dont la température était de 34^{+10}_{-4}°C, ce qui est en accord avec les températures d'homogénéisation obtenues par microthermométrie (médiane = 34±5°C). La similitude entre les pentes des droites d'évaporation mesurées et expérimentales montre que le vent avait peu d'impact sur l'évaporation lors de la formation des dépôts de halite. Les compositions isotopiques de l'hydrogène et de l'oxygène de vingt échantillons de halite provenant de la mine de Realmonte en Sicile définissent une droite d'évaporation dont l'extrapolation jusqu'à l'intersection avec la droite des eaux météoriques (MWL) permet la caractérisation de la source de l'eau avec des valeurs de δD et de δ^{18}O respectivement égales à -60±10‰ et -8.5±1.5‰. Ces résultats indiquent que les grandes quantités de halite déposées en Sicile résultent de l'évaporation d'une eau de mer mélangée à une fraction importante d'eau météorique provenant en grande partie des fleuves alpins.

Experimental determination of δD–δ^{18}O trajectories during water evaporation: The record of temperatures and wind velocities in water inclusions of synthetic and natural halites

Thomas Rigaudier[1], Christophe Lécuyer[1,*], Véronique Gardien[1], Jean-Pierre Suc[1] and François Martineau[1]

[1] Laboratoire UMR CNRS 5125 'PaléoEnvironnements et PaléobioSphère', Université Lyon 1, Lyon, Campus de la Doua, 69622 Villeurbanne, France.

* Corresponding author: clecuyer@univ-lyon1.fr

Keywords: water evaporation; δD; δ^{18}O; Rayleigh distillation; fluid inclusion; water temperature; halite; Sicily

Abstract – Deuterium and oxygen isotope fractionations between liquid and vapour water have been experimentally–determined during evaporation of a NaCl solution (35 $g.L^{-1}$) as a function of water temperature and wind velocity. In the case of a null wind velocity, slopes 'a' of $\delta D–\delta^{18}O$ trajectories of residual waters hyperbolically decrease with increasing water temperatures in the range 23°C–47°C. For wind velocities ranging from 0.8 to 2.2 $m.s^{-1}$, slopes of the $\delta D–\delta^{18}O$ trajectories linearly increase with increasing wind velocity at a given water temperature. These experimental results can be modelled by using Rayleigh distillation equations taking into account wind–related kinetics effects. Deuterium and oxygen isotope compositions of water inclusions trapped by the precipitated halite crystals were determined by micro–equilibration techniques. These isotopic compositions accurately reflect those of the surrounding residual waters during halite growth. Isotopic compositions of water inclusions in natural halite from the Messinian deposits of Sicily suggest precipitation temperatures of 34^{+10}_{-4}°C that match the homogenization temperatures obtained by microthermometry (median = 34±5°C). The similarity between the measured and experimental slopes of the $\delta D–\delta^{18}O$ evaporation trajectories suggest that the effect of wind was negligible during the genesis of these halite deposits. Hydrogen and oxygen isotope compositions of twenty halite samples from the Realmonte mine in Sicily define a linear trend whose extrapolation until intersection with the Meteoric Water Line allows the characterization of the water source with δD and $\delta^{18}O$ values of -60±10‰ and -8.5±1.5‰, respectively. These results reveal that the huge amounts of halite deposited in Sicily result from the evaporation of seawater mixed with a dominant fraction (≥ 50%) of meteoric waters most likely deriving from alpine fluvial discharge.

1) Introduction

Superficial water cycle plays a major role in the transfer of heat at Earth's surface through the genesis, transport and condensation of humid air masses. These physical processes generate large isotopic fractionations for both water hydrogen and oxygen that are mainly controlled by Rayleigh distillation and air temperature during condensation and also by relative air humidity and wind velocity during evaporation (Craig and Gordon, 1965). Therefore stable isotope compositions of precipitations are related to air temperature of formation and trajectories of humid air masses (Dansgaard, 1964). In the case of evaporating water, the unsaturated overlying air layer causes out of equilibrium isotopic fractionation that can be complicated by wind velocity which modifies the structure of the limit layer at the water–air interface (Craig and Gordon, 1965).

Surface waters can be trapped as fluid inclusions in various neoformed minerals such as quartz filling in fractures of crustal rocks; they have been used, for example, to estimate paleoaltitudes during the evolution of mountain belts (Blisniuk and Stern, 2005; Mulch and Chamberlain, 2007). Water inclusions in calcite precipitated as speleothems in caves have been also studied to reconstruct past mean air temperatures (Schwarcz et al., 1976; Matthews et al., 2000; Dennis et al., 2001). Residual evaporated waters are commonly trapped in evaporitic minerals and especially within one of critical interest, NaCl or halite, which is nominally H– and O–free. Hydrogen and oxygen isotope compositions of water inclusions in halite have been determined for identifying fluid sources and mixing processes. They should also reflect the temperature at which water was trapped in the crystal structure, wind velocity and relative air humidity at the water–air interface.

Therefore, we designed a set of experiments where NaCl salt was dissolved in waters of known isotopic compositions that were monitored over the course of evaporation until halite precipitated. Fluid inclusions were also analyzed to check the validity of the compositions they record with regard to the evaporation of a seawater–like solution. The potential of δD and $\delta^{18}O$ of fluid inclusions in natural halite to be proxies of surface water temperatures and wind velocity was tested by studying halite from the large marine salt deposits of Sicily generated during the Messinian crisis in the Mediterranean sea about 5 my ago (Decima and Wezel, 1973; Lugli et al., 1999). Temperatures of halite precipitation were determined by microthermometric measurements of water inclusions and compared to those deduced from their δD–$\delta^{18}O$ pairs. Finally, the origin of water that led to the formation of these huge salt deposits is discussed in terms of mixing between marine and fresh waters.

2) Experimental precipitation of halite from seawater–like solutions

Pure grade sodium chloride was dissolved in 500 mL of double deionized water until to obtain an aqueous solution with a salinity of 35 $g.L^{-1}$. Water derives from Rhône river and has $\delta^{18}O$ and δD values close to -10.5‰ and -80‰, respectively, $\delta^{18}O$ and δD variations in the range -10.96‰ to -9.76‰ and -89.4‰ to -70.9‰, respectively (Tables 1 and 2), from one experiment to another one reflect seasonal variations in the oxygen isotope composition of Rhône river. This aqueous solution was placed in a 4 L translucent polycarbonate rectangular tank itself partly immerged in a thermostated bath. The bottom of the tank was cleaned, dried and polished between each experiment. All the experiments have been run in an air–conditioned room at a temperature of 21±1°C. Evaporating water was regularly sampled through time for δD and $\delta^{18}O$ analysis. After complete water evaporation, NaCl crystals have been also sampled for isotopic analysis of their water inclusions (Table 3). A first set of

experiments was performed without wind at temperatures of 23°C, 26.5°C, 28°C, 29.5°C, 36°C and 47°C (Table 1). A second set of experiments was performed at a constant temperature of 36°C (temperature without wind) for wind velocities of 0.8 $m.s^{-1}$, 1.5 $m.s^{-1}$ and 2.2 $m.s^{-1}$ (Table 2). Wind was generated by a fan whose velocity was measured by an anenometer. Wind was responsible for a decrease of the superficial water temperature as indicated in Table 2.

3) Analytical techniques

Salinity and temperature

Temperature and conductivity (converted into salinity) were measured at the surface of evaporating waters during each sampling stage with a multi-parameter WTW Multi 340ik (Tables 1 and 2). Above 300 $g.L^{-1}$, precision became very poor because of an out of scale calibration complicated by the very thin layer of residual water precluding a complete immersion of the multi–parameter electrode.

Deuterium and oxygen isotope measurements of waters

Aliquots of 200 µl of water were automatically reacted at 313 K with CO_2 and H_2 (in presence of a Pt catalyst) and analyzed using a MultiPrep™ system on line with a GVI IsoPrime™ dual inlet IRMS. Reproducibility of D/H and $^{18}O/^{16}O$ measurements was established at about ±1‰ and ±0.1‰, respectively, by scaling raw data to the "true" isotopic ratios of SMOW, SLAP and GISP international standards. Corrections of the hydrogen and oxygen isotope ratios due to changes in the salinity–dependent fractionation factors between

CO_2 and H_2O and H_2O and H_2 have been taken into account according to Lécuyer et al. (2009) and Martineau et al. (in prep.).

Deuterium and oxygen isotope measurements of water inclusions in halite

Water trapped in halite was extracted by thermal decrepitation. 50 to 150 mg of millimetre–sized grains of halite was dried overnight at 110°C in an oven then loaded in a quartz tube and degassed at 80˚C under vacuum for at least 90 minutes. Water was then extracted by heating samples up to 800°C during 15 minutes. Water blanks were very low over the complete set of experiments without contributing more than 1% of the total amount of water extracted from fluid inclusions.

Water collected during the decrepitation of fluid inclusions, in the range 50-200 μmoles, was transferred to a microequilibration vessel to which 5–10 μmoles of CO_2 were added. The H_2O and CO_2 of known amount and isotopic composition were then allowed to exchange oxygen isotopes at 25˚C for two days. After this time, equilibration was complete and the equilibrated samples of H_2O and CO_2 were separated cryogenically. The $\delta^{18}O$ values of the water samples were calculated using the mass balance equation (1) of Kishima and Sakai (1980). Precisions obtained during the experiments for $\delta^{18}O$ values of H_2O were close to 0.5‰.

$$(1)\ \delta^{18}O\,H_2O = \left(\delta^{18}O\,CO_2(f) - \delta^{18}O\,CO_2(i)\right)\left(2\frac{[CO_2]}{[H_2O]}\right) + \left(1 + \frac{\delta^{18}O\,CO_2(f)}{1000}\right)\frac{1000}{\alpha_{CO_2\text{-}H_2O}} - 1000$$

with α CO_2-H_2O = 1.0412 at T= 25˚C (O'Neil and Adami, 1969)

$\delta^{18}O$ CO_2 (f) = $\delta^{18}O$ of CO_2 equilibrated after two days with H_2O

$\delta^{18}O$ CO_2 (i) = $\delta^{18}O$ of CO_2 before equilibrium with H_2O = 15.3±0.1 (SMOW)

$[CO_2]$ and $[H_2O]$ are the amounts of the two gases in μmoles

After equilibration, the same water was collected into a silica glass tube containing about 500 mg of fine–grained chromium metal. This water was then reduced by Cr at 1000°C during 5 minutes to produce H_2 gas for which the D/H ratio was determined by using a dual–inlet GV Prism™ mass spectrometer. External reproducibility of D/H measurements was established at about ±3‰ by scaling raw data to the VSMOW-SLAP scale. Water amounts of samples, required to solve equation (1), were determined by comparison with a series of water samples of known weights ranging from 0.5 μl to 3.5 μl. After expansion of H_2 into a constant volume of the mass spectrometer sample inlet, the amount of gas was estimated from the voltage of mass 2 collector. Uncertainty associated with the determined amount of water is close to ±0.05 μl. Internal reproducibility of D/H analyses of reference waters is better than 1.5‰.

Microthermometry of fluid inclusions in natural evaporites

Halite of Messinian age (5.6–5.3 My) was sampled in the Realmonte mine, south Sicily. The samples were selected and prepared following the methods of Roberts and Spencer (1995) and Lowenstein et al. (1998). Halite samples were clipped into about 5 mm across and 500 μm thick wafers and mounting on microscope cover glasses with polyepoxy resin. Fluid inclusions selected for this study (Figure 3) did not initially contain vapour bubbles at room temperature (25°C) in order to avoid the measurement of high homogenization temperatures that do not reflect the real temperatures of halite formation

(Roberts and Spencer, 1995). Selected halite samples were placed in small containers with desiccant to prevent condensation on crystals surfaces, and cooled to -20°C in a freezer for three days in order to nucleate vapour bubbles. Microthermometric observations were carried out using a Linkam Inc. Heating–Freezing stage, calibrated with synthetic fluid inclusions (pure water: ice melting temperature of 0.0°C and critical homogenization temperature of 374.1°C; pure CO_2-H_2O: CO_2 melting temperature of -56.6°C ; clathrate : melting temperature of 10°C). Condensation of water vapour on the sample inside the chamber was reduced by addition of desiccant. Samples were transferred to the precooled Linkam Inc. Heating–Freezing stage as quickly as possible to avoid uncontrolled heating. Samples were heated by 5°C per minute from -10°C to 15°C and more slowly (1°C per minute) from 15°C to 50°C. Homogenization temperatures of fluid inclusions were recorded with an accuracy of ±0.5 °C (Table 3).

4) Results

Halite crystals and their water inclusions

The mode of crystallization of halite during these experiments have been already described by Roedder (1984b). Precipitated crystals are typically what Roedder (1984b) called “hopper crystals”. Evaporation at the surface of the NaCl solution provokes the nucleation of floating tiny tablets resulting from surface tension at the aqueous solution–air interface (Figure 1). Crystals grew at the edges forming their tabular crystals with depressed centres (Figure 2C) as a result of floating lower and lower as they grew heavier. The fastest growth direction is perpendicular to (111) which means towards the cube corners (Figure 2C). Mean surface of isolated halite crystals decreases with increasing temperature; 4.17±0.01

mm^2 (n = 229) at 25°C; 2.24±0.01 mm^2 (n = 406) at 31°C and 1.87±0.01 mm^2 (n = 181) at 47°C (Figure 1).

Aligned fluid inclusions underline the successive growth steps, their shape is described as 'a rounded negative cube' according to Roedder (1984b). They have a large range of sizes from a few μm to up to 100 μm (Figure 2A and B). Thermal decrepitation of water inclusions under vacuum reveal that synthetic halite crystals contain from 0.9 to 4.6 wt% H_2O (Table 3).

δD and $\delta^{18}O$ variations of evaporating waters with temperature

Compositions of evaporated waters have been reported in a δD–$\delta^{18}O$ space along with the Meteoric Water Line (MWL) (Craig, 1961a; Dansgaard, 1964). Experiments performed without wind reveal that the data can be linearly fitted for each considered water temperature ranging from 23°C to 47°C (Figure 4). Slopes of all these linear equations are much lower (from 3.3 to 5.4) than that of the MWL close to 8. These lines constitute a set of "isotherms" for which the slope 'a' decreases with increasing water temperature according to the following hyperbolic equation:

(2) $$a = \exp\left(\frac{297.5 \pm 217.1}{T^2} + \frac{16.5 \pm 10.9}{T}\right) + 1.75 \pm 0.27 \qquad R^2 = 0.992$$

Curvature of equation (2), which is reported in Figure 5, shows that slopes of the δD–$\delta^{18}O$ evaporation trajectory equations constitute a quantitative and sensitive indicator of the surface water temperature in the range 20–35°C. For the mean slope of the MWL (a≈8), a temperature of 18°C is calculated and could correspond to the mean air temperature of tropical, subtropical and Mediterranean–like climates where most evaporation processes take place on Earth's surface. This possible explanation of the slope of the MWL is valid only at

the condition that the mean air humidity that prevailed during our experiments is close enough to the mean Earth air humidity under latitudes comprised between 0° and 40°.

δD and $\delta^{18}O$ variations of evaporating waters with wind velocity

In the same δD–δ^{18}O space, data constitute again a set of linear equations as a function of wind velocity ranging from 0 to 2.2 m.s^{-1} with slopes again much lower than that of the MWL (Figure 6). Temperature of the bath was set at 36°C, however the measured surface water temperature decreased down to 31.5°C–33.5°C in the presence of wind. Therefore, slope values have been corrected from the temperature effect described in Figure 5. All slope values were thus calculated for a temperature of 36°C that was set for the experiment performed without wind. Slopes of the four δD–δ^{18}O equations increase linearly within the considered restricted range of wind velocity according to the following equation (Figure 7):

(3) $a = 0.786(\pm 0.025)Wv - 3.872(\pm 0.035)$ $R^2 = 0.998$

The slope of equation (3) is a quantitative indicator of wind velocity at the water–air interface for a given surface water temperature up to a wind velocity of 2.2 m.s^{-1}.

δD and $\delta^{18}O$ values of water inclusions in halite

1–Synthetic halite

Hydrogen and oxygen isotope compositions of fluid inclusions from halite precipitated at 23°C, 28°C, 36°C and 47°C (Table 3) are close to the compositions of residual waters which are located at the end of corresponding isotopic trajectories of water evaporation (Figure 8). Among the three aliquots of about 100 mg that were taken from the experimental sample FI–23, aliquot FI–23–C has significantly lower δD and $\delta^{18}O$ values considering the analytical uncertainties, however the isotopic pair lies on the water evaporation trajectory (Figure 8). These results reveal that isotopic variability occurs at this sample scale and should be taken into account during the interpretation of data obtained from natural samples.

2–Natural halite

Twenty δD–$\delta^{18}O$ pairs have been determined for water inclusions in halite samples from the Realmonte mine in Sicily (Table 4). Most halite samples contain from 0.1 to 0.4 wt% of water except samples REA1 to REA3 which have 3.3 to 7.9 wt% of water. Hydrogen and oxygen isotope compositions range from -39‰ to 31‰ and from -2.5‰ to 14.6‰, respectively. It is noteworthy that the most water–rich samples have the highest δD and $\delta^{18}O$ values (Table 4). In a δD–$\delta^{18}O$ space (Figure 9), all data from the Realmonte mine plot below the MWL and can be fitted according to the following linear equation:

(4) $\delta D = 3.82(\pm 0.43)\delta^{18}O - 26.41(\pm 2.49)$ $R^2 = 0.815$

This equation represents the isotopic trajectory of water evaporation that led to the precipitation of halite during the Messinian crisis, the line intersects the MWL for δD and

$\delta^{18}O$ values of -60±10‰ and -8±1‰, respectively, thus indicating that the water source is not pure seawater (Figure 9).

3–Homogenization temperature of fluid inclusions in natural halite

Sixty-seven homogenization temperatures (Th) have been measured on sample REA–11 (Table 5). Th values range from 21.8°C to 41.5°C with a median value of 34°C and a standard deviation of 5°C (Figure 10). It is noteworthy that eighteen measurements give Th values close to 38°C (Figure 10).

5) Discussion

δD and $\delta^{18}O$ records of water inclusions in halite

Deuterium and oxygen isotope compositions of water inclusions in experimental halite match those of residual waters generated at the end of evaporative trajectories for temperatures of 23°C, 28°C, 36°C and 47°C (Figure 8). Fluid inclusions are continuously trapped during the growth of halite, however crystal growth is fast and only starts when the sursaturation of the aqueous solution with respect to halite is reached. Most fluid inclusions occur at the periphery of halite crystals because the volume of the crystal increases with the cube of the mean radius. Therefore δD and $\delta^{18}O$ values of water inclusions in halite record the last stages of water evaporation.

The water mass and fraction–dependent isotopic mass balance equations for the stagnant evaporative open water layer of our experimental apparatus, are written as following:

(5) $$\frac{dV}{dt} = -E$$

(6) $$\delta_L = \delta^* - \left(\delta^* - \delta o\right) f^m$$ (Gonfiantini, 1986)

where for equation (5), V is the volume of water in the tank, t the time and E the evaporation flux. For equation (6), δ_L is the isotopic composition of the evaporating water, δ_o is the initial composition of water, f is the fraction of remaining water and δ^* is the limiting isotopic composition of water under local conditions which is defined as following:

(7) $$\delta^* = \frac{\left(h\,\delta_A + \varepsilon\right)}{\left(h - \frac{\varepsilon}{1000}\right)}$$ (Gat and Levy, 1978; Gat, 1981)

δ_A is the isotopic composition of ambient moisture, h is the hygrometry and ε is the total isotopic fractionation summing the equilibrium fractionation component ε^* and the kinetic fractionation component ε_k that are respectively defined as following:

(8) $$\varepsilon^* = \left(\alpha_{L/V}\right).1000$$

where the thermo–dependent fractionation factor $\alpha_{L/V}$ is given by Majoube (1971),

(9) $$\varepsilon_k = (1-h).\theta.n.Cd$$

with n the turbulence parameter (n=1 for an overlying stagnant air layer; n=2/3 for a moderate wind speed and n = 0.5 for a strong wind speed), Cd is the coefficient of diffusivity between isotopes of the same element (Cd = 28.55‰ for $^{18}O/^{16}O$ and 25.115‰ for D/H) and θ describes the relationship (10) between h_N the humidity of the free atmosphere and $h_{N'}$ the humidity at the interface between the turbulently mixed sublayer and the diffusive sublayer as developed in Craig–Gordon (1965)'s linear resistance model:

(10) $$\theta = \frac{(1-h_{N'})}{(1-h_N)}$$

This model, extensively developed in Gibson (2002), describes the relationships observed between the D/H and $^{18}O/^{16}O$ ratios of the evaporating stagnant water as a function of its salinity. Evaporation experiments have been performed during either the cold or warm seasons in Lyon, France (Table 6). Therefore, both D/H and $^{18}O/^{16}O$ ratios of atmospheric vapour for each experiment were calculated by considering the seasonal variations in the isotopic compositions of meteoric waters known for the eastern part of France (IAEA database). Results of best fits for the complete set of experiment are summarized in Table 6. The experiment performed at T=36°C shows in detail how the hydrogen (δD_L) and oxygen ($\delta^{18}O_L$) isotope ratios of evaporating waters increase with salinity (Figure 11) according to the best fits obtained from equation (6):

(11) $$\delta D_L = 38.8(\pm 12.2) - \left(38.8(\pm 12.2) - (-82.5)\right) f^{(0.72\pm 0.12)} \qquad R^2 = 0.986$$

$$(12) \quad \delta^{18}O_L = 22.31(\pm 2.54) - \left(22.31(\pm 2.54) - (-10.27)\right) f^{(0.73 \pm 0.10)} \qquad R^2 = 0.991$$

It is noteworthy that these isotopic ratios can be considered to vary linearly with salinity ranging from 35 to 50 $g.L^{-1}$ as observed for marine waters of the Mediterranean (Pierre et al., 1986) and Red Seas (Craig, 1966).

Slopes of δD–$\delta^{18}O$ trajectories as a function of temperature and wind velocity

The model described above is also used to simulate the influence of water temperature or wind velocity on the slope of the δD–$\delta^{18}O$ evaporation trajectories. By combining two equations similar to (6) for both D/H and $^{18}O/^{16}O$ isotopic systems, f does not need to be known anymore, thus reducing the source of analytical uncertainties in the calculation of trajectory slope as a function of θ. For a n value of 1 that corresponds to a stagnant water layer (wind speed = 0) and a near constant θ value of 0.51±0.05 (Table 6), the decreasing slope of these isotopic trajectories with the increasing temperatures mostly results from changes in the isotopic fractionation factors. The increasing slope of the isotopic trajectories with the increasing wind velocity is explained by decreasing θ values from 0.51 to 0.36 (Table 6), which means that an increasing wind velocity is responsible for a decrease in the thickness of the diffusion sublayer above the air–water interface.

Potential applications to natural evaporites

The Messinian crisis

Some peculiar environments are suffering a negative hydrological budget which is characterized by an evaporation-precipitation ratio larger than 1. Such arid environments are illustrated by the examples of the Dead and Aral seas in the Middle East or Salt Lake in Utah, USA and the Atacama Desert in northern Chile. In the past, one of the most spectacular phenomena ever recorded was the "Messinian crisis" that took place 5.96 to 5.32 My ago (Krijgsman et al., 1999), and which symbolizes the partial drying of the Mediterranean Sea (Hsü et al., 1973 ; Clauzon et al., 1996). The Mediterranean Sea generated large deposits of evaporitic minerals such as gypsum or halite whose total mass was estimated to be $7.88.10^{18}$ kg according to Blanc (2000). Except the arid conditions, the reconstruction of climatic modes is highly delicate since the sedimentary record does not contain any carbonated or phosphatic skeletal remain of macrofossils. The absence of preserved biominerals therefore precludes the use of oxygen isotope paleothermometers as it could be expected in the presence of foraminifera, molluscs or fish teeth. Messinian halite deposits from Sicily were preserved from aerial exposures and post-depositional fluid–mineral interactions (Lugli et al., 1999), thus they most likely preserved their original water inclusions trapped during crystal growth.

Source of water and precipitation temperature of halite deposits in Sicily

Slopes of δD–$\delta^{18}O$ evaporation trajectories have been shown to be highly sensitive to both water temperature and wind speed. These slopes can be determined in the past if δD–

$\delta^{18}O$ pairs of water inclusions allow the determination of a high–quality linear regression. In that case, the intersection with the Meteoric Water Line will provide the isotopic compositions of the water source. Comparison between the temperature deduced from microthermometric data and from the slope of the δD–$\delta^{18}O$ evaporation trajectory allow the estimation of wind velocity by combining equations (2) and (3).

Hydrogen and oxygen isotope compositions of Messinian halite samples from the Realmonte mine, Sicily, define a linear trend (R^2 = 0.815) whose extrapolation until intersection with the MWL allows determining the water source composition with δD and $\delta^{18}O$ values of -60±10‰ and -8.5±1.5‰ (Figure 9), respectively. These low isotopic values mean that the source water that precipitated halite was Mediterranean Sea Water (MSW) mixed with a significant fraction of fresh waters. The composition of the fresh water end–member can be estimated from that of Alpine rivers that discharge in the western Mediterranean Basin. Indeed, Rhône, Danube and Pô rivers, for example, have δD and $\delta^{18}O$ values close to -80‰ and -10‰, respectively. However, during the Messinian crisis, corrections must be applied to isotopic values (about -2.5‰ and -0.3‰ per 100 m) because of an altitude effect (Bortolami, 1978) resulting from a low–stand sea–level which was about 1000 m to 2000 m lower than now (Clauzon, 1982; Gorini et al., 2005; Babault et al. 2006). Consequently, the δD and $\delta^{18}O$ values of fluvial discharges from Pyrenean, Alpine and Atlas mountains could have been as low as -120‰ and -16‰, respectively. Considering this possible range of values for the isotopic fresh water end–member and a seawater end–member similar to present–days (δD = 8‰ and $\delta^{18}O$ = 1.6‰), the MSW that generated the Messinian halite deposits was mixed with at least 50% to 75% of freshwater. This mass balance calculation supports the hypothesis that river water fluxes played a major role in the hydrological budget of the western Mediterranean Sea as it was already deduced from

hydrological budget modelling (Flecker et al., 2002; Gladstone et al., 2007; Gargani et al., 2008).

According to equation (2), the slope of the regression line defined by the isotopic compositions of water inclusions in natural halite from the Messinian deposits of Sicily indicates precipitation temperatures of 34^{+10}_{-4}°C that match the homogenization temperatures obtained by microthermometry (median = 34±5°C). Therefore, the similarity between the measured and experimental slopes of the $\delta D–\delta^{18}O$ evaporation trajectories suggest that the effect of wind was negligible during the genesis of these halite deposits. However, large uncertainties lead to consider that the mean apparent isotopic temperature is lower than the maximum value of 41±1°C recorded by fluid inclusion microthermometric data. The apparent difference of 7±1°C can be translated into a wind velocity of about 0.3 $m.s^{-1}$ responsible for an increasing of the evaporation trajectory slope. This calculation, however, also depends on the past values of relative air humidity and isotopic compositions of atmospheric moisture that could have been different from those prevailing during our experiments. Consequently, at the first order, we consider that the wind effect was negligible regarding the good agreement between microthermometric data and isotopic temperatures.

These temperatures could seem very high for surface water; however Roberts and Spencer (1995) and Lowenstein (1998) already measured similar temperatures in halite fluid inclusions of salted lakes in the Death Valley, California. It must be kept in mind that most of evaporation processes should take place during the sunny and hottest hours of the day. Consequently, such air–water interface temperatures cannot be compared to that deduced from the oxygen isotope compositions of carbonate or phosphate–secreting aquatic invertebrates.

6) Conclusions

Experimental precipitation of halite has shown that the hydrogen and oxygen isotope compositions of their water inclusions record the isotopic trajectories of water evaporation. Combination of microthermometric data with hydrogen and oxygen isotope compositions of water inclusions in halite potentially leads to the estimation of both temperature and wind velocity at the water–air interface during crystal growth. The application of this method to the Messinian halite deposits in Sicily reveals surface water temperatures of at least 35°C along with a negligible wind velocity effect. In addition, hydrogen and oxygen isotope compositions of these water inclusions define a linear trend crosscutting the Meteoric Water Line at δD and $\delta^{18}O$ values indicating that the water source that generated the Messinian halite deposits contained at least 50% to 75% of freshwater mixed with seawater. This result suggests that river water fluxes from Pyrenean, Alpine and Atlas mountains, played a major role in both the hydrological budget of the western Mediterranean Sea and the precipitation of the huge salt deposits during the Messinian crisis.

Acknowledgements – The authors thank G. Broillet who made the thick sections in halite, M. Dubois for his advice in the domain of microthermometric analyses, F. Fourel and L. Simon for their assistance in the stable isotope laboratory. Funding of this project was ensured by both French CNRS and IUF (CL).

References

Babault J., Loget N., Van den Driessche J., Castelltort S., Bonnet S. and Day Ph. (2006) Did the Ebro basin connect to the Mediterranean before the Messinian salinity crisis? *Geomorphology* **81**, 155-165.

Blanc, P.-L. (2000) Of sills and straits: a quantitative assessment of the Messinian Salinity Crisis. *Deep-Sea Res*. **47**, 1429– 1460.

Blisniuk P.M. and Stern L.A. (2005) Stable isotope paleoaltimetry: A critical review. *Am. J. Sci.* **305**, 1033-1074.

Bortolami G.C., Ricci B., Susella G.F. and Zuppi G.M. (1978) Isotope hydrology of the Val Corsaglia Maritime Alps, Piedmont, Italy. In *Isotopes in Hydrology* International Atomic Energy Agency, Vienna. pp 327-350.

Clauzon G. (1982) Le canyon messinien du Rhône: une preuve décisive du dessicated deep-basin model (Hsü, Cita et Ryan, 1973). *Bull. Soc. géol. France* **24**, 597–610.

Clauzon G., Suc J.-P., Gautier F., Berger A. and Loutre M.-F. (1996) Alternate interpretation of the Messinian salinity crisis: Controversy resolved? *Geology* **24**, 363-366.

Craig H. (1961a) Isotopic variations in meteoric waters. *Science* **133**, 1702-1703.

Craig H. (1966) Isotopic composition and origin of the Red Sea and Salton Sea geothermal brines. *Science* **54**, 1544-1547.

Craig H. and Gordon L.I. (1965) Deuterium and oxygen-18 variations in the ocean and the marine atmosphere. In *Stable Isotopes in Oceanographic Studies and Paleotemperatures* (ed. E. Tongiorgi.). Lab. Geol. Nucl. pp. 9-130.

Dansgaard W. (1964) Stable isotopes in precipitation. *Tellus* **16**, 436-468.

Dennis P.F., Rowe P.J. and Atkinson T.C (2001) The recovery and isotopic measurement of water from fluid inclusions in speleothems. *Geochim. Cosmochim. Acta* **65**, 871-884.

Decima A. and Wezel F.C. (1973) Late Miocene evaporites of the Central Sicilian Basin. In *Initial Reports of the Deep Sea Drilling Project, Leg 42 (1)* (eds. Ryan W.B.F. and Hsü K.J). Government Printing Office, Washington D.C., U.S. pp 1234-1240

Flecker R., DeVilliers S. and Ellam R.M. (2002) Modelling the effect of evaporation on th Salinity–$^{87}Sr/^{86}Sr$ relationship in modern and ancient marginal–marine systems : the Mediterranean Messinian Salinity Crisis. *Earth Planet. Sci. Lett.* **3**, 258-266.

Gargani J., Moretti I. and Letousey J. (2008) Evaporite accumulation during the Messinian Salinity Crisis: The Suez Rift case. *Geoph. Res. Lett.* **35**, L02401.

Gat J.R. (1981) Lakes. In: *Stable Isotope Hydrology; Deuterium and Oxygen-18 in the Water Cycle* (eds, J.R. Gat and R. Gonfiantini). IAEA Techn. Rep. Ser. 210. pp 203-221.

Gat J.R. and Levy Y. (1978) Isotope hydrology of inland sabkhas in the Bardawil area. *Sinai. Limnol. Oceanog.* **23**, 841-850.

Gibson J.J. (2002) Short-term evaporation and water budget comparisons in shallowArtic lakes using non-steady isotope mass balance. *J. Hydrol.* **264**, 242-261.

Gladstone R., Flecker R., Valdes P., Lunt D. and Markwick P. (2007) The Mediterranean hydrologic budget from a Late Miocene global climate simulation. *Palaeogeography, Palaeoclimatology, Palaeoecology* **251**, 254-267.

Gonfiantini R. (1986) Environmental isotopes in lake studies. In *Handbook of Environmental Isotope Geochemistry* (eds. P. Fritz and J.C. Fontes). Vol. 3, Elsevier. pp. 113-168.

Gorini C., Lofi J., Duvail C., Dos Reis A.T., Guennoc P., Lestrat P. and Mauffret A. (2005) The Late Messinian salinity crisis and Late Miocene tectonism: Interaction and consequences on the physiography and post-rift evolution of the Gulf of Lions margin. *Mar. Petrol. Geol.* **22**, 695–712.

Hsü K. J. , Ryan W. B. F. and Cita M. B. (1973) Late Miocene desiccation of the Mediterranean. *Nature* **242**, 240–244.

Kishima N. and Sakai H. (1980) O-18 and deuterium determination on a single water sample of a few milligrams. *Anal. Chem.* **52**, 356-358.

Krijgsman W., Hiigeni F.J, Raffi I., Sierro F.J. and Wilson D.S. (1999) Chronology, causes and progression of the Messinian salinity crisis. *Nature* **400** (6745), 652–655.

Lécuyer C., Gardien V., Rigaudier T., Martineau F., Fourel F. and Cros A. (2009) Oxygen isotope fractionation and equilibration kinetics between CO_2 and H_2O as a function of salinity of aqueous solutions. *Chem. Geol.*, **264**, 221-233.

Lowenstein T.K., Li J. and Brown C.N. (1998) Paleotemperatures from fluid inclusions in halite : method verification and a 100,00 year paleotemperature record, Death Valley, CA. *Chem. Geol.*, **150**, 223-245.

Lugli S., Schreiber B.C. and Triberti B. (1999) Giant Polygons in the Realmonte salt (Agrigento, Sicily). *J. Sed. Res.* **69**, 764-771.

Majoube M. (1971) Fractionnement en oxygene-18 et en deuterium entre l'eau et sa vapeur. *J. Chim. Phys.*, **68**, 1423-1436.

Matthews A., Ayalon A and Bar-Matthews M. (2000). D/H ratios of fluid inclusions of Soreq cave (Israel) speleothems as a guide to the Eastern Mediterranean Meteoric Line relationships in the last 120 ky. *Chem. Geol.* **166**: 183-191.

Mulch A. and Chamberlain C.P. (2007) Paleoaltimetry: geochemical and thermodynamic approaches. *Rev. Min. Geochim.* **66**, 89-118.

O'Neil J.R. and Adami L.H. (1969) The oxygen isotope partition function ratio of water and the structure of liquid water. *J. Phys. Chem.* **73**, 1553-1558.

Pierre C., Vergnaud-Grazzini C., Thunron D. and Saliege J.F. (1986) Compositions isotopiques de l'oxygene et du carbone des masses d'eau en Mediterranee. *Mem. Soc. Geol. It. Al.* **36**, 165-174.

Roberts S.M. and Spencer R.J. (1995) Paleotemperatures preserved in fluid inclusions in halite. *Geochim. Cosmochim. Acta* **59**, 3929-3942.

Roedder E. (1984b) The fluids in salt. *The American Mineralogist* **69**, 413-419.

Schwarcz H.P., Harmon R.S., Thompson P. and Ford D.C. (1976) Stable isotope studies of fluid inclusions in speleothems and their paleoclimatic significance. *Geochim. Cosmochim. Acta* **40**, 657-665.

Table captions

Table 1: Temperature effects on δD and $\delta^{18}O$ variations of evaporated waters in the case of a null wind velocity and relatively constant hygrometry. Temperatures of water range from 23°C to 47°C. These isotopic compositions are used in order to draw the δD–$\delta^{18}O$ trajectories shown in Figure 4.

Table 2: Wind effect on δD and $\delta^{18}O$ variations of evaporated waters in the case of a constant bath temperature (36°C). Note the wind velocity effect on the decrease of the surface water temperature.

Table 3: δD and $\delta^{18}O$ values of water inclusions in synthetic halite precipitated from 23°C to 47°C without wind.

Table 4: δ D and $\delta^{18}O$ values of water inclusions in natural Messinian halite from the Realmonte mine, Sicily.

Table 5: Homogenization temperatures of water inclusions from a Messinian halite sample of the Realmonte mine, Sicily.

Table 6: Results of parameters modelling of the hydrogen and oxygen isotope compositions of evaporating waters by using the fraction–dependent developed by Gonfiantini (1986). δ_A, the hydrogen and oxygen isotope compositions of ambient moisture, were set at -130‰ and -17.5‰, respectively, except for experiments performed during the summer season during

which values were estimated to be -110‰ and -15‰, respectively. The turbulence parameter, n, was set at 1 for all the calculations. See text for detailed explanations.

Figure captions

Figure 1: Photographs of synthetic halite crystals which grew at three different temperatures of 25°C (A); 29.5°C (B) and 47°C (C). The mean size of isolated synthetic crystals decreases with increasing temperature.

Figure 2: Synthetic halite crystals hosting water inclusions.

A: Photomicrograph of primary fluid inclusions with cubic shapes. Some inclusions such as the one at the bottom of the picture contain a large bubble of gas.

B. Densely packed band of primary fluid inclusions outlying the growth stages of the halite crystal.

C. NaCl "hopper" crystal which grew at a temperature of 25°C.

Figure 3: Messinian natural halite crystals (Realmonte mine, Sicily) hosting water inclusions.

A. A fragment of chevron structure with free–vapour bubble inclusions at room temperature.

B. Relic of chevron structure with single-phase fluid inclusions.

Figure 4: δD and $\delta^{18}O$ variations of evaporated waters as a function of water temperatures ranging from 23°C to 47°C. Paired data constitute a set of linear equations which all slopes are significantly lower than that of the Meteoric Water Line (MWL). All the lines are rooted in the MWL at values corresponding to the composition of the deionized water used for all

the experiments. Small variations in the δD and $\delta^{18}O$ values result from seasonal changes in the composition of the water originating from the Rhône river, Lyon, France. Linear regressions for each evaporation trajectory are the following: T=23°C: $\delta D=5.37(\pm0.30)\delta^{18}O-31.39(\pm2.20)$ ($R^2=0.991$); T=26.5°C: $\delta D=4.57(\pm0.18)\ \delta^{18}O-36.28(\pm1.49)$ ($R^2=0.994$). T=28°C: $\delta D=4.31(\pm0.13)\ \delta^{18}O-39.17(\pm1.48)$ ($R^2=0.997$). T=29.5°C: $\delta D=4.25(\pm0.22)\delta^{18}O-38.81(\pm2.32)$ ($R^2=0.992$). T=36°C: $\delta D=3.83(\pm0.07)\ \delta^{18}O-43.57(\pm0.77)$ ($R^2=0.996$). T=47°C: $\delta D=3.33(\pm0.02)\delta^{18}O-39.57(\pm0.30)$ ($R^2=0.999$).

Figure 5: Variations in the slope of the $\delta D-\delta^{18}O$ equations of Figure 4 as a function of water temperature. Data are described by a hyperbolic regression according to equation (2). Note that extrapolation to an infinite slope indicates a water temperature close to the melting point of ice.

Figure 6: δD and $\delta^{18}O$ variations of evaporated waters as a function of wind velocity for a constant water temperature of 36°C. Paired data constitute a set of linear equations which all slopes are significantly lower than that of the Meteoric Water Line (MWL). Linear regressions for each evaporation trajectory are the following: Wv=0 $m.s^{-1}$: $\delta D=3.85(\pm0.04)\delta^{18}O-42.34(\pm0.54)$ ($R^2=0.998$); Wv=0.8 $m.s^{-1}$: $\delta D=4.06(\pm0.08)\ \delta^{18}O-38.98(\pm0.76)$ ($R^2=0.997$). Wv=1.5 $m.s^{-1}$: $\delta D=4.85(\pm0.17)\ \delta^{18}O-32.37(\pm1.07)$ ($R^2=0.988$). Wv=2.2 $m.s^{-1}$: $\delta D=5.22(\pm0.16)\delta^{18}O-26.83(\pm1.00)$ ($R^2=0.992$).

Figure 7: Variations in the slope of the $\delta D-\delta^{18}O$ equations of Figure 6 as a function of wind velocity at a constant water temperature of 36°C. Data are described by a linear regression according to equation (3). Wind has been responsible for a decrease in surface water

temperature (Table 2), thus the slopes values have been corrected from the temperature effect described in Figure 5.

Figure 8: δD and $\delta^{18}O$ values of fluid inclusions from synthetic halite precipitated from 23°C to 47°C are reported along with the corresponding δD–$\delta^{18}O$ trajectories of evaporated waters.

Figure 9: δD and $\delta^{18}O$ values of fluid inclusions from natural halite (Realmonte mine, Sicily) reported along with the Meteoric Water Line (MWL) and the Mediterranean Sea Water (MSW). Paired data are described by a linear regression whose slope indicates an apparent isotopic temperature of 34^{+10}_{-4}°C assuming a null wind velocity. This temperature matches the mean homogenization temperature determined by microthermometry (Figure 10). The regression line: δD =3.82(±0.43)$\delta^{18}O$-26.41(±2.49) (R^2=0.815) intersects the MWL at δD and $\delta^{18}O$ values of -60(±10)‰ and -8(±2)‰, respectively, thus indicating that the water source of the Sicilian evaporites was dominated by freshwater mixed with seawater. Dashed lines define the error envelope at a 95% confidence level.

Figure 10: Frequency histogram of homogenization temperatures of water inclusions from a Messinian halite sample (REA-11) of Realmonte mine, Sicily. The mean value is 34±5°C while maximum values reach up to 42°C.

Figure 11: Variations in δD and $\delta^{18}O$ values of evaporating waters as a function of salinity for a temperature of 36°C. Data are described by two power laws which result from the fraction–dependent model developed by Gonfiantini (1986). The best fits correspond to equations (11) and (12).

A

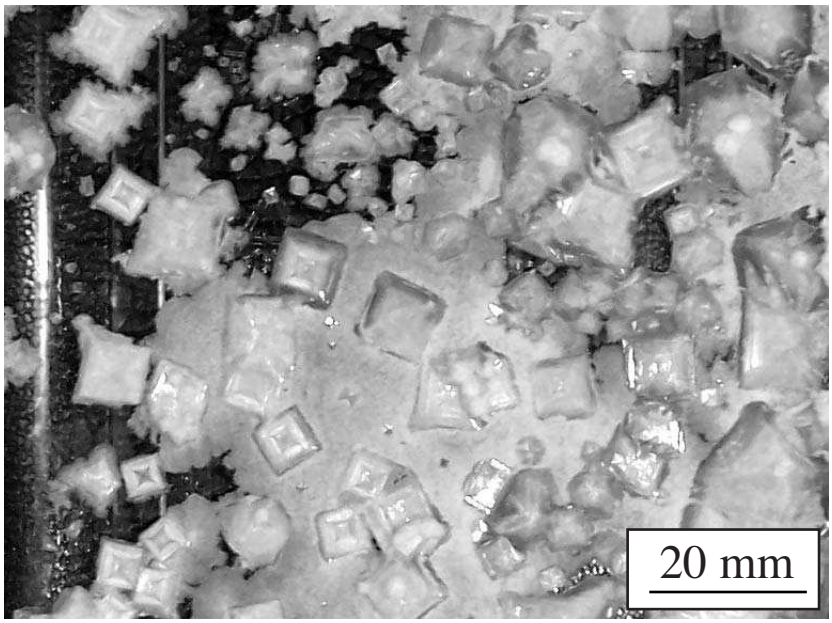

B

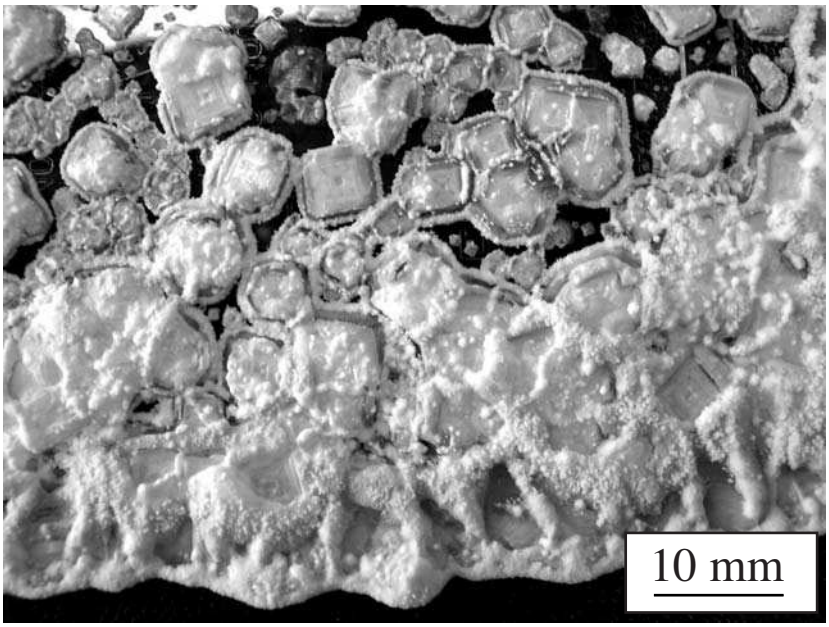

C

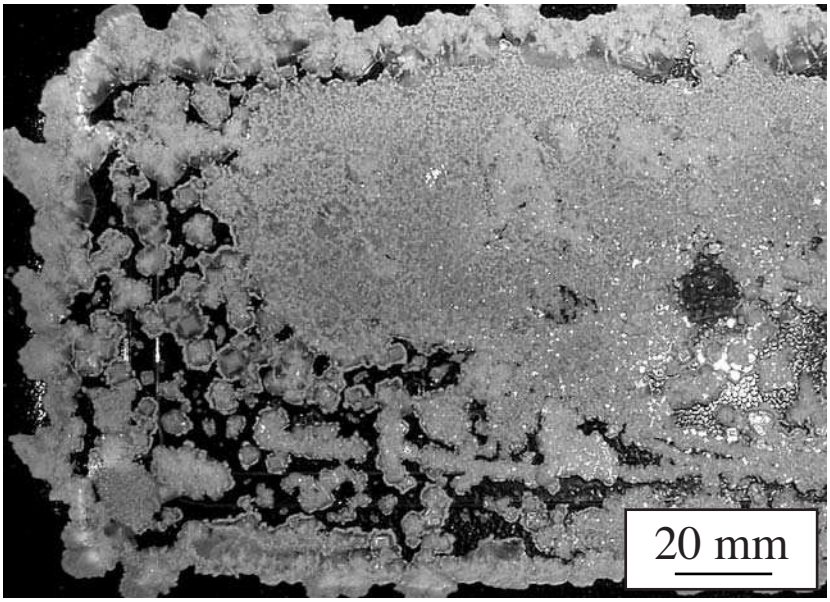

FIG. 1 – Photographs of synthetic halite crystals which grew at three different temperatures of 25°C (A); 29.5°C (B) and 47°C (C). The mean size of isolated synthetic crystals decreases with increasing temperature.

A

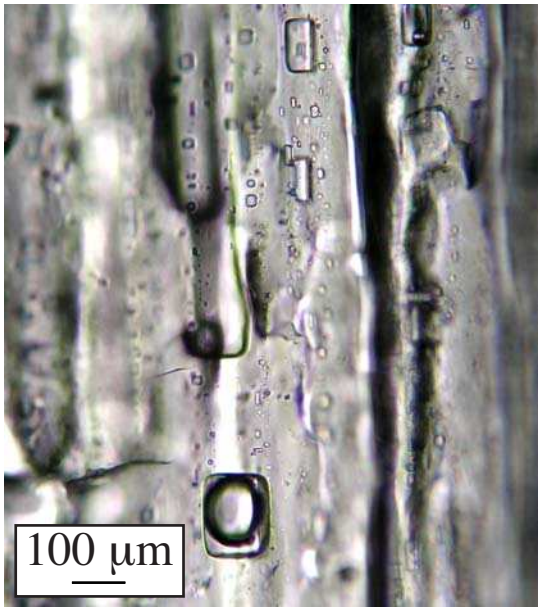

B

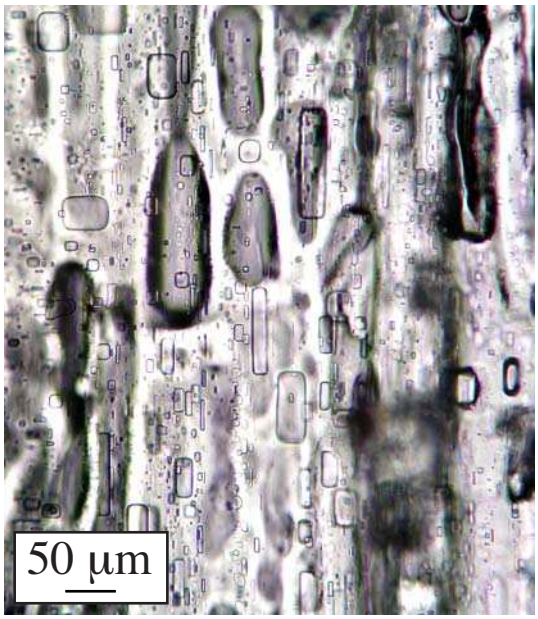

C

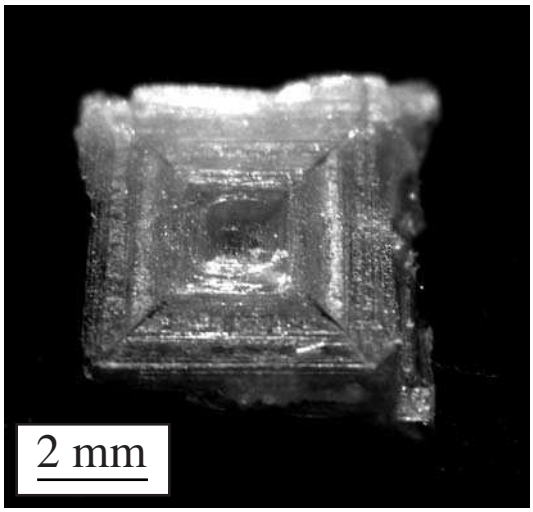

FIG. 2 – Synthetic halite crystals hosting water inclusions. A: Photomicrograph of primary fluid inclusions with cubic shapes. Some inclusions such as the one at the bottom of the picture contain a large bubble of gas ; B. Densely packed band of primary fluid inclusions outlying the growth stages of the halite crystal ; C. NaCl "hopper" crystal which grew at a temperature of 25°C.

A

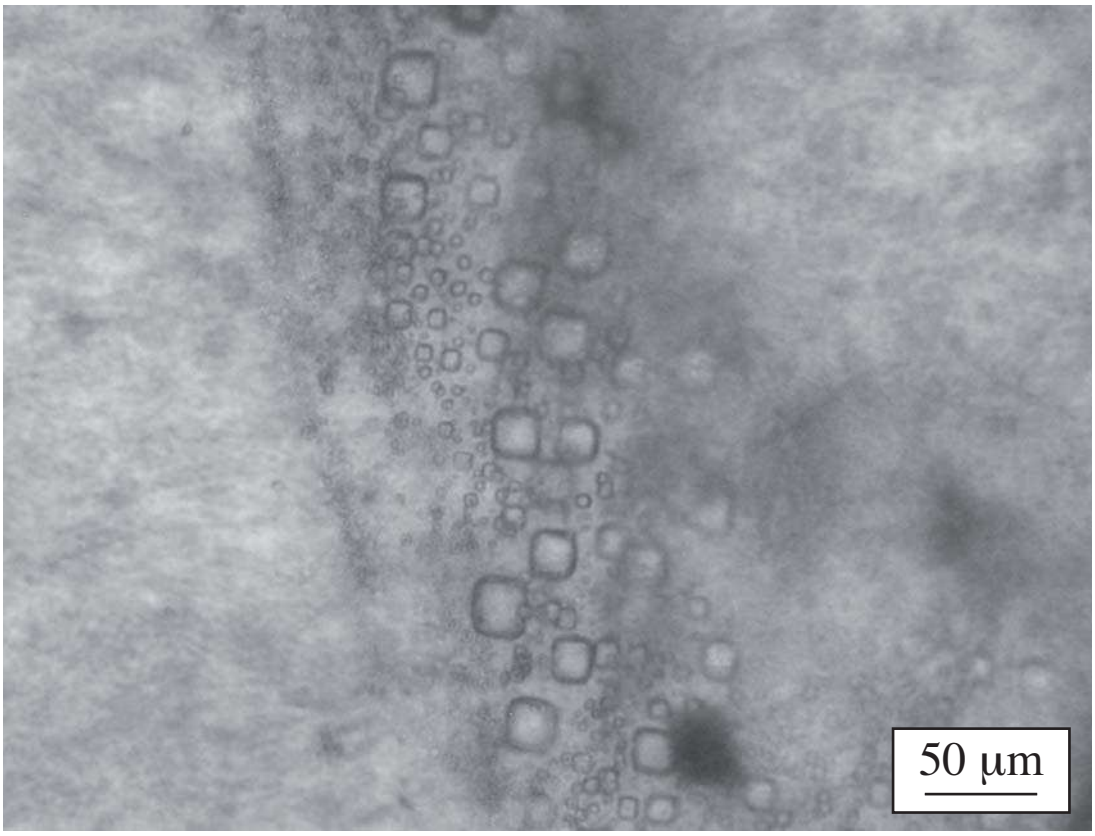

B

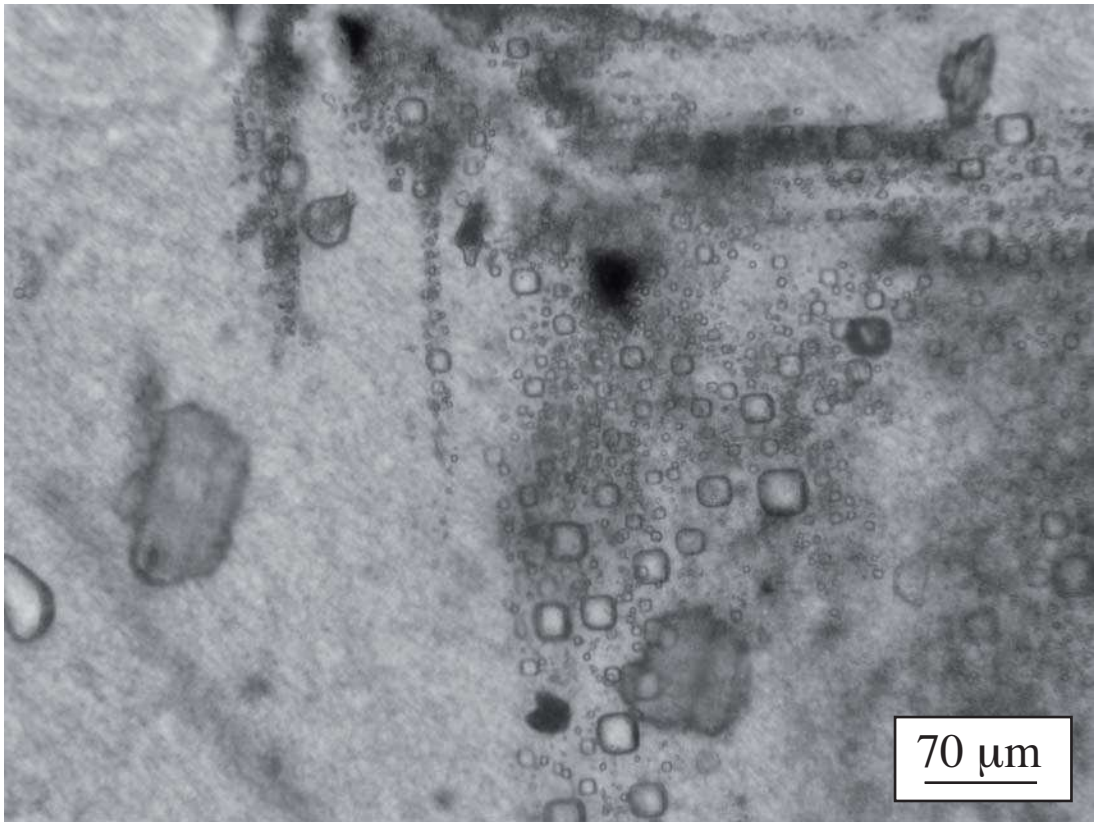

FIG. 3 – Messinian natural halite crystals (Realmonte mine, Sicily) hosting water inclusions ; A. A fragment of chevron structure with free–vapour bubble inclusions at room temperature ; B. Relic of chevron structure with single-phase fluid inclusions.

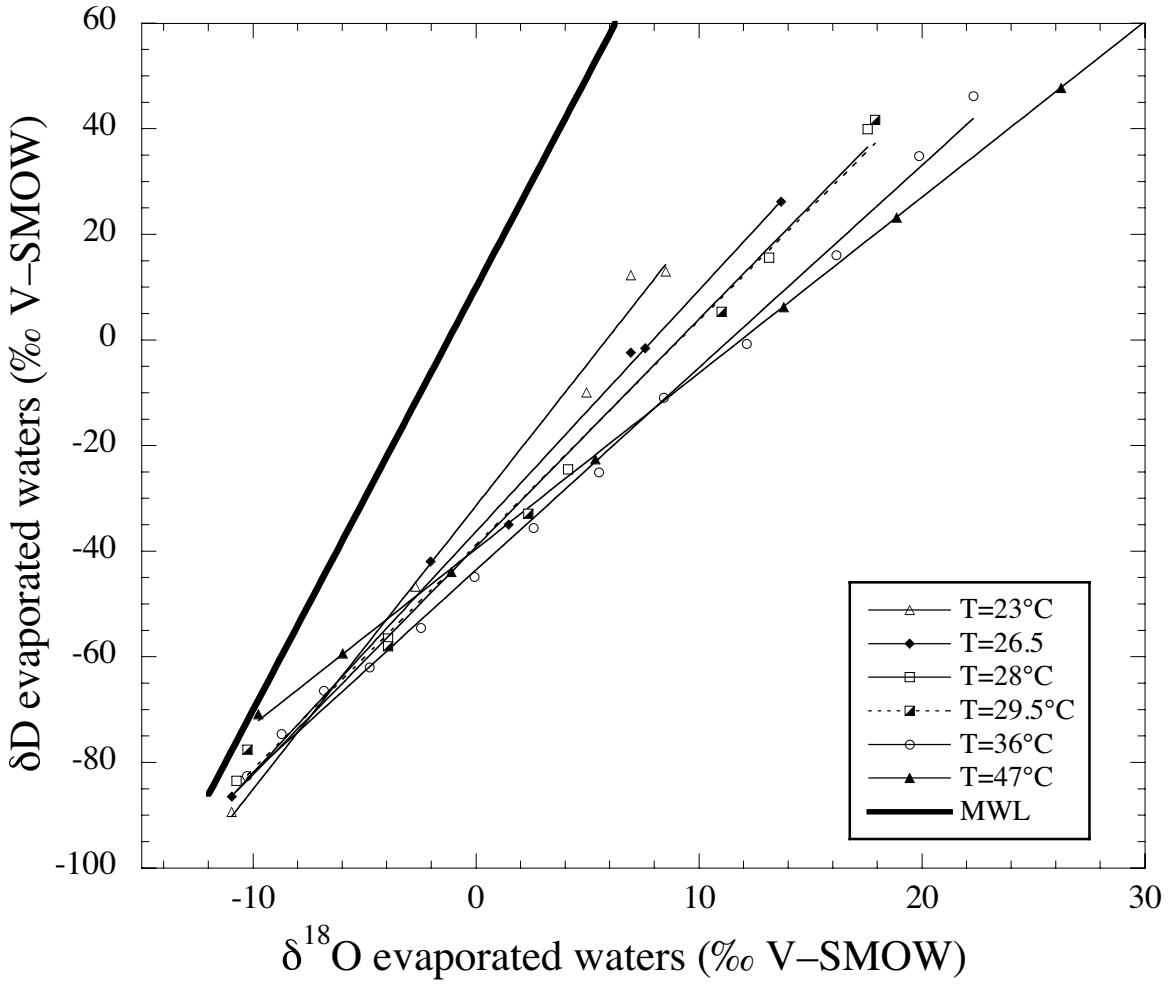

FIG. 4 – δD and $\delta^{18}O$ variations of evaporated waters as a function of water temperatures ranging from 23°C to 47°C. Paired data constitute a set of linear equations which all slopes are significantly lower than that of the Meteoric Water Line (MWL). All the lines are rooted in the MWL at values corresponding to the composition of the deionized water used for all the experiments. Small variations in the δD and $\delta^{18}O$ values result from seasonal changes in the composition of the water originating from the Rhône river, Lyon, France. Linear regressions for each evaporation trajectory are the following:

T=23°C: $\delta D=5.37(\pm0.30)\delta^{18}O-31.39(\pm2.20)$ ($R^2=0.991$)
T=26.5°C: $\delta D=4.57(\pm0.18)\delta^{18}O-36.28(\pm1.49)$ ($R^2=0.994$)
T=28°C: $\delta D=4.31(\pm0.13)\delta^{18}O-39.17(\pm1.48)$ ($R^2=0.997$)
T=29.5°C: $\delta D=4.25(\pm0.22)\delta^{18}O-38.81(\pm2.32)$ ($R^2=0.992$)
T=36°C: $\delta D=3.83(\pm0.07)\delta^{18}O-43.57(\pm0.77)$ ($R^2=0.996$)
T=47°C: $\delta D=3.33(\pm0.02)\delta^{18}O-39.57(\pm0.30)$ ($R^2=0.999$).

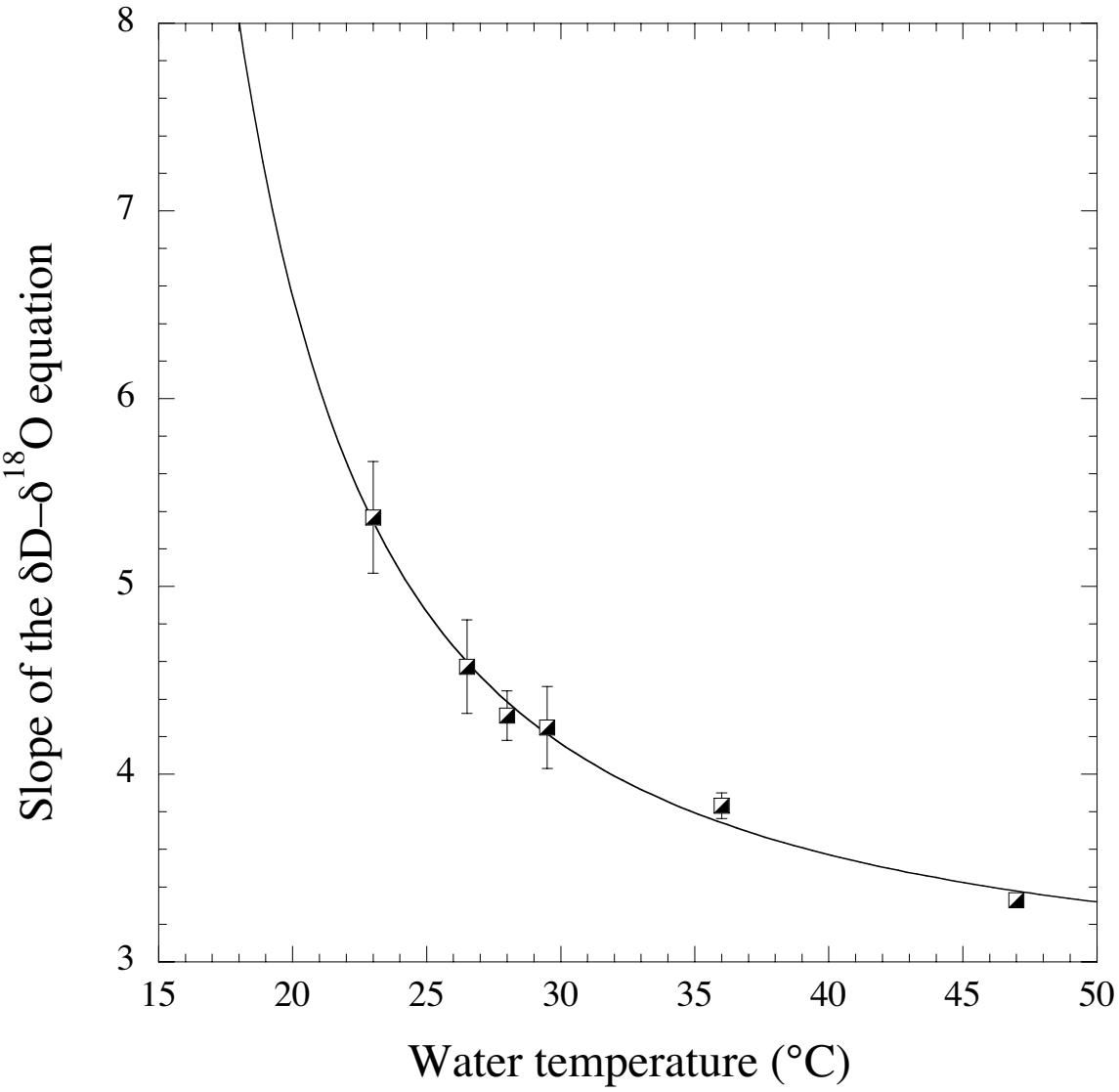

FIG. 5 – Variations in the slope of the δD–$\delta^{18}O$ equations of Figure 4 as a function of water temperature. Data are described by a hyperbolic regression according to equation (2). Note that extrapolation to an infinite slope indicates a water temperature close to the melting point of ice.

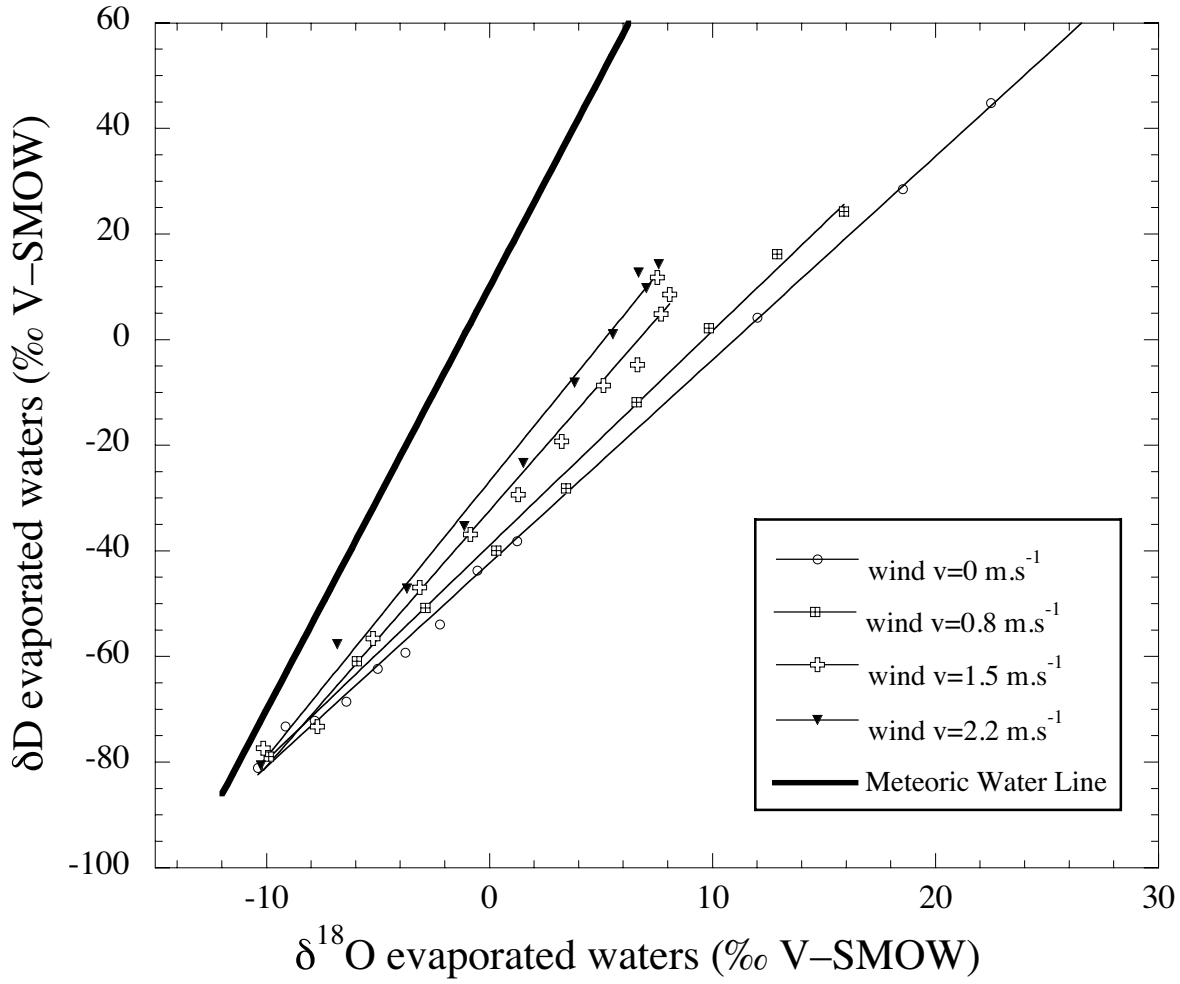

FIG. 6 – δD and $\delta^{18}O$ variations of evaporated waters as a function of wind velocity for a constant water temperature of 36°C. Paired data constitute a set of linear equations which all slopes are significantly lower than that of the Meteoric Water Line (MWL). Linear regressions for each evaporation trajectory are the following:
Wv=0 m.s-1: $\delta D=3.85(\pm0.04)\delta^{18}O-42.34(\pm0.54)$ ($R^2=0.998$)
Wv=0.8 m.s-1: $\delta D=4.06(\pm0.08)\delta^{18}O-38.98(\pm0.76)$ ($R^2=0.997$)
Wv=1.5 m.s-1: $\delta D=4.85(\pm0.17)\delta^{18}O-32.37(\pm1.07)$ ($R^2=0.988$)
Wv=2.2 m.s-1: $\delta D=5.22(\pm0.16)\delta^{18}O-26.83(\pm1.00)$ ($R^2=0.992$)

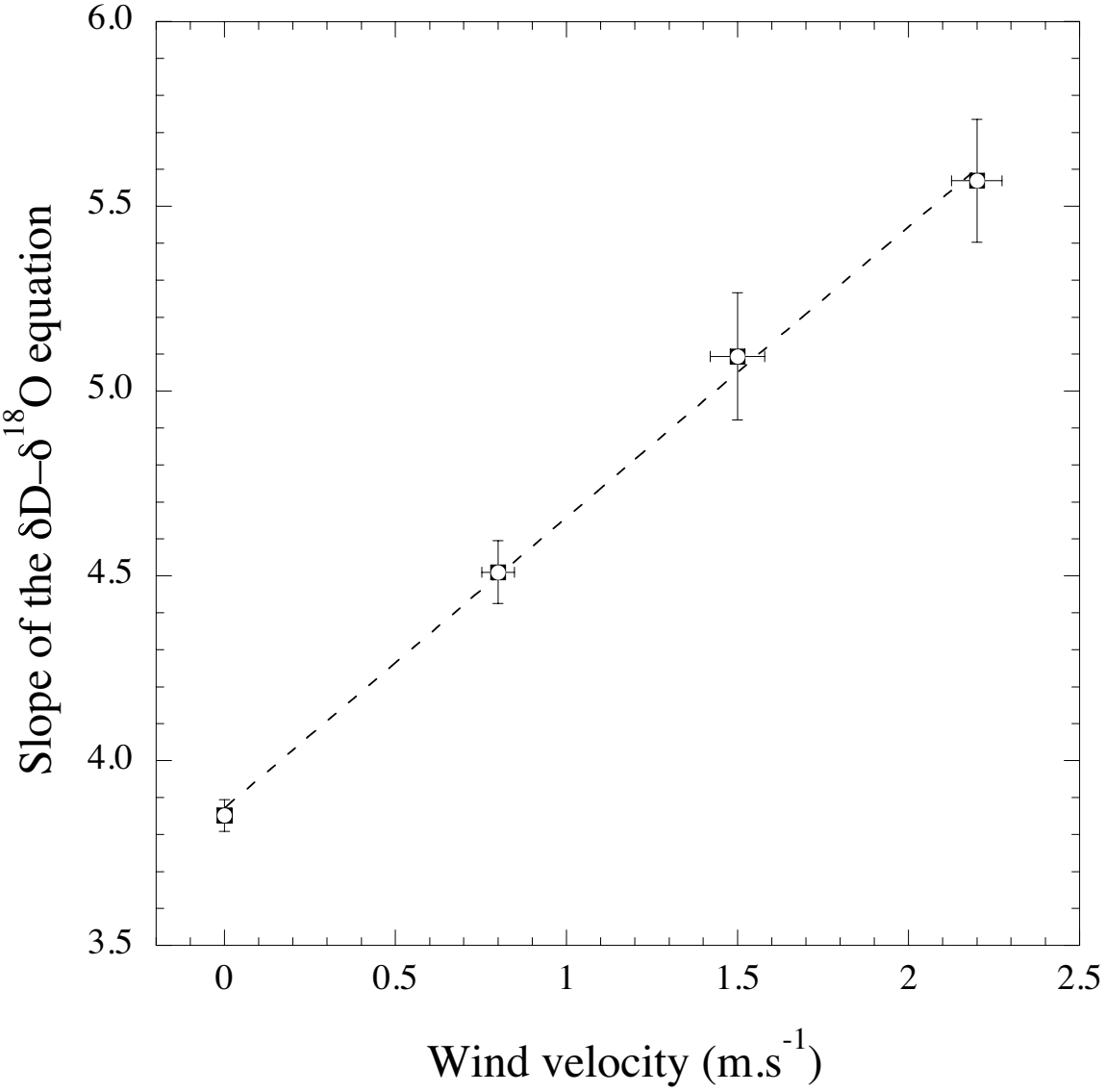

FIG. 7 – Variations in the slope of the $\delta D–\delta^{18}O$ equations of Figure 6 as a function of wind velocity at a constant water temperature of 36°C. Data are described by a linear regression according to equation (3). Wind has been responsible for a decrease in surface water temperature (Table 2), thus the slopes values have been corrected from the temperature effect described in Figure 5.

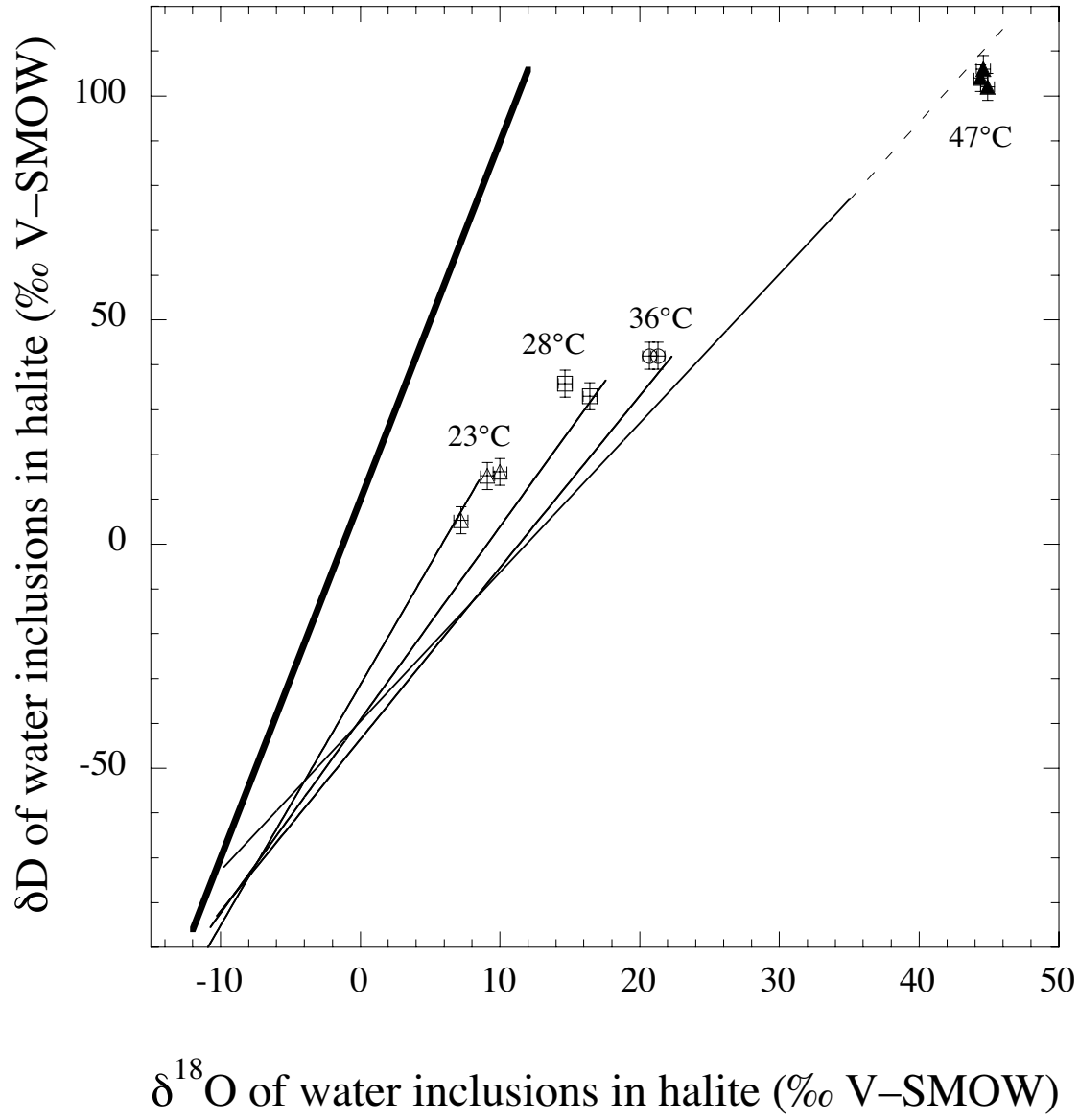

FIG. 8 – δD and $\delta^{18}O$ values of fluid inclusions from synthetic halite precipitated from 23°C to 47°C are reported along with the corresponding δD–$\delta^{18}O$ trajectories of evaporated waters.

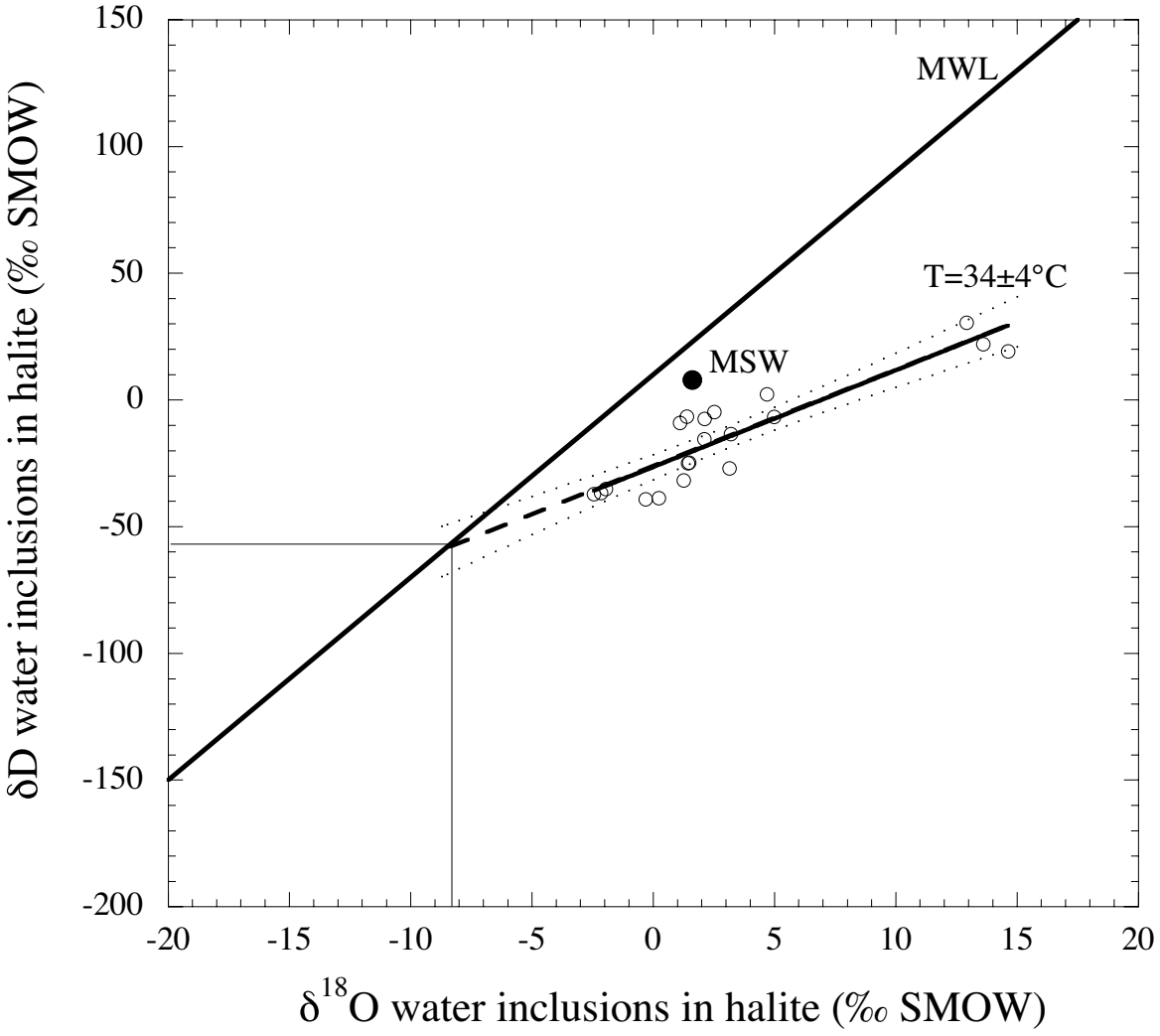

FIG. 9 – δD and $\delta^{18}O$ values of fluid inclusions from natural halite (Realmonte mine, Sicily) reported along with the Meteoric Water Line (MWL) and the Mediterranean Sea Water (MSW). Paired data are described by a linear regression whose slope indicates an apparent isotopic temperature of ˚C assuming a null wind velocity. This temperature matches the mean homogenization temperature determined by microthermometry (Figure 10). The regression line: $\delta D = 3.82(\pm 0.43)\delta^{18}O - 26.41(\pm 2.49)$ ($R^2=0.815$) intersects the MWL at δD and $\delta^{18}O$ values of -60(±10)‰ and -8(±2)‰, respectively, thus indicating that the water source of the Sicilian evaporites was dominated by freshwater mixed with seawater. Dashed lines define the error envelope at a 95% confidence level.

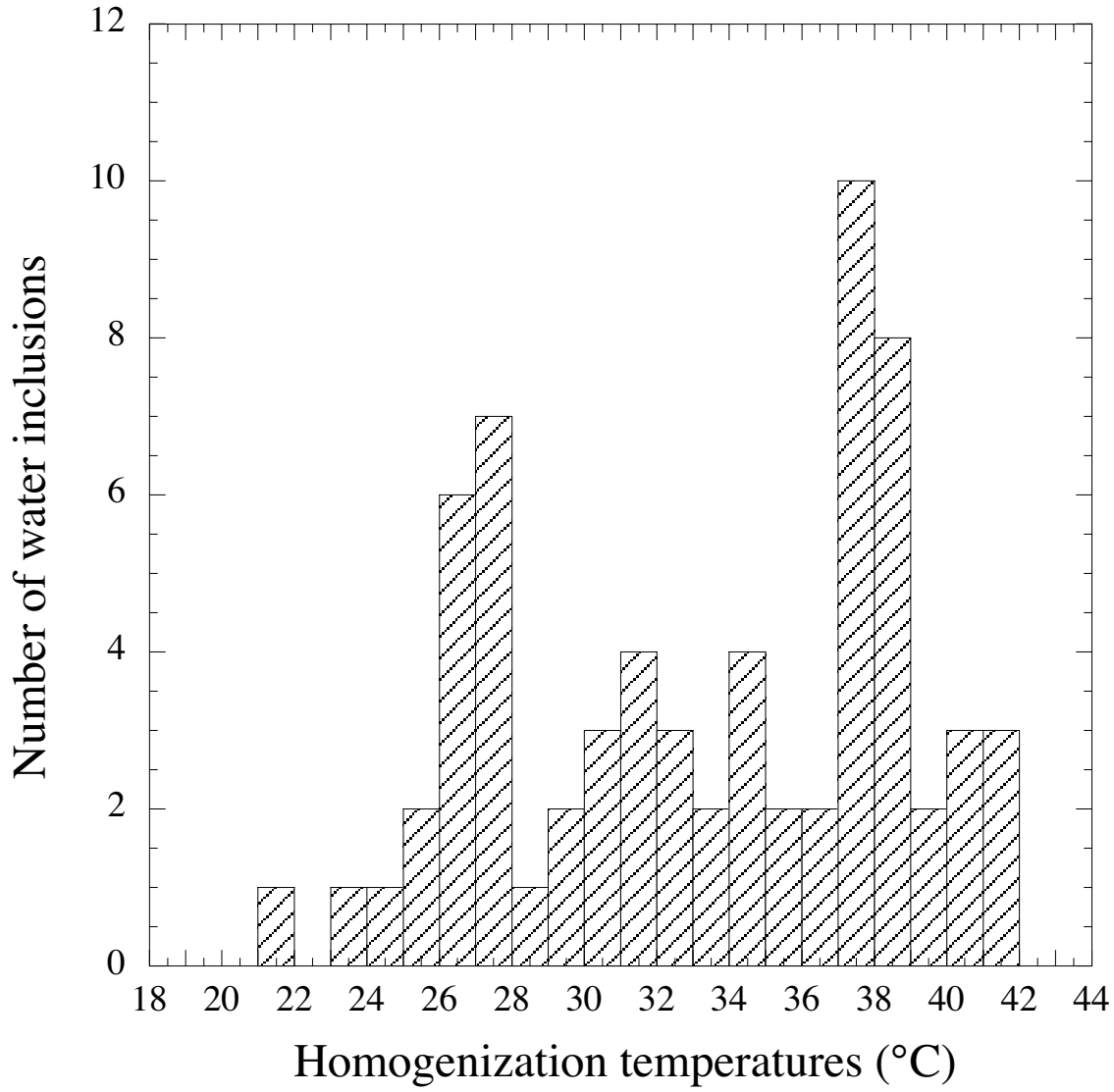

FIG. 10 – Frequency histogram of homogenization temperatures of water inclusions from a Messinian halite sample (REA-11) of Realmonte mine, Sicily. The mean value is 34±5°C while maximum values reach up to 42°C.

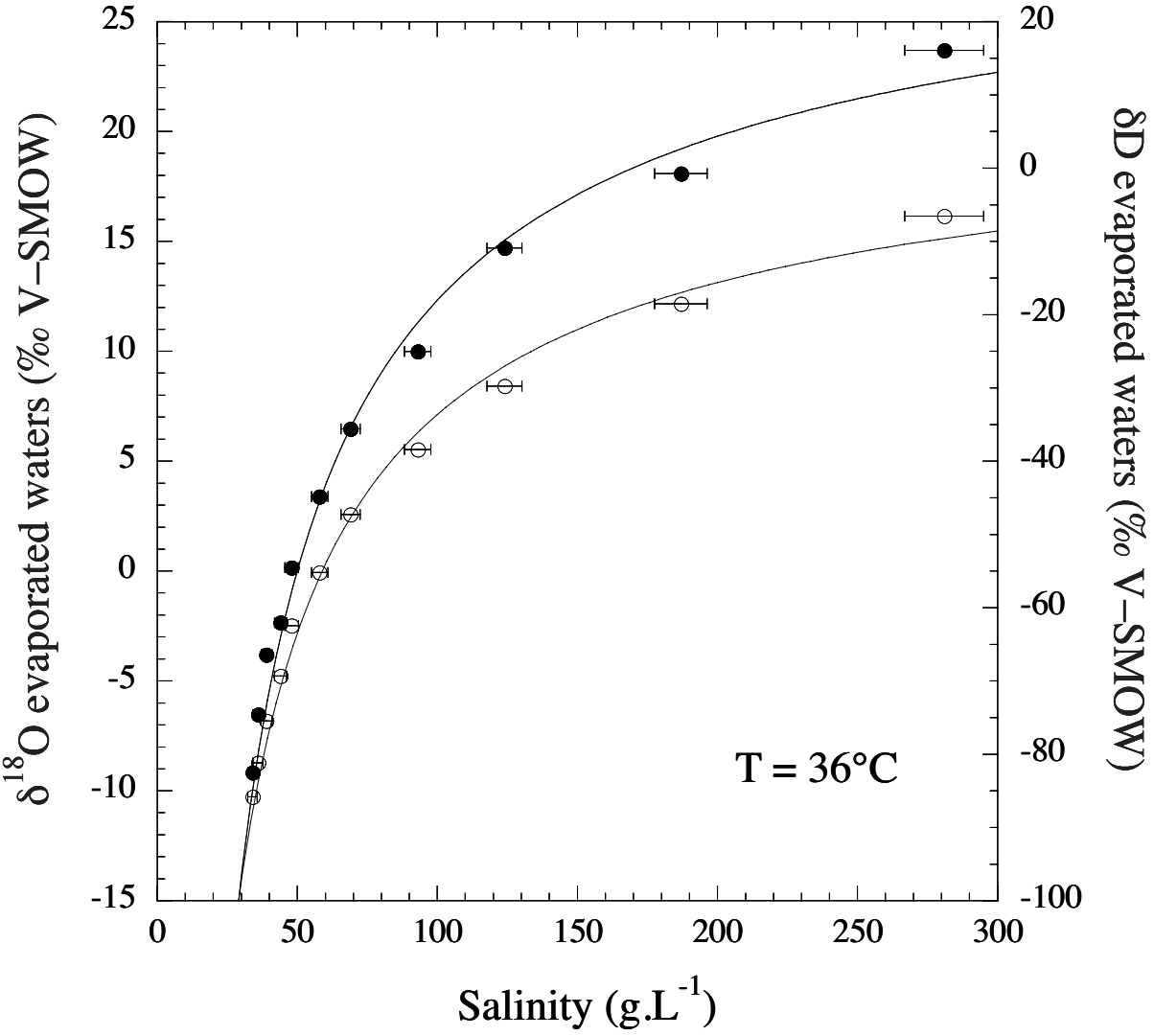

FIG. 11 – Variations in δD and $\delta^{18}O$ values of evaporating waters as a function of salinity for a temperature of 36°C. Data are described by two power laws which result from the fraction–dependent model developed by Gonfiantini (1986). The best fits correspond to equations (11) and (12).

Sample	Evaporation (h)	Temperature (°C)	Hygrometry (h_N) Wt %	Salinity ($g.L^{-1}$)	$\delta^{18}O\ H_2O$ (‰ V–SMOW)	$\delta D\ H_2O$ (‰ V–SMOW)
NaCl-1	0	23	53	35	-10.96	-89.4
NaCl-2	24	23	53	48	-2.71	-46.7
NaCl-3	48	23	53	78	4.96	-9.9
NaCl-4	72	23	53	120	8.51	13.0
NaCl-5	96	23	53	n.d.	6.94	12.2
NaCl-6	0	26.5	48	35	-10.94	-86.5
NaCl-7	18	26.5	48	49	-2.03	-42.0
NaCl-8	24	26.5	48	59	1.47	-35.0
NaCl-9	48	26.5	48	86	6.94	-2.4
NaCl-10	48	26.5	48	92	7.59	-1.6
NaCl-11	72	26.5	48	165	13.69	26.2
NaCl-12	0	28	53	35	-10.73	-83.4
NaCl-13	12	28	53	47	-3.94	-56.5
NaCl-14	24	28	53	91	4.13	-24.5
NaCl-15	36	28	53	300	13.15	15.6
NaCl-16	48	28	53	n.d.	17.56	39.9
NaCl-17	0	29.5	53	35	-10.25	-77.6
NaCl-18	8	29.5	53	46	-3.94	-58.0
NaCl-19	16	29.5	53	68	2.35	-32.9
NaCl-20	24	29.5	53	190	11.02	5.3
NaCl-21	32	29.5	53	350	17.9	41.7
NaCl-22	0	36	46	34	-10.27	-82.5
NaCl-23	2	36	46	36	-8.73	-74.6
NaCl-24	4	36	46	39	-6.82	-66.4
NaCl-25	6	36	46	44	-4.77	-62.0
NaCl-26	8	36	46	47	-2.47	-54.5
NaCl-27	10	36	46	57	-0.07	-44.8
NaCl-28	12	36	46	70	2.58	-35.6
NaCl-29	14	36	46	93	5.52	-25.0
NaCl-30	16	36	46	124	8.42	-10.9
NaCl-31	18	36	46	187	12.15	-0.8
NaCl-32	20	36	46	281	16.15	16.1
NaCl-33	22	36	46	n.d.	19.86	34.9
NaCl-34	23	36	46	n.d.	22.31	46.2
NaCl-35	0	47	45	35	-9.76	-70.9
NaCl-36	2	47	45	42	-5.97	-59.4
NaCl-37	4	47	45	62	-1.10	-43.9
NaCl-38	6	47	45	116	5.36	-22.6
NaCl-39	8	47	45	365	13.81	6.3
NaCl-40	9	47	45	n.d.	18.87	23.2
NaCl-41	10	47	45	n.d.	26.25	47.7
NaCl-42	11	47	45	n.d.	34.99	77.5

TAB. 1 – Temperature effects on δD and $\delta^{18}O$ variations of evaporated waters in the case of a null wind velocity and relatively constant hygrometry. Temperatures of water range from 23°C to 47°C. These isotopic compositions are used in order to draw the δD–$\delta^{18}O$ trajectories shown in Figure 4.

Sample	Evaporation	Wind velocity	Temperature	Hygrometry (h_N)	Salinity	$\delta^{18}O\ H_2O$	$\delta D\ H_2O$
	(h)	$m.s^{-1}$	(°C)	Wt %	($g.L^{-1}$)	(‰ V–SMOW)	(‰ V–SMOW)
NaCl-43	0	0	36	38	34	-10.39	-81.1
NaCl-44	3	0	36	38	35	-9.15	-73.2
NaCl-45	6	0	36	38	36	-7.84	-72.1
NaCl-46	9	0	36	38	39	-6.42	-68.5
NaCl-47	12	0	36	38	41	-5.02	-62.3
NaCl-48	15	0	36	38	47	-3.77	-59.2
NaCl-49	18	0	36	38	53	-2.22	-53.9
NaCl-50	21	0	36	38	61	-0.55	-43.7
NaCl-51	24	0	36	38	66	1.24	-38.1
NaCl-52	40	0	36	38	124	12.02	4.2
NaCl-53	48	0	36	38	224	18.53	28.5
NaCl-54	52	0	36	38	n.d.	22.49	44.8
NaCl-55	56	0	36	38	n.d.	27.29	63.7
NaCl-56	0	0.8	31.5	40	36	-9.90	-78.9
NaCl-57	3	0.8	31.5	40	42	-5.95	-60.9
NaCl-58	5	0.8	31.5	40	50	-2.86	-50.8
NaCl-59	7	0.8	31.5	40	63	0.31	-39.9
NaCl-60	9	0.8	31.5	40	83	3.44	-28.1
NaCl-61	11	0.8	31.5	40	112	6.60	-11.8
NaCl-62	13	0.8	31.5	40	159	9.84	2.2
NaCl-63	15	0.8	31.5	40	n.d.	12.90	16.2
NaCl-64	17	0.8	31.5	40	n.d.	15.90	24.2
NaCl-65	0	1.5	33.5	54	36	-10.15	-77.3
NaCl-66	2	1.5	33.5	54	39	-7.71	-73.3
NaCl-67	4	1.5	33.5	54	44	-5.22	-56.6
NaCl-68	6	1.5	33.5	54	50	-3.13	-46.9
NaCl-69	8	1.5	33.5	54	55	-0.86	-36.9
NaCl-70	10	1.5	33.5	54	65	1.29	-29.4
NaCl-71	12	1.5	33.5	54	74	3.23	-19.3
NaCl-72	14	1.5	33.5	54	101	5.11	-8.7
NaCl-73	16	1.5	33.5	54	140	6.64	-4.8
NaCl-74	18	1.5	33.5	54	221	7.70	4.9
NaCl-75	20	1.5	33.5	54	n.d.	8.08	8.6
NaCl-76	22	1.5	33.5	54	n.d.	7.53	11.8
NaCl-77	0	2.2	32.5	53	34	-10.24	-80.6
NaCl-78	2	2.2	32.5	53	39	-6.83	-57.7
NaCl-79	4	2.2	32.5	53	48	-3.70	-47.1
NaCl-80	6	2.2	32.5	53	60	-1.13	-35.3
NaCl-81	8	2.2	32.5	53	79	1.53	-23.4
NaCl-82	10	2.2	32.5	53	99	3.82	-8.1
NaCl-83	12	2.2	32.5	53	124	5.55	1.0
NaCl-84	14	2.2	32.5	53	235	7.04	9.8
NaCl-85	16	2.2	32.5	53	n.d.	7.59	14.3
NaCl-86	18	2.2	32.5	53	n.d.	6.69	12.7

TAB. 2 – Wind effect on δD and $\delta^{18}O$ variations of evaporated waters in the case of a constant bath temperature (36°C). Note the wind velocity effect on the decrease of the surface water temperature.

Halite Sample#	Precipitation T (°C)	Water amount Wt%	δD H_2O (‰ V-SMOW)	$\delta^{18}O$ H_2O (‰ V–SMOW)
FI-23-A	23	2.3	15.2	9.1
FI-23-B	23	1.9	16.1	10.0
FI-23-C	23	2.0	5.3	7.2
FI-28-A	28	3.3	33.0	16.4
FI-28-B	28	3.2	35.8	14.7
FI-36-A	36	0.9	42	20.7
FI-36-B	36	1.0	42	21.3
FI-47-A	47	4.0	106	44.6
FI-47-B	47	4.5	104	44.4
FI-47-C	47	4.6	102	44.9

TAB. 3 – δD and $\delta^{18}O$ values of water inclusions in synthetic halite precipitated from 23°C to 47°C without wind. δD–$\delta^{18}O$ trajectories shown in Figure 4.

Halite Sample#	Water amount wt%	δD H_2O (‰ V-SMOW)	$\delta^{18}O$ H_2O (‰ V–SMOW)
REA-1	3.3	31	12.9
REA-2	4.6	22	13.6
REA-3	7.9	19	14.6
REA-4	0.1	-27	3.1
REA-5	0.1	-25	1.5
REA-6	0.2	-9	1.1
REA-7	0.2	2	4.7
REA-8	0.2	-7	1.4
REA-9	0.1	-39	-0.3
REA-10	0.1	-37	-2.5
REA-11	0.2	-37	-2.2
REA-12	0.2	-25	1.4
REA-13	0.3	-35	-2.0
REA-14	0.3	-39	0.2
REA-15	0.3	-15	2.1
REA-16	0.4	-7	2.1
REA-17	0.4	-5	2.5
REA-18	0.2	-7	5.0
REA-19	0.3	-13	3.2
REA-20	0.2	-32	1.3

TAB. 4 – δD and $\delta^{18}O$ values values of water inclusions in natural Messinian halite from the Realmonte mine, Sicily.

Sample REA–11 IF #	Th (°C)	Sample REA–11 IF #	Th (°C)
1	26.5	34	41.5
2	27.4	35	26.1
3	28.9	36	26.7
4	29.7	37	26.9
5	30.4	38	27.2
6	30.5	39	27.2
7	30.8	40	27.8
8	37.4	41	26.6
9	25.9	42	29.4
10	27.3	43	31.0
11	31.5	44	31.8
12	32.5	45	34.7
13	34.6	46	34.1
14	33.8	47	35.1
15	35.3	48	37.4
16	37.2	49	37.9
17	37.2	50	38.9
18	37.9	51	40.7
19	32.6	52	21.8
20	38.8	53	24.8
21	25.6	54	26.6
22	38.7	55	27.0
23	38.9	56	27.6
24	39.6	57	23.4
25	39.8	58	31.4
26	40.4	59	32.1
27	41.4	60	33.5
28	41.1	61	37.4
29	36.2	62	37.0
30	37.5	63	38.0
31	37.6	64	38.6
32	38.2	65	34.1
33	40.0	66	36.3
		67	38.5

TAB. 5 – Homogenization temperatures of water inclusions from a Messinian halite sample of the Realmonte mine, Sicily.

Temperature (°C)	Wind velocity $m.s^{-1}$	Hygrometry (h_N) wt %	θ	$h_{N'}$
23	0	53	0.49	0.77
26.5	0	48	0.54	0.72
28	0	53	0.55	0.74
29.5	0	53	0.54	0.75
36	0	46	0.53	0.71
47	0	45	0.42	0.77
36	0	38	0.51	0.68
31.5	0.8	40	0.44	0.73
33.5	1.5	54	0.43	0.80
32.5	2.2	53	0.36	0.83

TAB. 6 – TResults of parameters modelling of the hydrogen and oxygen isotope compositions of evaporating waters by using the fraction–dependent developed by Gonfiantini (1986). δA, the hydrogen and oxygen isotope compositions of ambient moisture, were set at -130‰ and -17.5‰, respectively, except for experiments performed during the summer season during which values were estimated to be -110‰ and -15‰, respectively. The turbulence parameter, n, was set at 1 for all the calculations. See text for detailed explanations.

Chapitre 6

Les inclusions fluides dans les granites : sources et mélanges des fluides de la croûte supérieure.

6.1.

Fluid sources and mixing during the magmatic and post-magmatic evolution of the Soultz–sous–Forêts granite (France) : Evidence from the satble isotope compositions (H, C et O) of CO_2 and water from fluid inclusions in quartz and their host rocks.

Mise en évidence des sources des fluides et des mélanges pendant l'évolution magmatique et post–magmatique du granite de Soultz–sous–Forêts (France) par l'analyse des compositions isotopiques (H, C et O) du CO_2 et de l'eau des inclusions fluides des quartz et des roches encaissantes.

Résumé

Le dôme granitique de Soultz–sous–Forêts, localisé dans le Graben du Rhin (Alsace, France), est caractérisé par un gradient géothermique élevé et est par conséquent considéré comme l'un des meilleurs exemples en Europe pour démontrer le potentiel du concept Hot Dry Rock pour la géothermie. L'intrusion granitique datée à 331 Ma se compose d'un monzogranite métalumineux riche en Ca, Mg et K, avec une teneur élevée en éléments lithophiles (Th, U, REE). L'altération pénétrative du granite et la présenc e de microstructures indiquent que le domaine a subi une migration de fluides active et complexe à l'origine de la transformation des feldspaths en barytine, des plagioclases en argile et de la chloritisation de la biotite et de l'amphibole. La présence d'inclusions fluides dans les différentes générations de quartz du granite offre l'opportunité d'étudier les sources des fluides et leurs zones de mélange dans la croûte. Les compositions isotopiques (H, C et O) de CO_2 et H_2O des inclusions fluides dans les quartz ont été mesurées. La distribution avec la profondeur des quantités de CO_2 et des valeurs de $\delta^{13}C$ constituent une preuve de l'existence de processus de mélange dans la croûte entre deux sources distinctes de carbone dérivant pour l'une des carbonates sus–jacents ($\delta^{13}C$ = -2‰ PDB) et pour l'autre de la croûte profonde ou du manteau supérieur ($\delta^{13}C$ = -9‰ PDB). La composition isotopique des échantillons de roche totale révèle une troisième source de carbone ($\delta^{13}C$ = -20‰ PDB), de moindre importance, qui pourrait résulter de l'oxydation in situ de minéraux carbonés comme le graphite. La distribution des données dans un espace δD–$\delta^{18}O$ montre que l'eau associée au CO_2 dans les inclusions fluides primaires est constituée en grande partie d'eau météorique mélangée à des petites quantités d'eau juvénile. Les inclusions fluides dans le quartz peuvent donc représenter les paléo–précipitations contemporaines de la cristallisation du granite. Les valeurs de δD et $\delta^{18}O$ plus élevées que celles des eaux météoriques actuelles reflètent les températures moyennes de l'air plus élevées (d'environ 6°C) qui régnaient dans cette région à l'Oligocène quand le rift s'est formé.

Fluid sources and mixing during the magmatic and post-magmatic evolution of the Soultz-sous-Forêts granite (France): Evidence from the stable isotope compositions (H, C, and O) of CO_2 and water from fluid inclusions in quartz and their host rocks.

Gardien[1*] Véronique, Lecuyer[1] Christophe, Rabinowicz[2] Michel, Rigaudier[1] Thomas, Dubois[3] Michel and Martineau[1] François.

1: UMR CNRS 5125 PEPS, Université Claude Bernard Lyon 1, 2 Rue Raphaël Dubois, 69622 Villeurbanne cedex. France.

2: UMR 5562 Observatoire Midi Pyrénées, 14 Rue Edouard Belin, 31400 Toulouse France

3: UMR 8157, Université Lille 1, UFR Sciences de la Terre, bldg SN5, 59655 Villeuneuve d'Ascq

*C*orresponding author:* UMR 5125 CNRS – PEPS, Université Lyon 1,2 Rue Raphaël Dubois, 69622 Villeurbanne.
E-Mail: veronique.gardien@univ-lyon1.fr
Tel: 33 (0) 4 72 73 14 79
Fax: 33 (0) 4 72 44 83 82

Abstract – Soultz-sous-Forêt granitic dome which is located in the Rhine Graben, Alsace, France, presents a high geothermal gradient and is therefore considered as one of the best example in Europe for demonstrating the potentiality of the Hot Dry Rock concept (HDR). The granitic intrusion dated at 331 Ma consists of a metaluminous Ca, Mg, K-rich monzogranite with a high content in lithophilic (Th, U, REE) elements and a high K-calc-alkaline composition in agreement with a main crustal origin influenced by a mantle–derived component. Penetrative alteration of the granite body and the presence of sealed open microstructures indicate that the area experienced a complex and active fluid migration which was responsible for the hepatisation of the feldspars, the argilisation of the plagioclase and the chloritisation of both biotite and amphibole. Quartz forms either anhedral crystals with ondulose extinction that represent inherited magmatic grains or euhedral recrystallized grains related to the more recent Rhine continental rift evolution. The presence of fluid inclusions in the various generations of quartz gave the opportunity to study the source of fluids and mixing processes that operated during the long-lived fluid circulation in the granite. Stable isotope compositions (H, C and O) of CO_2 and H_2O have been measured in the quartz–bearing fluid inclusions. Amounts of CO_2 and $\delta^{13}C$ decreasing with depth reveal two distinct sources of carbon that mixed in the crust, most likely derived from the overlying carbonates ($\delta^{13}C$ = -2 ‰ PDB) and from the deep seated-crust ($\delta^{13}C$ = -9 ‰ PDB). The carbon isotope composition of bulk granites indicates a third source of carbon of minor importance that could be expressed as graphite ($\delta^{13}C$ = -20‰ PDB). The distribution of data in a δD–$\delta^{18}O$ space indicates that the water trapped in quartz grains mainly comes from meteoric waters. These fluid inclusions could thus represent the paleo-precipitations contemporaneous of both the crystallization and sub-solidus cooling stage of the monzogranite pluton. Higher δD and $\delta^{18}O$ values than the present–day meteoric waters could reflect higher mean air temperatures that prevailed in this area during the Oligocene when the rift formed.

Key words: granite, fluids inclusion, stable isotope, mantle carbon dioxide, meteoric water

1) Introduction

Fluids play a fundamental role in the evolution of the Earth's crust. Vectors of heat and chemical elements, they affect many physical and chemical properties of their host minerals and rocks (Karato, 1990; Keppler and Smyth, 2006). Hence, documenting fluid-rock interactions is important to understand crustal processes. Hydrothermal activity is well documented in oceanic ridges whatever the tectonic context of spreading ridge, back to fore arc basins. In such a geodynamic context, convection of seawater is localized at the ridge, the most permeable part of the oceanic crust. The high thermal regime, the thin or absent sedimentary cover and the development of fractures due to extension make the oceanic crust permeable enough to promote the hydration and the changes in the chemical composition of the oceanic lithosphere (Hart, 1973). As the high water pressure at the bottom of the ocean floor inhibits complete magma degassing during partial melting of the upper mantle, volatile elements remains partly trapped, thus facilitating their identification and relative abundance (Moore, 1970; Schiling et al., 1980; Bottinga and Javoy, 1990; Farley et al., 1995; Saal et al., 2002). Fluids trapped as inclusions in minerals are also studied for understanding the influence of mantle degassing on the chemistry of both the hydrosphere and atmosphere.

Identification of fluid sources as well as the quantification of their relative fluxes within the continental crust remains a difficult task to achieve. Indeed, the high degree of heterogeneity in the composition of the continental crust and the complexity of igneous processes involving deep-seated and surface-derived fluid phases constitute barriers to the quantification of fluid motions between Earth’s envelopes. For example, the crust belonging to stable craton undergoes less devolatilization than that in orogenic domains (Ranero et al., 2003). Previous studies have also revealed heterogeneities in the fluid distribution with depth. Aqueous saline fluids are dominant through the granitic basement at the upper structural level

(Aquilina et al., 1997) suggesting that the continental upper crust must be considered to behave as an aquifer. It is also generally accepted that CO_2 is the dominant fluid that occurs in the deepest part of the crust (e.g. Touret, 1971; Andersen et al., 1993; Pili et al., 1997; Santosh and Tsunogae, 2003), being of deep-crust to upper mantle origin with a $\delta^{13}C$ value of about -7‰ PDB (Javoy et al., 1986; Kyser, 1986; Cartigny et al., 2001). However, the lower crust and lithospheric mantle xenoliths that were sampled by volcanoes have demonstrated that water (dominated by OH^- with possibly minor H_2O in plagioclase) content varies from 0 to 100 ppm (mostly < 50 ppm) and from 100 to 1000 ppm (mostly > 200 ppm) for bulk peridotites and granulites, respectively (Bell and Rossman, 1992; Demouchy et al., 2006; Peslier and Luhr, 2006; Xia et al., 2006 ; Grant et al., 2007). These results corroborate studies performed on fluid inclusions in granulitic terrains showing that brines and N_2 are two additional common fluids that occur in granulites (Swanenberg, 1980; Touret and Dietvorst, 1983; Andersen et al., 1993; Touret, 1995).

It needs to be still explored to what extent CO_2 of mantle provenance and H_2O from fluid envelopes can penetrate and mix into the upper continental crust. Continental rifts offer a favourable context to study this fluid circulation because the thickness of the crust is reduced and extensional tectonics creates pathways for fluid migration. Moreover rifting is very often associated with both high thermal regime and mantle upwelling leading to its partial melting. Such mantle-derived magmas are then able to intrude the lower continental crust in which they induce anatexis and crustal magma generation (Bingen et al., 1993; Debon and Lemmet, 1999).

Soultz-sous-Forets site in the Rhine graben was selected for illustrating the Europe Hot Dry Rock (HDR) concept because of its high geothermal gradient (Gérard and Kalppelmeyer, 1987). A deep drilling (-5090 m) was performed throughout the Tertiary sedimentary cover and the Hercynian granitic basement. Available geochronological data offer the opportunity to constrain the timing of fluid circulation through this section of upper continental crust. Therefore, stable isotope compositions (H, C, and O) of CO_2 and water from fluid inclusions in

quartz and their host rock have been determined in order to identify fluid sources and mixing during the magmatic and post-magmatic evolution of the Soultz-sous-Forêts monzogranite.

2) Geological setting

The Rhine graben is part of the European Cenozoic Rift System (ECRIS) that extends from the North Sea coast in Germany to the Mediterranean Sea (Fig. 1A). The rift formed during the Oligocene results from an extension stage along with mantle upwelling related to the Alpine Orogeny (Villemin et al., 1986; Dezes et al., 2004) that promoted the upper mantle exhumation at a depth of -24 km (Prodehl et al., 1992). The Rhine depression is an asymmetric graben filled with Triassic to Tertiary sediments of 1400 m (western part) to 3500 m (eastern part) in thickness (Fig. 1 B and C). The thickest Tertiary series is mainly composed of marls and clays from Eocene to Oligocene in age (Schnaebele, 1948), the thin Triassic series being made of the three classical facies: Keuper, Muschelkalk and Buntsandstein (Kappelmeyer and Gérard, 1989). The sedimentary cover lies over a Hercynian basement affected by N10 normal faults (Fig. 1B and 1C), contemporaneous to the Oligocene extension re-activating pre-existing late Hercynian to Mesozoic crustal discontinuities (Schumacher, 2002).

Four deep boreholes (EPS1 = 2227 m fully cored; GPK1 = 3600 m cuttings; GPK2 = 5093 m mainly cuttings and cored between 5040 m and 5093 m, GPK3 = 5100 m cuttings) were drilled in the region of Soultz-Sous-Forêts with the objective to study structural, mechanical and thermal properties of the heat exchanger (Genter and Traineau, 1992; Ledésert et al., 1999; Hooijkaas et al., 2006). Based on the petrography and structures (subhorizontal K-feldspar megacrysts fabric) of the rocks intersected by the four boreholes, the basement in the Soultz-sous-Forêts was identified as a massive porphyritic monzogranite laccolithic body or the roof of a diapir like-intrusion (Edel et al, 2007). At the interface between the sedimentary cover and the monzogranite basement a paleo-weathering surface (at a depth of -1420 m to -1545 m) is interpreted as a Hercynian paleo-relief (Hooijkaas et al., 2006). Below -1545 m, the massive porphyritic monzogranite is affected by fractures localised between -2090 and -2170

m and at -2700 m and -3200 m (Fig. 2). The fractures are sealed by illite, calcite and geodic quartz (Sample 79 encountered at -2200 m) (Smith et al., 1998). At greater depth the monzogranite is intruded by two-mica granite (Hooijkaas et al., 2006).

Available data were obtained so far from core sections recovered in EPS1 (full section) and GPK2 (bottom of the section) boreholes. Pressure and temperature calculations indicate that the monzogranite underwent an early stage of crystallization (700-750°C, 3±0.5 kb) in a deep-seated magma chamber (9-12 km) followed by an adiabatic stage of consolidation at a depth of 5 km (Stussi et al., 2002). Geochemical ($^{87/86}$Sr initial ratio = 0.7085) and petrological (monzogabbrodiorite to quartz-monzonite enclaves) criteria indicate that the monzogranite has a crustal origin contaminated by a mantle-derived magma (Rummel, 1991; Stussi et al., 2002). Age emplacement of the porphyritic granite is dated between 331±9 Ma and 334.0+3.8–3.5 Ma (U/Pb on Zircon; Cocherie et al. 2004). The fine-grained two-micas granite intruded the monzogranite at 327±7 Ma (U/Pb method on zircon; Alexandrov et al., 2001; Cocherie et al. 2004). Cooling ages range between 325±6Ma (Rb/Sr method on whole rock; Rummel, 1991) and 320±5Ma (K/Ar method on feldspar; Dubois et al., 1994) to 319.8±0.6Ma $^{(40}$Ar/^{39}Ar method on micas; Stussi et al., 2002).

The monzogranite is affected by two types, pervasive and channelized hydrothermal alterations (Fig. 3). Pervasive alteration took place on a large scale in the granite and corresponds to the static replacement of biotite by hydrogarnet associated with chloritization (brunsvigite) and of plagioclase by sericite and calcite and to the development of neoformed epidote (Genter and Traineau, 1992; Ledésert et al., 1999; Stussi et al., 2002). The development of hydrogarnet as first Ca-Al is interpreted as an early alteration of plutonic rocks by low X_{CO2} fluids during post-magmatic cooling (Stussi et al., 2002). The channelized hydrothermal alteration developed in relation with the formation of a complex network of fault segments, dominated by N–S trends in accordance with the geometry of the local Soultz-sous-Forêts horst structure (Dezayes et al., 2004). The authors observed that fractures are filled with

illite, hematite, geodic quartz, carbonates and sulfides (Traineau et al., 1991). The fractures vary in width from few millimetres to centimetres and are bounded by a secondary hydrothermal alteration haloes that are several meters thick. Widespread ages obtained on illite range from 62 Ma to 17 Ma (Jacquemont, 2002) and are correlated with the extensional tectonics responsible for the Rhine Graben formation. However, the too large range in ages does not allow a precise dating of the hydrothermal alteration events. The deeper fine-grained two micas granite has a different type of vein alteration. Fractures appear with a thinner alteration halo and the spectral gamma-ray response suggests a uranium enrichment matching the fracture locations (Genter et al., 1995).

Previous studies that were dedicated to the recovered samples have also demonstrated that past to modern fluid circulations were recorded in fluid inclusions and in sealed microstructures and veins (Dubois et al., 1996; Smith et al., 1998) within both the sedimentary cover and the granitic basement. The authors described an earlier (most likely Late Hercynian) fluid stage recorded in rare fluid inclusions planes affecting the monzogranite quartz grains. Most of the studied inclusions are aqueous, except a few CO_2-rich fluid inclusions found in granite basement and in quartz veins. Raman analyses detected that no other volatiles component except CO_2 are present in fluid inclusion in quartz of the granite basement, although N_2 was also found in fluid inclusions in quartz veins. The minimum P-T conditions of entrapment are 350°C and 2.2 kb (Dubois et al., 1996). Remnants of the more recent (most likely post-Oligocene) fluid flows are the fluid inclusions trapped in authigenic quartz and barite in veins involving numerous fracturing and self sealing events. Fluid inclusion salinity is similar to modern brines. This and the oxygen isotope compositions of quartz suggest that quartz vein growth may be active at the present day (Dubois et al., 1996; Smith et al., 1998).

3) Petrology of the studied rocks

The porphyritic monzogranite cored between -1440 m and -2200 m in EPS1 borehole (Fig. 4A) contains centimetre-sized pink K-feldspar perthitic megacrysts set in a granular matrix of mm-sized quartz and K-feldspar. The reddish colour of the rock is a consequence of the granite weathering. Most of the primary iron-bearing minerals (biotite, magnetite and amphibole) are partially altered into chlorite, iron-hydroxide or hematite depending on the degree of alteration (Fig. 4B). Magnetite, titanite, apatite, allanite and zircon occur as accessory minerals. Calcite from pervasive hydrothermal alteration may also be present in fractures (Fig. 3C). Sample 79 (Fig. 2) provides an example of open fractures sealed by geodic quartz found at different depths in granites. The photomicrograph of the sample (Fig. 4E) shows typical pyramidal habits of a first generation of quartz surrounded by a second generation of quartz overgrowths. The absence of intra-crystalline deformation structures indicates that this quartz is probably linked to the present hydrothermal system and has not been affected by a deformation stage posterior to its growth.

The two-mica granite collected at -5058m depth in GPK-2 borehole is very fine-grained granite and characterized by the occurrence of primary muscovite flakes (fig. 4D). Geochemical data (in particular REE) indicate that the two-micas intrusion is a crystallization product of the potassic magma at the origin of the porphyritic pluton (Cocherie et al., 2004). This two-mica granite was encountered below about -4500 m in other boreholes suggesting that between -1400 m and - 4500 m depth, several post-magmatic two-micas granitic dikes have intruded the monzogranite pluton (Traineau et al., 1991).

4) Fluid inclusion petrography

Fluid inclusions are quantities of liquid or mixtures of liquid plus vapour trapped as impurities within the tiny crystal lattice of minerals. Their sizes range from submicroscopic up to several hundred micrometers in diameter and typical masses are in order of nanograms.

Most fluid inclusions preserve the chemical and physical properties of the original parent fluid from which they were formed. Fluids inclusions content might therefore be considered as direct sample of the volatile phase which circulated through the lithosphere and their chemical analyses might provide both the composition and density of these geologically important fluid phases. Following the criteria developed by Roedder (1984) and Touret (2001), microstructural observations made at room temperature under the microscope allows the discrimination between “primary inclusions” and “secondary inclusions”.

In the Soultz-sous-Forets granite we observed both primary and secondary fluid inclusions trapped in magmatic quartz. Fluids in primary inclusions in magmatic quartz crystals were trapped during crystal growth. These inclusions, of about 15 μm in size, occur isolated or clustered in quartz (Fig. 3F). Their shape depends on the crystal lattice of the host mineral and temperature of entrapment; it is hexagonal in quartz and rectangular in plagioclase. These primary fluid inclusions are supposed to represent the magmatic fluid trapped during the first stage of crystallisation. Secondary inclusions are trail-bound, showing irregular shape and commonly occur along fractures that intersect the crystallographic surfaces (Fig. 3G). It means that fluids in secondary fluid inclusions were trapped at any time after the growth of the host crystal stopped and sampled post-magmatic fluids.

5) Analytical techniques

Ten samples of the monzogranite taken at depth comprised between -1400 and -1930 m and one sample of cm-sized quartz of a sealed fracture from the bottom (-2200 m) of the EPS 1 borehole and one sample of the two micas granite taken at depth of -5048 m from GPK2 borehole were selected for stable isotope analysis. Samples were crushed down to mm-sized granulate and quartz was hand-picked-under binocular.

Extraction of fluid inclusions

Fluids trapped in granites were extracted by thermal decrepitation on a vacuum line. About 1 g of millimetre–sized quartz grains was washed with diluted nitric acid and rinsed with doubly deionised water before drying overnight at 110°C in an oven. Samples were loaded in a quartz glass tube and outgassed at 110˚C for at least 2 h. Step heating fixed on the basis of homogenisation temperatures observed by microthermometry was considered as the best protocol to separate fluids from primary and secondary fluid inclusions. Ideally, it is expected that fluids of secondary inclusions forming micro cracks would be totally released at temperatures that did not exceed 300°C whereas most fluids from primary inclusions would be collected at temperatures in the range of 700–800°C. For each heating step, fluids contained in mineral inclusions were collected for at least 20 min. This method does not guarantee however complete separation of fluids from both generations of fluid inclusions without some cross-contamination of the high–temperature generation by the low-temperature ones. Indeed, if the decrepitation temperature of the inclusions depends on the internal pressure inside the inclusions, it also depends on their size as well as the strength of surrounding minerals. Consequently, small secondary fluid inclusions tend to decrepitates at higher temperatures approaching those of primary inclusions. Similarly, the smallest primary inclusions could escape decrepitation performed at about 700°C even though no sizable amount of water has been extracted at temperatures up to 800°C. Finally, carbon dioxide and water were separated using a cryogenic trap cooled with a mixture of ethanol and liquid N2 maintained at -70°C. Water was collected into a silica glass tube containing about 300 mg of fine–grained pure grade chromium metal. Water blanks were very low over the complete set of experiments without contributing more than 5% of the total amount of water extracted from fluid inclusions.

Extraction of carbon dioxide and water from bulk samples

Whole rock samples were crushed into a very fine powder (implying the opening of the two types of fluid inclusions). An amount of 150 to 200 mg of rock powder was loaded into a quartz tube and heated at 150°C for 1 h in vacuum to remove any adsorbed water from the sample. Sample was further heated up with a torch until complete melting inducing the release of water from hydrous minerals. The Pyrex™ vacuum extraction line was maintained at a temperature of 80°C over the complete experiment to avoid water condensation on the inner sides of the experimental apparatus. Carbon dioxide and water were separated by using ethanol-liquid N_2 cryogenic trap. Using a liquid nitrogen trap, water was collected into a silica tube containing about 300 mg of chromium metal. This protocol was adapted from both methods developed by Vennemann and O'Neil (1993) and Morrison et al. (2001). Residual gases not condensable in liquid nitrogen are mainly composed of H_2 produced during the oxidation of the FeO component of silicates by water. If this amount of H_2 is one order of magnitude lower than the amount of water released during the melting of the granite samples, its D/H ratio is about from 150‰ to 300‰ lower than that of water according to thermodynamic calculations performed by Cerrai et al. (1954) and experiments made by Simon (2003) in the temperature range 600°C–1200°C. Therefore, a quantitative oxidation of this H_2 to water in a CuO furnace at 500°C is necessary to avoid the acquisition of D/H ratios shifted towards too high values. Water amounts of bulk rocks and fluid inclusions were determined by comparison with a series of water samples of known weights ranging from 0.5 μl to 1.5 μl. After reduction and expansion of H_2 into a constant volume of the mass spectrometer sample inlet, the amount of gas was estimated from the voltage of mass 2 collector. Uncertainty associated with the determined amount of water is close to ±0.05 μl.

Water collected during the decrepitation of fluid inclusions, in the range 35-125 μmoles, was transferred to a microequilibration vessel to which 10–15 μmoles of isotopically

CO_2 were added. Then H_2O were left to equilibrate oxygen isotopes at 25 ˚C for three days. When equilibration was completed and the equilibrated samples of H_2O and CO_2 were separated cryogenically. The $\delta^{18}O$ values of the water samples were calculated using the mass balance equation (1) of Kishima and Sakai (1980). Precisions obtained during the experiments for $\delta^{18}O$ values of H_2O were close to 0.5‰.

$$(1)\quad \delta^{18}O\,H_2O = \left(\delta^{18}O\,CO_2(f) - \delta^{18}O\,CO_2(i)\right)\left(2\frac{[CO_2]}{[H_2O]}\right) + \left(1 + \frac{\delta^{18}O\,CO_2(f)}{1000}\right)\frac{1000}{\alpha_{CO_2\text{-}H_2O}} - 1000$$

With α CO_2-H_2O = 1.0402 at T= 30˚C (O'Neil and Adami, 1969)

$\delta^{18}O$ CO_2 (f) = $\delta^{18}O$ of CO_2 equilibrated after three days with H_2O

$\delta^{18}O$ CO_2 (i) = $\delta^{18}O$ of CO_2 before equilibrium with H_2O = 26.95±0.05 (SMOW)

[CO_2] and [H_2O] are the amounts of the two gases in μmoles

Isotope ratio measurements of carbon dioxide and water

Carbon isotope composition of purified carbon dioxide from primary and secondary fluid inclusions was measured with a dual–inlet GV Prism™ mass spectrometer, the internal reproducibility was about ±0.3‰. Carbon dioxide amount was determined by using a calibrated Keller™ pressure gauge; the associated uncertainty is close to ±2 μmoles. At 1000°C during 5 minutes, water was reduced by Cr to produce H_2 gas for which the D/H ratio was determined by using a dual–inlet GV Prism™ mass spectrometer. External reproducibility of D/H measurements was established at about ±3‰ by scaling raw data to the "true" isotopic ratios of SMOW, SLAP and GISP international standards. Aliquots of these international standard waters were selected in the range 0.5–1.5 μl which sizes are comparable to those of analyzed natural samples. D/H measurements of most samples have been duplicated and the internal reproducibility is close to ±3‰. Repeated analyses of the international standard

NBS30 provided a mean δD value of –66.4±3.1‰ (n = 11) to be compared to the recommended value of –65.7‰.

6) Results of the isotopic values of carbon dioxide and water

$^{13}C/^{12}C$ ratios of fluid inclusions and bulk rocks

Four monzogranite and one two-mica granite samples have been selected for the analysis of fluid inclusions (Table 1). Studied monzogranite samples contain very few primary fluid inclusions but are characterized by abundant secondary fluid inclusions which are located in healed micro cracks affecting quartz grains. Fluid inclusions extracted at high temperatures provided an amount of CO_2 high enough (6 to 25 μmoles.g^{-1} of quartz) to be analyzed. Fluid inclusions released at temperatures below 350°C did not provide detectable amounts of CO_2, they are however H_2O-rich. These results are in agreement with previous microthermometric studies (Dubois et al., 1996). Carbon isotope compositions and amounts of CO_2 from fluid inclusions trapped in the quartz grains of the monzogranite are reported versus the depth below surface (Tables 1 and 2, Figure 4). The most superficial samples occurring below the sedimentary series (between -1400 m and -1480 m) host the fluid inclusions which contain the highest amounts of CO_2 (up to 60 μmoles g^{-1}) with a $\delta^{13}C$ value of -3±0.5‰ (VPDB). For the deepest samples located at -1500 m and below -1700 m, the amount of CO_2 is about 20 μmoles.g^{-1} and to about 5 μmoles.g^{-1}, respectively, along with progressive decreasing $\delta^{13}C$ values from -7.5‰ to -9‰ with depth (Figure 4). The good quality of data fitting (r^2 = 0.95) between the $\delta^{13}C$ value of CO_2 and its relative abundance suggests a mixing between at least two carbon dioxide reservoirs. One end-member could be of superficial origin with a $\delta^{13}C \geq$ -3‰ and the second one of deep-seated origin which is characterized by a more negative $\delta^{13}C \leq$ -9‰ (Figure 5). The $\delta^{13}C$ value of -7.1‰ VPDB obtained for the carbon extracted from the fluid inclusions of quartz grains from the two-mica granite (Table 2) is comparable to that

recorded in the carbon dioxide from monzogranite samples located close to -1500 m depth. Geodic quartz of sample 79 provides only H_2O.

Bulk granite analyses were also performed in order to track other possible sources of solid carbon in the Soultz monzogranite. Two groups of values can be distinguished with respect to both the depth and the amount of CO_2 (Table 3, figure 6A and B). Bulk $\delta^{13}C$ values between -8.1‰ to -2.9‰ were obtained for monzogranite samples recovered between -1740 m and -1400 m and the amount of C released as CO_2 during the pyrolysis of powdered rocks range from 435 to 2224 ppm. Below -1700 m, the amount of C and its isotopic composition lie between 87 and 121 ppm and between -20‰ and -14‰, respectively. The two-mica granite has a bulk $\delta^{13}C$ value of -41.9‰ (Table 3).

D/H and $^{18}O/^{16}O$ ratios of fluid inclusions

Four monzogranite samples and one two-mica granite sample have been selected for the measurement of D/H ratios in fluid inclusions that were released within two ranges of decrepitation temperatures: the first one between 100±20°C and 350±50°C and the second one between 350±50°C and 750±50°C. Data compiled in Table 1 reveal that primary fluid inclusions contain both water and carbon dioxide whereas secondary fluid inclusions only contain water. This indicates that the two-step heating procedure we established was likely to be able to separate 'primary' from 'secondary' fluid inclusions. However, δD values of primary fluid inclusions range from -51‰ to -43‰ (mean δD = -48±2.6‰) and are bracketed by the δD values of the secondary fluid inclusions that range from -66‰ to -38‰ (mean δD = -49±12‰). Thus, both generations of fluid inclusions have trapped waters of similar isotopic compositions derived from meteoric waters or released by partial dehydration of the rocks intruded by the granitic pluton. Therefore, for the complete collection of samples, the D/H ratios have been measured for the fluid inclusions released in the highest range of temperatures (Table 2) to avoid interferences of the isotopic signature from the fluid flow of lowest

temperature. These fluid inclusions from monzogranites have δD values that range from -59‰ to -40‰ with a mean value of -50‰ (Table 2) which does not differ from the preliminary measurements presented in Table 1. It is noteworthy that there is no relation between the δD values of fluid inclusion and the depth of sampling (Table 2). Except for sample sγ4 which has a very low $\delta^{18}O$ value of -15.7‰, $\delta^{18}O$ values of these fluid inclusions range from -7.4 to -3.7‰ with a mean value of -5.7‰ (Table 2). Water inclusions in geodic quartz from sample 79 have a relative low δD value of -63.8‰ with a corresponding $\delta^{18}O$ value of -10.4‰ (Table 2). Water inclusions with δD and $\delta^{18}O$ values both negative mean derived from meteoric waters; moreover the distribution of these data in a δD–$\delta^{18}O$ space (Figure 7) reveals that four samples (Sγ1, Sγ6, Sγ12 and Sγ18) lie on or close to the meteoric water line (MWL). However samples Sγ2, Sγ3, Sγ10 and Sγ13 have δD and $\delta^{18}O$ values that deviate from the MWL in the direction of lower δD and higher $\delta^{18}O$ values which could suggest the existence of a second water end-member.

D/H ratios of bulk rocks

Hydrogen isotope compositions of bulk rock monzogranites range from -68‰ to -45‰ (SMOW) independently of both the water content of the rock or the sampling depth (Table 3). The δD value of -48‰ for the two-mica granite is bracketed by the range of monzogranite δD values (Table 3). Offsets between hydrogen isotope compositions of water inclusions and their host rocks range from -16‰ to +20‰.

7) Discussion

Water-rock interactions

It is now generally admitted that aqueous fluids are required to promote partial melting of the continental crust. Stable isotope studies of the products resulting from crust melting have the potential to determine the source and the amounts of these aqueous fluids (e.g. Taylor, 1968; Taylor, 1977; Wickham and Taylor, 1985; Taylor, 1988). These fluids may come from external reservoirs in context of rifting (seawater) and subduction or continental collision (meteoric waters) (see Taylor, 1988 for a review) or they can be recycled through dehydration of previously hydrated surrounding rocks (e.g. Fourcade and Allègre, 1981). As it was commonly demonstrated, because of the ubiquitous ^{18}O –depleted character of meteoric waters, interaction of such waters with igneous rocks at temperatures above 200–300°C generate low $\delta^{18}O$ hydrothermally-altered igneous rocks (Taylor, 1977; Taylor and Sheppard, 1986). An ^{18}O–enrichment of igneous rocks may be produced at lower temperatures as already documented during weathering (Lawrence and Taylor, 1971) as well as in the superficial zones of certain hydrothermal systems (Criss et al., 1984). We cannot also exclude that aqueous fluid with positive $\delta^{18}O$ values could have been released during the heating of intruded pelites or metabasites. Such a hypothesis has been already proposed as a source of aqueous fluids that interacted with the Hercynian granites from the Pyrenees (Fourcade and Allègre, 1981).

Many studies were dedicated to the processes of hydrothermal and weathering alterations of plutons that took place into the continental crust. Most of these studies involved the hydrogen or oxygen isotope compositions of alteration products (e.g. clays, secondary quartz) or minerals highly sensitive to post-solidus oxygen isotope exchange with aqueous fluids such as feldspars (Criss and Taylor, 1986). Only a few studies focused on the stable isotope compositions of the hydrothermal fluids trapped as tiny fluid inclusions in secondary minerals. This indirect sampling and analysis of hydrothermal fluids facilitate the identification

of fluid sources, mixing zones in the crust and their evolution through water–rock interactions as already exemplified when applied to the oceanic crust (Gregory et al., 1989; Ito and Clayton, 1983; Alt et al., 1986).

Sources of carbon

Distribution with depth of the amount of carbon dioxide and of its carbon isotope composition constitutes and evidence for mixing processes between surface-derived and deep-seated sources of carbon (Figure 5A). The surface reservoir of carbon dioxide, characterized by the highest amounts of CO_2 and $\delta^{13}C$ (close to -3.3‰) values could result from the decarbonation or dissolution of the overlying sedimentary carbonates (Figures 5A and 5B). The 'deep reservoir' characterized by low amounts of CO_2 and $\delta^{13}C$ values close to -9‰ (Figure 5) could be of deep crustal or shallow mantle origin (e.g. Baker, 1988; Moecher et al., 1994). Part of the circulating CO_2 with low $\delta^{13}C$ values relative to PDB could also have been produced by in *situ* oxidation of mineralized carbon such as graphite that was identified as trace amounts in the altered zones of the pluton. This graphite could result from the thermal maturation of sedimentary organic matter whose $\delta^{13}C$ remained close to -25‰ over the Earth's history (Schidlowski, 2001).

Sources of water

Paired δD–$\delta^{18}O$ values for fluid inclusions from monzogranite quartz are distributed along a rough trend which is anchored in the MWL at δD and $\delta^{18}O$ values of -40‰ and -6‰, respectively. The $\delta^{18}O$–δD paired values of fluid inclusions 'rooted' close the MWL could represent the paleo-precipitations contemporaneous of the crystallization and sub-solidus cooling stage of the monzogranite pluton. These values are comparable to present–day δD and

$\delta^{18}O$ values of meteoric waters (Figure 7) in Alsace, France, which are close to -60‰ and -9‰, respectively (Daux et al., 2005) .

This isotopic offset could reflect higher mean air temperatures that prevailed in this area during the Oligocene when the rift formed. During the Oligocene, climate in Western Europe was warmer than today as shown by paleobotanical data (Mosbrugger et al., 2005; Utescher et al., 2009), oxygen isotope compositions of terrestrial vertebrate remains (Maridet et al., 2007) and molluscs or foraminifera from the North Atlantic Ocean (Zachos et al., 2001). Mean air temperatures higher by about a few degrees Celsius are in agreement with δD and $\delta^{18}O$ values of meteoric waters 20‰ and 3‰ higher, respectively, which correspond to an increase in mean air temperatures of about 6° (Von Grafenstein et al., 1996).

The presence of samples that plot on the right side of the MWL (Figure 7) could indicate that the oxygen isotope composition of water inclusions was modified through sub-solidus isotopic exchange with the host quartz. Wet diffusion of oxygen in quartz is however slow at temperatures below 700°C (Giletti and Yund, 1984) and the ^{18}O-enrichment of fluid inclusions by several ‰ implies a very slow cooling rate of the pluton. It is noteworthy that data plotted in Figure 7 draw a rough trend in the direction of a possible “hidden” second end–member characterized by lower δD and higher $\delta^{18}O$ values. This rough isotopic trend could be a mixing line reflecting the discrete presence of magmatic water still preserved in the so-called ‘primary fluid inclusions’. Magmatic quartz sampled in a non-altered section of the granite cored in EPS1 borehole has a $\delta^{18}O$ value close to 10‰ (Yardley et al., 1995). This means that the $\delta^{18}O$ of magmatic water should have been close to 5–7‰ according to the known fractionation equations for quartz-water (Bottinga and Javoy, 1975) and assuming that the closure temperature of oxygen diffusion in quartz is close to 600°C as it was documented in several granitic plutons (Giletti, 1986). Extrapolating fluid inclusion data in Figure 7 to a $\delta^{18}O$ value of 5–7‰ lead to infer a δD value of -120 to -80‰ which is compatible with known or estimated compositions of magmatic waters (Sheppard, 1986 and reference therein). This

rough calculation suggests that the pervasive circulation of hydrothermal waters of meteoric origin nearly completely erased the isotopic signature of the magmatic water reservoir of small size comparatively. These results suggest that the introduction of meteoric water took place early in the crystallization of the granite during post-magmatic cooling. Introduction of water has been most likely favoured by the development of discrete microfractures that developed throughout the pluton in relation with the volume change during cooling. This hypothesis agree with thermometric data indicating that primary fluids in cluster and healed microfractures in quartz were trapped at temperatures of at least 350°C and 150-340°C respectively (Dubois et al., 1996). More over according to Tenzer et al. (1991), the orientation of the healed microfractures in quartz (N120°E) might be related to a Hercynian episode.

Metamorphic hydrous minerals are expected to be at least 30‰ deuterium-depleted relative to the water from which they were formed according to natural observations (e.g. Früh–Green et al., 1996) and laboratory experiments (e.g. Suzuoki and Epstein, 1976; Graham et al., 1984). Data compiled in Table 2 and Table 3 reveal that δD values of fluid inclusions are similar to or lower than the δD values of several of their corresponding bulk rocks. These observations suggest that water from some granite-forming hydrous minerals has not the same source than waters trapped in the fluid inclusions of quartz. Indeed, under low water-rock ratios, secondary minerals such as chlorite or sericite can partially inherit the hydrogen isotope composition of the biotite they replaced. Therefore, bulk D/H ratios of most monzogranites most likely reflect the composition of water released during the monzogranite intrusion that produced a partial dehydration of the surrounding rocks, the source of this water being most likely exclusively of crustal origin (Fu et al., 2003; Chen et al., 2007).

Fluid inclusions from sample sγ79 of geodic quartz have hydrogen and oxygen isotope compositions close to those of present-day meteoric waters. This quartz was most likely deposited within a fracture that recently developed throughout the monzogranitic dome. Geodic quartz occurring in veins has $\delta^{18}O$ values that range from 12 to 18‰ (SMOW) with a

mean value of 15‰ (Smith et al., 1998). Assuming that this neoformed quartz precipitated in oxygen isotope equilibrium with the meteoric waters having a $\delta^{18}O$ value of -6±0.5‰, temperatures of the hydrothermal waters were in the range 110°C–160°C, which are comparable to the temperatures measured in the present-day upwelling hot waters (Pauwels et al., 1993).

Mixing of fluids

All the primary inclusions of the monzogranite and the two mica granite (decrepitating at T > 600°C) contain CO_2 and H_2O. The two distinct $\delta^{13}C$ values (-3.3‰ and -7‰) indicate that CO_2 derived either from the overlying sedimentary carbonates or shallow mantle (magma). The water associated with the CO_2 in primary inclusions derived from surface continental water possibly mixed with a small amount of juvenile water. The surface water equilibrated at temperature generally hotter (by about 6°C) than the present day aquifers in the Rhine Valley. How to explain the mixing of surface and deep seated fluids in the same primary inclusions trapped during the crystallization of magmatic mineral?

We will consider the hypothesis which states that the water percolating from the surface through the cracks network following the low temperature elastic contraction of the granite merges with juvenile waters at a temperature > 600°C. At that temperature the granite is still ductile therefore; we have to envisage a process of fluids percolation that is different to the propagation of a ~350°C cracking front triggered by hydrothermal cooling (Norton and Knight, 1977; Norton and Taylor, 1979; Parmentier, 1981). The question is how to connect low temperature (meteoric) and high temperature (juvenile) fluids at the late step of crystallisation of the granite? The emplacement of the pluton dated at 340 and 325 Ma (Edel et al, 2007) in the Variscan Saxo-Thuringian zone occurred within a 40 km wide North-30°-40° sinistral wrench-zone which experienced 43 km of displacement. The structural data within the granite records a subsolidus horizontal foliation marked by the preferential orientation of biotite and feldspars due to NE-SW oriented flow (Edel et al., 2007) suggesting a horizontal compression field $\vec{\sigma}_1$ pointing North-30°-40°. The fabric being essentially horizontal, we deduce that $\vec{\sigma}_3$

also points on a horizontal direction, while $\vec{\sigma}_2$ is vertical and small. The $(\vec{\sigma}_1,\vec{\sigma}_3)$ plane being horizontal an orthogonal direction to $\vec{\sigma}_3$, i.e. the $(\vec{\sigma}_1,\vec{\sigma}_2)$ plane is vertical and parallel to strike. Shearing of partially molten plastic rock can segregate the interstitial melt on planes orthogonal to $\vec{\sigma}_3$ (Stevenson, 1989; Richardson, 1998; Rabinowicz and Vigneresse, 2004 and Rabinowicz and Toplis, 2009). The transport of the interstitial melt into these planes requires a relatively high strain (γ). When the viscosity (η_s) of the solid fraction of the mush is independent of melt concentration (ϕ) a strain γ of about 10 is required to transport the melt into $(\vec{\sigma}_1,\vec{\sigma}_2)$ - planes (Rabinowicz and Vigneresse, 2004). Alternatively, when the solid viscosity η_s decreases with melt concentration ϕ, a strain γ value of 1 is required to confine melt in $(\vec{\sigma}_1,\vec{\sigma}_2)$ - planes (Stevenson, 1989; Richardson, 1998; Rabinowicz and Toplis, 2009). Experimental works on granitic or mantle mush suggest that the effective viscosity of the mush drops by about one order of magnitude when ϕ is about 1 to 10 vol % (Kelemen, et al., 1997; Scott and Kohlstedt, 2006). Thus, we suggest that the North-30°-40° wrench-zone have provided the shear $\gamma \sim 1$ necessary to concentrate ~5-10% in volume of leucocratic melt in vertical $(\vec{\sigma}_1,\vec{\sigma}_2)$ - planes just after the consolidation of the granite mush at ~700°C.

A much debated point concerns the spacing of the melt planes formed during shear. Stevenson (1989) suggested that the spacing is inversely proportional to 1/*a,* where *a* represents the size of the solid grains. This argument is used by several authors to explain metric to hectometric distant melt layers in a granitic or mantle mush (Kelemen et al., 1997). More precisely, it was suggested that the characteristic distance between the melt layers is lower than the compaction length *L* of the mush (Richarson, 1998; Hall and Parmentier, 2000; Holtzman et al., 2003; Rabinowicz and Vigneresse, 2004; Katz et al., 2006; Kohlstedt and Zimmerman, 2009; King, et al., 2009). A more recent work yields to the result that the characteristic distance of the shear bands should be actually proportional to the size of the solid grains *a* (Rabinowicz and Toplis, 2009). But, when the mush is stressed and the interstitial melt is buoyant, the height of the shear band is seen to be proportional to the compaction length *L* (Rabinowicz and Toplis, 2009). Actually, the stress field

in Soultz is essentially horizontal and leucosome melt is buoyant. The compaction length equation writes:

$$L = \sqrt{\frac{\eta_s k}{\eta_f \phi}} \qquad (1)$$

Where η_s, η_f, and k represents the solid and fluid viscosity, and the mush permeability, respectively. Close to its solidus, the solid viscosity η_s of granite is ~10^{18} Pa.s, (Rabinowicz and Vigneresse, 2004 and references therein). Besides, the permeability k range of a several millimetre grain size plastic mush with a melt concentration of about 5% is 10^{-12}-10^{-13}m^2 (i.e. Rabinowicz and Toplis, 2009 and references therein). Finally, at the end of the crystallization process, the leucosome melt, concentrating the essential part of the water contained in the granite, results to contain about 5 % in weight of H_2O, and thus has a relatively low viscosity η_f ~10^4 Pa.s. The former parameter values imply that the compaction length *L* is ~10 m (Equ. 1).

Accordingly, we deduce that, at a temperature of ~550°C, the crystallization of the leucosome melt lead to the development of vertical quartz veins with a spacing of several ~a= 3-4 mm millimetres forming a connected network on a height ~L = 10m. Macroscopic observations of cored samples show that quartz grains distribution is clearly connected in a vertical direction but not in the horizontal one. Indeed on the basal section of the cored granite quartz formed isolated rounded grains (figure, 10-A). On this section no preferred orientation of biotite or plagioclase is observed. Biotite grains occur as automorph rectangular magmatic minerals. On longitudinal sections on the contrary, quartz grains are organised as vertical ribbons of 1 or 2 cm length and the spacing between quartz ribbons is about few millimetres (typical grain size of the minerals constituting the matrix of the granite). These quartz ribbons,

representing the product of crystallisation of the SiO_2 rich veins generated during shear are discordant to the foliation plane made of biotite and feldspar (Figure 10-B).

Quartz grains being essentially anhydrous, the water contained in the silica melt is exsolved and trapped either as primary inclusions nested inside magmatic quartz grains or on grain-grain boundaries. The quartz veins represent about 5 to 10% of the rock volume and have exsolved about 5 % in weight of fluid initially dissolved in the leucosome melt. Because of the low density (~600kg/m^3) of super-critical water, it is deduced that the exsolved water represents up to 30% of the volume occupied by the quartz veins, and up to 3 % oh the entire volume of the granite. Because of the small grain size of the quartz veins (3-4 mm) and the weak surface tension between water and quartz, the interstitial water film representing 30% of the quartz volume would constitute a connected network free to percolate through the rock.

As long as the granitic mush is at temperature above $0.8 \times T_s$ ~450°C (T_s = solidus of quartz i.e. ~550°C) the quartz grains remain ductile. The deformation of the granite imposed by the large scale tectonic stresses will partition into the ductile quartz veins (~5-10 % of the bulk volume of the granite). A large strain (γ_v ~10) experienced by the quartz ductile veins will contribute only moderately to the global strain γ_g of the granite because $\gamma_g = \sim \gamma_v \times 5\% = 0.5$ if $\gamma_v = 10$.

Accordingly, it is likely that the deformation of the quartz veins lead to the squeeze of the interstitial water into vertical lenses 3-4 mm-distant and oriented parallel to the $(\vec{\sigma}_1, \vec{\sigma}_2)$ -planes of the global stress field. The viscosity of sub-solidus quartz η_s being > 10^{18} Pa.s (Fontaine et al., 2003 and references therein), the exsolved fluid concentration ϕ in the vertical quartz veins representing 30% of the quartz volume, the fluid network effective permeability k being > 10^{-12}-10^{-13}m^2, and the viscosity η_f of water at 450°C-550° being <10^{-4} Pa.s the compaction length *L* results to be incredibly large: > 100 km (see Equ. 1). This proves that the juvenile waters will forms a vertically connected network crossing the whole viscous cap overriding the granitic mush.

When the temperature drops below the ductile threshold of quartz, (T° lower than 0.8×550°C: i.e. about 450°C), the mechanical stability of the system is reinforced and the hydraulic continuity of the water network in the solidified granite will be preserved. However there is a critical height over which the hydraulic network should collapse when the excess pressure resulting from the buoyancy of water of density ~600kg/m^3 inside granite of density ~2700kg/m^3, exceeds its brittle threshold, ~100 MPa. Using, the former values, we see that the brittle threshold is reached when the connected hydraulic height exceeds 5 km. Then, juvenile water planes will be triggered and water will pool at the place where $\vec{\sigma}_3$ rotates to the vertical. Such mechanism was invoked by Bons (2001) in order to explain generation of the large quartz deposits found in Australian Achaean Granites. As we do not observe such quartz deposits in the Soultz-Sous-Forêts granite we conclude that the hydraulic continuity of juvenile water never exceeded a few kilometre of height.

Moreover, when the temperature dropped below the cracking temperature of granite, i.e. a temperature < 350°C, connection between hydrothermal and juvenile waters is unavoidable. Initially, the permeability of the connected network should have been high enough, $k \sim 10^{-12}$-10^{-13}m^2, for the development of porous flow convection through the whole hydraulically connected layer (Norton and Knight, 1977; Norton and Taylor, 1979; Parmentier, 1981). The juvenile waters being very salted they must be much heavier than the hydrothermal waters at the same temperature. Therefore, thermohaline convection should develop with a light "cold" hydrothermal water layer floating over heavy and "hot" juvenile water layer. Diffusion of salt, of heat and mixing of hydrothermal and juvenile water will occur at the boundary of both layers. It will lead to the isotopic mixing recorded in the primary inclusions. Moreover, because of the strong solubility variation of silica with temperature, salinity and pH precipitation of quartz will rapidly occurs (Parmentier, 1981; Rabinowicz et al., 1985). It will rapidly heal the whole granitic layer which eventually will remain extremely impermeable: i.e. presenting an intrinsic permeability k of $\sim 10^{-18}$-10^{-20}m^2.

8) Conclusions

The preservation of primary fluid inclusions in quartz from the Soultz-sous-Forêts monzogranite gives the opportunity to study fluid mixing in the continental crust and the water-rock interactions operating during the long-lived fluid circulation in the monzogranite. The biphasic primary fluid inclusions observed in quartz grains are composed of carbon dioxide from two main sources: sedimentary carbonates ($\delta^{13}C$ = -2‰V-PDB) and deep-seated crust/upper mantle ($\delta^{13}C$ = -7‰V-PDB). A minor part of the circulating CO2 could also correspond to the oxidation of mineralized carbon such as graphite. The distribution of data in δD –$\delta^{18}O$ diagram indicates that the water presents in the fluid inclusions with the carbon dioxide, has a meteoric origin possibly mixed with juvenile water. The hydrogen and oxygen compositions of the meteoric water define à trend that cross-cut the Meteoric Water Line at δD and $\delta^{18}O$ values of -40 ‰ and -6‰ respectively. These values could represent the precipitation contemporaneous to the early stage of the pluton intrusion and sub-solidus cooling; it indicates à mean air temperature about 6°C higher than the present day air temperature.

The melange of meteoric and deep-seated fluid in quartz takes place from the early stage of the intrusion of the pluton in the crust to post-cooling stage. The emplacement of the pluton occurred in a North30-40° wrench zone that have provided the shear $\gamma \sim 1$ necessary to concentrate the ultimate leucocratic melt in vertical ($\vec{\sigma}_1, \vec{\sigma}_2$) - planes (~5-10% in volume) after the consolidation of the granite mush at ~700°C. The crystallization of the leucocratic melt lead to the development of vertical quartz veins with a spacing of several ~a= 3-4 mm millimetres forming a connected network on a height ~L = 10m. When the temperature drops below the ductile threshold of quartz, (T° lower than 0.8×550°C: i.e. about 450°C), the mechanical stability of the system is reinforced and the hydraulic continuity of the water network in the solidified granite will be preserved. The permeability of the connected network should have been high enough, $k \sim 10^{-12}$-10^{-13} m^2, for the development of porous flow convection through the whole hydraulically connected layer (Norton and Knight, 1977; Norton

and Taylor, 1979; Parmentier, 1981). The juvenile waters being very salted they must be much heavier than the hydrothermal waters at the same temperature. Therefore, thermohaline convection should develop with a light “cold” hydrothermal water layer floating over heavy and “hot” juvenile water layer. This can explain the mixing of surface and deep seated fluids in the same primary inclusions trapped during the crystallization of magmatic mineral

Acknowledgements – The authors thank F. Fourel, and C. Chelouah, for their assistance in the laboratory.

References

Alexandrov P., Royer J.J. and Deloule E. (2001) 331 ± 9 Ma emplacement age of the Soultz monzogranite (Rhine Graben basement) by U/Pb ion-probe zircon dating of samples from 5 km depth, *C.R. Acad. Sci. (Paris), Sèrie II* **332**, 747–754.

Alt J. C., Muehlenbachs K., and Honnorez J. (1986) An oxygen isotopic profile through the upper kilometer of the oceanic crust, DSDP Hole 504B. *Earth Planet. Sci. Lett.* **80**, 217–229.

Andersen T., Austrheim H., Burk, E.A.J. and Elvevold S. (1993) N_2 and CO_2 in deep crustal fluids: evidence from the Caledonides of Norway. *Chem. Geol.* **108**, 113–132.

Aquilina L., Pauwels H., Genter A. and Fouillac C. (1997) Water–rock interaction processes in the Triassic sandstone and the granitic basement of the Rhine Graben: geochemical investigation of a geothermal reservoir. *Geochim. Cosmochim. Acta* **61**, 4281–4295.

Baker A.J. (1988) Stable isotope evidence for limited fluid infiltration of deep crustal rocks from the Ivrea Zone, Italy. *Geology* **16**, 492–495.

Bataillé A. (2004) Modélisation de la circulation thermoconvective en milieu fracturé : application à la géothermie des Roches Chaudes et Fracturées à Soultz–sous–Forêts (France). Ph. D. thesis, Université Paul Sabatier, Toulouse.

Bell D.R. and Rossman G.R. (1992) Water in Earth's mantle: the role of nominally anhydrous minerals. *Science* **255**, 1391–1397.

Bingen B., Demaiffe D., Hertogen J., Weis D. and Michot J. (1993) K-rich calc-alkaline augen gneisses of Grenvillian age in the SW Norway: migling of mantle-derived and crustal components. *J. Geol.* **101**, 763–778.

Bons P.D. (2001) The formation of large quartz veins by rapid ascent of fluids in mobile hydrofractures. *Tectonophysics* **336**, 1–17.

Bottinga Y. and Javoy M. (1975) Oxygen isotope partitioning among the minerals in igneous and metamorphic rocks. *Rev. Geophys.* **13**, 401–418.

Bottinga Y. and Javoy M. (1990) Mid-ocean ridge basalt degassing: bubble growth and ascent. *Chem. Geol.* **81**, 255–270.

Brun J.P., Wenzel F. and ECORS-DEKORP team (1991) Crustal scale structure of the southern Rhine graben from ECORS-DEKORP seismic reflection data. *Geology* **19**, 758–762.

Cartigny P., Jendrzejewski N., Pineau F., Petit F., and Javoy M. (2001) Volatile (C, N, Ar) variability in MORB, and the respective roles of mantle source heterogeneity and degassing: the case of the Southwest Indian Ridge. *Earth Planet. Sci. Lett.* **194**, 241–257.

Cerrai E., Marchetti R., Renzoni R., Roseo L., Silvestri M. and Villani S. (1954) A thermal method for concentrating heavy water. *Chem. Eng. Prog. Symp.* **50**, 271-280.

Chen R.X., Zheng Y.F., Gong B., Zhao Z.F., Gao T.S., Chen B. and Wu Y.B. (2007) Origin of retrograde fluid in ultrahigh–pressure metamorphic rocks : Constraints from mineral hydrogen isotope and water content changes in eclogite–gneiss transitions in the Sulu orogen. *Geochim. Cosmochim. Acta* **71**, 2299–2325.

Cocherie A., Guerrot C., Fanning M. and Genter A. (2004) Datation U-Pb of two granites types from Soultz (Rhine Graben, France). *C. R. Geosciences* **336**, 775–787.

Criss R.E., Ekren E.B. and Hardyman R.F. (1984) Casto ring zone: A 4,500 km^2 fossil hydrothermal system in the Challis volcanic field, central Idaho. *Geology* **12**, 331–334.

Criss R.E. and Taylor H.P. (1986) Meteoric-hydrothermal systems. In *Stable Isotopes in High Temperature Geological Processes.* (eds. J.W. Valley, H.P. Taylor and J.R. O'Neil), Mineral. Soc. Am., **vol. 16**, 373–424.

Daux V., Lécuyer C., Adam F., Martineau F. and Vimeux F. (2005) Oxygen isotope composition of human teeth and the record of climate changes in France (Lorraine) during the last 1700 years. *Climatic Change* **70**, 445–464.

Debon F. and Lemmet M. (1999) Evolution of Mg/Fe ratios in late Variscan plutonic rocks from the external crystalline massifs of the Alps. (France, Italy, Switzerland). *J. Petrology* **40**, 1151–1185.

Demouchy S., Jacobsen S.D., Gaillard F. and Stern C.R. (2006) Rapid magma ascent recorded by water diffusion profiles in mantle olivine. *Geology* **34**, 429–432.

Dezayes C., Genter A. and Gentier S. (2004) Fracture Network of the EGS geothermal reservoir at Soultz–sous-Forêts (Rhine Graben, France). *Geotherm. Resour. Council Trans.* **28**, 213–218.

Dezes P., Schmid S.M. and Ziegler P.A. (2004) Evolution of the European Cenozoic Rift System: interaction of the Alpine and Pyrenean orogens with their foreland lithosphere. *Tectonophysics* **389**, 1–33.

Doebl F. and Olbrecht W. (1974) An isobath map of the Tertiary base in the Rhine graben. In *Approaches to taphrogenesis* (eds. J.H. Illies and K. Fuchs), Schweizerbart'sche Verlagsbuchhandlung, Stuttargt, 71–72.

Dubois et al., 1994

Dubois M., Ayt Ougougdal M., Meere P., Royer J.J., Boiron M-C. and Cathelineau M. (1996) Temperature of paleo-to modern self-sealing within a continental rift basin: the fluid inclusion data (Soultz sous Forets, Rhine graben, France). *Eur. J. Mineral.* **8**, 1065–1080.

Edel J.B., Schulmann K. and Rotstein Y. (2007) The Variscan inheritance of the Upper Rhine Graben: evidence of reactivation in the Lias, Late Eocene-Oligocene up to the recent. *Int. J. Earth Sci.* **96**, 305–325.

Farley K.A., Maier-Reimer E., Schlosser P. and Broecker W.S. (1995) Constraints on mantle ^{3}He fluxes and deep-sea circulation from an oceanic general circulation model. *J. Geophys. Res.* **100**, B3, 3829–3839.

Fontaine F.J., Rabinowicz M. and Boulègue J. (2003) Hydrothermal processes at Milos Island (Greek Cyclades) and the mechanisms of compaction–induced phreatic eruptions. *Earth Planet. Sci. Lett.* **210**, 17–33.

Fourcade S. and Allègre C.J. (1981) Trace element behavior in granite genesis – a case study: the calc-alkalic plutonism association from the Querigut complex (Pyrénées, France). *Contrib. Mineral. Petrol.* **76**, 177–195.

Früh-Green G., Plas A., Lécuyer C. (1996) Petrologic and stable isotope constraints on hydrothermal alteration and serpentinization of the EPR shallow mantle at Hess Deep (Site 895). In *Proc. ODP, Sci. Results, 147* (eds. C. Mével, K.M. Gillis, J.F. Allan and P.S. Meyer), College Station, TX (Ocean Drilling Program), 255–291.

Fu B., Touret J.L.R. and Zheng Y.-F. (2003) Remnants of premetamorphic fluid and oxygen isotopic signatures in eclogites and garnet clinopyroxenite from the Dabie–Sulu terranes, eastern China. *J. Metam. Geol.* **21**, 561–578.

Genter A. and Traineau H. (1992) Borehole EPS1, Alsace, France: preliminary geological results from granite core analyses for Hot Dry Rock research. *Sci. Drilling* **3**, 205–214.

Genter A., Traineau H., Dezayes C., Elsass P., Ledésert B., Meunier A. and Villemin T. (1995) Fracture analysis and reservoir characterization of the granitic basement in the HDR Soultz project (France). *Geotherm. Sci. Tech.* **4**, 189–214.

Gerard A. and Kappelmeyer O. (1987) The Soultz-sous-Forêts project and its specific characteristics with respect to the present state of experiments with HDR. *Geothermics* **16**, 393–399.

Giletti B.J. (1986) Diffusion effects on oxygen isotope temperatures of slowly cooled igneous and metamorphic rocks. *Earth Planet. Sci. Lett.* **77**, 218–228.

Giletti B.J. and Yund R.A. (1984) Oxygen diffusion in quartz. *J. Geophys. Res.* **89**, 4039–4046.

Graham C.M., Viglino J.A. and Harmon R.S. (1984) Experimental study of hydrogen-isotope exchange between aluminous chlorite and water and of hydrogen diffusion in chlorite. *Amer. Mineral.* **72**, 566–579.

Grant K.J., Ingrin J., Lorand J.P. and Dumas P. (2007) Water partitioning between mantle minerals from peridotite xenoliths. *Contrib. Mineral. Petrol.* **154**, 15–34.

Gregory R.T., Criss R.E. and Taylor H.P. (1989) Oxygen isotope exchange kinetics of mineral pairs in closed and open systems: applications to problems of hydrothermal alteration of igneous rocks and precambrian iron formations. *Chem. Geol.* **75**, 1–42.

Hall C.E. and Parmentier E.M. (2000). Spontaneous melt localization in a deforming solid with viscosity variations due to water weakening. *Geophys. Res. Lett.* **27**, 9–12.

Hart R.A. (1973) Geochemical and geophysical implications of the reaction between seawater and the oceanic crust. *Nature* **243**, 76-78.

Holtzman B.K., Groebner N., Zimmerman M., Ginsberg S. and Kohlstedt D. (2003) Stress–driven melt segregation in partially molten rocks. *Geochem. Geophys. Geosyst.* **4**, Art. No. 8607.

Hooijkaas G.R., Genter A. and Dezayes C. (2006) Deep seated geology of the granite intrusions at the Soultz EGS site based on 5 km depth boreholes. *Geothermics* **35**, 484–506.

Ito E. and Clayton R. N. (1983) Submarine metamorphism of gabbros from the Mid-Cayman Rise: An oxygen isotopic study. *Geochim. Cosmochim. Acta* **47,** 535–546.

Jacquemont B. (2002) Etude des interactions eau–roche dans le granite de Soultz–sous–Forêts. Quantification et modélisation des transferts de matière par les fluides. Ph. D. thesis, Université Louis Pasteur, Strasbourg.

Javoy M., Pineau F. and Delorme H. (1986) Carbon and nitrogen isotopes in the mantle. *Chem. Geol*. **57**, 41-62.

Kappelmeyer O. and Gérard A. (1989) The European project at Soultz-sous-Forets. In: *Proc. 4th Intl. Seminar on the Results of EC Geothermal Energy Research and Demonstration Florence* 27–30 April, Kluwer, 283–334.

Karato S. (1990) The role of hydrogen in the electrical conductivity of the upper mantle. *Nature* **347**, 272–273.

Katz R.F., Spiegelman M. and Holtzman B. (2006). The dynamics of melt and shear localization in partially molten aggregates. *Nature* **442**, 676–679.

Kelemen P.B., Hirth G., Shimizu N., Spiegelman M. and Dick H.J.B. (1997). A review of melt migration processes in the adiabatically upwelling mantle beneath oceanic spreading ridges. *Philosophical Transactions of the Royal Society of London, series A- Mathematical physical and engineering sciences* **355**, 283–318.

Keppler H. and Smyth J.R. (2006) Water in Nominally Anhydrous Minerals. *Mineral. Soc. Am.* **62**,Washington D.C. 478 pp.

King D.S.H., Zimmerman M.E. and Kohlstedt D.L. (2009). Stress–driven melt segregation in partially molten olivine-rich rocks deformed in Torsion. *J. Petrol.*, 10.1093/petrology/egp062.

Kishima N. and Sakai H. (1980) O-18 and deuterium determination on a single water sample of a few milligrams. *Anal. Chem.* **52**, 356-358.

Kohlstedt D.L., Zimmerman M.E. and Mackwell S.J. (2009) Stress-driven melt segregation in partially molten feldspathic rocks. *J. Petrol.,* doi:10**.**1093/petrology/egp043

Kyser T.K. (1986) Stable isotope variations in the mantle. In *Stable isotopes in high temperature geological processes.* (eds. J.W. Valley, H.P. Taylor and J.R. O'Neil), Review in Mineralogy **16**, Mineralogical Society of America. 141–164.

Lawrence J.R. and Taylor H.P. (1971) Deuterium and oxygen-18 correlation: clay minerals and hydroxides in quaternary soils compared to meteoric waters. *Geochim. Cosmochim. Acta* **35**, 993–1003.

Ledésert B., Berger G., Meunier A., Genter A. and Bouchet A. (1999) Diagenetic-type reactions related to hydrothermal alteration in the Soultz-sous-Forêts granite, France. *Eur. J. Miner.* **11**, 731–741.

Maridet O., Escarguel G., Costeur L., Mein P., Hugueney M. and Legendre S. (2007) Small mammals (rodents and lagomorphs) European biogeography from the Late Oligocene to the mid Pliocene. *Global Ecol. Biogeogr.* **16**, 529–544.

Moecher D.P., Valley J.W. and Essene E.J. (1994) Extraction and carbon isotope analysis of CO_2 from scapolite in deep crustal granulites and xenoliths. *Geochim. Cosmochim. Acta* **58**, 959–967.

Moore J.G. (1970) Water content of basalt erupted on the ocean floor. *Contrib. Miner. Petrol.* **28**, 272-279.

Morrison J., Brockwell T., Merren T., Fourel F. and Phillips A.M. (2001) Online high–precision stable hydrogen isotopic analysis on nanoliter water samples. *Anal. Chem.* **73**, 3570–3575.

Mosbrugger V., Utescher T. and Dilcher D.L. (2005) Cenozoic continental climatic evolution of Central Europe. *PNAS* **102**, 14964–14969.

Norton D. and Knight J. (1977) Transport phenomena in hydrothermal systems: cooling plutons. *Am. J. Earth Sci.* **277**, 937–981.

Norton D. and Taylor H.P.J. (1979) Quantitative simulation of the hydrothermal systems of crystallizing magmas on the basis of transport and oxygen isotopic data: an analysis of the Skaergaard intrusion. *J. Petrol.* **20**, 421–448.

O'Neil J.R. and Adami L.H. (1969) The oxygen isotope partition function ratio of water and the structure of liquid water. *J. Phys. Chem.* **73**, 1553-1558.

Parmentier E.M. (1981) Numerical experiments on O18 depletion in igneous intrusion cooling by ground water convection. *J. Geophys. Res.* **86**, 7131–7144.

Pauwels H., Fouillac C. and Fouillac A.M. (1993) Chemistry and isotopes of deep geothermal saline fluids in the Upper Rhine Graben: Origin of compounds and water–rock interactions. *Geochim. Cosmochim. Acta* **57**, 2737–2749.

Peslier A.H. and Luhr J.F. (2006) Hydrogen loss from olivines in mantle xenoliths from Simcoe (USA) and Mexico: mafic alkalic magma ascent rates and water budget of the sub-continental lithosphere. *Earth Planet. Sci. Lett.* **242**, 302–319.

Prodehl C., Mueller St., Glahn A., Gutscher M. and Haak V. (1992) Lithospheric cross section of the European Cenozoic Rift System (ECRIS). In *Geodynamic of rifting* (ed. P.A. Ziegler) *Tectonophysics* **208**, 113-138.

Rabinowicz M., Dandurand J.L., Jakubowski M. Schott J. and Cassan J.P. (1985) Convection in a North Sea oil reservoir; inferences on diagenesis and hydrocarbon mitigation. *Earth Planet. Sci. Lett.* **74**, 387–404.

Rabinowicz M. and Toplis M.J. (2009) Melt segregation in the lower part of the partially molten mantle zone beneath an oceanic spreading center: numerical modelling of the combined effects of shear segregation and compaction. *J. Petrol.* **50**, 1071–1106.

Rabinowicz M. and Vigneresse J.L. (2004) Melt segregation under compaction and shear channeling: application to granitic magma segregation in a continental crust. *J. Geophys. Res.* **109**, doi:10.1029/2002JB002372.

Ranero C.R., Phipps Morgan J., McIntosh K.D. and Reichert C. (2003) Bending, faulting, and mantle serpentinization at the Middle America trench. *Nature* **425**, 367–373.

Richardson C.N. (1998) Melt flow in a variable viscosity matrix. *Geophys. Res. Lett.* **277**, 937–981.

Roedder E. (1984) Fluid Inclusions. *Mineralogical Society of America, Reviews in Mineralogy* **12**, Washington D.C., 644 pp.

Rummel F. (1991) Physical properties of the rock in the granitic section of borehole GPK-1, Soultz-sous-Forêts. *Geotherm. Sci. Tech.* **3**, 199–216.

Saal A.E., Hauri E.H., Langmuir C.H. and Perfit M.R. (2002) Vapour undersaturation in primitive mid-ocean-ridge basalt and the volatile content of Earth's upper mantle. *Nature* **419**, 451-455.

Santosh M. and Tsunogae T. (2003) Extremely high density pure CO_2 fluid inclusions in a garnet granulite from southern India. *J. Geol.* **111**, 1–16.

Schidlowski M. (2001) Carbon isotopes as biogeochemical recorders of life over 3.8 Ga of Earth history: evolution of a concept. *Precamb. Res.* **106**, 117–134.

Schilling J.G., Bergeron M.B. and Evans R. (1980) Halogens in the mantle beneath the North Atlantic. *Phil. Trans. R. Soc. Lond.* **297**, 147-178.

Schnaebele R. (1948) Monographie géologique du champ pétrolifère de Péchelbronn. *Mem. Serv. Carte Géol. Alsace Lorraine* **7**, p. 254.

Schumacher M.E. (2002) Upper Rhine Graben: role of pre-existing structures during rift evolution. *Tectonics* **21**, 10.1029/2001TC900022.

Scott T. and Kohlstedt D.L. (2006) The effect of large melt fraction on the deformation behaviour of peridotite. *Earth Planet. Sci. Lett.* **246**, 177–187.

Simon L. (2003) Quelques exemples de modélisations géochimiques des interactions entre les enveloppes terrestres. Ph. D. thesis, Ecole Normale Supérieure de Lyon.

Smith M.P., Savary V., Yardley B.W.D., Valley J.W., Royer J.J. and Dubois M. (1998) The evoluton of the deep flow regim at Soultz sous Forets, Rhine graben, eastern France : Evidence from a composite quartz vein. *J. Geophys. Res.* **103**, B11, 27223–27237.

Stevenson D.J. (1989) Spontaneous small scale melt segregation in partial melts undergoing deformation. *Geophys. Res. Lett.* **16**, 1067–1070.

Stussi J., Cheilletz A., Royer J. Chevremont P. and Feraud G. (2002) The hidden monzogranite of Soultz-sous-Forêts (Rhine Graben, France). Mineralogy, petrology and genesis. *Géologie de la France* **1**, 45–64.

Suzuoki T. and Epstein S. (1976) Hydrogen isotope fractionation between OH–bearing minerals and water. *Geochim. Cosmochim. Acta* **40**, 1229–1240.

Swanenberg H.C. (1980) Fluid inclusions in high grade metamorphic rocks from SW *Norway. Geol. Ultraiectina* **25**, 1–147.

Taylor H.P. (1968) The oxygen isotope geochemistry of igneous rocks. *Contrib. Mineral. Petrol.* **19**, 1–71.

Taylor H.P. (1977) Water/rock interactions and the origin of H_2O in granitic batholiths. *J. Geol. Soc. London*. **133**, 509–558.

Taylor H.P. (1988) Oxygen, hydrogen, and strontium isotope constraints on the origin of granites. *Trans. Royal Soc. Edinburgh* **79**, 317–338.

Taylor H.P. and Sheppard S.M.F. (1986) Igneous rocks: I. Processes of isotopic fractionation and isotope systematics. In *Stable Isotopes in High Temperature Geological Processes.* (eds. J.W. Valley, H.P. Taylor and J.R. O'Neil). *Mineral. Soc. Am.* **16**, 227–271.

Tenzer H., Mastin L. and Heinemann B. (1991) Detremination of planar discontinuities and borehole geometry in the crystalline rocks of the borehole GPK1 at Soultz-sous Forets. *Geotherm. Sci. Tech.* **3**, 31-67.

Touret J. (1971) Le faciès granulitique en Norvège Méridionale II : Les inclusions fluides. *Lithos* **4**, 423–436.

Touret J. (1995) Fluid regile in southern Norway, the record of fluid inclusions. In *The deep Proterozoic crust in the North Antlantic Provinces*. (eds. A.C. Tobi and J.L.R. Touret), NATO ASI Ser. C. Reidel Publishing Company. 517–549.

Touret J. (2001) Fluids in metamorphic rocks. *Lithos* **55**, 1–25.

Touret J. and Dietvorst P. (1983) Fluid onclusions in migmatites. In *Migmatites* (ed. J.R. Ashworth), Blackie, Glassgow, 265-288.

Traineau H., Genter A., Cautru J., Fabriol H. and Chevremont P. (1991) Petrography of the granite massif from drill cutting analysis and well log interpretation in the geothermal HDR borehole GPK1 (Soultz, Alsace, France). *Geotherm. Sci. Tech.* **3**, 1–29.

Utescher T., Mosbrugger V., Ivanov D. and Dilcher D.L. (2009) Present–day climatic equivalents of European Cenozoic climates. *Earth Planet. Sci. Lett.* **284**, 544–552.

Vennemann T.W. and O'Neil J.R. (1993) A simple inexpensive method of hydrogen isotope and water analysis of minerals and rocks based on zinc reagent. *Chem. Geol.* **103**, 227–234.

Villemin T., Alvarez F. and Angelier J. (1986) The Rhine graben : extension, subsidence and uplift. *Tectonophysics* **128**, 45–59.

Von Grafenstein U., Erlenkeuser H., Müller J., Trimborn P. and Alefs J. (1996) A 200 year mid-European air temperature record preserved in lake sediments : An extension of the δ^{18}O-air temperature relation in the past. *Geochim. Cosmochim. Acta* **60**, 4025–4036.

Wickham S.M. and Taylor H.P. (1987) Stable isotope constraints on the origin and depth of penetration of hydrothermal fluids associated with Hercynian low-pressure regional and crustal anatexis in the Pyrenées. *Contrib. Mineral. Petrol.* **95**, 255–268.

Xia Q.K., Yang X.Z., Deloule E., Sheng Y.M. and Hao Y.T. (2006) Water in the lower crustal granulite xenoliths from Nushan, eastern China. *J. Geophys. Res.* **111,** 10.1029/2006JB004296.

Yardley B.W., Meere A., Cathelineau M. and Valley J. (1995) Are quartz veins forming under Strasbourg today? A stable isotope study of veins quartz from Soult-sous-Forêts. *Terra Nova abstr.* **7**, 185.

Zachos J.C., Pagani M., Sloan L., Thomas E. and Billups K. (2001) Trends, rhythms, and aberrations in global climate, 65 Ma to present. *Science* **292**, 686–693.

Figures captions

Figure 1: **A:** Tertiary rift system (ECRIS) of Western Europe showing the Cenozoic faults system (black lines) and the rift related sedimentary basin (light grey). **B:** Isobaths map of the pre-Tertiary basement, after Doebl and Olbrecht (1974) and Edel et al., (2007). **C:** Interpretive A-B cross section of the ECORS Rhine graben profile (after Brun et al., 1991).

Figure 2: Location of the GPK1, GPK2 and EPS1 boreholes on a vertical cross section of the Soultz-sous-Forêts area. Pictures of the different monzogranite types and of the two-mica granite drilled in EPS1 and GPK2 boreholes. **A:** Aspect of the altered monzogranite affected by a cataclastic event and quartz vein post-dating the cataclastic event. **B:** Aspect of the propylitic facies by pervasive alteration of monzogranite. C: Standard porhyritic monzogranite. D: Geodic quartz sealing fractures.

Figure 3: Schematic representation of the different fracturing and alteration events occurring in the granitic basement (after Bataillé, 2004). Temperature and mineralogical assemblages developed during the hydrothermal alteration are from petrologic observations (Stussi et al., 2001), salinity of the fluid interacting with the rock is deduced from fluid inclusion studies (Dubois et al., 1996, Smith et al 1998).

Figure 4: Photomicrographs of the different types of monzogranite. **A:** Centimetre size K-feldspar+ biotite + plagioclase + quartz. **B:** Chlorite and serricite development at the expense of biotite and K-feldspar respectively due to the pervasive alteration of the monzogranite, note the cloudy aspect of the K-feldspar. **C:** Calcite, epidote and quartz vein post-dating the pervasive alteration in the monzogranite. **D:** Photomicrograph of the two-mica granite. **E:** Photomicrograph of quartz crystals from a 2200m depth quartz vein in the monzogranite revealing at least two growth steps. **F:** Isolated primary fluid inclusions in quartz grain. **G:** Trail-bound of secondary fluid inclusions sealing micro cracks in quartz grains.

Figure 5: A -Variations in the amount of CO_2 in fluid inclusions per gram of monzogranite from Soultz-sous-Forêts (Alsace, France) and, B - Variations of its $\delta^{13}C$ as a function of depth in the borehole EPS-1.

Figure 6: Variations in the $\delta^{13}C$ of CO_2 in fluid inclusions as a function of the amount of CO_2 in fluid inclusions per gram of monzogranite. The correlation line suggests a mixing between two sources of carbon derived from superficial carbonates and the deep crust or shallow mantle.

Figure 7: A -Variations in the amount of C in the monzogranite from Soultz-sous-Forêts (Alsace, France) and, B - Variations of its $\delta^{13}C$ as a function of depth in the borehole EPS-1.

Figure 8: Variations in a δD–$\delta^{18}O$ space of the compositions of fluid inclusions from quartz of monzogranite and of geodic quartz (sγ79) occurring in veins crosscutting the monzogranite dome.

Figure 9: Schematic representation of the fluid sources affecting fluid composition trapped in quartz grains from the granitic basement. The arrows indicate possible fluid inputs to the granitic basement.

Figure 10: Photomicrographs of the cored monzogranite. A: Basal section. B: Longitudinal section (Bio: biotite; K–fld: potassic feldspar; Plg: plagioclase; Qtz: quartz). See text for more explanations.

Table captions

Table 1: Amount of CO_2, $\delta^{13}C$ and δD values of carbon dioxide and water extracted from fluid inclusions decrepitated at low (350°C) and high (700°C) temperatures. Depth sampling are reported for four monzogranite samples (Sγ1, Sγ10, Sγ13 and Sγ18) taken in EPS1

borehole and one two-mica granite (Sγ28) taken in GPK2 borehole (Soultz-sous-Forêts, Alsace, France).

Table 2: Amounts of CO_2 in fluid inclusions per gram of monzogranite from Soultz-sous-Forêts (Alsace, France) along with its $\delta^{13}C$, and δD–$\delta^{18}O$ values of water from fluid inclusions.

Table 3: $\delta^{13}C$ values and amounts of C along with δD values of water from bulk monzogranites (Sγ1 to Sγ18) and in one sample from the two-mica granite (Sγ28).

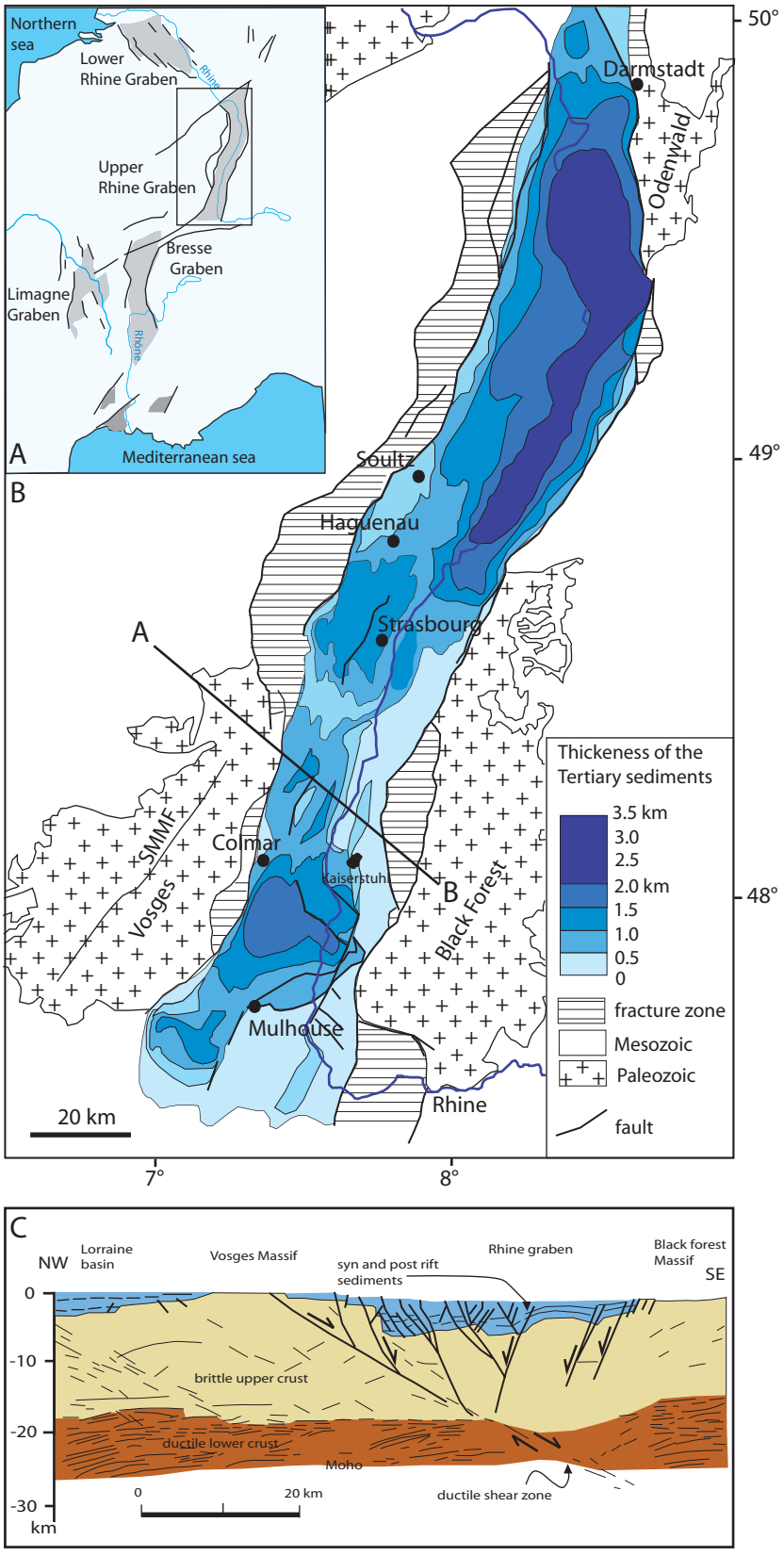

FIG. 1 – A: Tertiary rift system (ECRIS) of Western Europe showing the Cenozoic faults system (black lines) and the rift related sedimentary basin (light grey). B: Isobaths map of the pre-Tertiary basement , after Doebl and Olbrecht (1974) and Edel et al., (2007). C: Interpretive A-B cross section of the ECORS Rhine graben profile (after Brun et al., 1991).

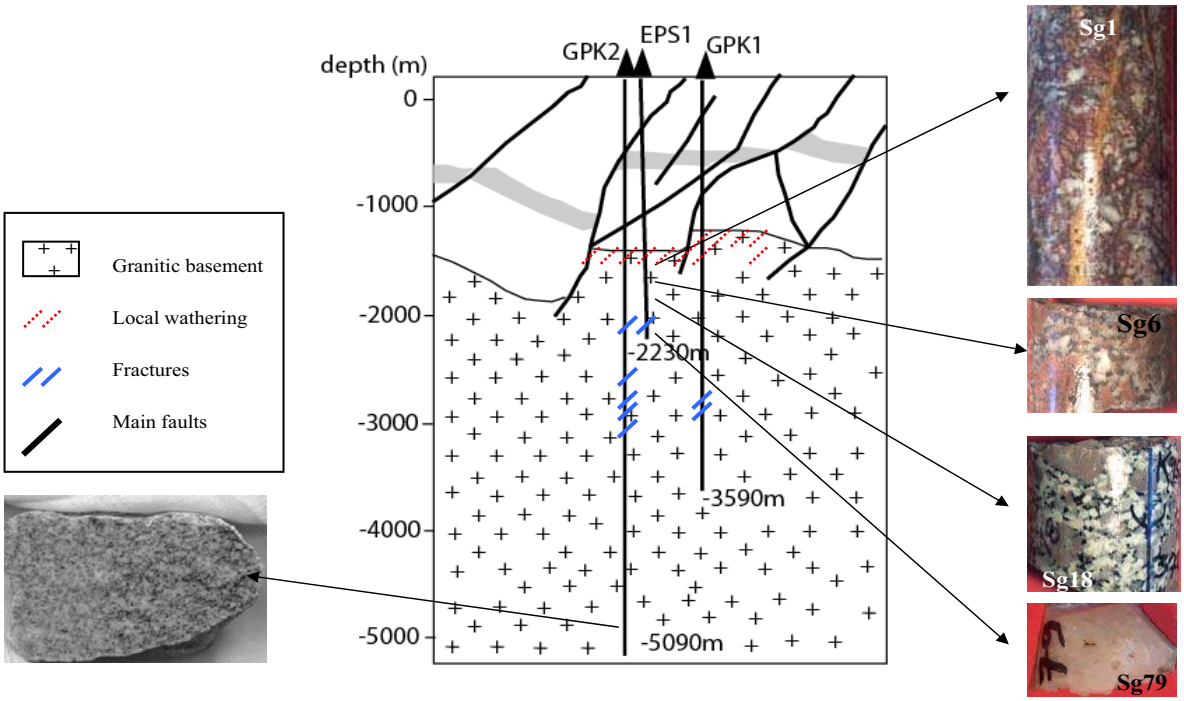

FIG. 2 – Location of the GPK1, GPK2 and EPS1 boreholes on a vertical cross section of the Soultz-sous-Forêts area. Pictures of the different monzogranite types and of the two-mica granite drilled in EPS1 and GPK2 boreholes. A: Aspect of the altered monzogranite affected by a cataclastic event and quartz vein post-dating the cataclastic event. B: Aspect of the propylitic facies by pervasive alteration of monzogranite. C: Standard porhyritic monzogranite. D: Geodic quartz sealing fractures.

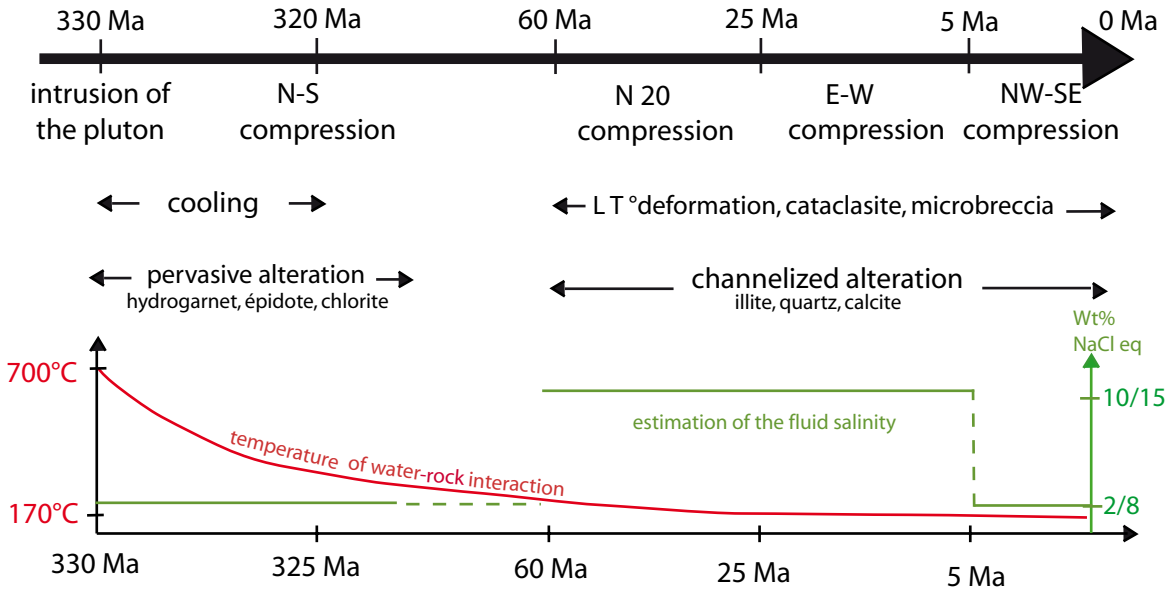

FIG. 3 – Schematic representation of the different fracturing and alteration events occurring in the granitic basement (after Bataillé, 2004). Temperature and mineralogical assemblages developed during the hydrothermal alteration are from petrologic observations (Stussi et al., 2001), salinity of the fluid interacting with the rock is deduced from fluid inclusion studies (Dubois et al., 1996, Smith et al 1998).

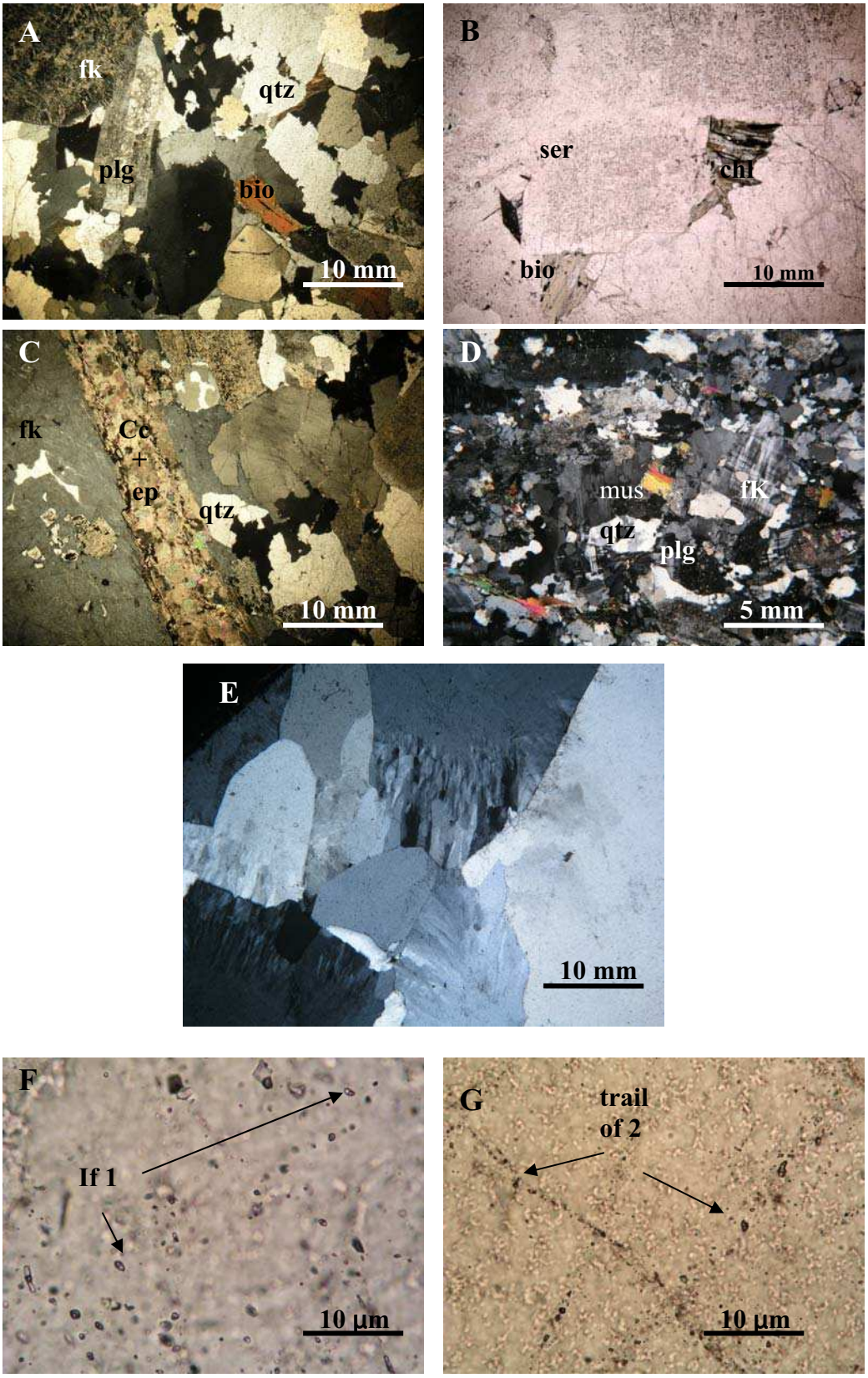

FIG. 4 – Photomicrographs of the different types of monzogranite. A: Centimetre size K-feldspar + biotite + plagioclase + quartz. B: Chlorite and serricite development at the expense of biotite and K-f feldspar respectively due to the pervasive alteration of the monzogranite, note the cloudy aspect of the K-feldspar. C: Calcite, epidote and quartz vein post-dating the pervasive alteration in the monzogranite. D: Photomicrograph of the two-mica granite. E: Photomicrograph of quartz crystals from a 2200 m depth quartz vein in the monzogranite revealing at least two growth steps. F: Isolated primary fluid inclusions in quartz grain. G: Trail-bound of secondary fluid inclusions sealing micro cracks in quartz grains.

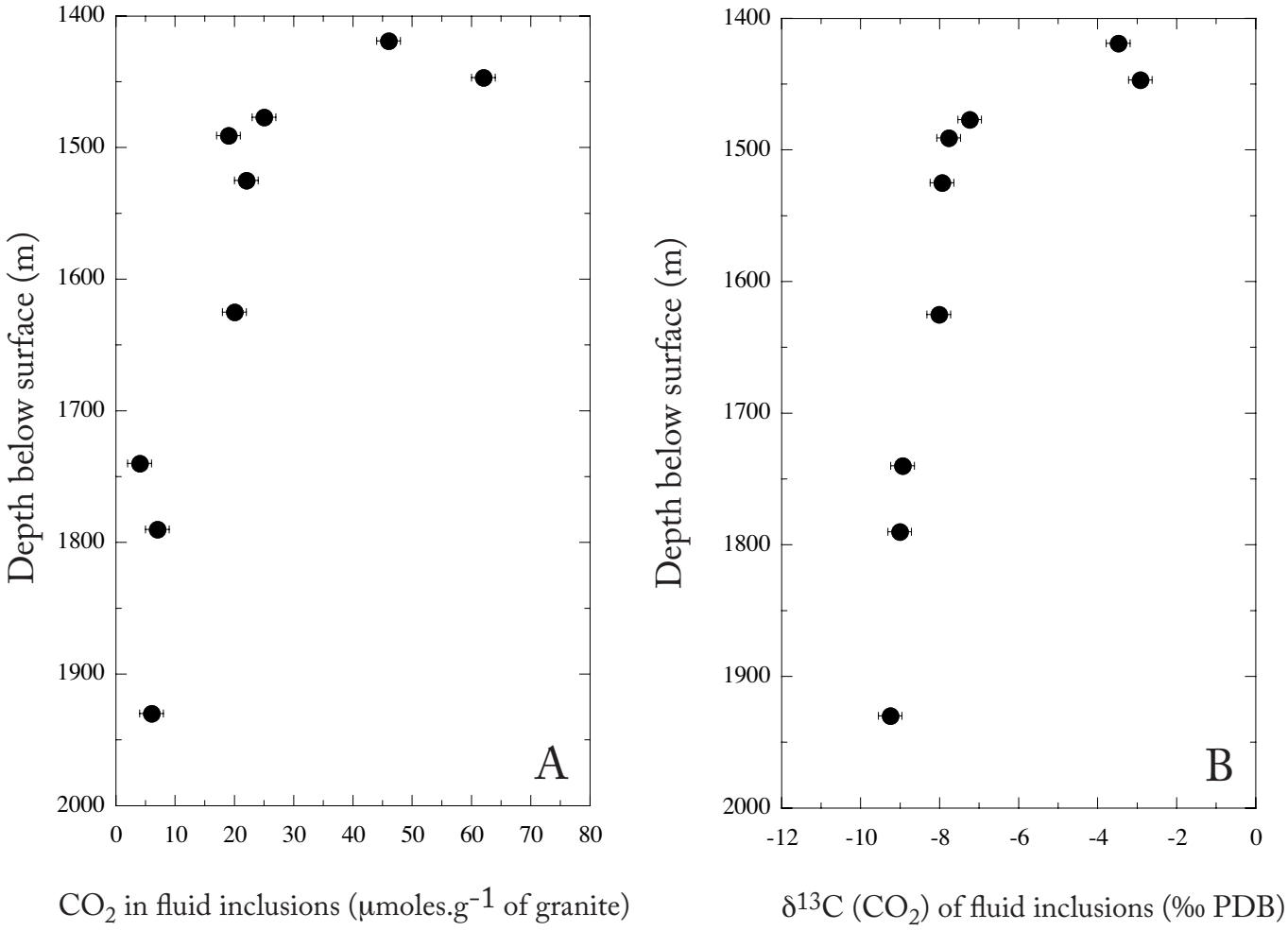

FIG. 5 – A -Variations in the amount of CO_2 in fluid inclusions per gram of monzogranite from Soultz-sous-Forêts (Alsace, France) and , B - Variations of its $\delta^{13}C$ as a function of depth in the borehole EPS-1.

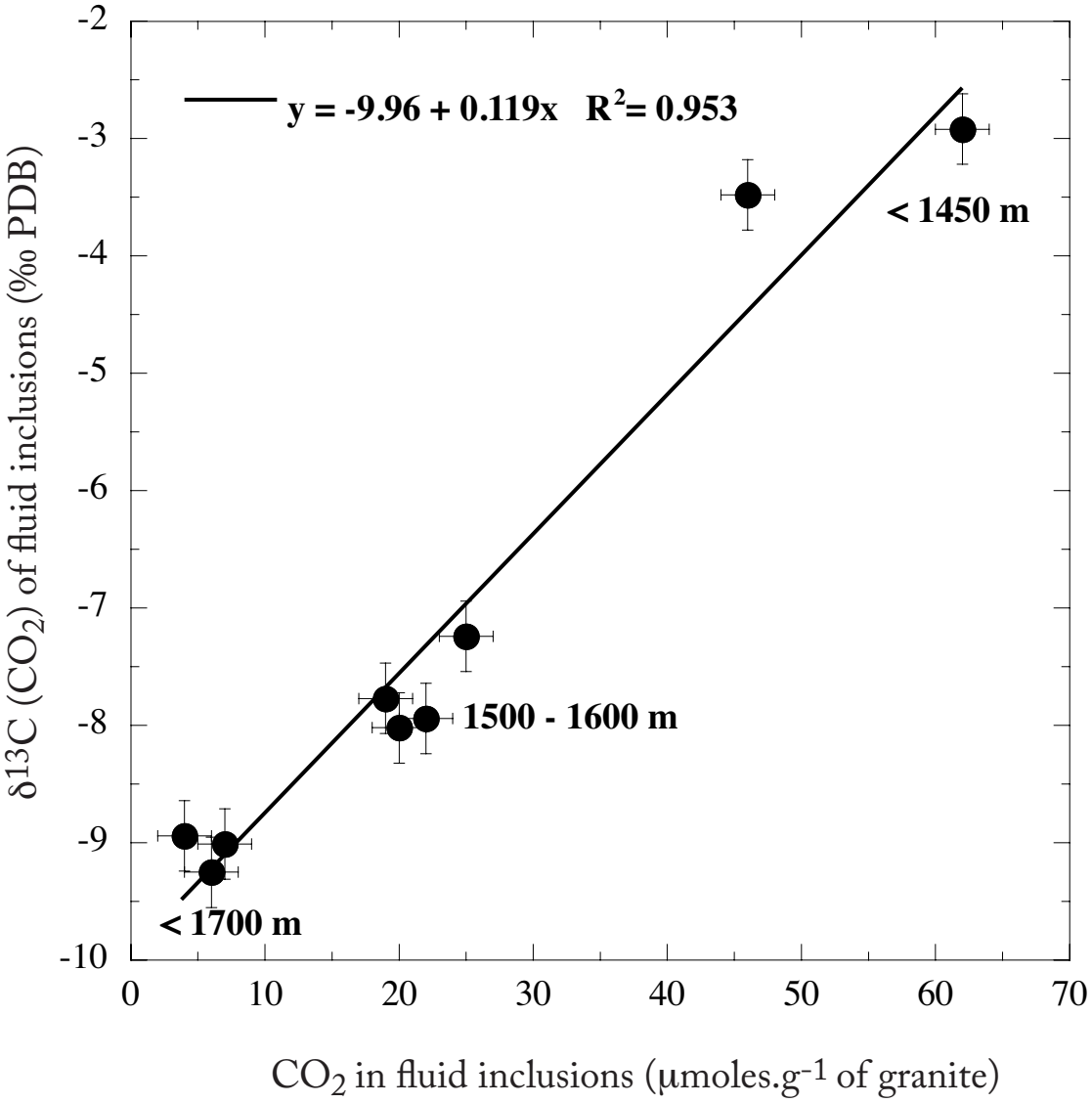

FIG. 6 – Variations in the d^{13}C of CO_2 in fluid inclusions as a function of the amount of CO_2 in fluid inclusions per gram of monzogranite. The correlation line suggests a mixing between two sources of carbon derived from superficial carbonates and the deep crust or shallow mantle.

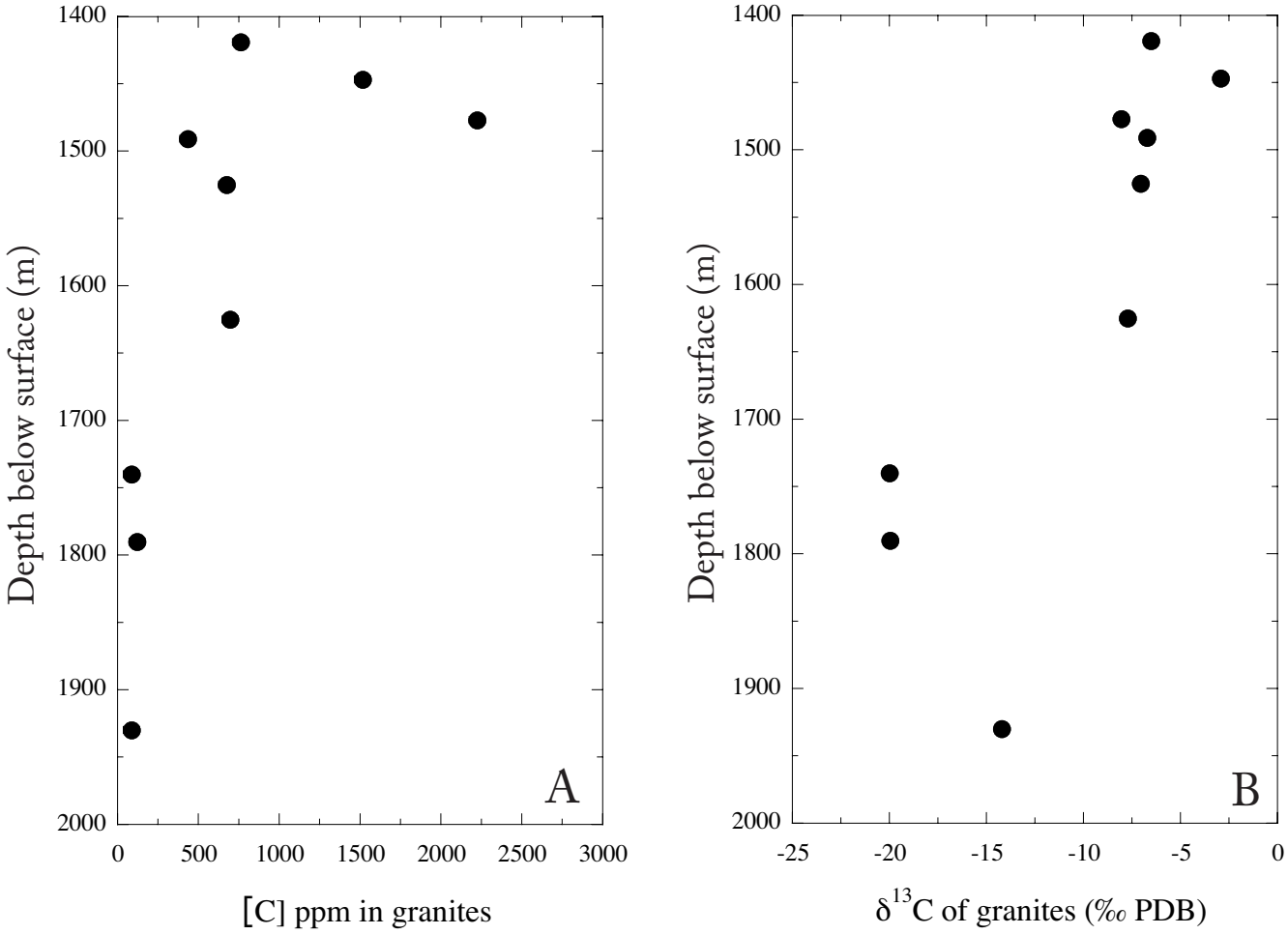

FIG. 7 – A -Variations in the amount of C in the monzogranite from Soultz-sous-Forêts (Alsace, France) and, B - Variations of its $\delta^{13}C$ as a function of depth in the borehole EPS-1.

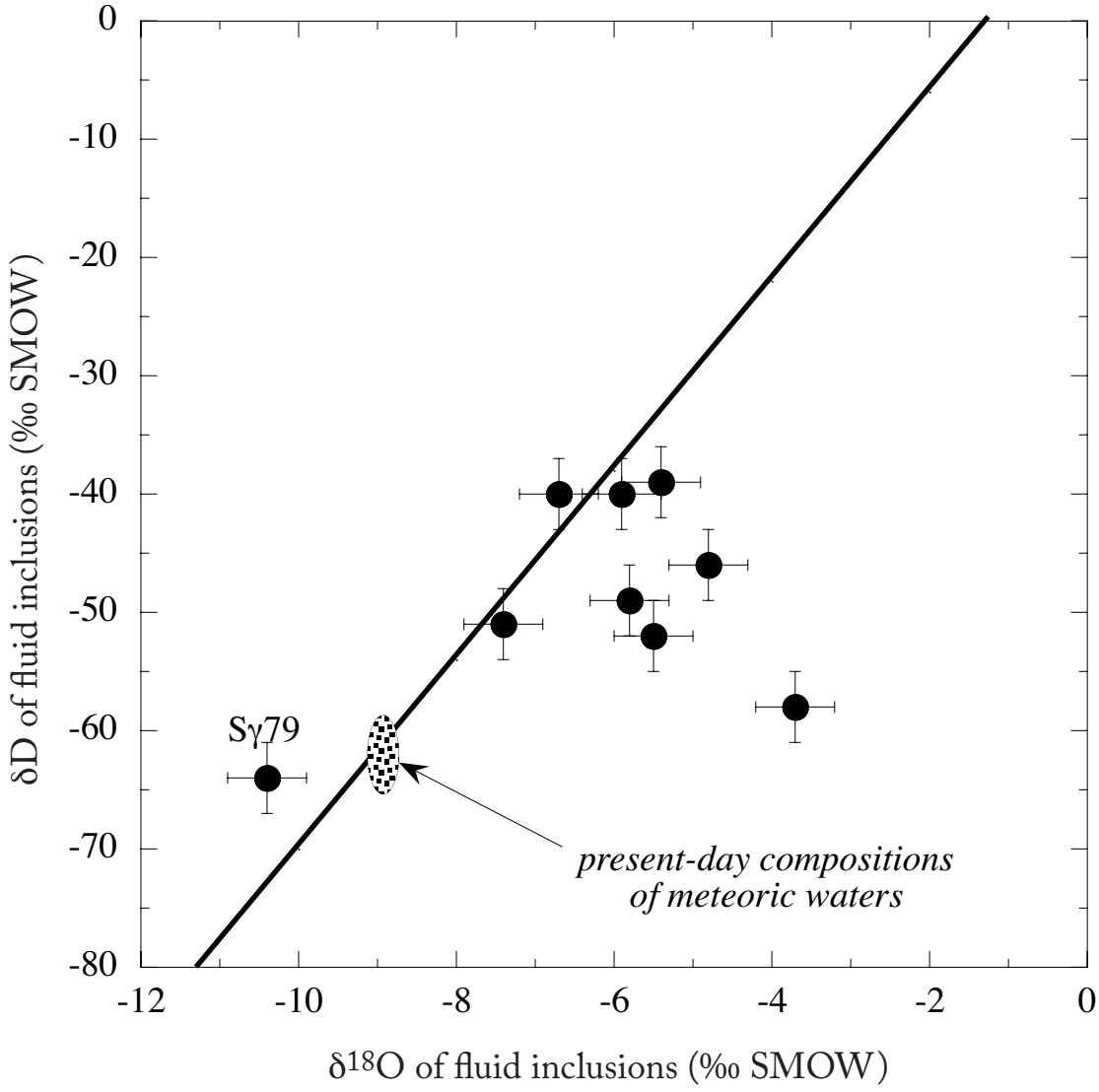

FIG. 8 – Variations in a δD–δ^{18}O space of the compositions of fluid inclusions from quartz of monzogranites and of geodic quartz (sγ79) occurring in veins crosscutting the monzogranite dome.

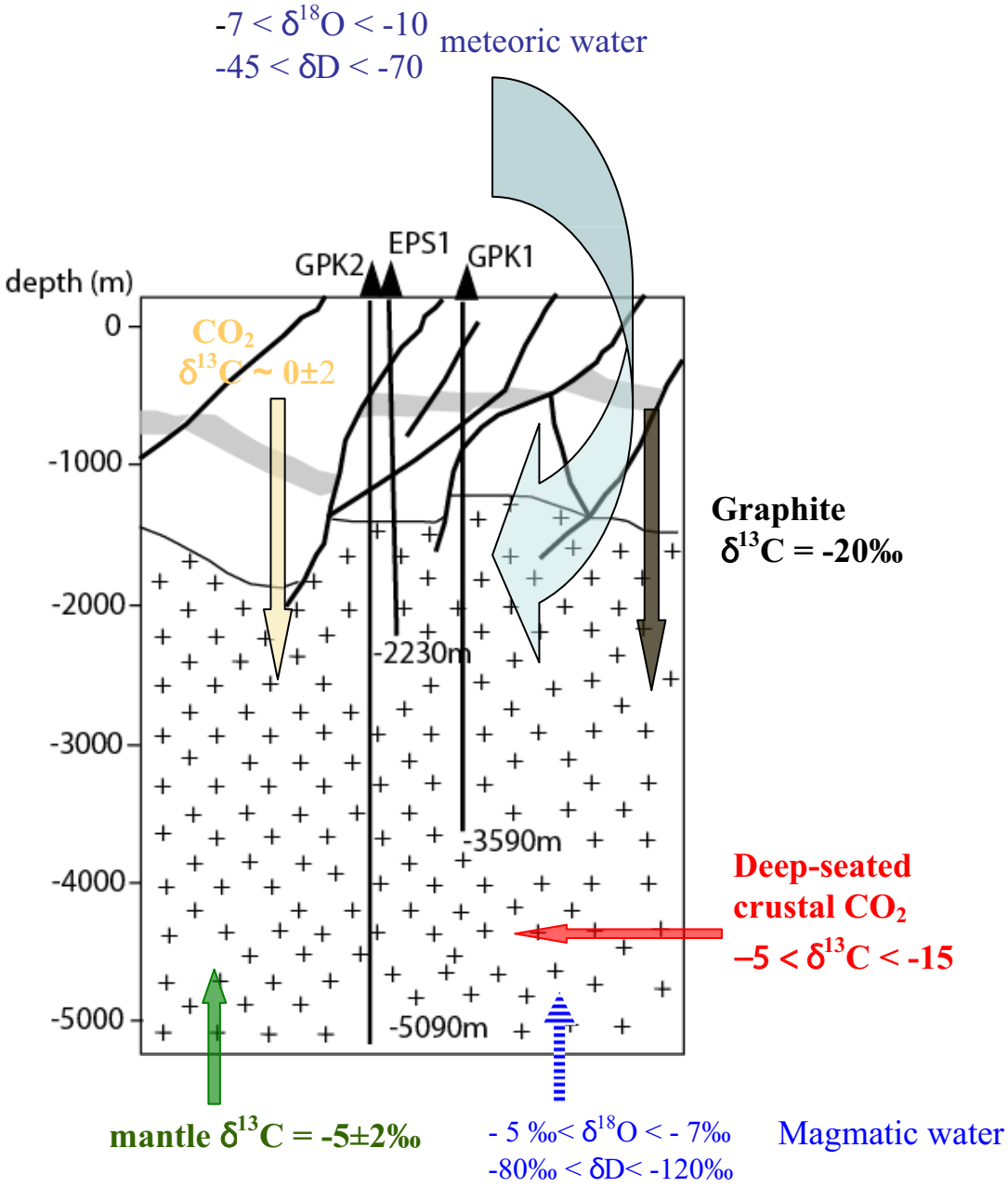

FIG. 9 – Schematic representation of the fluid sources affecting fluid composition trapped in quartz grains from the granitic basement. The arrows indicate possible fluid inputs to the granitic basement.

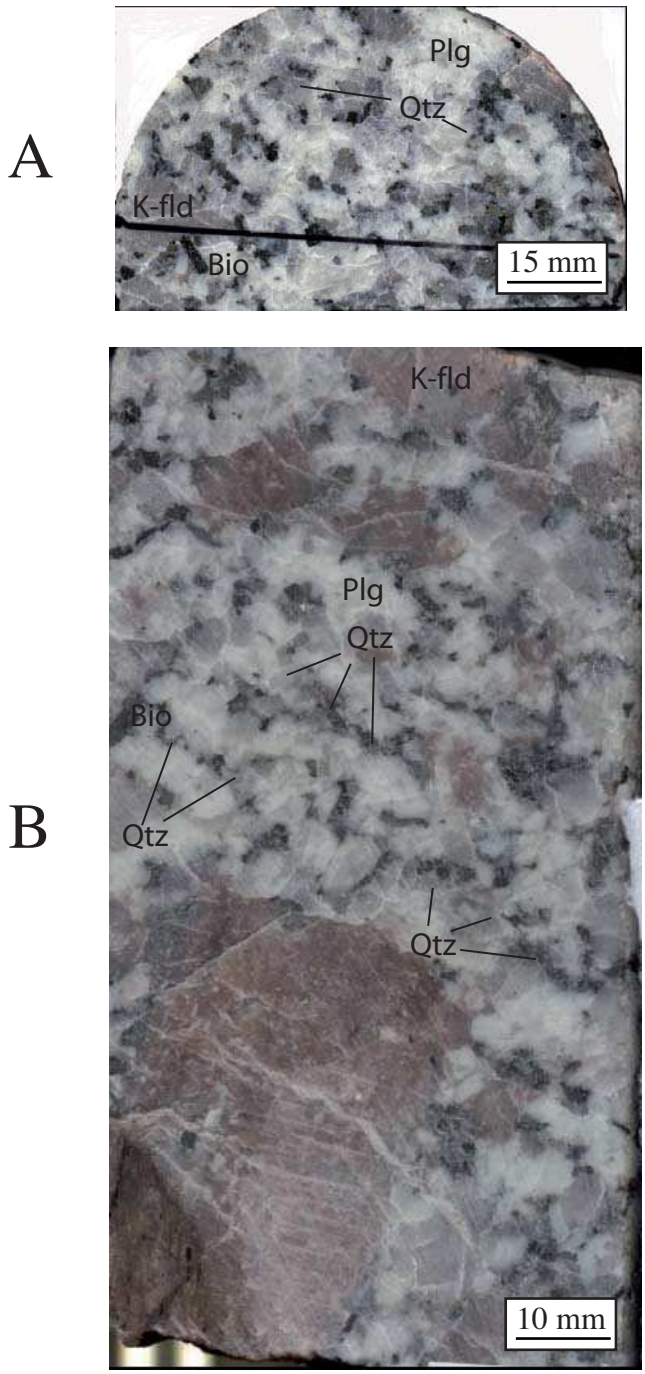

FIG. 10 – Photomicrographs of the cored monzogranite. A: Basal section. B: Longitudinal section (Bio: biotite; K–fld: potassic feldspar; Plg: plagioclase; Qtz: quartz). See text for more explanations.

Sample	Depth (m)	T (°C)	μmoles CO_2	$\delta^{13}C$ CO_2	δD H_2O
Sγ1	1419	350	ε	n.d.	-38.3
		700	13.4	-3.35	-49.5
Sγ10	1625	350	ε	n.d.	-44.2
		700	25	-7.82	-44.9
Sγ13	1790	350	ε	n.d.	-46.6
		700	8.8	-9.17	-50.7
Sγ18	1930	350	ε	n.d.	-66.2
		700	6	-8.42	-42.6
Sγ28	5058	350	ε	n.d.	-39.9
		700	4	-7.1	-51.6

TAB. 1 – Amount of CO_2, $\delta^{13}C$ and δD values of carbon dioxide and water extracted from fluid inclusions decrepitated at low (350°C) and high (700°C) temperatures. Depth sampling are reported for four monzogranite samples (Sγ1, Sγ10, Sγ13 and Sγ18) taken in EPS1 borehole and one two-mica granite (Sγ28) taken in GPK2 borehole (Soultz-sous-Forêts, Alsace, France).

sample	depth (m)	μmoles CO_2 /g rock (f.i.)	$\delta^{13}C$ CO_2	δD H_2O (f.i.)	$\delta^{18}O$ H_2O (f.i.)
Sγ1	1419	46	-3.48	-40	-5.9
Sγ2	1447	62	-2.92	-58	-3.7
Sγ3	1477	25	-7.24	-49	-5.8
Sγ4	1491	19	-7.77	-59	-15.7
Sγ6	1525	22	-7.94	-51	-7.4
Sγ10	1625	20	-8.02	-46	-4.8
Sγ12	1740	4	-8.94	-39	-5.4
Sγ13	1790	7	-9.01	-52	-5.5
Sγ18	1930	6	-9.25	-40	-6.7
Sγ79	2200	-	n.d.	-64	-10.4
Sγ28	5058	4	-7.1	-52	-

TAB. 2 – Amounts of CO_2 in fluid inclusions per gram of monzogranite from Soultz-sous-Forêts (Alsace, France) along with its $\delta^{13}C$, and δD–$\delta^{18}O$ values of water from fluid inclusions.

sample	depth (m)	ppm C	$\delta^{13}C$ (C)	δD
Sγ1	1419	761	-6.5	-56
Sγ2	1447	1516	-2.9	-45
Sγ3	1477	2224	-8.1	-68
Sγ4	1491	435	-6.7	-49
Sγ6	1525	675	-7.1	-53
Sγ10	1625	697	-7.7	-53
Sγ12	1740	87	-20.0	-57
Sγ13	1790	121	-20.0	-50
Sγ18	1930	87	-14.2	-45
Sγ28	5058	827	-41.9	-48

TAB. 3 – Amount of CO_2, $\delta^{13}C$ and δD values of carbon dioxide and water extracted from fluid inclusions decrepitated at low (350°C) and high (700°C) temperatures. Depth sampling are reported for four monzogranite samples (Sγ1, Sγ10, Sγ13 and Sγ18) taken in EPS1 borehole and one two-mica granite (Sγ28) taken in GPK2 borehole (Soultz-sous-Forêts, Alsace, France).

Chapitre 7

Les inclusions fluides dans les granulites : nature, sources et mélanges des fluides à l'interface croûte - manteau supérieur.

7.1.

CO_2 and H_2O sources and transfers at the crust–mantle boundary: $\delta^{13}C$ and δD of fluid inclusions in granulites.

Sources et trnsferts de CO_2 et H_2O à l'interface croûte–manteau: $\delta^{13}C$ et δD des inclusions fluides dans les granulites.

Résumé

Les rapports isotopiques de l'hydrogène de H_2O et du carbone de CO_2 ont été déterminés pour des granulites d'âge Précambrien (3,3 Ga) à Miocène (18 Ma). L'eau (–97‰ < δD < –55‰) et le dioxyde de carbone (valeur de $\delta^{13}C$ moyenne = –6.3 ±3.4‰) des inclusions primaires riches en CO_2 sont principalement d'origine mantellique. Les inclusions secondaires riches en H_2O contiennent des fluides d'origine crustale (–139‰ < δD < –86‰) tels que des eaux météoriques et du dioxyde de carbone provenant de l'oxydation de la matière organique ($\delta^{13}C$ ~ -15‰) ou de la décarbonation des carbonates sédimentaires ($\delta^{13}C$ ~ -2,5‰). Les valeurs de δD (–142‰ à –52‰) des minéraux hydratés des granulites (amphibole et biotite) ne peuvent pas être reliées aux compositions isotopiques des eaux piégées dans les inclusions primaires ou secondaires. Ces valeurs sont plus probablement reliées à des événements crustaux tels que l'évolution métamorphique rétrograde des granulites. Les compositions isotopiques de l'hydrogène et du carbone des granulites semblent être reliées aux évolutions isotopiques des cycles globaux de l'eau et du carbone. La relative stabilité des compositions isotopiques du carbone à travers le temps pour le CO_2 des inclusions primaires des granulites peut refléter au premier ordre la stabilité de la composition isotopique du carbone du manteau supérieur tout au long de l'histoire de la Terre. En revanche, les valeurs de δD obtenues sur la roche totale des granulites diminuent d'environ 25 ±5‰ entre l'Archéen et le Miocène, avec un changement rapide qui s'est produit il y a 2 Ga et qui pourrait refléter la mise en place d'une atmosphère oxydante à la surface de la Terre.

CO_2 and H_2O sources and transfers at the crust-mantle boundary: $\delta^{13}C$ and δD of fluid inclusions in granulites

Thomas Rigaudier[1], Véronique Gardien[1], Christophe Lécuyer[1,2], Laurent Simon[3] and François Martineau[1].

[1]UMR CNRS 5125 PaléoEnvironnements et PaléobioSphère, Université Lyon 1, Campus de la DOUA, Bâtiment Géode, 69622 Villeurbanne Cedex, France

[2]Institut Universitaire de France, Paris, France.

[3]UMR-CNRS 5023, Laboratoire d'Ecologie des Hydrosystèmes Fluviaux, Université Lyon 1, Campus de la DOUA, 69622 Villeurbanne Cedex, France

Keywords: granulite, mantle, crust, fluid inclusion, stable isotope, carbon dioxide, water

Abstract – Hydrogen isotope ratios of H_2O and carbon isotope compositions of CO_2 were measured in fluid inclusions from granulites that formed from Precambrian (3.3 Ga) to Miocene (18 Ma) either in subduction or collision contexts. Water (–97‰ < δD <–55‰) and carbon dioxide (mean $\delta^{13}C$ value = –6.3±3.4‰) in primary CO_2–rich fluid inclusions could mainly derive from a mantle source. Secondary H_2O –rich inclusions are most likely dominated by fluids of crustal origin (–139‰ < δD <–86‰) such as meteoric waters and carbon dioxide resulting from either the oxidation of organic matter ($\delta^{13}C$ as low as –15‰) or decarbonation of sedimentary carbonates ($\delta^{13}C$ as high as –2.5‰). Hydrogen isotope compositions of granulite–forming hydrous minerals (amphibole and biotite) cannot be related to the compositions of waters trapped either in primary or secondary inclusions. Bulk δD values which range from –142‰ to –52‰ are most likely related to crustal events such as the retrograde metamorphic evolution of granulites which can themselves have inherited from the composition of a partly hydrated protolith. Hydrogen and carbon stable isotope compositions of granulites seem to be related to the secular isotopic evolution of the global carbon and water cycles. The rather constancy of carbon isotope compositions through time for CO_2 in primary fluid inclusions of granulites could reflect at first order the constancy of carbon isotope composition of the upper mantle over the Earth's history. By contrast, δD values of bulk granulites decrease by about 25±5‰ from the Archean to the Miocene, with an abrupt change that took place about 2 Gy ago, and could reflect the onset of Earth's oxic surface conditions.

1. Introduction

Granulite is a key lithology in the composition of the lower crust and its genesis at about 5–10 kb and 600–800°C is associated with both water and carbon dioxide fluxes that take place at the crust–mantle boundary. Granulite genesis is considered to operate under high CO_2 activities relative to water (e.g. Touret, 1971; Coolen, 1982; Andersen et al., 1997; Pili et al., 1997; Tsunogae et al., 2002; Santosh and Tsunogae, 2003). Various models were proposed to explain the low activities of water and the dehydration of the lower crust under granulitic facies conditions. Newton et al. (1980) suggest that the crust metamorphosed under granulite facies conditions is infiltrated by an important amount of CO_2 of mantellic or crustal origin. In the absence of a meaning CO_2 infiltration, the weak activities of water could be produced by plugging during melting reactions (Powell, 1983). Another possibility is that the granulitic metamorphism is set up in an already dehydrated crust (Lamb and Valley, 1984). If granulites are formed according to one of the last two models then the quantities of CO_2 will be low in the crust under granulitic facies conditions. Therefore, the identification of these fluid sources and their relative flux amplitudes not only play a role in our understanding of granulite genesis, heat transfer and rheology of the lower crust but also of water and carbon cycle dynamics through time.

Tiny fluid inclusions trapped in silicates of the granulite paragenesis (pyroxene, garnet, quartz) constitute the only direct remnants of the fluids that circulated at the time of granulite genesis. Combination of microthermobarometry and stable isotope analysis of primary fluid inclusions in granulites can potentially lead to identify the mantle or crustal origin of water and carbon dioxide at the P–T conditions at which they were trapped in the lower crust. Carbon isotope composition of CO_2 and hydrogen isotope composition of H_2O may vary through time as a response to large scale interactions between Earth's envelopes. Mantle

degassing, continental growth, hydrothermal activity, plate subduction and the onset of an oxic atmosphere most likely contributed to modify the long–term compositions of carbon and water in the mantle, crustal and ocean reservoirs (e.g. Glassley, 1983; Holland, 1984; Alt, 1995; Taylor and McLennan, 1995). Moreover, the relative contributions of fluids derived from surficial and deep sources may be associated with a given geodynamic context in which granulites were generated. Granulites form either in subduction, extension or collision contexts where decarbonation of carbonate rocks or dehydration of previously hydrated protolith (by meteoric or marine waters) could also contribute in addition to water and carbon dioxide derived from mantle degassing.

Therefore we determined both δD values of H_2O and $\delta^{13}C$ values of CO_2 from fluid inclusions along with the bulk δD values of their host granulites sampled worldwide and that formed from Precambrian (3.3 Ga) to Miocene (18 Ma) either in subduction, extension or collision contexts. The resulting database is firstly used to discuss the role of fluids in the genesis and evolution of granulites and whether or not their stable isotope compositions could constitute a geochemical signature of their geotectonic environments. Secondly, this geochemical record in granulites is examined as a possible new way to track the long–term stable isotope evolution of carbon and water cycles.

2. Sample description and analytical procedures

2.1. Samples

A suite of Precambrian (3.3 Ga) to Miocene (18 Ma) metamorphic rocks corresponding to the granulites facies has been investigated for this study (sample locations and descriptions are given in Table 1 and Figure 1). These rocks have been formed either in

subduction or collision zones. The mineralogical compositions (Table 1) of granulites indicate basic (GAL 26-10, CZ2, EAR 34), acidic (GD 04.167, YR DDU) and intermediate (SZ 35b, L 647) compositions.

Basic granulites:

- Sample GAL 26–10 (Figure 2a) is a basic anhydrous orthogranulite with a granoblastic texture. The well-preserved granulitic assemblage consists of orthopyroxene, clinopyroxene, plagioclase, quartz, K-feldspar, and iron oxide. Retrograde metamorphism is limited to the development of secondary biotite and bastite in replacement of feldspars and pyroxenes, respectively. Undulose extinctions in quartz, feldspars and pyroxenes indicate intracrystalline deformation.

- Sample CZ2 (Figure 2b) consists of green amphibole, sericitized plagioclase, garnet and biotite. Amphibole and plagioclase corona that developed around poikilitic garnet suggest high temperature retrogression of an eclogite. A second generation of biotite developed after amphibole.

- Sample EAR 34 (Figure 2c) is a basic hydrated granulite consisting of a quartzo–feldspathic matrix containing millimetre-length poikiloblastic garnet in equilibrium with amphibole grains. Garnet porphyroblasts are rich in quartz, plagioclase, pyroxene and iron oxide inclusions. Biotites are elongated in the foliation plane and amphiboles rim both iron oxides and pyroxenes.

Intermediate granulites :

- Sample SZ35b (Figure 3a) is characterized by a foliation plane marked by two intercalated layers of feldspar plus cordierite and garnet plus biotite. Relics of highly retrogressed pyroxene are associated with garnet and biotite. Cordierite is pseudomorphosed

into pinnite and white mica. Garnet and biotite are retromorphosed into chlorite. Quartz and feldspars grains contain many biotite inclusions.

- Sample L647 (Figure 3b) consists of poikiloblastic garnet, quartz, feldspar, zircon, biotite and orthopyroxene elongated in a foliation plane. A coronitic texture of secondary biotite and ilmenite developed after orthopyroxene. The occurrence of sub-grains in quartz and the development of a foliation plane both indicate a high temperature deformation.

Acidic granulites:

- Sample GD–04–167 (Figure 4a) consists of an assemblage of quartz, alkali-feldspar, biotite and garnet. Biotite occurs in corona around garnets.

- Sample YR–DDU (Figure 4b) is composed of cordierite, quartz, feldspar and iron oxide. This sample is characterized by a typical granulitic texture with 120° angles between linear grain boundaries and which is devoid of retrograde paragenesis. A small intracrystalline deformation of quartz is highlighted by the presence of sub-grains. Rare chlorite occurs in fractures within garnets.

2.2. Fluid inclusion petrography

Fluid inclusions are tiny quantities of liquid or mixtures of liquid plus vapour trapped as impurities within the crystal lattice of minerals. Their sizes range from submicroscopic up to several hundred micrometers in diameter and typical masses are in order of nanograms. Most fluid inclusions preserve the chemical and physical properties of the original parent fluid from which they were formed. The fluids are therefore considered to be direct samples of the volatile phase which circulated through the lithosphere and their chemical analysis provide both the composition and density of these geologically important fluid phases.

Following the criteria developed by Roedder (1984), Touret (2001) and Van den Kerkhof (2001), microstructural observations made at room temperature under the microscope allows the discrimination between “primary inclusions” and “secondary inclusions”.

Fluids in primary inclusions were trapped during crystal growth. These inclusions, of about 20 μm in size, occur isolated or clustered in garnet, quartz, plagioclase or pyroxene (Figure 5). Their form depends on the crystal lattice of the host mineral: it is hexagonal in quartz and garnet and rectangular in plagioclase. In granulites, these primary fluid inclusions are assumed to represent the metamorphic fluid trapped during the peak metamorphic conditions whereas secondary inclusions sample fluids trapped during the retrograde metamorphic phase. It means that fluids in secondary fluid inclusions were trapped at any time after the growth of the host crystal stopped. These secondary fluid inclusions are trail-bound, showing irregular shape and sealed fractures that intersect the crystallographic surfaces (Figure 5). Fluid inclusions in microcracks formed during crystal growth are defined as the so–called ‘pseudo-secondary’ inclusions.

2.3. Analytical techniques

Extraction of fluid inclusions

Fluids trapped in granulites were extracted by thermal decrepitation. About 1 g of millimetre–sized grains of anhydrous minerals (quartz, plagioclase, pyroxene and garnet) were washed with diluted nitric acid and rinsed with double deionised water before drying overnight at 110°C in an oven. Samples were loaded in a quartz glass tube and degassed at 110˚C under vacuum for at least 2 h. Step heating fixed on the basis of homogenisation temperatures observed by microthermometry was considered as the best protocol to separate fluids from primary and secondary fluid inclusions. Ideally, it is expected that fluids of

secondary inclusions forming microcracks would be totally released at temperatures close to 350±20°C, whereas most fluids from primary inclusions would be collected at temperatures of 700±20°C. For each heating step, fluids contained in mineral inclusions were collected for at least 20 min. This method does not ensure however to separate fluids from both generations of fluid inclusions without some contamination of the high–temperature generation by the lower one. Indeed, if the decrepitation temperature of the inclusions depends on the internal pressure inside the inclusions, it also depends on their size as well as the strength of surrounding minerals. Consequently, small secondary fluid inclusions tend to decrepitate at higher temperatures approaching those of primary inclusions. Similarly, the smallest primary inclusions could escape decrepitation performed at about 700°C even though no sizable amount of water has been extracted at temperatures up to 800°C. Finally, carbon dioxide and water were separated by using cryogenic traps and non condensable gases were purged. Water was collected into a silica glass tube containing about 300 mg of fine–grained chromium metal. Water blanks were very low over the complete set of experiments without contributing more than 5% of the total amount of water extracted from fluid inclusions.

Extraction of water from bulk samples

Whole rock samples were crushed into a very fine powder with a ball mill grinder (implying the opening of the two types of fluid inclusions). An amount of 150 to 200 mg of rock powder was loaded into a quartz glass tube and heated at 150°C for 1 h under vacuum to remove any atmospheric water adsorbed on the sample. Sample was further heated up with a torch until complete melting inducing the release of water from hydrous minerals. The pyrex™ vacuum extraction line was maintained at a temperature of 80°C over the complete manipulation to avoid water condensation on the inner sides of the experimental apparatus.

Using a liquid nitrogen trap, water was collected into a silica tube containing about 300 mg of chromium metal as reduction agent to convert H_2O to H_2. This off-line protocol was adapted from the off-line water reduction method with zinc (Vennemann and O'Neil, 1993) and from the on-line water reduction method using Cr (Morrison et al., 2001) in order to achieve a good analytical reproducibility and to overcome fractionation due to hydrogen-Zn reactions (Demény, 1995). Residual gases not condensable in liquid nitrogen are mainly composed of H_2 produced during the oxidation of the FeO component of silicates by water. Despite this amount of H_2 is one order of magnitude lower than the amount of water released during the melting of the granulite samples, its D/H ratio is about from 150‰ to 300‰ lower than that of water according to thermodynamic calculations performed by Cerrai et al. (1954) and experiments made by Simon (2003) in the temperature range 600°C–1200°C. Therefore, a quantitative oxidation of this H_2 to water in a CuO furnace at 500°C is performed to avoid the acquisition of D/H ratios shifted towards too high values.

Isotope ratio measurements of carbon dioxide and water

Carbon isotope composition of purified carbon dioxide from primary and secondary fluid inclusions was measured with a dual–inlet GV Prism™ mass spectrometer. The internal reproducibility was about ±0.3 and ±0.5‰ for samples sizes lower and upper than 10 μmoles, respectively. Carbon dioxide amount was determined by using a calibrated Keller pressure gauge with an associated uncertainty close to ±2 μmoles.

Water was reduced by Cr at 1000°C during 5 minutes to produce H_2 gas for which the D/H ratio was determined by using a dual–inlet GV Prism™ mass spectrometer. External reproducibility of D/H measurements was established at about ±3‰ by scaling raw data to the VSMOW-SLAP scale. Aliquots of international standard waters (VSMOW, SLAP and GISP) were selected in the range 0.5–1.5 μl which sizes are comparable to those of analyzed

samples. Internal reproducibility of D/H analyses of reference waters is better than 1.5‰. D/H measurements of most samples have been duplicated and the external reproducibility of fluid inclusions and bulk silicates analyses is close to ±3‰. Repeated analyses of the international standard NBS30 provided a mean δD value of –66.6±3.2‰ (n = 11) to be compared to the recommended value of –65.7‰.

3. Results

3.1. CO_2 abundance in fluid inclusions

Observations under the microscope combined to Raman and micro-thermometric analyses revealed that the CO_2–rich primary inclusions are less abundant than the H_2O–rich secondary inclusions. At 700°C, granulites released from about 50 ppm to 3500 ppm with a mean value of 900 ppm whereas at a temperature of 350°C from about 5 ppm to 65 ppm (25 ppm in average) of CO_2 were only released (Table 2). Whatever the age of the sample and the context in which the granulitic metamorphism developed, primary inclusions contain about 40 times more CO_2 than secondary inclusions.

3.2. Stable isotope compositions of fluid inclusions

$^{13}C/^{12}C$ and D/H ratios of fluid inclusions

Secondary fluid inclusions are characterized by δD values that range from –139‰ to –86‰ (Table 2), lower by about 35‰ than those measured in primary fluid inclusions (–97‰ < δD < –55‰). Hydrogen isotope compositions of primary fluid inclusions in the two granulites formed in a collision context are also significantly higher than those coming from a subduction environment (Table 2).

Carbon isotope compositions and amounts of carbon dioxide in both primary and secondary inclusions from granulites formed in a collision context describe a hyperbolic mixing curve (Figure 6). One end–member is characterized by a small pool of carbon (a few ppm) with negative $\delta^{13}C$ values of at least –20‰ whereas the second one of larger size (a few thousands ppm) tends to have a $\delta^{13}C$ close to 0‰. In the case of granulites formed in a context of subduction, $\delta^{13}C$ values of primary fluid inclusions range from –14.7‰ to –2.5‰ whereas secondary inclusions are characterized by a narrow range from –13.7‰ to –10.5‰. The carbon isotope compositions of these two generations of fluid inclusions do not show any correlation with the amounts of carbon dioxide or with the geological age of their host granulites (Table 2; Figure 7).

D/H ratios of bulk rocks

Hydrogen isotope compositions of bulk granulites range from –142‰ to –52‰ (Table 2). Except the case of Namche–Barwa (Himalaya) samples, the lowest δD values (–79‰ < δD < –65‰; mean value = –72‰) were recorded in the youngest granulites (post Paleo-Proterozoic) that are also those generated in a subduction context. By comparison, other granulites that formed in a collision context have δD that range from –61‰ to –52‰ with a mean value of –58‰ (Table 2). Bulk δD values of granulites decrease with their geological age of formation with a jump in values that took place between 2 Gy and 1.5 Gy ago (Figure 8).

4. Discussion

4 .1. Isotopic compositions of granulites and fluid sources

In granulites formed in a collision context, carbon dioxide in fluid inclusions derives from at least two sources (Figure 6): one low-carbon source (LC) with $\delta^{13}C < -15‰$ and [CO2] < 20 ppm, and a second, high-carbon, source (HC) with $\delta^{13}C \sim -2‰$ and [CO2] > 2000 ppm. The low $\delta^{13}C$ values of most secondary fluid inclusions, associated with low carbon dioxide content, indicate that they are dominated by LC source. Vry et al. (1988) and Crawford and Valley (1990) have shown that the $\delta^{13}C$ values of CO_2 trapped in granulites of sedimentary origin or contaminated by a sedimentary source are lower than –15‰. LC source probably derive from the oxidation of graphite itself resulting from the thermal maturation of sedimentary organic matter whose $\delta^{13}C$ remains close to -25‰ over the Earth's history (Schidlowski, 2001).

A second source of carbon dioxide trapped in granulite fluid inclusions could come from the decarbonation of carbonated rocks, a process which can take place at depth as suggested by the results of the experimental work carried out by Biellmann et al. (1993). The carbon isotope composition of HC source is close to the $\delta^{13}C$ of 0±2‰ of marine carbonates, a value that remains constant since the Precambrian (Schidlowski, 2001). Marine carbonates can thus be identified as the main component of HC source since the carbon isotope fractionation between carbonates and carbon dioxide is very small at high pressure and high temperature (Martinez et al., 1994; Sharp et al., 2003). The CO_2–rich primary fluid inclusions, which $\delta^{13}C$ values are slightly negative, are dominated by HC source and probably derive from the decarbonation of marine carbonates. The relative poor quality of

data fitting (r^2 = 0.56) to a hyperbolic mixing curve suggests that a third carbon end–member cannot be excluded (Figure 6). Fluid inclusions with carbon isotope compositions in the range –8.9 to –4.5‰ and intermediate CO2 content (14 – 563 ppm) are compatible with the contribution of a shallow mantle source. The carbon content of the shallow mantle is estimated between 30 and 60 ppm from carbon fluxes or from the chemistry of mid-ocean ridge basalts (MORBs) according to Jambon (1994) and Saal et al. (2002), and the $\delta^{13}C$ of the shallow mantle lies between -6 and -3.5‰ (Cartigny et al, 2001).

Granulites formed in a subduction context have also a large range of $\delta^{13}C$ values (from -14.7‰ to -2.6‰; Table 2). However the absence of any significant correlation with the C abundance in fluid inclusions precludes the identification of carbon reservoirs and their potential mixing relationships that were possibly masked by additional mechanisms such as partial degassing.

Hydrogen isotope compositions of primary fluid inclusions (δD values from –97‰ to -82‰) in granulites formed in a subduction context are compatible with a mantle–derived source of water which has a mean value of -80±20‰ (Sheppard and Epstein, 1970; Kuroda et al., 1977; Boettcher and O'Neil, 1980; Javoy, 1980; Chaussidon et al., 1991; Deloule et al., 1991). The interpretation of these D/H ratios remains however ambiguous because meteoric waters may have the same compositions as waters derived from mantle degassing. Granulite genesis itself may also fractionate the hydrogen isotope composition of circulating water through crustal degassing, however relative high P–T conditions should restrict the amplitude of this isotopic fractionation. Therefore it is most likely that the D/H ratios of water inclusions in anhydrous minerals closely reflect the composition of circulating water. High-grade metamorphic hydrous minerals are expected to be at least 30‰ deuterium-depleted relative to their forming water according to natural observations (e.g. Früh–Green et al., 1996) and laboratory experiments (e.g. Suzuoki and Epstein, 1976; Graham et al., 1984) for the temperature range of interest between 600°C and 900°C. Data compiled in Table 2 reveal

that δD values of primary and secondary fluid inclusions are close to or much lower than the δD values of their corresponding bulk rocks. These observations suggest that water from hydrous minerals has not the same source that waters trapped in both primary and secondary inclusions from the nominally–anhydrous granulitic minerals. Therefore we propose that bulk D/H ratios reflect the composition of hydrous silicates that formed during the retromorphic evolution of granulites, the source of this water being most likely exclusively of crustal origin (Fu et al., 2003; Chen et al., 2007).

Isotopic compositions of granulites that formed in both geodynamic contexts need to be examined as a function of time in the frame of the dynamics of global carbon and water cycles.

4.2. Isotopic compositions of granulites and the evolution of carbon and water cycles

Large carbon and hydrogen isotope fractionations are associated with inorganic or biologically–mediated reactions that involve CO_2– CH_4 and H_2O – H_2 species (e.g. Schidlowski, 1987; Des Marais et al., 1992; Karhu and Holland, 1996). Therefore, changes in the carbon and hydrogen isotope compositions of CO_2 and H_2O at the global scale could reflect variations in the redox state of both Earth's hydrosphere and atmosphere through time. The history of the rise in atmospheric oxygen can be drawn from numerous geological and geochemical evidence. The presence of mass-independent fractionation (MIF) in sulphur isotopes infers an atmospheric pO_2 level before 2.4 Ga lower than 10^{-5} bar (Pavlov and Kasting, 2002). Sedimentary successions older than 2.45 Ga are characterized by the presence of uraninite, siderite and pyrite (Rassmussen and Buick, 1999; England et al., 2002), iron deposits in shallow aquatic environments (Beukes and Klein, 1990) and non–oxidized paleosols (Rye and Holland, 1998). Sedimentary deposits younger than 2.2 Ga

contain ferric iron–rich levels (« Red Beds »; Chandler, 1980), sulfate–rich evaporites and strongly oxidized paleosols (Rye and Holland, 1998; Holland, 1999). The whole geological record therefore argues in favour of a major increase of the oxygen partial pressure in the Earth's atmosphere between 2.45 and 2.2 Ga, even though few authors argue in favour of an early oxidized atmosphere (e.g. Ohmoto et al., 2001).

Carbon isotope compositions of primary fluid inclusions range from –14.7‰ to –2.5‰ and do not show any trend with geological time (Figure 7). A mean $\delta^{13}C$ value of –6.3±3.4‰ is compatible with a dominant mantle–derived source of carbon dioxide ($\delta^{13}C$ = -6 to -3.5‰; Cartigny et al, 2001) that was trapped in primary fluid inclusions during granulite genesis. The carbon isotopic record preserved in granulites is therefore consistent with the observations that the $\delta^{13}C$ of mantle rocks, mostly sampled from carbonatites and peridotitic diamonds, have remained constant through most of the Earth's history (Deines et al., 1993; Cartigny et al., 2004) despite imbalance in the long-term carbon isotope cycle (Coltice et al., 2004). Chromium and vanadium contents of basaltic rocks indicate that mantle fO_2 did not significantly change through time (Canil, 1999; Delano, 2001) and consequently the carbon speciation in mantle–derived rocks was most likely large dominated by CO_2. The restricted range of carbon isotope compositions of CO_2 in primary fluid inclusions of granulites could therefore reflect at the first order the constancy of the carbon isotopic composition of the upper mantle. Uprising of an oxidizing atmosphere about 2 Gy ago cannot be therefore recorded in the primary fluid inclusions of granulites.

Low $\delta^{13}C$ values of secondary fluid inclusions could indeed result from methane–based bacterial metabolic activity (e.g. Archaea) considering that the $\delta^{13}C$ values of the methane released by these bacteria are low as –50±20‰ (e.g. Alperin et al., 1988 ; Valentine et al., 2004 ; Proskurowski et al., 2008). Without any striking evidence, reducing conditions

at Earth's surface before 2 Ga are perhaps recorded in the lowest $\delta^{13}C$ values (from –21‰ to –16‰) of carbon dioxide from secondary fluid inclusions that trapped crustal–derived fluids.

Assuming that the δD values of bulk granulites reflects the evolution of the hydrogen isotope composition of crustal water that interacted with granulites during their retrograde metamorphism, the observed decreasing isotopic trend (Figure 8) could be explained by the onset of Earth's oxidizing surface conditions that took place about 2.2 Gy ago. The evolution of the ocean D/H ratio is mainly driven by atmospheric escape (Hunten et al., 1987) and deuterium exchange between hydrogen gas and water vapour (Robert et al., 2000). Hydrothermal reactions at mid-ocean ridges can produce H_2 through silicate oxidation reactions such as $2Fe^{2+} + 3H_2O = Fe_2O_3 + 4H^+ + H_2$. In an O_2-rich atmosphere and sulphate-rich oceans, H_2 produced by such a reaction is rapidly oxidized. Under reducing Archean sulphate-poor oceans, hydrothermal reactions could produce an enhanced flux of H_2 by silicate oxidation by water (Kump and Seyfried, 2005), H_2 that will subsequently escape to space. The large hydrogen isotope fractionation between H_2 and H_2O (Cerrai et al., 1954; Simon, 2003) will lead to the production of residual water enriched in deuterium under reducing conditions compared to deuterium–depleted water under oxidizing ocean-atmosphere conditions. Carbon and hydrogen isotope compositions of granulites could be considered as new valuable proxies of the dynamics of global carbon and water cycles.

5. Conclusions

Hydrogen and carbon isotope compositions of fluid inclusions along with the bulk δD values of their host granulites sampled worldwide lead to underline the following results:

- At least three distinct sources of water participated to the metamorphic genesis and retromorphosis evolution of granulites. D/H ratios of water in primary inclusions of anhydrous minerals closely reflect the composition of circulating water at the time of the

granulitic metamorphic event. This water could originate from mantle degassing processes with δD values that range from –97 to –55‰. Secondary fluid inclusions have lower δD values from -139‰ to –86‰ that are compatible with a source of crustal origin such as meteoric waters that were trapped during or after the exhumation of granulite in the conditions of brittle deformation. Hydrogen isotope compositions of granulite–forming hydrous minerals (amphibole and biotite) cannot be related to the compositions of waters trapped either in primary or secondary inclusions. Bulk δD values are most likely related to crustal events such as the retrograde metamorphic evolution of granulites which can themselves have inherited from the composition of a partly hydrated protolith.

- Carbon isotope compositions of CO_2 in primary inclusions also argue in favour of the dominant presence of a mantle–derived source of carbon for granulites generated in both subduction and collision contexts. Mixing relationships between amounts of carbon dioxide and their $\delta^{13}C$ values in both primary and secondary inclusions from granulites formed in a collision context suggest at least two additional sources of carbon derived from the oxidation of organic matter and the decarbonation of sedimentary carbonates.

- Stable isotope compositions of granulites cannot be easily related to their geodynamic environment. However, they could reflect the secular isotopic evolution of the global carbon and water cycles. The rather constancy of carbon isotope compositions through time along with a mean $\delta^{13}C$ value of –6.3±3.4‰ for CO_2 in primary fluid inclusions of granulites could reflect the constancy of the carbon isotope composition of the upper mantle. By contrast, bulk δD values of granulites that decrease by about 25±5‰ from the Archean to the Miocene, with an abrupt change that took place about 2 Gy ago, could reflect the onset of Earth's oxidizing surface conditions.

References

Alperin M.J., Reeburgh W.S., Whiticar M.J. and Oremland R.S. 1988. Carbon and hydrogen isotope fractionation resulting from anaerobic methane oxidation. In : Global Biogeochemical Cycles (ed. J.J. McCarthy). American Geophysical Union, Washington.

Alt J.C. (1995) Subseafloor processes in mid-ocean ridge hydrothermal systems. In Seafloor hydrothermal systems; physical, chemical, biological, and geological interactions (S.E. Humphris, R.A. Zierenberg, L.S. Mullineaux, R.E. Thomson, Eds.) Geophys. Monograph., Am. Geophys. Union, Washington DC, 91, pp. 85–114.

Andersen T., Whitehouse M.J. and Burke E.A.J. 1997. Fluid inclusions in Scourian granulites from the Lewisian complex of NW Scotland : evidence for CO_2–rich fluid in Late Archaean high–grade metamorphism. Lithos, 40 : 93-104.

Barbey P., Raith M., 1990. The granulit belt of Lapland. In: Vielzeuf D., Vidal Ph. (Eds.), Granulites and Crustal Evolution, NATO ASI Series. Kluwer, Dordrecht, pp. 111-132.

Beukes, N.J. & Klein, C. (1990) Geochemistry and sedimentology of a facies transition –- from microbanded to granular iron–formation –- in the early Proterozoic Transvaal Supergroup, South Africa. Precamb. Res. 47, 99–139.

Biellmann C., Gillet P ., Guyot F., Peyronneau J. and Reynard B. (1993). Experimental evidence for carbonate stability in the Earth's lower mantle. Earth Planet. Sci. Lett. 118: 31–41.

Boettcher, A.L. and O'Neil, J.R., 1980. Stable isotope, chemical and petrographic studies of high pressure amphiboles and micas: evidence for metasomatism in the mantle source regions of alkali basalts and kimberlites. Am. J. Sci., 280A: 594-621.

Boillot G., Agrinier P., Beslier M.O., Cornen G., Froitzheim N., Gardien V., Girardeau J., Gil-Ibarguchi J., Kornprobst J., Moullade M., Schärer U., Vanney J.R., 1995. A lithospheric syn-rift shear zone at the ocean-continent transition: preliminary results of the Galinaute II cruise (Nautile dives on the Galicia Bank, Spain). C.R. Acad. Sci. Paris, 321: 1171-1178.

Canil D. (1999) Vanadium partitioning between orthopyroxene, spinel and silicate melt and the redox states of mantle source regions for primary magmas. Geochim. Cosmochim. Acta 63, 557–572.

Cartigny, P., Jendrzejewski, N., Pineau, F., Petit, E. and Javoy, M. (2001) Volatile (C, N, Ar) variability in MORB and the respective roles of mantle source heterogeneity and

degassing: The case of the southwest Indian, Earth Planet. Sci. Lett., 194, 241-257.

Cartigny, P., Stachel, T., Harris, J. F. and Javoy, M., 2004. Constraining diamond metasomatic growth using C- and N- stable isotopes: examples from Namibia. Lithos, 77: 359-373.

Cerrai E., Marchetti R., Renzoni R., Roseo L., Silvestri M., and Villani S. (1954) A thermal method for concentrating heavy water. Chem. Eng. Prog. Symp. 50, 27-280.

Chandler, F.W. (1980) Proterozoic redbed sequences of Canada. Can. Geol. Surv. Bull. 311.

Chaussidon, M., Sheppard, S.M.F. and Michard, A., 1991. Hydrogen, sulphur and neodymium isotope variations in the mantle beneath the EPR at 12°50'N. In H.P. Taylor, J.R. O'Neil and I.R. Kaplan (Editors), Stable Isotope Geochemistry: A Tribute to Samuel Epstein. Geochem. Soc. Spec. Pub., 3: 325-337.

Chen R.-X., Zheng Y.-F., Gong B., Zhao Z.-F., Gao T.-S., Chen B. and Wu Y.-B. 2007. Origin of retrograde fluid in ultrahigh-pressure metamorphic rocks : Constraints from mineral hydrogen isotope and water content changes in eclogite–gneiss transitions in the Sulu orogen. Geochim. Cosmochim. Acta, 71 : 2299-2325.

Coltice N., Simon L. and Lécuyer C. 2004. Carbon isotope cycle and mantle structure. Geophys. Res. Lett., 31, No. 5, L05603, doi :10.1029/2003GL018873.

Coolen J.J.M.M.M. 1982. Carbonic fluid inclusions in granulites from Tanzania–A comparison of geobarometric methods based on fluid density and mineral chemistry. Chem. Geol., 37 : 59-77.

Crawford, W. A. and Valley, J. W., 1990. Origin of graphite in the Pickering Gneiss and the Franklin Marble, Honey Brook Upland, Pennsylvania Piedmont, Geol. Soc. Am. Bull., 102: 807–811.

Daly J.S., Balagansky V.V., Timmerman M.J., Whitehouse M.J., De Jong K., Guise P., Bogdanova S. Gorbatschev R., Bridgwater D., 2001. Ion microprobe U-Pb zircon geochronology and isotopic evidence for trans-crustal suture in the Lapland-Kola Orogen, northern Fennoscandian Shield. Precambrian Research, 102, 289-314.

Deines, P., Harris, J.W. and Gurney, J.J., 1993. Depth–related carbon isotope and nitrogen concentration variability in the mantle below the Orapa kimberlite, Bostwana, Africa. Geochim. Cosmochim. Acta, 57: 2781–2796.

Delano, J.W. (2001) Redox history of the Earth's interior since 3900 Ma: Implications for prebiotic molecules. Origins Life Evol. B. 31, 311–341.

Deloule, E., Albarède, F. and Sheppard, S.M.F., 1991. Hydrogen isotope heterogeneities in the mantle from ion probe analysis of amphiboles from ultramafic rocks. Earth Planet. Sci. Lett., 105: 543-553.

Demény, A. (1995) H isotope fractionation due to hydrogen-zinc reactions and its

implications on D/H analysis of water samples. Chem. Geol., 121, 19-25.

Des Marais, D.J., Strauss, H., Summons, R.E., Hayes, J.M. (1992) Carbon isotope evidence for the stepwise oxidation of the Proterozoic environment. Nature 359, 605–609.

Desmurs L., 1997. Etude pétrologique et géochronologique de la croûte continentale de la marge de Galice. DEA à l'université Lyon 1, 28 pp.

England, G.L., Rasmussen, B., Krapez, B., Groves, D.I. (2002) Palaeoenvironmental significance of rounded pyrite in siliciclastic sequences of the Late Archaean Witwatersrand Basin: oxygen-deficient atmosphere or hydrothermal alteration? Sedimentology 49, 1133–1156.

Früh-Green, G., Plas, A. and. Lécuyer, C., 1996., Petrologic and stable isotope constraints on hydrothermal alteration and serpentinization of the EPR shallow mantle at Hess Deep (Site 895). In: Mével C., Gillis K.M., Allan J.F. and Meyer P.S. (Editors). Proc. ODP, Sci. Results, 147: College Station, TX (Ocean Drilling Program), pp. 255–291.Galimov, E.M., 1991. Isotope fractionation related to kimberlite magmatism and diamond formation. Geochim. Cosmochim. Acta, 55: 1697-1708.

Fu B., Touret J.L.R. and Zheng Y.-F. 2003. Remnants of premetamorphic fluid and oxygen isotopic signatures in eclogites and garnet clinopyroxenite from the Dabie–Sulu terranes, eastern China. J. Metamorphic Geol., 21: 561-578.

Gardien V., Arnaud N., Desmurs L., 2000. Petrology and Ar-Ar dating of granulites from the Galicia Bank (Spain) : African craton relics in Western Europe. Geodinamica Acta, 13, 103-117.

Glassley W.E. 1983. The role of CO_2 in the chemical modification of deep continental crust. Geochim. Cosmochim. Acta, 47: 597-616.

Graham, C.M., Viglino, J.A. and Harmon, R.S., 1984, Experimental study of hydrogen-isotope exchange between aluminous chlorite and water and of hydrogen diffusion in chlorite. Amer. Mineral., 72, 566–579.

Holland, H.D. (1984) The chemical evolution of the atmosphere and oceans. Princeton University Press, Princeton.

Holland, H.D. (1999) When did the Earth's atmosphere become oxic? A reply. Geochem. News 100, 20–22.

Holzer L., Frei R., Barton J.M., Kramers J.D., 1998. Unraveling the record of successive high grade events in the Central Zone of the Limpopo Belt using Pb single phase dating of metamorphic minerals. Precambrian Research, 87, 87-115.

Hunten, D.M., Pepin, R.O., Walker, J.C.G. (1987) Mass fractionation in hydrodynamic escape. Icarus, 69, 532-549.

Jambon, A. (1994) Earth degassing and large-scale geochemical cycling of volatile elements. In: Volatiles in magmas (eds. M.R. Carroll and J.R. Holloway) Mineral. Soc. Am., Washington D.C., pp. 479-517.

Javoy, M., 1980. $^{18}O/^{16}O$ and D/H ratios in high temperatures peridotites. C.N.R.S. Colloques internationaux, n°272: 279-287.

Karhu, J. & Holland, H.D. (1996) Carbon isotopes and the rise of atmospheric oxygen. Geology 24, 867–870.

Kröner A., Jaeckel P., Brandl G., Nemchin A.A., Pidgeon R.T., 1999. Single zircon ages for granitoid gneisses in the Central Zone of the Limpopo Belt, Southern Africa and geodynamic significance. Precambrian Research, 93, 299-337.

Kröner A., Wendt J.I., Milisenda C., Compston W., Maphala R., 1993. Zircon geochronology and Nd systematics of the Ancient Gneiss Complex, Swaziland, and implications for crustal evolution. Bulletin of the Swaziland Geological Survey and Mines Department 11, 15-37.

Kump, L.R., Seyfried, W.E. (2005) Hydrothermal Fe fluxes during the Precambrian: effect of low oceanic sulfate concentrations and low hydrostatic pressure on the composition of black smokers. Earth Planet. Sci. Lett., 235, 654-662.

Kuroda, Y., Suzuoki, T. and Matsuo, S., 1977. D/H ratios of the coexisting phlogopite and richterite from mica nodules and a peridotite in South African kimberlites. Contrib. Mineral. Petrol., 52: 315-318.

Lamb, W., Valley, J.W., 1984. Metamorphism of reduced granulites in low CO_2 vapour–free environnement. Nature, 312, 56-58.

Maboko M.A.H., 1997. P-T conditions of metamorphism in the Wami River granulite complex, central coastal Tanzania: implications for Pan-African geotectonics in the Mozambique Belt of eastern Africa. Journal of African Earth Sciences, 24, n°1/2, 51-64.

Martinez I., Agrinier P., Schärer U. and Javoy M., 1994, A SEM–ATEM and stable isotope study of carbonates from the Haughton impact crater, Canada. Earth Planet. Sci. Lett., 121, 559–574.

Melzer M., 2001. Pan-African granulites in the Precambrian basement of eastern Tanzania: a geochemical, fluid inclusions and P-T history, DEA de l'Université de Clermont-Ferrand II.

Ménot R.P., Pêcher A., Rolland Y., Peucat J.J., Pelletier A., Duclaux G., Guillot S., 2005. Structural setting on the Neoarchean terrains in the Commonwealth Bay Area (143-145°E), Terre Adélie Craton, East Antarctica. Gondwana Research, 8, n°1, 1-9.

Möller A., 1995. Pan-African granulites and early proterozoic eclogites in the Precambrian basement of eastern Tanzania: P-T-t history and crustal evolution of the Complex Mozambique Belt. Thèse de l'université de Kiel.

Morrison J., Brockwell T., Merren T., Fourel F. and Philipps A. 2001. On-Line High-Precision Stable Hydrogen Isotopic Analyses on Nanolitre Water Samples. Analytical Chemistry. 73, 3570-3575.

Muhongo S., Kröner A., Nemchin A.A., 2001. Single zircon evaporation and SHRIMP ages for granulite facies rocks in the Mozambique Belt of Tanzania. Journal of Geology, 109, 171-190.

Muhongo S., Tuisku P., Mtoni Y., 1999. Pan–African pressure-temperature evolution of the Merelani area in the Mozambique Belt in northeast Tanzania. Journal of African Earth Sciences, 29, n°2, 353-365.

Muhongo S., Tuisky P., 1996. Pan-African high pressure isobaric cooling: evidence from the mineralogy and thermobarometry of the granulite-facies rocks from Uluguru mountains, eastern Tanzania. Journal of African Earth Sciences, 23, n°3, 443-463.

Newton, R.C., Smith, J.V., Windley, B.F., 1980. Carbonic metamorphism, granulites and crustal growth. Nature, 288, 45-50.

Ohmoto, H., Yamaguchi, K.E., and Ono, S. (2001). Questions regarding Precambrian sulfur isotope fractionation. Science, 292, 1959a.

Pavlov, A.A., Kasting, J.F. (2002) Mass-independent fractionation of sulfur isotopes in Archean sediments: strong evidence for an anoxic Archean atmosphere. Astrobiology, 2, 27-41.

Peucat J.J., Ménot R.P., Monnier O., Fanning C.M., 1999. The Terre Adélie basement in the East-Antarctica Shield: geological and isotopic evidence for a major 1,7 Ga thermal event ; comparison with the Gawler Craton in South Australia. Precambrian Research, 94, 205-224.

Pili E., Sheppard S.M.F., Lardeaux J.-M., Martelat J.-E. and Nicollet C. 1997. Fluid flow vs. Scale of shear zones in the lower continental crust and the granulite paradox. Geology, 25 : 15-18.

Powell, R., 1983. Processes in granulite-facies metamorphism. in: Migmatites, Melting and Metamorphism, Atherton, M.P., Gribble, C.D., Eds., Nantwich, Shiva, 127-139.

Proskurowski G., Lilley M.D. and Olson E.J. 2008. Stable isotopic evidence in support of active microbial methane cycling in low-temperature diffuse flow vents at 9°50'N East Pacific Rise. Geochim. Cosmochim. Acta, 2005-2023.+

Rassmussen, B. & Buick, R. (1999) Redox state of the Archean atmosphere; evidence from detrital heavy minerals in ca. 3250-2750 Ma sandstones from the Pilbara Craton, Australia. Geology 27, 115–118.

Robert, F., Gautier, D., Dubrulle, B. (2000) The Solar System D/H: Observations and theories. Space Sci. Rev., 92, 201-224.

Roedder, E., 1984. Fluid inclusions. Review in Mineralogy (Mineralogical Society of America), vol. 12, 644p.

Rye, R. & Holland, H.D. (1998) Paleosols and the evolution of atmospheric oxygen: a critical review. Am. J. Sci. 298, 621–672.

Saal, A.E., Hauri, E.H., Langmuir, C.H., Perfit, M.R. (2002) Vapour undersaturation in primitive mid-ocean-ridge basalt and the volatile content of Earth's upper mantle. Nature, 419, 451-455.

Sano, Y. and Marty, B., 1995, Origin of carbon in fumarolic gas from island arcs. Chem. Geol., 119, 265–274.

Santosh, M., Tsunogae, T., 2003. Extremely high density pure CO_2 fluid inclusions in a garnet granulite from southern India. Journal of Geology 111, 1–16.

Schaller M.., Steiner O., Studer I., Holzer L., Herweg M., Kramers J.D., 1999. Exhumation of Limpopo Central Zone granulites and dextral continent-scale transcurrent movement at 2000 Maalong the Palala Shear Zone, Northern Province, South Africa, Precambrian Research, 96, 263-288.

Schidlowski, M. (1987) Application of stable isotopes to early biochemical evolution on Earth. Ann. Rev. Earth. Planet. Sci. 15, 47–72.

Schidlowski, M. 2001. Carbon isotopes as biogeochemical recorders of life over 3.8 Ga of Earth history: evolution of a concept. Precambrian Res., 106: 117-134.

Sharp Z.D., Papike J.J. and Durakiewicz T., 2003, The effect of thermal decarbonation on stable isotope compositions of carbonates. Amer. Mineral., 88, 87–92.

Sheppard, S.M.F., Epstein, S., 1970. D/H and $^{18}O/^{16}O$ ratios of minerals of possible mantle or lower crustal origin. Earth Planet. Sci. Lett. 9, 232–239.

Simon L., 2003, Quelques exemples de modélisations géochimiques des interactions entre les enveloppes terrestres. PhD Thesis, Ecole Normale Supérieure de Lyon, France, 220 pp.

Suzuoki, T. and Epstein, S. 1976, Hydrogen isotope fractionation between OH–bearing

minerals and water. Geochim. Cosmochim. Acta, 40, 1229–1240.

Taylor, S. R., and S. M. McLennan (1995), The geochemical evolution of the continental crust, Rev. Geophys., 33, 241–265.

Touret, J.L.R., 1971. Le facies granulite en Norvège méridionale: II. Les inclusions fluides. Lithos, 4: 423–436s.

Touret, J.L.R., 2001. Fluids in metamorphic rocks. Lithos 55, 1–26.

Tsunogae, T., Santosh, M., Osanai, Y., Owada, M., Toyoshima, T., Hokada, T., 2002. Very high-density carbonic fluid inclusions in sapphirine-bearing granulites fromTonagh island in theArcheanNapier complex, eastAntarctica: implications for CO_2 infiltration during ultrahigh-temperature (T>1100°C) metamorphism. Contributions to Mineralogy and Petrology 143, 279–299.

Valentine D.L., Chidthaisong A., Rice A., Reeburgh W.S. and Tyler S.C. 2004. Carbon and hydrogen isotope fractionation by moderately thermophilic methanogens. Geochim. Cosmochim. Acta, 68: 1571-1590.

Van den Kerkhof A.M., Hein U.F., 2001. Fluid inclusion petrography. Lithos, 55, 27-47.

Vennemann T.W. and O'Neil J.R., 1993, A simple and inexpensive method of hydrogen isotope and water analyses of minerals and rocks based on zinc reagent. Chem. Geol., 103, 227–234.

Vry, J., Brown, P.E., Valley, J.W. and Morrison J., 1988, Constraints on granulite genesis from carbon isotope compositions of cordierite and graphite. Nature, 332: 66-68.

Table captions

Table 1: Petrology of Archean to Miocene granulites sampled worldwide. Opx: orthopyroxene; Cpx: clinopyroxene; Gt: garnet; Fs: feldspar; Cord: cordierite; Pl: plagioclase; Qtz: quartz; Bt1: primary biotite; Amph: amphibole; Bt2: secondary biotite; Pin: pinite; Zn: zircon; Ap: apatite; Ox: oxide; Sph: sphene; Chl: chlorite; Ilm: ilmenite.

Table 2: δD values of H_2O and $\delta^{13}C$ values of CO_2 from primary and secondary fluid inclusions along with the bulk δD values of their host granulites. Primary and secondary fluid inclusions (f.i.) have respectively been extracted at 700°C and 350°C, respectively, following a step heating procedure. Geological age, tectonic context and P–T conditions of granulitic metamorphism are given according to following sources from the literature: 1 = Kröner et al. (1993); 2 = Holzer et al. (1998), Kröner et al. (1999) and Schaller et al. (1999); 3 = Ménot et al. (2004); 4 = Barbey et al. (1990) and Daly et al. (2001); 5 = Peucat et al. (1999); 6 = Boillot et al. (1995), Desmurs (1997) and Gardien et al. (2000); 7 = Maboko (1997), Möller (1995), Muhongo et al. (1996; 1999; 2001) and Melzer (2001). N.d. = not determined.

Figure captions

Figure 1: Geographic location and age of metamorphism (from Archean to Miocene) of basic, intermediate and acidic granulites that were studied for their carbon (CO_2 in inclusions) and hydrogen (H_2O in inclusions and bulk rock) stable isotope compositions. Circles: granulites formed in a subduction context. Stars: granulites formed in a collision context.

Figure 2: Photomicrographs (plane light) of basic granulites.
A: Photomicrograph of sample GAL 26–10 which is a basic anhydrous orthogranulite with an isotropous granoblastic texture. Intracrystalline deformation is marked by undulose extinctions of quartz, feldspars and pyroxenes. The granulitic paragenesis which consists of orthopyroxene, clinopyroxene, plagioclase, quartz, K–feldspar, and Fe–Ti oxide is particularly well preserved. The retrograde metamorphism is limited to the development of micas at the expense of feldspars and to replacement of orthopyroxene rims by bastite.
B: Photomicrograph of sample CZ2 that is a garnet–bearing amphibolite, mainly composed of green amphibole associated with sericitized plagioclase. Corona of amphibole and plagioclase has developed around poikilitic garnet suggesting an eclogitic retrograde metamorphism at high temperature. Biotite also occurs as a retromorphic mineral. C: Photomicrograph of sample EAR34 that is a basic hydrous granulite with a quartzo-feldspathic matrix. Garnet contains inclusions of quartz, plagioclase, pyroxene and Fe–Ti oxide. Biotite underlines foliation and amphibole associated with automorphic garnet forms reaction rim around Fe–Ti oxide and pyroxene.

Figure 3: Photomicrographs of intermediate granulites.
A: Photomicrograph of sample SZ35b which is a metapelite with a granulitic paragenesis of low pressure. The foliated rock is marked by an alternation of feldspar + cordierite levels and garnet + biotite levels. Relics of retromorphosed pyroxene are associated with garnet + biotite levels. Cordierite is largely altered and occurs as clusters of pinnite and white mica. Garnet and biotite are retromorphosed into chlorite. Quartz and feldspars contain many biotite inclusions.
B: Photomicrograph of sample L647 which presents an inequigranular texture. Orthopyroxene (Opx) is lengthened within the foliation plane. Poikilitic garnet (Gt) includes

quartz, feldspars, zircons and primary biotite inclusions. Corona texture of secondary biotite (Bt) + ilmenite (il) has developed around destabilized orthopyroxene. The presence of sub-grains in quartz indicates a partial recrystallization of the quartzo-feldspathic matrix.

Figure 4: Photomicrographs of acidic granulites.
A: Photomicrograph of sample GD–04–167 with quartz (Qtz) and biotite (Bt) inclusions in garnet (Gt). Biotite developed corona around garnets.
B, C: Photomicrographs of sample YR–DDU which is mainly composed of cordierite (Cord), quartz (Qtz), feldspar (Fs) and Fe–Ti oxides (Ox) with a granulitic texture characterized by an angle of 120° between grains having linear grain boundaries. Intracrystalline deformation of quartz is revealed by the presence of sub-grains. No retromorphic paragenesis is observed except rare chlorite deposited in the fractures of garnet.

Figure 5: Photomicrographs of primary and secondary fluid inclusions in granulites.
A: Primary inclusions occur isolated with size and geometry depending on the crystal lattice of the host mineral.
B, C: Secondary inclusions occur aligned along microcracks and crosscut the crystal lattice.
D: Naking-down structure of secondary inclusions.

Figure 6: Variations in the $\delta^{13}C$ of CO_2 from primary and secondary fluid inclusions as a function of CO2 amount in granulites that formed in a collision context. The distribution of data can be described by a hyberbolic equation that suggests mixing between a ^{13}C-depleted CO_2–poor end–member (oxidation of graphite with organic matter as the ultimate source) and one or two CO_2–rich end–members (degassing of upper mantle peridotites and decarbonation of sedimentary carbonates) with $\delta^{13}C$ values that range from –8‰ and –2‰.

Figure 7: Variations through geological time of the $\delta^{13}C$ of CO_2 in primary fluid inclusions of granulites formed in collision and subduction contexts.

Figure 8: Variations through geological time of the bulk δD of granulites formed in collision and subduction contexts.

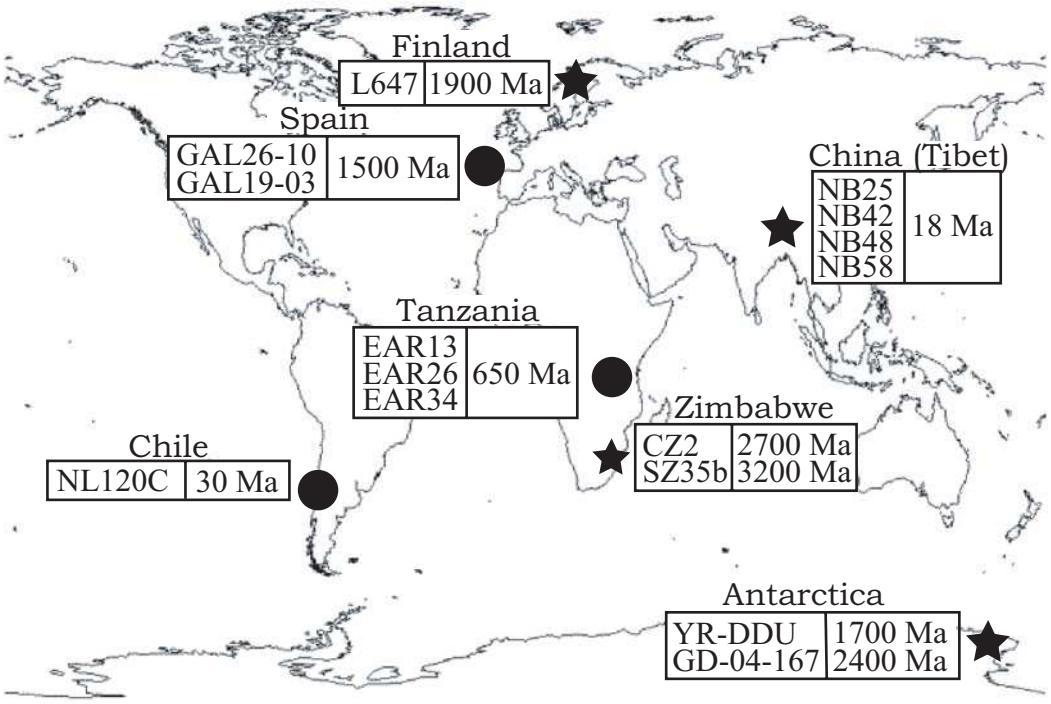

FIG. 1 – Geographic location and age of metamorphism (from Archean to Miocene) of basic, intermediate and acidic granulites that were studied for their carbon (CO_2 in inclusions) and hydrogen (H_2O in inclusions and bulk rock) stable isotope compositions. Circles: granulites formed in a subduction context. Stars: granulites formed in a collision context.

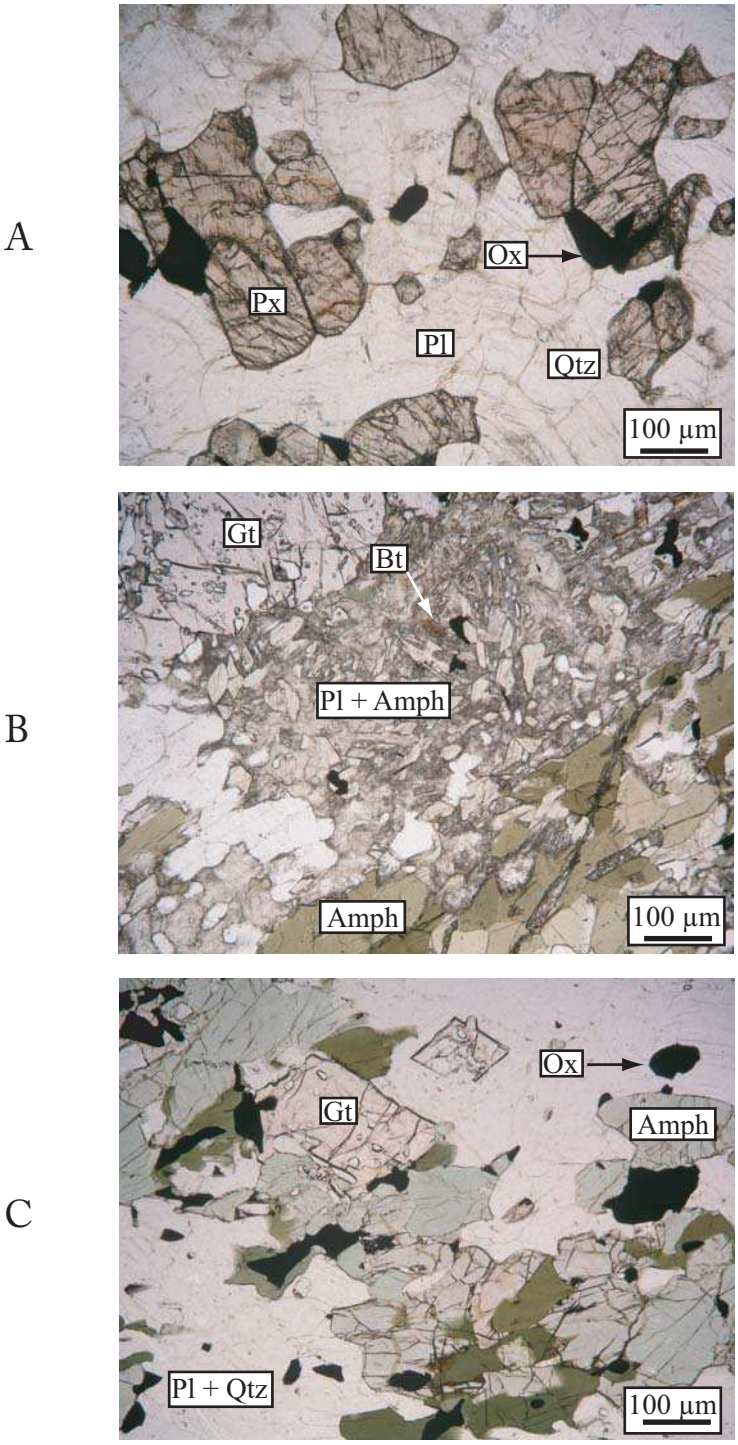

FIG. 2 – Photomicrographs (plane light) of basic granulites. A: Photomicrograph of sample GAL 26–10 which is a basic anhydrous orthogranulite with an isotropous granoblastic texture. Intracrystalline deformation is marked by undulose extinctions of quartz, feldspars and pyroxenes. The granulitic paragenesis which consists of orthopyroxene, clinopyroxene, plagioclase, quartz, K–feldspar, and Fe–Ti oxide is particularly well preserved. The retrograde metamorphism is limited to the development of micas at the expense of feldspars and to replacement of orthopyroxene rims by bastite. B: Photomicrograph of sample CZ2 that is a garnet–bearing amphibolite, mainly composed of green amphibole associated with sericitized plagioclase. Corona of amphibole and plagioclase has developed around poikilitic garnet suggesting an eclogitic retrograde metamorphism at high temperature. Biotite also occurs as a retromorphic mineral. C: Photomicrograph of sample EAR34 that is a basic hydrous granulite with a quartzo-feldspathic matrix. Garnet contains inclusions of quartz, plagioclase, pyroxene and Fe–Ti oxide. Biotite underlines foliation and amphibole associated with automorphic garnet forms reaction rim around Fe–Ti oxide and pyroxene.

A

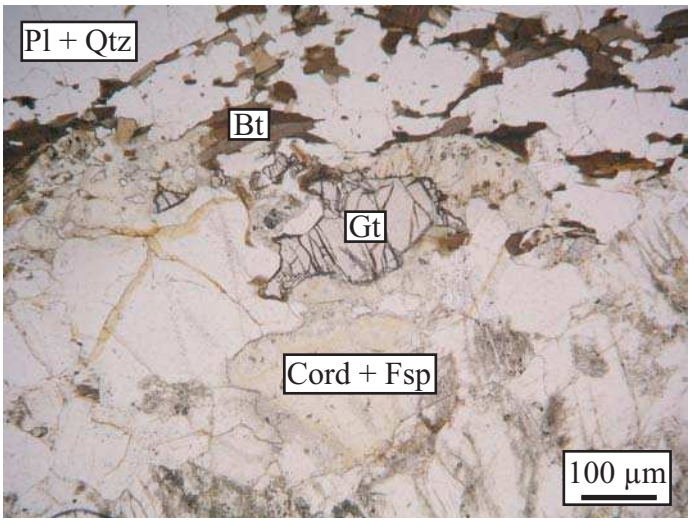

B

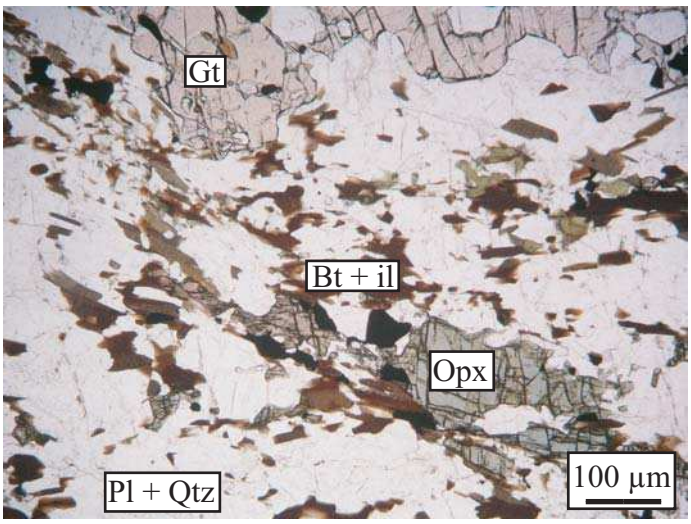

FIG. 3 – Photomicrographs of intermediate granulites. A: Photomicrograph of sample SZ35b which is a metapelite with a granulitic paragenesis of low pressure. The foliated rock is marked by an alternation of feldspar + cordierite levels and garnet + biotite levels. Relics of retromorphosed pyroxene are associated with garnet + biotite levels. Cordierite is largely altered and occurs as clusters of pinnite and white mica. Garnet and biotite are retromorphosed into chlorite. Quartz and feldspars contain many biotite inclusions. B: Photomicrograph of sample L647 which presents an inequigranular texture. Orthopyroxene (Opx) is lengthened within the foliation plane. Poikilitic garnet (Gt) includes quartz, feldspars, zircons and primary biotite inclusions. Corona texture of secondary biotite (Bt) + ilmenite (il) has developed around destabilized orthopyroxene. The presence of sub-grains in quartz indicates a partial recrystallization of the quartzo-feldspathic matrix.

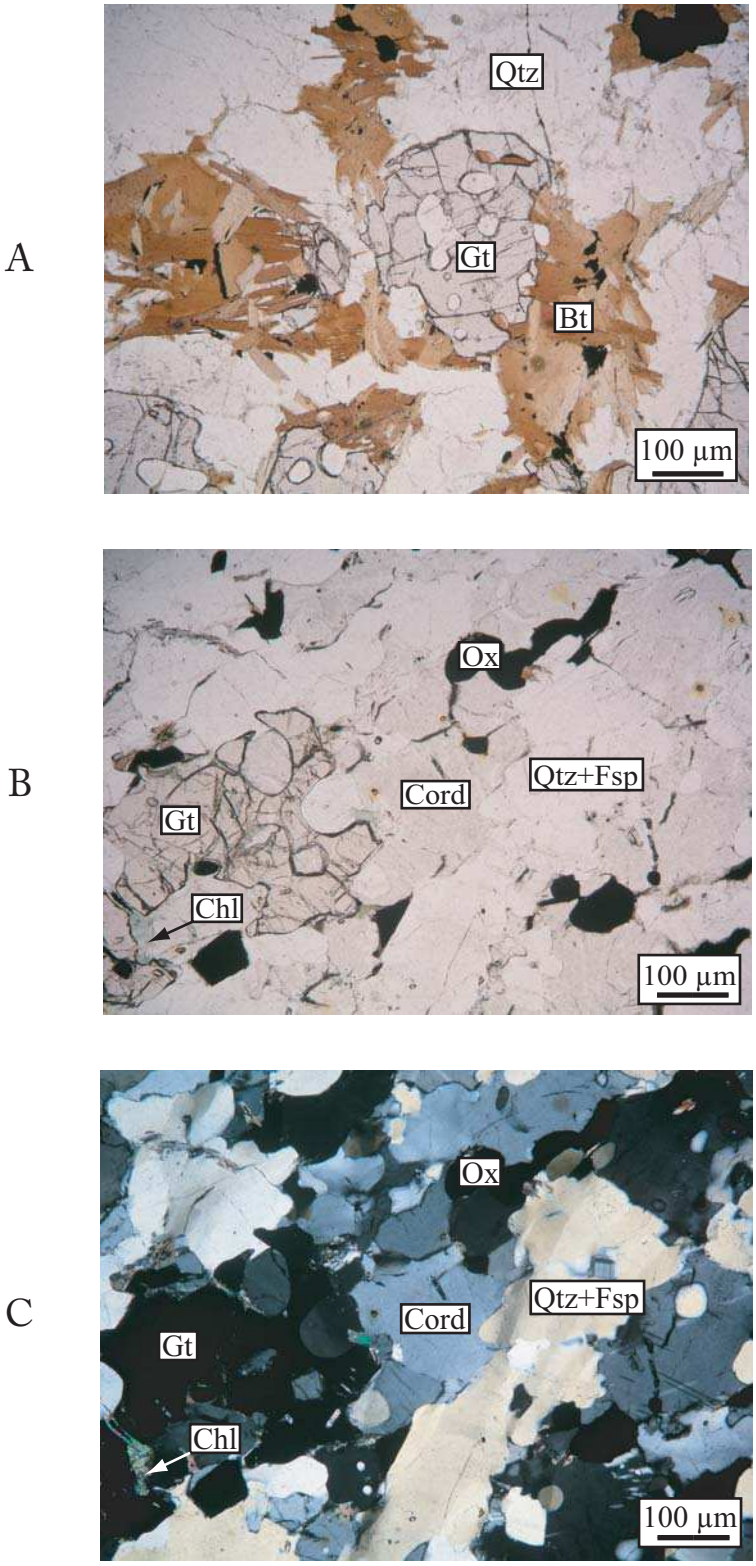

FIG. 4 – Photomicrographs of acidic granulites. A: Photomicrograph of sample GD–04–167 with quartz (Qtz) and biotite (Bt) inclusions in garnet (Gt). Biotite developed corona around garnets. B, C: Photomicrographs of sample YR–DDU which is mainly composed of cordierite (Cord), quartz (Qtz), feldspar (Fs) and Fe–Ti oxides (Ox) with a granulitic texture characterized by an angle of 120° between grains having linear grain boundaries. Intracrystalline deformation of quartz is revealed by the presence of sub-grains. No retromorphic paragenesis is observed except rare chlorite deposited in the fractures of garnet.

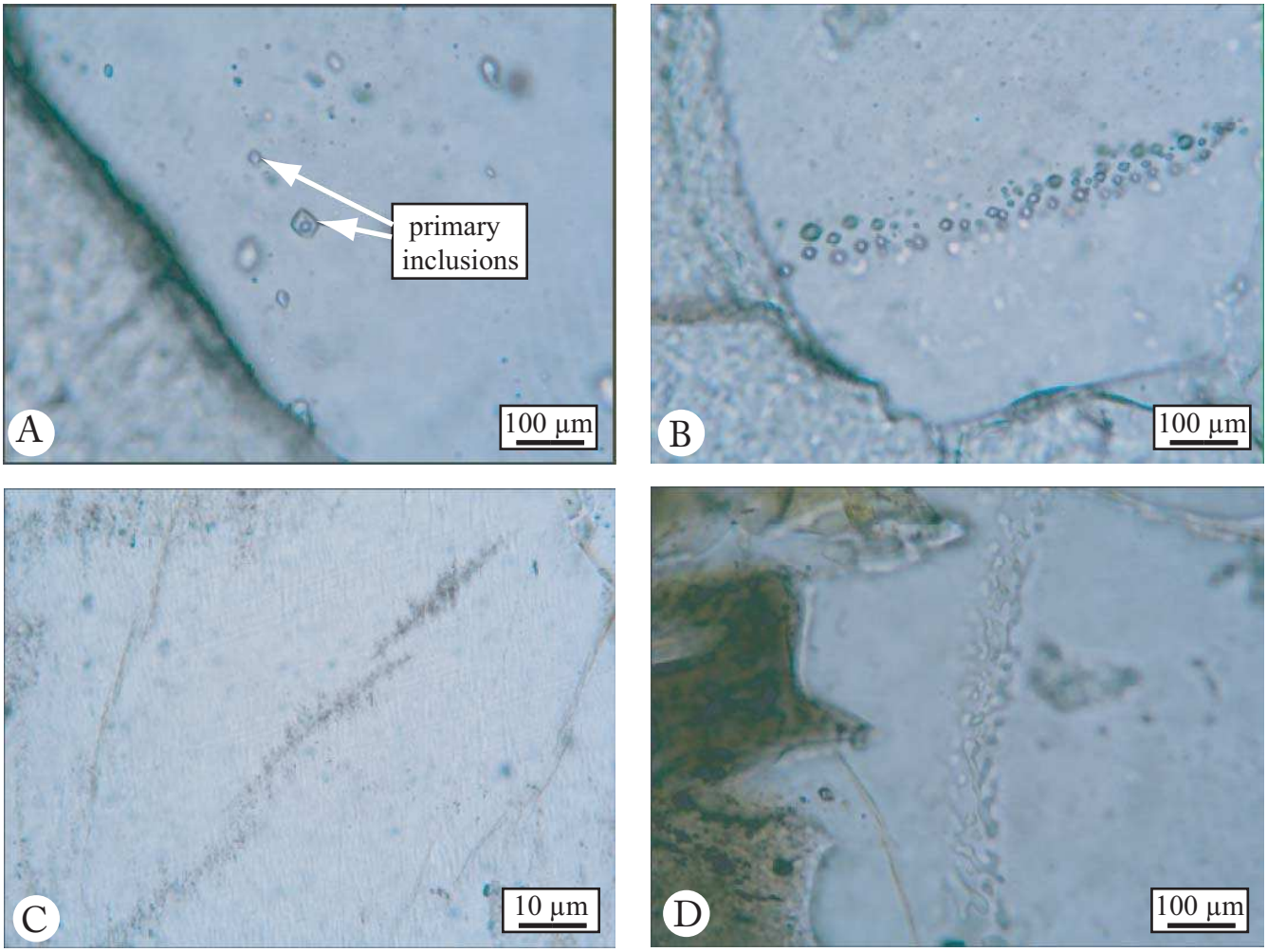

FIG. 5 – Photomicrographs of primary and secondary fluid inclusions in granulites. A: Primary inclusions occur isolated with size and geometry depending on the crystal lattice of the host mineral. B, C: Secondary inclusions occur aligned along microcracks and crosscut the crystal lattice. D: Naking-down structure of secondary inclusions.

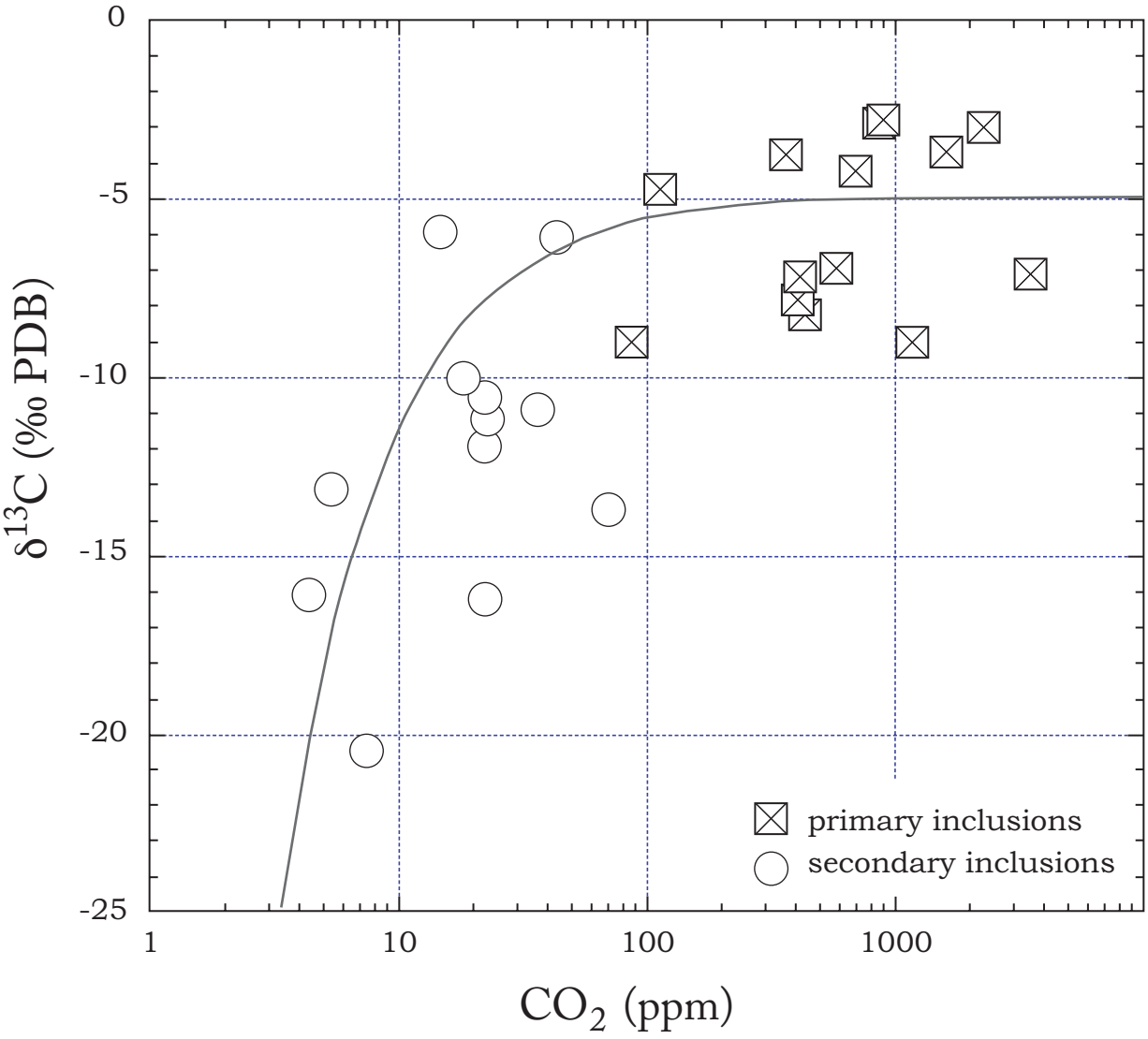

FIG. 6 – Variations in the $\delta^{13}C$ of CO_2 from primary and secondary fluid inclusions as a function of CO_2 amount in granulites that formed in a collision context. The distribution of data can be described by a hyberbolic equation that suggests mixing between a ^{13}C-depleted CO_2–poor end–member (oxidation of graphite with organic matter as the ultimate source) and one or two CO_2–rich end–members (degassing of upper mantle peridotites and decarbonation of sedimentary carbonates) with $\delta^{13}C$ values that range from –8‰ and –2‰.

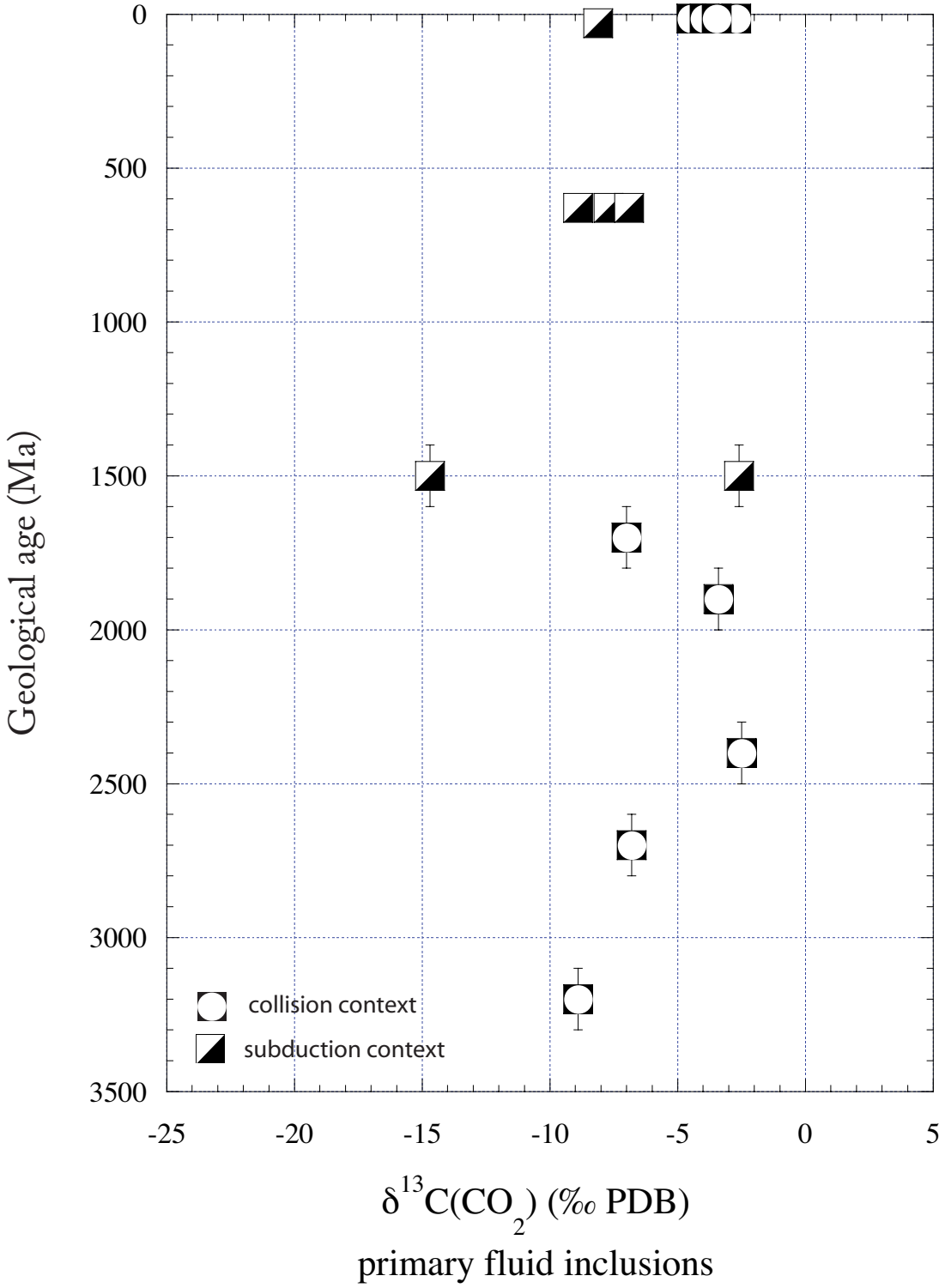

FIG. 7 – Variations through geological time of the $\delta^{13}C$ of CO_2 in primary fluid inclusions of granulites formed in collision and subduction contexts.

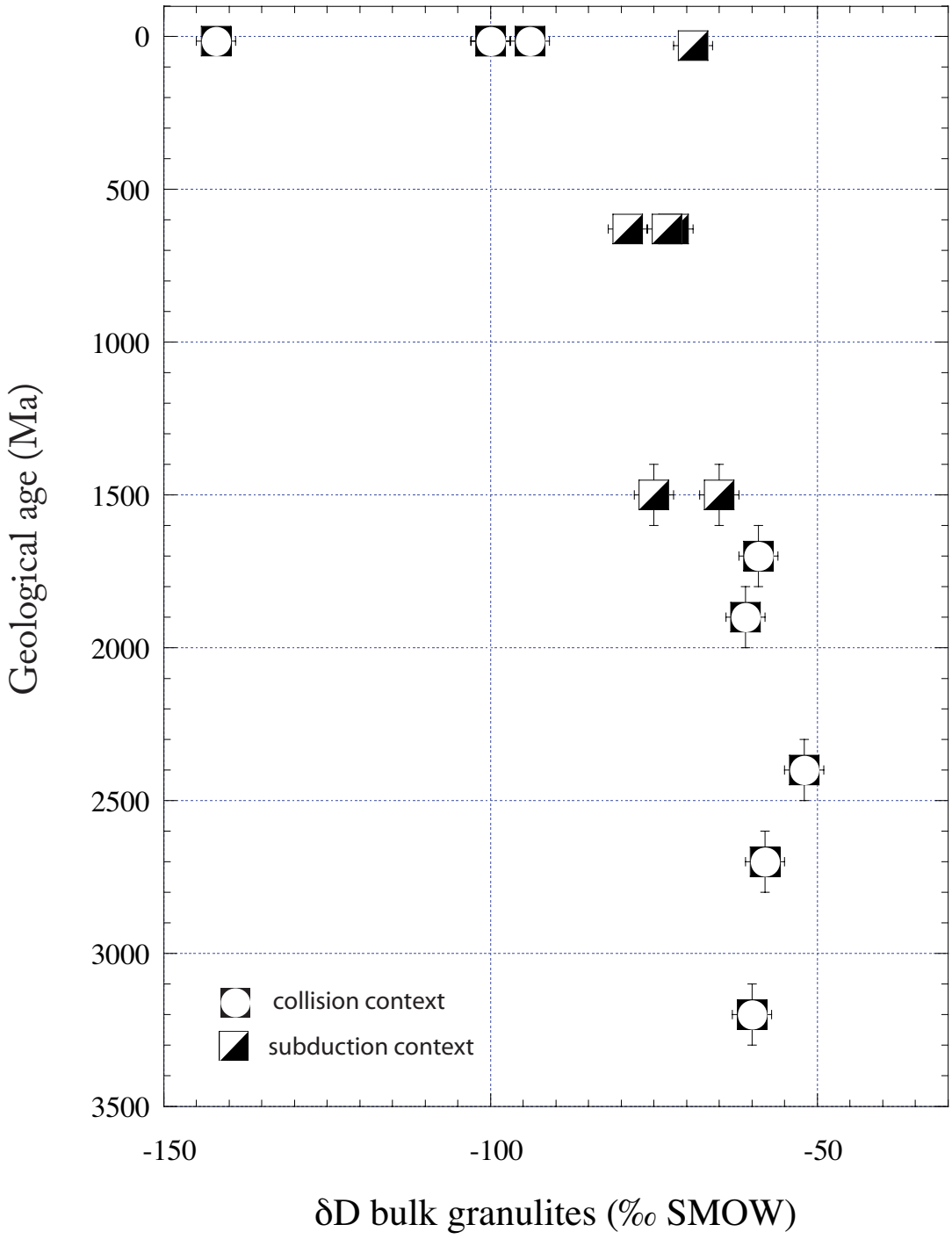

FIG. 8 – Variations through geological time of the bulk δD of granulites formed in collision and subduction contexts.

		Granulitic paragenesis								Retromorphic paragenesis			Accessory minerals			
samples	caractère	Opx	Cpx	Gt	Fs	cord.	Pl	Qtz	Bt 1	Amph	Bt 2	Pin	Zn	Ap	Ox	sph
CZ2	basic	○		XXX			XX	X		XXX	X		X		X	
GAL 26_10	basic	X	X		X		X	X					X		X	
EAR13	basic	X	X	XX			X	X	X	X			X		X	
EAR 26	basic	X	X	XX			X	X		X	X		X		X	
EAR 34	basic	X	X	XX			X	X	X	X	X		X		X	
GAL 19_03	basic	X		X	XX		XXX	X		XX	X		X		X	
NL120C	basic	○	○				XX						X		XXX	
NL129F	basic	○	○				XXX						X		XX	
SZ35b	Intermediate	○	○	XX	XXX	XX	X	XXX	X		XX ± Chl.	X ± white mica	X		X	
L647	intermediate	○	X	X	XXX		X	XXX			XX ± ilm.		X		X	
L940	acid	X		XX	XXX		X	X	X		X		X		X	X
GD_04_167	acid			XX	XX		X	XXX	X		XX		X		X	
YR_DDU	acid				XXX	XXX	X	XX			X	X	X		XX	

TAB. 1 – Petrology of Archean to Miocene granulites sampled worldwide. Opx: orthopyroxene; Cpx: clinopyroxene; Gt: garnet; Fs: feldspar; Cord: cordierite; Pl: plagioclase; Qtz: quartz; Bt1: primary biotite; Amph: amphibole; Bt2: secondary biotite; Pin: pinite; Zn: zircon; Ap: apatite; Ox: oxide; Sph: sphene; Chl: chlorite; Ilm: ilmenite.

Sample	Geographic location	Geotectonic context	Geological age (Ma)	Metamorphism P kb	Metamorphism T °C	δD bulk granulites ‰ SMOW	$[CO_2]$ f.i. (700°C) ppm	$\delta^{13}C$ (CO2) f.i. (700°C) ‰ PDB	δD (H_2O) f.i. f.i. (700°C) ‰ SMOW	$[CO_2]$ f.i. f.i. (350°C) ppm	$\delta^{13}C$ (CO_2) f.i. (350°C) ‰ PDB	δD (H_2O) f.i. (350°C) ‰ SMOW	Ref.
SZ35b	Zimbabwe	Collision	3200±100	n.d.	n.d.	-60	84	-8.9	-61	21	-16.3	n.d.	1
CZ2	Zimbabwe	Collision	2700±100	5–8	650-800	-58	563	-6.8	n.d.	4	-16.1	n.d.	2
GD-04-167	Antarctica	Collision	2400±100	7.5–10.5	750-850	-52	876	-2.5	n.d.	42	-5.9	n.d.	3
L647	Finland	Collision	1900±100	6.2–7.2	760-830	-61	1576	-3.4	-55	7	-20.6	-99	4
YR-DDU	Antarctica	Collision	1700±100	5–6	750	-59	405	-7	-56	14	-5.7	-102	5
GAL26-10	Spain	Subduction	1500±100	6–7	700-800	-75	898	-14.7	-97	67	-13.7	-139	6
GAL19-03	Spain	Subduction	1500±100	6–7	700-800	-65	867	-2.6	n.d.	5	-13.1	n.d.	
EAR13	Tanzania	Subduction	630±10	6–12	600-900	-72	392	-7.7	-88	21	-11.9	-86	
EAR26	Tanzania	Subduction	630±10	6–12	600-900	-79	1171	-8.9	n.d.	35	-10.8	n.d.	7
EAR34	Tanzania	Subduction	630±10	6–12	600-900	-73	3521	-6.9	n.d.	21	-10.5	n.d.	
NL120c	Chile	Subduction	30±10	n.d.	n.d.	-69	427	-8.1	-82	22	-11.1	-128	8
NB25	China (Tibet)	Collision	15±5	n.d.	n.d.	-100	2293	-2.7	n.d.	≈ 0	n.d.	n.d.	
NB48	China (Tibet)	Collision	15±5	n.d.	n.d.	-94	107	-4.47	n.d.	≈ 0	n.d.	n.d.	9
NB42	China (Tibet)	Collision	15±5	n.d.	n.d.	-142	675	-3.95	n.d.	≈ 0	n.d.	n.d.	
NB58	China (Tibet)	Collision	15±5	n.d.	n.d.	-100	351	-3.47	n.d.	≈ 0	n.d.	n.d.	

TAB. 2 – δD values of H_2O and $\delta^{13}C$ values of CO_2 from primary and secondary fluid inclusions along with the bulk δD values of their host granulites. Primary and secondary fluid inclusions (f.i.) have respectively been extracted at 700°C and 350°C, respectively, following a step heating procedure. Geological age, tectonic context and P–T conditions of granulitic metamorphism are given according to following sources from the literature: 1 = Kröner et al. (1993); 2 = Holzer et al. (1998), Kröner et al. (1999) and Schaller et al. (1999); 3 = Ménot et al. (2004); 4 = Barbey et al. (1990) and Daly et al. (2001); 5 = Peucat et al. (1999); 6 = Boillot et al. (1995), Desmurs (1997) and Gardien et al. (2000); 7 = Maboko (1997), Möller (1995), Muhongo et al. (1996; 1999; 2001) and Melzer (2001). N.d. = not determined.

7.2.

P–T evolution and fluid sources support a subduction–related origin for the Neoproterozoic Tanzanian granulite.

Evolution P–T et sources de fluides supposant la formation de granulites Néo–protérozoiques de Tanzanie dans un contexte de subduction.

Résumé

Les compositions isotopiques du carbone et de l'hydrogène de deux générations d'inclusions fluides et de la roche totale ont été déterminées pour des granulites du rift de Pangani (Rift Est Africain) et pour des granulites et des amphibolites à grenat du Namche–Barwa (Himalaya). Les valeurs de $\delta^{13}C$ (-8,9‰ à -5,4‰) du dioxyde de carbone et de δD (-97‰ à -75‰) de l'eau des inclusions fluides primaires des granulites de Pangani montrent que ces fluides sont principalement issus d'une source mantellique. Les valeurs de δD des granulites fortement rétromorphosées (–107‰ à –96‰) et de leurs inclusions aqueuses (-128‰ à -100‰) suggèrent la présence d'eau météorique lors de la rétromorphose contemporaine au développement de la biotite dans les plans de foliation. Les inclusions fluides primaires des granulites et amphibolites à grenat du Namche–Barwa (Himalaya) sont quant à elles caractérisées par des valeurs de $\delta^{13}C$ relativement hautes (–4,5‰ à –2,5‰) et des valeurs de δD basses (–142‰ à –94‰) suggérant une source d'origine crustale pour les fluides piégés lors du pic de métamorphisme. L'origine crustale des fluides des inclusions primaires des granulites du Namche–Barwa est compatible avec un contexte de formation de type collision continentale alors que les fluides d'origine mantellique des inclusions aqueuses primaires des granulites du rift de Pangani sont plus en accord avec un contexte de formation de type subduction.

P–T evolution and fluid sources support a subduction–related origin for the Neoproterozoic Tanzanian granulites

Gardien,[1] V., Lécuyer,[1] C., Rigaudier,[1] T., Burg [2]J.-P. and Mbede,[3] E.

1: UMR PEPS 5125, CNRS, UCB Lyon 1, 2 Rue Raphael Dubois, 696222 Villeurbanne, France

2: ETHZ Zurich Strukturgeologie Leonhardstrasse, 19CH-8092Zürich, Switzerland

3: Geology Dept, Box 35052, Dar es Salaam, Tanzania

Keywords: Granulites,Tanzania, EARS, P-T evolution, fluid inclusions, stables isotopes, CO_2

Abstract:

Carbon and hydrogen isotope compositions were determined for two generations of fluid inclusions and their host granulites from the Pangani Rift (eastern branch of the East African Rift System) and from the Namche-Barwa (Himalaya). The Pangani Rift's granulites include mafic and felsic granulites. The $\delta^{13}C$ values (-8.9‰ to -5.4‰) and δD values (-97‰ to -75‰) of primary carbonic and aqueous fluid inclusions are compatible with a dominantly mantle–derived source. The δD values of the highly retrogressed granulites (–107‰ to –96‰) and of their water inclusions (–128‰ to –100‰) suggest meteoritic water addition during retrogression coeval with the development of biotite in a foliation plane. Primary carbonic and aqueous fluid inclusions in granulites and garnet amphibolites from the Namche-Barwa (Himalaya) are characterized by relatively high $\delta^{13}C$ values (–4.5‰ to –2.5‰) and low δD values (–142‰ to –94‰) suggesting a major crustal-derived source for the fluid trapped during peak metamorphism and compatible with a continental collision–like context. The mantle–derived source for the carbonic and aqueous primary fluid inclusions from the Pangani Rift is more compatible with a subduction–like context.

Introduction

The Mozambique Belt (MB), a major suture of the late Neoproterozoic 'Pan African' orogen in eastern Africa, represents a suture zone between East and West Gondwana (Burke et al., 1977). Metamorphic rocks of the MB represent the root (mainly granulite facies rocks) of a deeply eroded orogeny exhumed through the Phanerozoic (Möller et al., 2000; Stern, 1994). Two tectonic interpretations are invoked for the formation of the granulites in the Pan-African Belt of Tanzania. The first interpretation, comparable to the collision-ocean closure model of Stern (1994), implies collision of East and West Gondwana causing high–grade metamorphism in East Africa between 800 and 600 Ma. The age of metamorphism has been repeatedly used to determine the age of collision, based on the assumption that the collision directly caused the granulite facies metamorphism (Kröner, 1993). The second interpretation (Meert et al., 1995, Kröner et al, 2001), based on paleomagnetic data and Ar-Ar dating of Neoproterozoic lavas from Tanzania, argues for a polyphased terrane accretion to form the Gondwana supercontinent because there is no evidence for a common polar-wander-path for East and West Gondwana before 550 Ma. Meert et al. (1995) suggested that the granulites formed during two orogenies: 1) the Pan-African orogeny considered to represent collision of India, Madagascar, Sri Lanka, part of Antarctica, Kalahari craton, Congo craton with the Arabian-Nubian shield between 850 and 650 Ma and associated with the closure of the northern part of the Mozambic Ocean; 2) the second orogeny happened at about 550 Ma implying amalgamation of the earlier Pan-African Orogen with Antarctica and Australia to form Gondwana.

Exhumation of the Mozambique belt, mainly related to extensional processes, finally formed

the Neogene East African Rift System (EARS). The main N-S structural trend of the Mozambique belt constrained the location where the crust was rifted (McConnel, 1972). Reactivation of former orogenic structures led to the exposure of Pan-African metamorphic series metamorphosed under granulite facies conditions. Extension related to the development of the Pangany rift is the only tectonic event occurring in this area after the Pan African orogeny. The reactivation of former structures during the Neogene extension localized the retromorphosis of the granulite facies rocks. Moreover, optical microscopy has demonstrated the presence of numerous primary and secondary fluid inclusions in the minerals. This metamorphic complex is therefore suitable for studying the stable isotope compositions of fluids that circulated in the lower continental crust in connection with tectonic processes. Therefore, we present microthermometric analyses and Raman microanalysis of two generations of fluid inclusions trapped in quartz, garnet, plagioclase and pyroxenes in order to track the origin and the history of the deep crustal fluids that participated to the genesis of these granulites. This fluid chemistry dataset is complemented by the first report to our knowledge of stable carbon and hydrogen isotope analyses of bulk rocks as well as of carbon dioxide and water which occur in the two generations of fluid inclusions. Thermobarometric calculation of the peak metamorphic conditions was also performed for deciphering the tectonic context – subduction versus collision - in which these granulites were generated.

Geological setting

The East African Orogeny

The last stage of the Gondwana super-continent assembly happened through a series of orogenic events responsible for the formation of the East African Orogeny (EAO) between 750

and 620 Ma (Stern, 1994). The EAO encompasses the Arabian–Nubian shield to the north, formed by accretion of arc terranes, and the polycyclic Mozambique Belt, resulting from major landmass collisions. The term 'Pan-African' is usually attributed to the EAO and to several other orogenic belts formed between 800 Ma and 450 Ma in Africa and adjacent Gondwana landmasses (Kuski et al., 2003, Collins and Pisarevsky, 2005, Collins, 2006), although the term originally defined thermo-tectonic events that happened around 500 Ma (Kennedy, 1964). The Mozambique Belt, described by Holmes (1951) extends from Ethiopia to Mozambique with an average N–S orientation. These terranes are subdivided into three main units based on geographical arguments, and which are the Western, Central and Eastern granulites (Hepworth, 1972). Peak granulite facies event has been dated at 655–615 Ma (review in Meert, 2003) and gave temperature and pressure conditions of 700–900ºC and 8–14 kb (Appel et al., 1998; Coolen, 1980; Möller, 1995; Muhongo and Tuisku, 1996, Sommer et al., 2003; Fritz et al., 2005). However the Eastern granulites experienced an anticlockwise P-T evolution characterized by a slow isobaric cooling in the amphibolite facies conditions before the onset of exhumation (Appel et al., 1998; Möller, 1995; Muhongo et al., 1999, Hauzenberger et al., 2004), whereas the Western granulites experienced a clockwise P-T evolution characterized by an isothermal decompression before final exhumation (Sommer et al., 2003, 2008). Microthermometric studies of fluid inclusions in the Western granulites (Sommer et al, 2008) have shown the presence of nearly pure CO_2 primary inclusions trapped in migmatites associated with the granulites and interpreted as CO_2-bearing brines immiscible under the conditions of the granulite facies metamorphism. Coolen et al (1982) described carbonic fluid inclusions in the Eastern granulites yielding pressures of 7 to 13 kb and interpreted as close to the peak of metamorphism.

Several Pan-African granulite complexes outcrop in Tanzania and in the northern part of

Mozambique, forming a fault–bounded mountain range with a broad N–S alignment. From the north of Tanzania, the Eastern Granulites group that form the Pare and Usambara Mountains (Fig. 1) are intercalated between two similar units of metasediments, namely the Umba steppe and Masai Steppe groups. In this area, the regional foliation dips ca. 30° toward the NE (Fig. 2) and is subparallel to the bedding. These structures and several lithological repetitions are attributed to several westward thrusts. Their kinematic direction would be parallel to the N240 stretching lineation (Shackleton, 1993).

Sample description

The thirty–four analyzed samples have been collected from five sampling sites distributed from the SE to the NW ends of the rift (Usangi and Usambara sites, respectively), one of them being located on the rift footwall (Kajiungeni site) (Fig. 1). In order to determine the origin of the mafic granulitic facies rocks, major and trace elements were determined by X–Ray Fluorescence analysis. Samples were crushed in an agate mortar, then major and trace element compositions were determined by fusion of glass discs and powder pellets, respectively. Bulk rock analyses are reported in Table 1 and indicate that the mafic granulites derived from an igneous protolith of basaltic to andesitic and rhyolitic compositions. Representation of the composition of the samples in an AFM diagram suggests a tholeiitic to calc-alkaline affinity (Fig. 3).

Mineral associations

The granulites are characterized by various mineralogical assemblages which result from both the protolith composition and subsequent metamorphic transformations. Granulite compositions vary from mafic pyroxene–bearing granulites (Fig. 4-A-B-C), to scarce pyroxene–free felsic granulites (Fig. 4-D-E-F). The main assemblage of the mafic granulite is characterized by the

paragenesis Qzt+Pl+Px±Grt±Hbl. In most samples, the retrograde metamorphism is characterized by the occurrence of amphibole and biotite (Fig. 4-G-H-I). Ilmenite, zircon and apatite and rare crystals of rutile and calcite developed as secondary minerals. All samples display a variably developed foliation principally marked by biotite, ilmenite (Fig. 4-D) and sillimanite for the felsic granulites (Fig. 4-E). Garnet stretched and elongated in the foliation plane, folded ortopyroxene, quartz ribbon and biotite both elongated in the foliation plane suggest that the deformation took place during and after the metamorphic climax.

Garnets have three distinct habitus. The first one (Grt I) consists of cm-sized poikilitic and xenomorphic porphyroblasts (Fig. 4-A) and contains inclusions of quartz, plagioclase, pyroxene and Fe–Ti oxides. This first generation of garnet is intergrown with orthopyroxene and clinopyroxene and this is interpreted to be representative of their early prograde growth. Millimeter automorphic garnets represent the second habitus (Grt II) (Fig. 4-C and 4-G), and contain rare inclusions of quartz, plagioclase, amphibole and biotite. This second generation of garnet is interpreted as an equilibrium texture formed at peak conditions reached during the granulites facies metamorphism. The third habitus (Grt III) corresponds to garnet associated with quartz in coronas around ilmenite (Fig. 4-J), and to the rim of Grt II crystals. Some garnets (Grt I) of the sillimanite-bearing granulite are flattened parallel to the foliation (Fig. 4-E).

Pyroxenes have two habitus. The most common (Px II) consists of millimeter-sized orthopyroxene (Opx) and clinopyroxene (Cpx) often in textural equilibrium with Grt I (Fig. 4-A). Some Opx II are folded and stretched along the foliation. Scarce, destabilized Opx surrounded by Px II and Grt I, are relics of the first pyroxene generation (Opx I). The corona texture can be explained by the reaction:

Opx + Pl ➔ Grt + Cpx + Qtz

This reaction illustrates the transition between medium- to high-pressure granulite facies conditions with the assemblage Grt + Pl + Qtz on the high-pressure side of the reaction. Occurrence of this texture in orthopyroxene-bearing branulites is a good indicator of isobaric cooling (e.g. Harley, 1989). Stretched quartz and plagioclases are always present in the granulites (Fig. 4-D). Green hornblende is occasionally found as porphyroclasts in equilibrium with Grt II (Fig. 4-C) and in symplectite textures surrounding pyroxene II. Biotite lays in the foliation and also occurs as corona around oxides, pyroxene, amphibole and garnet (Fig. 4-D).

Fluid Inclusions

Fluid inclusions are tiny quantities of liquid and/or vapour trapped within minerals. Their size ranges from submicroscopic up to several hundred micrometers in diameter and typical masses are in order of nanograms. Microstructural observations under the optical microscope may allow the discrimination between “primary inclusions” or “peak metamorphic conditions” formed during mineral growth and “secondary inclusions” or “retrograde” formed thereafter (Touret, 2001). Various sources of evidence suggest that many fluid inclusions preserve the chemical and physical properties of the original parent fluid from which they were formed. The fluids are therefore considered to be direct samples of the volatile phases that circulated through the lithosphere and their chemical analysis provides information on both the composition and density of these fluids. Two types of fluid inclusions are observed (Fig. 5), (1) isolated inclusions of 20 μm in size in quartz, plagioclase, garnet and pyroxene (primary inclusions) and (2) inclusions occurring along trails (secondary inclusions).

Analytical techniques

Microprobe analysis

Twelve samples were selected for microprobe analyses in order to accomplish a thermo-barometric study. Phase compositions where obtained using the CAMECA SX100 microprobe (University of Clermont-Ferrand, France) using silicate and Fe-oxide for calibration at a 15 kV acceleration potential. The beam current was 20 nA, and the counting time for each element was 10 s. Representative mineral compositions are reported in Table 2.

Raman micro-analysis

Analyses of fluids in individual inclusions in minerals were made with a Dilor Microdil-28 multi-channel laser Raman micro spectrometer at the LST of the ENS Lyon using a 514 nm Ar-ion laser source of excitation. Peak integrals of the different components have been recalculated to mol% following the principle outlined by Touray et al. (1985) and using the relative Raman scattering cross-section as discussed by Debussy et al (1989) after calibrating the instrument with synthetic gas mixtures of known composition and density. Fluid inclusions have been checked for the presence of CO_2, N_2, CH_4, H_2S, hydrocarbons and carbonaceous daughter minerals as well as graphite.

Microthermometry analyses

Microthermometry measurements of fluid inclusions were carried out with a Linkam THM 600 Heating/freezing stage with accuracy of 0.1° C at –56.6°C and of 1°C at 374°C. Temperature measurements were calibrated with a set of artificial inclusions. Fluid inclusions were frozen with liquid N_2 (–196°C). The cooling temperature permits determining the nature of the chemical system of the fluid. Slow heating allows determining the fluid melting point that was compared to

pure systems (0°C for H_2O and -56.6°C for CO_2). The homogenisation temperature of the fluid leads the fluid density to be calculated and the vapour–liquid curve, which provides the relationship between density, pressure and temperature, is inferred from its chemical composition. A heating stage also allows determining the fluid density from which one can deduce the trapping pressure and temperature. Molar volumes of pure CO_2 fluid inclusions were calculated with the MacFlinCor™ software using the homogenisation temperature (Th). MacFlinCor™ was developed to process laboratory data obtained on fluid inclusions as well as to calculate P-T isochors for fluid composed of H_2O, CO_2, N_2, CH_4 and NaCl (Brown and Hagemann, 1994, 1995).

Stable isotopes

Extraction of fluid inclusions

Fluids trapped in granulites were extracted by thermal decrepitation. Five hundred mg to one g of millimetre–sized grains of nominally anhydrous minerals (quartz, plagioclase, pyroxene and garnet) were washed with diluted nitric acid then with double deionised water before drying overnight at 110°C in an oven. Next, samples were then loaded in a silica glass tube and degassed at 110˚C for at least 2 h. Step heating fixed on the basis of homogenisation temperatures observed by microthermometry was considered as the best protocol to separate fluids from primary and secondary fluid inclusions. Ideally, it is expected that fluids of secondary inclusions forming micro-cracks would be totally released at temperatures close to 350±20°C, whereas most fluids from primary inclusions would be collected at temperatures of 700±20°C. For each heating step, fluids contained in mineral inclusions were collected for at least 20 min. This method does not however ensure that fluids were extracted from both generations of fluid inclusions without some

contamination of the high–temperature generation by the lower one. Indeed, decrepitation temperature of the inclusions depends on the internal pressure inside the inclusions, their size as well as the strength of the host, and the distance of the inclusion from the grain surface. Consequently, small secondary fluid inclusions tend to decrepitate at higher temperatures approaching those of primary inclusions. Similarly, the smallest primary inclusions could escape decrepitation performed at about 700°C even though no sizable amount of water has been extracted at temperatures up to 800°C. Finally, carbon dioxide and water were separated by using cryogenic traps. Water was collected into a silica glass tube containing about 300 mg of fine–grained chromium metal. Water blanks were very low over the complete set of experiments without contributing more than 5% of the total amount of water extracted from fluid inclusions.

Extraction of water from bulk samples

Whole-rock samples were crushed into a very fine powder (implying the opening of the two types of fluid inclusions). An amount of 150 to 200 mg of rock powder was loaded into a silica glass tube and heated at 150°C for 1 h in vacuum to remove any atmospheric water adsorbed on the sample. Sample was further heated up with a torch until complete melting inducing the release of water from hydrous minerals. The pyrex™ vacuum extraction line was maintained at a temperature of 80°C over the complete manipulation to avoid water condensation on the inner sides of the experimental apparatus. Using a liquid nitrogen trap, water was collected into a silica tube containing about 300 mg of chromium metal. This protocol was adapted from both methods developed by Vennemann and O'Neil (1993) and Morrison et al. (2001). Residual gases not condensable in liquid nitrogen are mainly composed of H_2 that is produced during the oxidation of the FeO component of silicates by water. If this amount of H_2 is one order of

magnitude lower than the amount of water released during the melting of the granulite samples, its D/H ratio is about from 150‰ to 300‰ lower than that of water according to thermodynamic calculations performed by Cerrai et al. (1954) and experiments made by Simon (2005) in the temperature range 600°C–1200°C. Therefore, a quantitative oxidation of this H_2 to water by passing through a CuO furnace at 500°C is necessary to avoid the acquisition of D/H ratios shifted towards too high values.

Isotope ratio measurements of carbon dioxide and water

Carbon isotope composition of purified carbon dioxide was measured with a dual–inlet GV Prism™ mass spectrometer. At 1000°C during 5 minutes, water was reduced by Cr to produce H_2 gas for which the D/H ratio was determined by using either a dual–inlet MAT–Finnigan™ DeltaE mass spectrometer for the bigger samples or a dual–inlet GV Prism™ mass spectrometer for the small samples. External reproducibility of D/H measurements was established at about ±3‰ by scaling raw data to the "true" isotopic ratios of SMOW, SLAP and GISP international standards (Fig. 6). Aliquots of these international standard waters were selected in the range 0.5–1.5 μl which sizes are comparable to those of analyzed natural samples, except for two samples (EAR4 and EAR6) that provided lower amounts of water (Table 1). D/H measurements of most samples have been duplicated and the internal reproducibility varied from ±1.5 to ±6.7‰ (Table 1). Repeated analyses of the international standard NBS30 provided a mean δD value of –66.8±2.8‰ (n = 8) to be compared to the recommended value of –65.7‰. Water amounts of samples were determined by comparison with a series of water samples of known weights ranging from 0.5 μl to 1.5 μl. After expansion of H_2 into a constant volume of the mass spectrometer sample inlet, the amount of gas was estimated from the voltage of mass 2 collector (Fig. 7). Uncertainty associated

with the determined amount of water is close to ±0.05 μl.

Results

Mineral chemistry

Garnets: Four garnet families were identified by microprobe analysis (Table 2). Garnets from the EAR 2 sillimanite–bearing granulite make the first one. Their compositions are $Alm_{56.7-65}$, $Py_{29.6-38.7}$, $Gr_{35.5-5.3}$, $Sp_{1.0-1.4}$. The second family is observed exclusively in sample EAR 5; it has a relatively homogeneous composition with <2 % of variation in end–members: $Alm_{48.6-50.4}$, $Py_{30.0-31.9}$, $Gr_{16.3-16.9}$, $Sp_{2.7-2.9}$. The third family includes garnets from sample EAR 14; it is also rather homogeneous with a composition range $Alm_{70.0-70.8}$, $Py_{6.1-7.5}$, $Gr_{18.7-20.0}$, $Sp_{2.8-3.1}$, and <1.5 % in variation for each end-member content. Garnets from other samples (family 4) are characterized by an important compositional variation: $Alm_{54.4-63.1}$, $Py_{16.1-25.4}$, $Gr_{16.4-19.2}$, $Sp_{1.9-6.1}$. The four different families of garnet are due to the different whole rock composition of the studied samples (Fig 8A). However in family D, the most variable garnet composition, two (Grt I and II) or sometimes three generations of garnet (Grt I, II and III) are present in the same sample. In that case we observed systematically that garnet composition evolved to pyrope-rich/almandine-poor (Grt I) to a pyrope-poor/almandine-rich (Grt II and Grt III) composition (Fig. 8B).

Pyroxenes: Clinopyroxenes have less than 10 % of variation in end–member composition: $En_{33.3-40.5}$, $Fs_{11.4-20.0}$, $Wo_{44.1-48}$ (Table 2). Using Morimoto nomenclature (1988), clinopyroxenes have diopside to augite compositions. Their tetrahedral and octahedral aluminium occupancy is

variable (Al^{IV} $_{0.050\text{-}0.11}$, Al^{VI} $_{0.02\text{-}0.12}$). According to Morimoto's nomenclature (1988), all orthopyroxenes (Opx) are enstatites that span two groups (Fig. 9) characterized by an important difference in Mg content; Opx I corresponds to Mg-poor enstatite ($En_{55.7\text{-}57.1}$) whereas the second generation, Opx II, is a Mg-rich enstatite ($En_{65.9\text{-}68.4}$).

Feldspars: All analyzed feldspars are unzoned (Table 2). They are divided between andesine and oligoclase groups within the composition range $Ab_{0.53\text{-}0.81}$, $An_{0.18\text{-}0.46}$, $Orth_{0.01\text{-}0.03}$.

Amphiboles: Three groups of amphiboles were analyzed (Table 2) in mafic granulites. According to Leake's classification (1978), the first group corresponds to ''Ferro Pargasitic Hornblendes'' and occurs as retrograde corona after kinked Opx I (Fig. 4G and group A in Fig 10). These Mg-rich amphiboles have Mg # comprised between 0.634 and 0.661. The second group belongs to the ''Ferroan-Pargasites'' with Mg # comprised between 0.504 and 0.565. This hornblende occurred in equilibrium with Grt II (Fig. 4H and group B in Fig. 10). The third group, composed of ''Ferro-Pargasites'' occurred as elongated minerals in the foliation plane of the more stretched mafic granulites (Fig. 4I and group C in Fig. 10). These Fe-rich amphiboles ($Fe_{3.1\text{-}3.2}$, $Mg_{1.3\text{-}1.5}$, $Al_{1.9\text{-}2.2}$, $Na_{0.6}$) have Mg # ranging from 0.266 to 0.301.

Biotites: All samples (Table 2) contain Mg-rich biotites ($Fe_{1.22\text{-}1.70}$, $Mg_{2.96\text{-}3.73}$) except those from sample EAR 14, which are Fe-rich ($Fe_{2.93\text{-}3.03}$, $Mg_{1.75\text{-}2.19}$).

Thermobarometry

The metamorphic evolution of Tanzanian granulites was assessed by combining the identification of distinct mineralogical textures with the occurrence of hydrated retrograde mineral

minerals of known chemistry. Pressure-temperature calculations have been performed by using the software TWEEQU (Berman, 1991; version 2.02) and the thermodynamic dataset was provided by Berman (1988; 1990).

The typical granulite facies paragenesis Gt-Px-Qz-Pl was used to calculate the pressure and temperature conditions reached during the peak of metamorphism. Calculations were done using different generations of minerals, as for example the three garnet types. In several samples, we have further calculated equilibrium conditions using pairs of mineral core-inclusion, and mineral rim-mineral in the matrix in order to define the PT evolution trend during the mineral growth. The acidic and intermediate granulites (EAR 2 and EAR 10) were used for calculation of the P–T conditions during deformation. They have been calculated from compositions of stretched pyroxene and garnet. The last stage of the retrograde path is associated with the development of amphibole and biotite. Hammarstrom and Zen (1986) have established an empirical Al-in-hornblende barometer for calc-alkaline rocks of tonalite and granodiorite compositions. Since this pioneering study, several authors (Hollister et al., 1987, Johnston and Rutherford, 1989; Rutter et al., 1989; Schmidt 1992; Ague, 1997) tested and confirmed that the proposed hornblende barometer can also be used to determine pressure emplacement of granitic rocks from 2.5 -13 kb with a precision of 0.6 kb. We used the barometer developed by Hammarstrom and Zen (1986) and the compositional grid from Spear (1993) based on the aluminium content in hornblende. The retrograde path has also been constrained using the compositional grid from Spear (1993) based on the plagioclase composition.

The composition of granulitic minerals (Gt-Px-Qz-Pl) provided P–T conditions ranging from 7.6 to 14.1 kb and from 595°C to 850ºC. These P–T conditions match the kyanite stability field and, to a lesser degree, the sillimanite stability field (Table 3). Usambara samples delivered the

highest pressure range (10.2-14.1 kb) for temperature conditions ranging from 660°C to 795ºC (Fig. 11). Due to the high temperature conditions reached during granulite facies metamorphism, relics of the early (prograde) stage are very rare and very often provided by inclusions (Opx) instead of mineral zonation. Calculations using both rim and core compositions of a Grt I – Opx II couple (sample EAR 4) indicated a cooling of 120ºC (Table 3). Samples from Kilomen and Same were equilibrated at intermediate pressures between 8.4–10.3 kb and 680–790°C while samples from Kilomen provided P-T conditions between 9.3–11.3 kb and 620–650 °C (Table 3, Fig. 11). The lowest equilibrium pressures have been obtained from Usangi samples with P–T conditions of 7.6–11.1 kb and 595-850ºC (Table 3, Fig. 11). These results were obtained using Grt-Cpx II core and rim compositions, inclusions of Cpx II within Grt II, and finally rims of Grt II and Cpx II from the matrix. Temperatures obtained from core and rim compositions suggest a cooling by about 140 ºC during mineral growth. We did not perform probe traverses in garnet from our samples however previous studies (Moller, 1995, Appel et al., 1996) have demonstrated that some garnets of both felsic and mafic granulites from the same localities preserved a bell-shape prograde growth zoning.

Equilibrium P-T conditions calculated from stretched and reoriented garnet, pyroxenes and biotites, differ substantially in each sample, and are sometimes very close to conditions obtained for undeformed granulites. The estimated temperatures are of 580ºC and 900°C for the mafic granulite EAR 14 and the intensively stretched granulite EAR 10, respectively (Table 3). Pressures were only estimated for the acid granulite EAR 2, between 9.3 kb and 10.6 kb (Table 3). P–T conditions estimated on the basis of the aluminium content of amphiboles using both the empirical barometer of Hammarstrom and Zen (1986) and the grid of Spear (1993) range from 730°C to 820°C and from 5.7 kb to 7.4 kb (Table 3).

Raman micro-analysis and micro thermometry data

Two major types of fluid inclusions have been distinguished with the Raman microanalysis, a CO_2 spectrum in primary and secondary fluid inclusions and an OH^- spectrum restricted to the secondary inclusions organized in trails (Fig. 12). These results are confirmed by the microthermometry analysis as CO_2 and aqueous fluid inclusions were observed in minerals (Table 4). Carbonic inclusions occur in garnet, pyroxene, plagioclase and quartz in the matrix, as well as in quartz inclusions within garnet. The CO_2–rich fluid inclusions in quartz inclusions homogenize into a liquid phase at temperatures comprised between –21.5°C and –13.2°C, translating into CO_2 densities in the range 0.98–1.02 $g.cm^{-3}$. The CO_2 rich-inclusions in quartz, pyroxene and plagioclase in the matrix homogenize into a liquid phase at temperatures from –36°C to –20°C translating into CO_2 densities of 1.06 to 1.15 $g.cm^{-3}$. The CO_2–rich fluid inclusions in the garnets homogenize in a temperature range of –43°C to –28.4°C, corresponding to densities of 0.99 to 1.11 $g.cm^{-3}$ (Table 4). The majority of the aqueous fluid inclusions occurring in matrix quartz have low salinities. Melting temperatures were in the range 160°C–340°C.

Stable isotope data

D/H of bulk rocks: Tanzanian samples have bulk δD values that lie in a relative large range from –107‰ to –72‰ and which are correlated to the amount of water trapped in hydrous silicates such as amphibole and biotite (Table 5 and Fig. 13). However, the analyzed samples present mineralogical differences related to their retrograde evolution. Samples EAR4, EAR6 and EAR20 have bulk δD values that range from –107‰ to –96‰ (Table 5). The three samples are retrogressed under amphibolite facies conditions. Retrogression gave rise to the development of amphibole and biotite in the foliation plane, indicating that the retrograde evolution is associated

with deformation. The other samples have bulk δD values that lie in a relatively narrow range from –87‰ to –72‰ (Table 5). They are characterized by limited retrogression which, when occurring, took place under medium pressure granulites facies conditions as testified by the development of a second generation of clinopyroxene and garnet.

Four samples from the core of the Namche-Barwa syntaxis (South Tibet) were studied as granulite references that were generated in a collision context. Three metapelites (NB25, NB48 and NB58) and one garnet amphibolite were chosen. Thermobarometric calculations yielded granulite facies conditions for the metapelites (720-760 °C; 8-10 kb) and amphibolite facies conditions (T> 600 °C, P> 8 kb) for the garnet amphibolites (Burg et al., 1998). Such P–T estimates are similar to the metamorphic conditions calculated for the Pangani samples (Table 3). The time of peak metamorphism at 16±2.5 Ma (Sm-Nd on whole rock and garnet fractions) obtained from the NB58 metapelite is related to continental collision (Burg et al., 1997, 1998). The three Namche-Barwa metasediments equilibrated under granulite facies conditions are characterized by low δD values ranging from -100‰ to -94‰ (Table 4). These δD values are similar to those obtained for the retrogressed Tanzanian samples EAR4, EAR5 and EAR20. The garnet amphibolite is characterized by a δD value of -142‰ (Table 4). The δD values of granulites from South Tibet are not correlated to the amount of water in bulk rocks (Table 5; Fig. 13).

D/H and $^{13}C/^{12}C$ of fluid inclusions: Assuming that no fractionation occurred during trapping of the fluids, both $\delta^{13}C$ and δD values of these inclusions may be considered to be those of the fluids circulating in the crust at the time of granulite formation. Tanzanian granulitic

samples (whatever the retrogression under amphibolite facies conditions) have $\delta^{13}C$ values that range from –8.9‰ to –5.4‰ with a mean $\delta^{13}C$ value of -7.4±1.2‰ (Table 4). The granulite samples from the Namche-Barwa (retrogressed or not under amphibolite facies conditions) are characterized by distinct isotopic compositions with higher $\delta^{13}C$ values ranging from –4.5‰ to –2.5‰ and with a mean value of –3.6±0.9‰ (Table 5). Water amounts from secondary fluid inclusions are in the range 100–200 ppm and are relatively low when compared to primary fluid inclusions that contain from 400 to 800 ppm of water (Fig. 14). Hydrogen isotope compositions of these two generations of inclusions are also distinct; at decrepitation temperatures of 350±20°C, secondary fluid inclusions from granulites EAR 6, 12 and 13 have δD values from -128‰ to -85‰, lower or similar to the D/H ratios obtained for primary fluid inclusions (-108‰ < δD < -83‰) that have been released at temperatures of 700±20°C (Table 4 and Fig. 14). High-grade metamorphic hydrous minerals are expected to be at least 30‰ deuterium-depleted relative to their forming water according to natural observations (e.g. Früh–Green et al., 1996) and laboratory experiments (e.g. Suzuoki and Epstein, 1976; Graham et al., 1984). Our data set reveals a distinct pattern with δD values of primary and secondary fluid inclusions that are about 10‰ to 30‰ lower than the δD values of their corresponding bulk rocks for which water was derived from the melting of hydrous phases. These results suggest that water from amphibole and biotite has not the same source as waters that were trapped in the primary and secondary inclusions from the nominally-anhydrous granulitic minerals. The correlation observed between the δD values and water amounts of bulk rocks suggests that D/H ratios of water were either fractionated during granulite formation and evolution or inherited from the composition of the protolith. Therefore, the D/H ratios of water inclusions can be considered as reliable proxies of

the hydrogen isotope composition of the water involved in the granulite facies metamorphism.

Interpretation and discussion

The thermobarometric conditions obtained for the mafic granulites are reported in Figure 15. Granulites from Usambara and Usangi have recorded the highest (14.1 kb) and the lowest pressures (7.6 kb) with temperatures ranging between 850ºC and 545ºC respectively. Results obtained with cores and rims of granulitic minerals indicate a cooling of about 100ºC during mineral growth and the P–T range of retromorphic conditions, deduced from amphibole chemistry, is consistent with this evolution path (Fig. 15). The presence of destabilized orthopyroxenes (Opx I) indicates the incursion in the granulite stability field corresponding to the experimentally determined "Opx-out" curve (Spear, 1993). This stage happened during the prograde path, suggesting an anticlockwise metamorphic evolution (Fig. 15), in agreement with the pressures obtained with the density of the primary fluid inclusions in garnets, pyroxenes and quartz. Estimated P–T conditions of the metamorphism peak (8-14 kb, 850ºC) are also consistent with previous studies of Pan-Africans rocks from the Mozambique belt, which provided P–T conditions in the ranges 700–900°C and 8–12 kb (Appel et al., 1998; Coolen, 1980; Möller, 1995; Muhongo and Tuisku, 1996; Hauzenberger et al., 2005).

Anticlockwise evolution of granulitic metamorphism is generally attributed to the contribution of an external heat source responsible for high temperatures during prograde metamorphism followed by a slow to nearly isobaric cooling. The most often proposed phenomena to explain this evolution is magmatic underplating and intrusions into the lower crust, inducing granulitic conditions. The geodynamic significance or even more the "reality" of anticlockwise P-T path are still in debate however, previous high-quality papers published in international journals present

anticlockwise P-T evolutions, as for example, for the Eastern Granulites (Eppel et al., 1998, Hauzenberger et al., 2004). Geochronological data indicate that the majority of protoliths are dated between 800 Ma to 1 Ga (Tenczer et al., 2006) whereas metamorphic conditions dated at 620 Ma (Möller et al., 1998, Muhongo et al, 2001; Kröner et al., 2003, Hauzenberger et al., 2007). The main structural features observed in the Eastern granulites basement are a subhorizontal to moderately E-dipping foliation and W-E mineral lineation. This foliation is associated with vertical flattened fold in the basement and N-S vertical parallel folds in the sedimentary cover (Fritz et al., 2009). The Western granulites are characterized by a clockwise P-T path dated between 640 and 620 Ma (Sommer et al., 2008) and the majority of the protoliths are dated between 2.3-2.6 and 1.8 Ga. The structure is characterized by a subhorizontal to moderately E-dipping foliation and E -W mineral lineation. General westward transport is illustrated by abundant top-to-the West shear zones. This contrast between Eastern and the Western granulites is interpreted as the results of metamorphism and deformation above the subducted lithospheric mantle (Fritz et al., 2009).

The granulite facies metamorphism is dated between 655 and 615 Ma (Meert, 2003). Paleomagnetic data indicate that the final assemblage between east and west Gondwana took place around 550 Ma (Meert et al., 1995). Appel et al. (1998) and Möller et al. (2000) proposed that magmatic underplating caused the metamorphism almost 70 Ma before continent–continent collision. More recently, Meert (2003) proposed that east Gondwana never formed a coherent block and that the formation of the super–continent resulted from several collision events between 750 and 530 Ma, the Mozambique collision belt being coeval with the granulite facies metamorphism (655–615 Ma). Meert (2003) proposed that magmatic underplating could have produced lithospheric delamination and subsequent intrusions of asthenospheric mantle beneath

the previously thickened crust. A similar contribution of heat by magmatic underplating is also mentioned beneath active continental margins (Harley, 1989). The WSW verging thrusts (Shackleton., 1993; Fritz et al 2009) show that the granulitic metamorphism took place in a convergence context. According to the thrust transport direction, we can therefore propose a model implying eastward subduction under a part of east Gondwana followed by continental collision. The magmatism related to the subduction under the active margin may have produced magmatic underplating at the origin of the high recorded pressures.

A subduction context can also be considered on the basis of the isotopic signatures of CO_2 and H_2O fluids trapped as inclusions in the Tanzanian granulites. They have $\delta^{13}C$ and δD values that are compatible with a mantle–derived source (Sheppard and Epstein, 1970; Kuroda et al., 1977; Boettcher and O'Neil, 1980; Javoy, 1980; Kyser and O'Neil, 1984; Chaussidon et al., 1991; Deloule et al., 1991; Lécuyer et al., 1998). Decarbonation of carbonates is the unlikely process to explain the carbon isotope composition of the carbon dioxide trapped in fluid inclusions because the carbon isotope fractionation dramatically decreases with increasing pressure as shown by Martinez et al. (1994) and Sharp et al. (2003). The $\delta^{13}C$ values suggest that oxidation of graphite, whose ultimate source is organic matter, was not involved as a source of carbon during the granulite genesis. In this case, the $\delta^{13}C$ values of CO_2 trapped in granulites of sedimentary origin or contaminated by a sedimentary source are lower than –15‰ (Vry et al., 1988; Crawford and Valley, 1990). Restricted but significant variations in carbon isotope compositions of CO_2 from Tanzanian granulites could reflect either mantle heterogeneities that are inferred from the large spectrum of diamond compositions (Galimov, 1991; Deines et al., 1993; Cartigny et al., 2004; Cartigny, 2005) or a slight crustal contamination. The interpretation of D/H ratios is ambiguous because meteoric waters may have the same compositions as waters derived from mantle degassing. Granulite genesis itself may also fractionate the hydrogen isotope composition of

circulating water through crustal degassing, however relative high PT conditions should restrict the amplitude of isotopic fractionation and the D/H ratios of water inclusions in anhydrous minerals could reflect the composition of circulating water. Both carbon and hydrogen isotope compositions of fluid inclusions suggest the dominant influence of mantle–derived fluids compatible with a subduction context for the genesis of Tanzanian granulites.

However, according to a number of authors (England and Thompson, 1984; Bohlen, 1987; Ellis, 1987; Harley, 1989; Bohlen, 1991) granulites with anticlockwise P-T paths are related to underplating of magma at the base of crust (loading the crust). Moreover, palaeomagnetic data (Meert et al., 1995) indicated that the closure of the southern Mozambique Ocean occurred at 550 Ma, that is almost 100 My after the granulite facies event dated between 650 and 620 Ma (Möller et al., 2000). Major element compositions of the granulitic protoliths indicate a tholeiitic to calc-alkaline affinity (Fig. 3 and Table 1). These data are consistent with the formation of the granulites at an active margin in a subduction context.

Granulites from the young Namche-Barwa syntax in Himalaya contain carbonic and aqueous fluids with isotopic compositions compatible with a crustal source involved during their genesis. Carbon isotope compositions are relatively high when compared to the assumed range of mantle compositions, they could reflect a contribution from carbonated sedimentary rocks for which $\delta^{13}C$ range from –2‰ to +5‰ since the Precambrian (Schidlowski, 2001). The relatively low δD values close to –100‰ compared to the assumed mantle range (δD = –80±10‰) could correspond to a contamination by meteoric waters of high altitude origin.

Conclusions

The thermo–barometric results presented in this study indicate an anticlockwise evolution of the granulitic facies metamorphism connected to both an external heat supply and a thickened crust (40–45 km). The high-grade metamorphism may result from lithospheric delamination and

subsequent intrusions of asthenospheric mantle beneath a crust previously thickened by continental collision. Another possibility is that a subduction zone below an active margin produced magmas underplated at the base of the lower crust and loading the crust a few million years before collision. Carbon and hydrogen isotope compositions of both CO_2 and H_2O fluids trapped as inclusions in the Tanzanian granulites are compatible with a dominantly contributing mantle-derived source. We thus proposed that the Tanzanian granulites were not caused directly by collision but in a subduction zone context.

References

Appel, P., Möller, A., Schenk, V., 1998. High-pressure granulite facies metamorphism in the Pan-African belt of eastern Tanzania: P-T-t evidence against granulite formation by continent collision. J. Metam. Geol. 16, 491–509.

Berman, R.G., 1988. Internally-consistent thermodynamic data for stoichiometric minerals in the system Na_2O-K_2O-CaO-MgO-FeO-Fe_2O_3-Al_2O_3-SiO_2-TiO_2-H_2O-CO_2. J. Petrol. 29, 445–522.

Berman, R.G., 1990. Mixing properties of Ca-Mg-Fe-Mn garnets. Am. Mineral. 75, 328–344.

Berman, R.G., 1991. Thermobarometry using multiequilibrium calculations: a new technique with petrologic applications. Can. Mineral. 29, 833–855.

Blundy, T.D., Holland, J.J.B., 1990. Calcic amphibole equilibria and a new amphibole-plagioclase geothermometer. Contrib. Mineral. Petrol. 104, 208–224.

Boettcher, A.L., O'Neil, J.R., 1980. Stable isotope, chemical and petrographic studies of high pressure amphiboles and micas: evidence for metasomatism in the mantle source regions of alkali basalts and kimberlites. Am. J. Sci. 280A, 594–621.

Bohlen, S.R., 1991. On the formation of granulites. J. Geol. 95, 617–632.

Brown, P.E., Hagemann, S,G.,1994. MacFlinCor: a computer program for fluid inclusion data reduction and manipulation. In: De Vivo and Frezzotti (Eds.), Fluid Inclusions in Minerals: Method and Applications, VP1 Press, 231–250.

Burg, J.P., Nievergelt, P., Oberli, F., Seward, D., Davy, P., Maurin, J.C., Diao, Z., Meier, M.,1997. Exhumation during crustal folding in the Namche-Barwa syntaxis. Terra Nova 9, 53–56.

Burg, J.P., Davy, P., Nievergelt, P., Oberli, F., Seward, D., Diao, Z., Meier, M., 1998. The Namche-Barwa syntaxis: evidence for exhumation related to compressional crustal folding. J. Asian Earth Sci. 16, 239–252.

Burke, K., Dewey, J.F., Kidd, W.S.F., 1977. World distribution of sutures: the sites of former oceans. Tectonophysics 40, 69–99.

Cartigny, P., 2005. Stable isotopes and the origin of diamond. Elements 1, 79–84.

Cartigny, P., Stachel, T., Harris, J. F., Javoy, M., 2004. Constraining diamond metasomatic growth using C- and N- stable isotopes: examples from Namibia. Lithos 77, 359–373.

Chaussidon, M., Sheppard, S.M.F., Michard, A., 1991. Hydrogen, sulphur and neodymium isotope variations in the mantle beneath the EPR at 12°50'N. In: Taylor, H.P., O'Neil, J.R., Kaplan, I.R. (Eds.), Stable Isotope Geochemistry: A Tribute to Samuel Epstein. The Geochemical Society, Special Publication, vol. 3, pp. 325–337.

Coolen, J.M., 1980. Chemical petrology of the Furua complex, Southern Tanzania. Ph. D Thesis, Vrije Universiteit, Amsterdam, GUA Papers of Geology, Series 1, nº13 pp.

Coolen, J.M., 1982. Carbonic fluid inclusions in granulites from Tanzania: a comparison of geobarometric methods based on fluid density and mineral chemistry. Chem. Geol. 37, 59–77.

Crawford, W.A., Valley, J.W., 1990. Origin of graphite in the Pickering Gneiss and the Franklin Marble, Honey Brook Upland, Pennsylvania Piedmont. Geol. Soc. Am. Bull. 102, 807–811.

Debussy, J., Porty, B., Ramboz, C., 1989. Advances in C-O-H-N-S fluid geochemistry based in micro-Raman spectrometry analyses on fluid inclusions. Eur. J. Mineral. 1, 517–534.

Deines, P., Harris, J.W., Gurney, J.J., 1993. Depth–related carbon isotope and nitrogen concentration variability in the mantle below the Orapa kimberlite, Bostwana, Africa. Geochim. Cosmochim. Acta 57, 2781–2796.

Deloule, E., Albarède, F., Sheppard, S.M.F., 1991. Hydrogen isotope heterogeneities in the mantle from ion probe analysis of amphiboles from ultramafic rocks. Earth Planet. Sci. Lett. 105, 543–553.

Dypvik, H., Hankel, O., Nilsen, O., Kaaya, C., Kilembe, E., 2001. The lithostratigraphy of the Karoo supergroup in the Kilombero Rift Valley, Tanzania. J. Afr. Earth Sci. 32, 451–470.

Fritz, H., Tenczer, V., Hauzenberger, C., Wallbrecher, E., Muhongo, S., 2009. Hot granulites nappes-Tectonic styles and thermal evolution of the Proterozoic granulite belts in East Africa. Tectonophysics, in press.

Früh-Green, G., Plas, A., Lécuyer, C., 1996. Petrologic and stable isotope constraints on hydrothermal alteration and serpentinization of the EPR shallow mantle at Hess Deep (Site 895). In: Mével, C., Gillis, K.M., Allan, J.F. and Meyer, P.S. (Eds). Proc. ODP, Sci. Results, 147: College Station, TX (Ocean Drilling Program), pp. 255–291.

Galimov, E.M., 1991. Isotope fractionation related to kimberlite magmatism and diamond formation. Geochim. Cosmochim. Acta 55, 1697–1708.

Graham, C.M., Powel, R.P., 1984. A garnet-hornblende geothermometer: Calibration, testing, and application to the Pelona schist, southern California. J. Metam. Geol. 2, 13–31.

Graham, C.M., Viglino, J.A., Harmon, R.S., 1984. Experimental study of hydrogen-isotope exchange between aluminous chlorite and water and of hydrogen diffusion in chlorite. Amer. Mineral. 72, 566–579.

Hauzenberger, C., Bauernhofer, A., Hoinkes, G., Wallbrecher, Mathu, E., 2004. Pan-African high pressure granulites from SE-Kenya: petrological and geothermobarometric evidence for polyphase evolution in the Mozanbique Belt. J. Afr. Earth Sci. 40, 245–268.

Hauzenberger, C., Robl, J., Stüwe ,W., 2005. Garnet zoning in high P granulite-facies metapelite,

Mozambique Belt SE Kenya: constraints on the cooling history. Europ. J. Mineral. 17, 43–55.

Hauzenberger, C., Sommer, H., Fritz, H., Bauernhofer, A., Kröner, A., Hoinkes, G., Wallbrecher, E., Thöni, M., 2007. SHRIMP U-Pb zircon Sm-Nd garnet ages from the granulite facies basement of SE Kenya: evidence for Neoproterozoic polycyclic assembly of the Mozambique Belt. J. Geol. Soc. London 164, 189–201.

Hammarstrom, J.M. and Zen, E.A., 1986. Aluminium in hornblende: An empirical igneous geobarometer. Am. Mineral. 71, 1297–1313.

Harley, S.L., 1989. The origin of granulites: a metamorphic perspective. Geol. Mag. 126, 215–247.

Hoinkes, G., 1986. Effect of grossular content in garnet on the partitioning of Fe and Mg between garnet and biotite. Contrib. Mineral. Petrol. 92, 393–399.

Holmes, A., 1951. The sequence of Pre-Cambrian orogenic belts in south and central Africa. In: Sandford, K.S., Blondel, F. (Eds.), 18th International Geological Congress. Association of African Geological Surveys, London, pp. 254–269.

Javoy, M., 1980. $^{18}O/^{16}O$ and D/H ratios in high temperature peridotites. C.N.R.S. Colloques internationaux, n°272: 279-287.

Kennedy, W.Q., 1964. The structural differentiation of Africa in the Pan-African (± 500 my) tectonic episode. Univ. Leeds, Res. Inst. African Geol., Annu. Rep. 8, 48–49.

Kishima, N., Sakai, H., 1980. Oxygen-18 and deuterium determination on a single water sample of a few milligrams. Anal. Chem. 52, 356–358.

Krogh, E.J., 1988. The garnet, clinopyroxene Fe-Mg geothermometer, a reinterpretation of existing experimental data. Contrib. Mineral. Petrol. 99, 44–48.

Kuroda, Y., Suzuoki, T., Matsuo, S., 1977. D/H ratios of the coexisting phlogopite and richterite

from mica nodules and a peridotite in South African kimberlites. Contrib. Mineral. Petrol. 52, 315–318.

Kuski, T.M., Stern, R.J., Tucker, R.D., 2003. Evolution of the East African and related orogens, and the assembly of Gondwana. Precamb. Res. 123, 81–85.

Kyser, T.K., O'Neil, J.R., 1984. Hydrogen isotope systematics of submarine basalts. Geochim. Cosmochim. Acta 48, 2123–2133.

Leake, B.E., 1978. Nomenclature of amphibole. Can. Mineral. 16, 105–124.

Lécuyer, C., Gillet, Ph., Robert, F., 1998. Hydrogen isotope composition of seawater and the global water cycle. Chem. Geol. 145, 253–265.

Maboko, M.A.H., 1997. P-T conditions of metamorphism in the Wami River granulite complex, central coastal Tanzania: implications for Pan-African geotectonics in the Mozambique Belt of eastern Africa. J. Afr. Earth Sci. 24, 51–64.

Martinez, I., Agrinier, P., Schärer, U., Javoy, M., 1994. A SEM–ATEM and stable isotope study of carbonates from the Haughton impact crater, Canada. Earth Planet. Sci. Lett. 121, 559–574.

McConnel, R.B., 1972. Geological Development of the Rift System of Eastern Africa. Geol. Soc. Am. Bull. 83, 2549–2572.

Meert, J.G., 2003. A synopsis of events related to the assembly of eastern Gondwana. Tectonophysics 362, 1–40.

Meert, J.G., Van der Voo, R., 1996. Paleomagnetic and 40Ar/39Ar study of the Sinay dolerite, Kenya, Implications for Gondwana assembly. J. Geol. 104, 131–142.

Meert, J.G., Van der Voo, R., Ayub, S., 1995. Paleomagnetic investigation of the Neoproterozoic Gagwe lavas and Mbozi complex, Tanzania and the assembly of Gondwana. Precamb. Res. 74, 225–244.

Möller, A., 1995. Pan-African granulites and early Proterozoic eclogites in the Precambrian basement of eastern Tanzania: P-T-t history and crustal evolution of the complex Mozambique Belt, PhD Thesis Christian-Albrechts-Universität Kiel, 206pp.

Möller, A., Mezger, K., Scenk, V., 2000. U-Pb dating of metamorphism and prolonged slow cooling of high pressure granulites in Tanzania, East Africa. Precamb. Res. 104, 123–146.

Morimoto, M., 1988. Nomenclature of pyroxenes. Am. Mineral. 73, 1123–1133.

Morrison, J., Brockwell, T., Merren, T., Fourel, F., Philipps, A., 2001. On-Line High-Precision Stable Hydrogen Isotopic Analyses on Nanolitre Water Samples. Anal. Chem. 73, 3570–3575.

Muhongo, S., Tuisku, P., 1996. Pan-African high pressure isobaric cooling: evidence from the mineralogy and thermobarometry of the granulite-facies rocks from the Uluguru Mountains, eastern Tanzania. J. Afr. Earth Sci. 23, 443–463.

Muhongo, S., Tuisku, P., Mtoni, Y., 1999. Pan-African pressure-temperature evolution of the Merelani area in the Mozambique Belt in northeast Tanzania. J. Afr. Earth Sci., 29, 353–365.

Muhongo, S., Kröner, A., Nemchin, A.A., 2001. Zircon ages from granulites facies rocks in the Mozambique Belt of Tanzania and implications for Gondwana assembly. J. Geol. 109, 171–189.

O'Neil, J.R., Adami, L.H., 1969. The oxygen isotope partition function ratio of water and the structure of liquid water. J. Phys. Chem. 73, 1553-1558.

Schidlowski, M., 2001. Carbon isotopes as biogeochemical recorders of life over 3.8 Ga of Earth history: evolution of a concept. Precamb. Res. 106, 117–134.

Sen, S.K., Bhattacharya, A., 1984. An orthopyroxene-garnet thermometer and its application to the

Madras charnockites. Contrib. Mineral. Petrol. 88, 64–71.

Shackleton, R., 1993. Tectonics of the lower crust: a view from the Usambara Mountains, NE Tanzania. J. Struct. Geol., 15, 663–671.

Sharp, Z.D., Papike, J.J., Durakiewicz, T., 2003. The effect of thermal decarbonation on stable isotope compositions of carbonates. Amer. Mineral. 88, 87–92.

Sheppard, S.M.F., Epstein, S., 1970. D/H and $^{18}O/^{16}O$ ratios of minerals of possible mantle or lower crustal origin. Earth Planet. Sci. Lett. 9, 232–239.

Simon, L., 2003. Quelques exemples de modélisations géochimiques des interactions entre les enveloppes terrestres. PhD Thesis, University of Lyon, France, 220 pp.

Sommer, H, Kröner, A, Hauzenberger, C, Muhongo, S., 2003. Metamorphic petrology and zircon geochronology of high-grade rocks from the CMB of Tanzani: crustal recycling of Archean and Paleoproterozoic material during the Pan-African orogeny. J. Metam. Geol. 21, 915–934.

Sommer, H., Hauzenberger, C., Fröner, A., Muhongo, S., 2008. Isothermal decompression history in the "Western granulites" terrain, central Tanzania: Evidence from reaction textures and trapped fluids in metapleites. J. Afr. Earth Sci. 51, 123–144.

Spear, F.S., 1993. Metamorphic Phase Equilibria and Pressure-Temperature-Time paths. Monograph Series. Mineral. Soc. Am. 799p

Stern, R.J., 1994. Arc assembly and continental collision in the Neoproterozoic East Africa Orogen: implications of consolidation of Gondwanaland. Ann. Rev. Earth Planet. Sci. 22, 319–351.

Suzuoki, T., Epstein, S. 1976, Hydrogen isotope fractionation between OH–bearing minerals and water. Geochim. Cosmochim. Acta 40, 1229–1240.

Touray, J.C., Beny, C., Dubessy, J., 1985. Micro-characterization of fluid inclusions in minerals by Raman microprobe. Scanning Electron Microscop. 1, 103–118.

Touret, J.L.R., 2001. Fluids in metamorphic rocks, Lithos 55, 1–25.

Tenczer, V., Hauzenberger, C., Fritz, CA., Whitehouse, M., Mogessie, A., Wallbrecher, E., Muhongo, S., Hoinkes, G., 2006. Anorthosites in the Eastern Granulites of Tanzania- new SIMS zircon U-Pb ages data, petrography and geochemistry. Precam. Res. 148, 85–114.

Vry, J., Brown, P.E., Valley, J.W., Morrison, J., 1988. Constraints on granulite genesis from carbon isotope compositions of cordierite and graphite. Nature 332, 66–68.

Vennemann, T.W., O'Neil J.R., 1993. A simple and inexpensive method of hydrogen isotope and water analyses of minerals and rocks based on zinc reagent. Chem. Geol. 103, 227–234.

Wernicke, B., 1985. Uniform-sense normal simple shear of the continental lithosphere. Can. J. Earth. Sci. 22, 108–125.

Zeyen, H., Volker, F., Wehrle, V., Fuchs, K., Sobolev, SV., Altherr ,R .,1997. Styles of continental rifting: crust-mantle detachment and mantle plumes. Tectonophysics 278, 1-4: 329–352.

Figure captions

Figure 1A: Studied area in the African continent and location of Mezosoic and Neogene rift systems. Age of the Madagascar drift is mentioned after Cochran (1998).

1B: Schematic Geological map of the Pangani rift. Samples sites are: 1 – Usangi; 2 – Kilomen; 3 – Same; 4 – Kajiungeni; 5 – Usambara.

Figure 2: Cross section of the Usambara Mountains parallel to the mineral lineation (modified after Shackelton, 1993).

Figure 3: Bulk rock chemical compositions of the granulite facies rocks plotted in an A(Na_2O+K_2O)-F(FeO)-M(MgO) diagram

Figure 4: Photomicrographs of granulites in plane-polarized light (A, C, E and F) and crossed-polarized light (B and D). **A-**Globular garnet (Grt I) and Cpx II elongated parallel to the foliation (trace showed by dashed line) (sample EAR 1). **B -** Equilibrium texture between automorph garnet (Grt II) and amphibole, and disequilibrium texture (corona) between Clinopyroxene II and orthopyroxene I (sample EAR6). **C -** Undeformed Qz + Pl + Cpx + Hb assemblage (sample EAR 29). **D -** Biotite and iron oxide grains elongated in the foliation plane (sample EAR 10). **E -** Garnet elongated in the foliation plane, associated with biotite and prismatic sillimanite (samples EAR 2). **F -** Quartz elongated in the foliation plane (sample EAR 16). **G**- Detail of equilibrium

texture between automorph garnet (Grt II) and amphibole; **H-** Coronitic retrograde amphibole around ortho and clinopyroxen. I- Coronitic retrograde biotite around amphibole. J- Third generation of garnet associated with quartz in cotonitic texture surrounding ilmenite.

Figure 5: Photomicrographs in plane-polarized light illustrating the primary (A) and secondary (B) fluid inclusions in quartz matrix, pyroxene (C) and garnet (D) of the granulite samples.

Figure 6: Calibration line scaling the measured D/H ratios to the "true" values certified for the international standards of water (SLAP, GISP and SMOW), also including the internal reference water which is a double deionised water derived from Rhône River, France. The equation obtained by a linear regression of data was used to calculate the D/H ratios of both bulk granulites and their water inclusions.

Figure 7: Calibration line scaling the measured intensity of mass 2 collector (H_2 gas) to water samples of known weights. The equation obtained by a linear regression of data was used to calculate the amount of water released during the pyrolysis of bulk granulites.

Figure 8 A: Chemical compositions of the four garnet families in a plot of %Alm vs % Pyr space. B: Composition of the 3 generations of garnets in the family D. Full symbol represents the first Grt I, open symbol Grt II and grey symbol GrtIII. The general evolution is an increase in the Mg (% pyrope) and a decrease in the Fe (% almandin) content during the growing of Grt I to Grt II. In EAR 4 the Fe content decreases and the Mg content remains constant during the development of

second generation of garnet, in EAR 20 the Mg content decreases and the Fe content remains constant during the development of Grt I to Grt III.

Figure 9: Chemical compositions of the first generation of Opx (full symbol) and of the second generation of Opx (open symbol) and of the Opx elongated in the foliation plane.

Figure 10: Chemical compositions of the 3 families of amphiboles.

Fig 11: Equilibrium P–T conditions calculated with the TWEEQU software (v 2.02). The 18 equilibrium states calculated with the program are listed, as well as the used additional thermometers and barometers (dashed curves on the graphs).

Figure 12: Spectrum signatures of the two types of fluid inclusions. A: CO_2 – rich fluid in primary inclusions in quartz, B: H_2O – rich fluid in secondary inclusions in quartz.

Figure 13: δD (‰ SMOW) of bulk Tanzanian (Open Square) and Himalayan (black and white Square) bulk granulites that are reported against the rate of rock hydration (wt% H_2O). Note the significant correlation between the two variables for the Tanzanian granulites ($r^2 = 0.778$; n = 10).

Figure 14: δD (‰ SMOW) of primary (filled square) and secondary (open circle) fluid inclusions hosted by bulk Tanzanian granulite samples (EAR 6; EAR12 and EAR13) which are reported against the concentration (ppm) of water inclusions.

Figure 15: Synthesis of the thermo-barometric results for the basic granulites and the possible mean P-T path for the retrograde metamorphism evolution. The equilibrium grids for plagioclases, amphiboles, garnets and aluminium silicates are from Spear (1993). The stippled lines represent the interpolations made for mineral stability conditions. The initial stage of the prograde path is pulled from a survey of Möller (1995, 1998) achieved on metapelites.

Table captions

Table 1: Bulk rock major compositions of the Tanzanian granulite facies rocks.

Table 2: Microprobe analyses of garnet, pyroxene, plagioclase, amphibole and biotite grains from the studied samples. Garnet types correspond to different habits described in the text. Different compositional families are specified. For Amphiboles, Mg # = Mg / (Mg + Fe + Mn), with the number of cations by structural unit.

Table 3: Thermo-barometric results for studied Tanzanian granulite samples. Mineral assemblages used for calculations are specified. B, C and I refer respectively to mineral border, mineral core, and inclusion. Frames group data obtained from the same mineral grains. Method used for P-T calculations: 1 for TWEEQU software, 2 for other calibrations.

Table 4: Results of microthermometry analyses of CO_2-rich fluid trapped in primary inclusions and of H_2O-rich fluid trapped in secondary inclusions in quartz, plagioclase, pyroxene and garnet.

Table 5: Carbon and hydrogen isotope compositions of CO_2 and H_2O fluids trapped in primary and secondary fluid inclusions from the quartz-feldspar fraction of the granulitic rocks. Letters in italic in the mineralogical description refer to retrograde minerals.

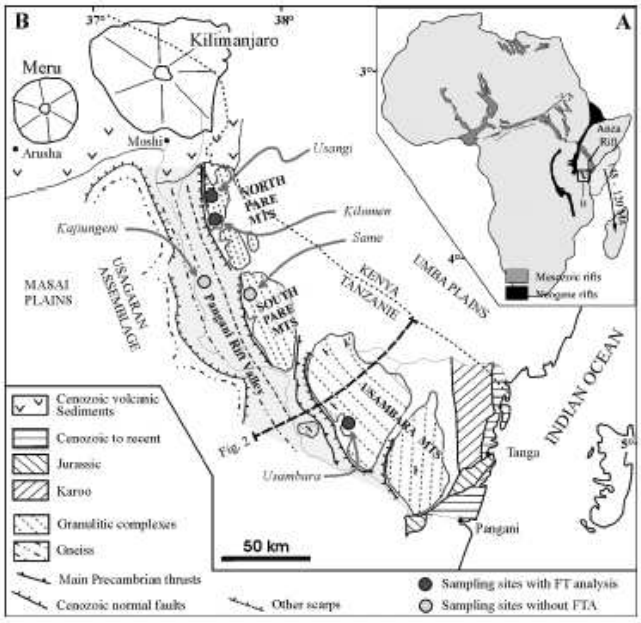

FIG. 1 – A: Studied area in the African continent and location of Mezosoic and Neogene rift systems. Age of the Madagascar drift is mentioned after Cochran (1998). B: Schematic Geological map of the Pangani rift. Samples sites are: 1 – Usangi; 2 – Kilomen; 3 – Same; 4 – Kajiungeni; 5 – Usambara.

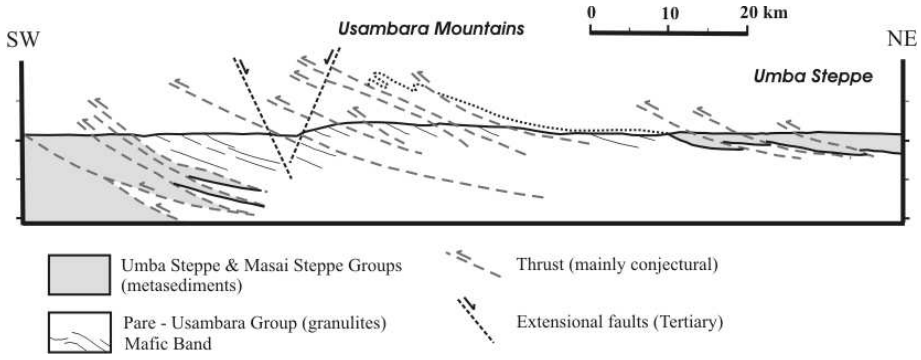

FIG. 2 – Cross section of the Usambara Mountains parallel to the mineral lineation (modified after Shackelton, 1993).

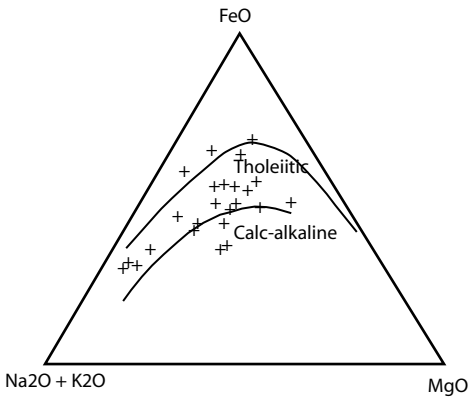

FIG. 3 – Bulk rock chemical compositions of the granulite facies rocks plotted in an $A(Na_2O+K_2O)$-F(FeO)-M(MgO) diagram.

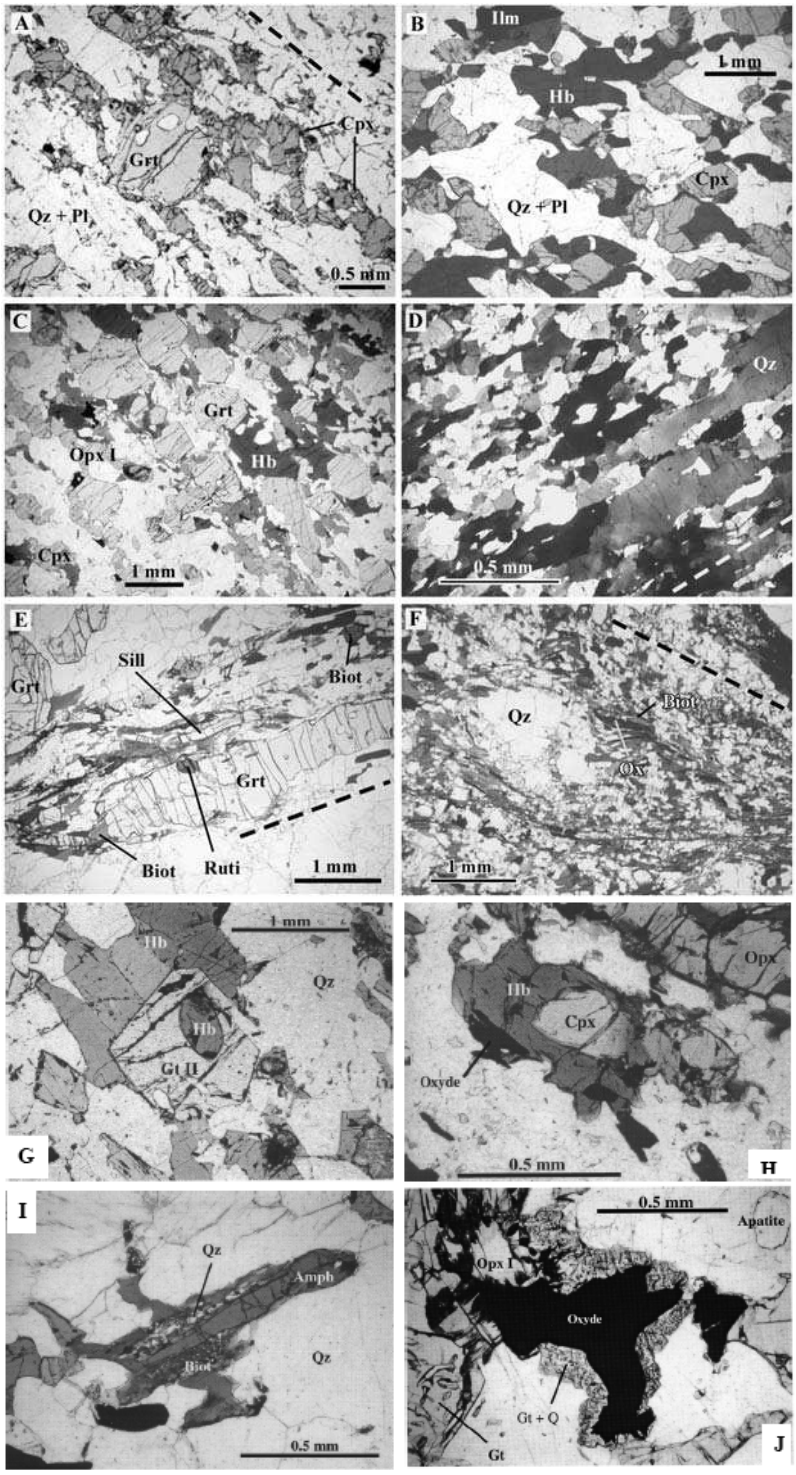

FIG. 4 – Photomicrographs of granulites in plane-polarized light (A, C, E and F) and crossed-polarized light (B and D). A: Globular garnet (Grt I) and Cpx II elongated parallel to the foliation (trace showed by dashed line) (sample EAR 1). B: Equilibrium texture between automorph garnet (Grt II) and amphibole, and disequilibrium texture (corona) between Clinopyroxene II and orthopyroxene I (sample EAR6). C: Undeformed Qz + Pl + Cpx + Hb assemblage (sample EAR 29). D: Biotite and iron oxide grains elongated in the foliation plane (sample EAR 10). E: Garnet elongated in the foliation plane, associated with biotite and prismatic sillimanite (samples EAR 2). F: Quartz elongated in the foliation plane (sample EAR 16). G: Detail of equilibrium texture between automorph garnet (Grt II) and amphibole; H: Coronitic retrograde amphibole around ortho and clinopyroxen. I: Coronitic retrograde biotite around amphibole. J: Third generation of garnet associated with quartz in cotonitic texture surrounding ilmenite.

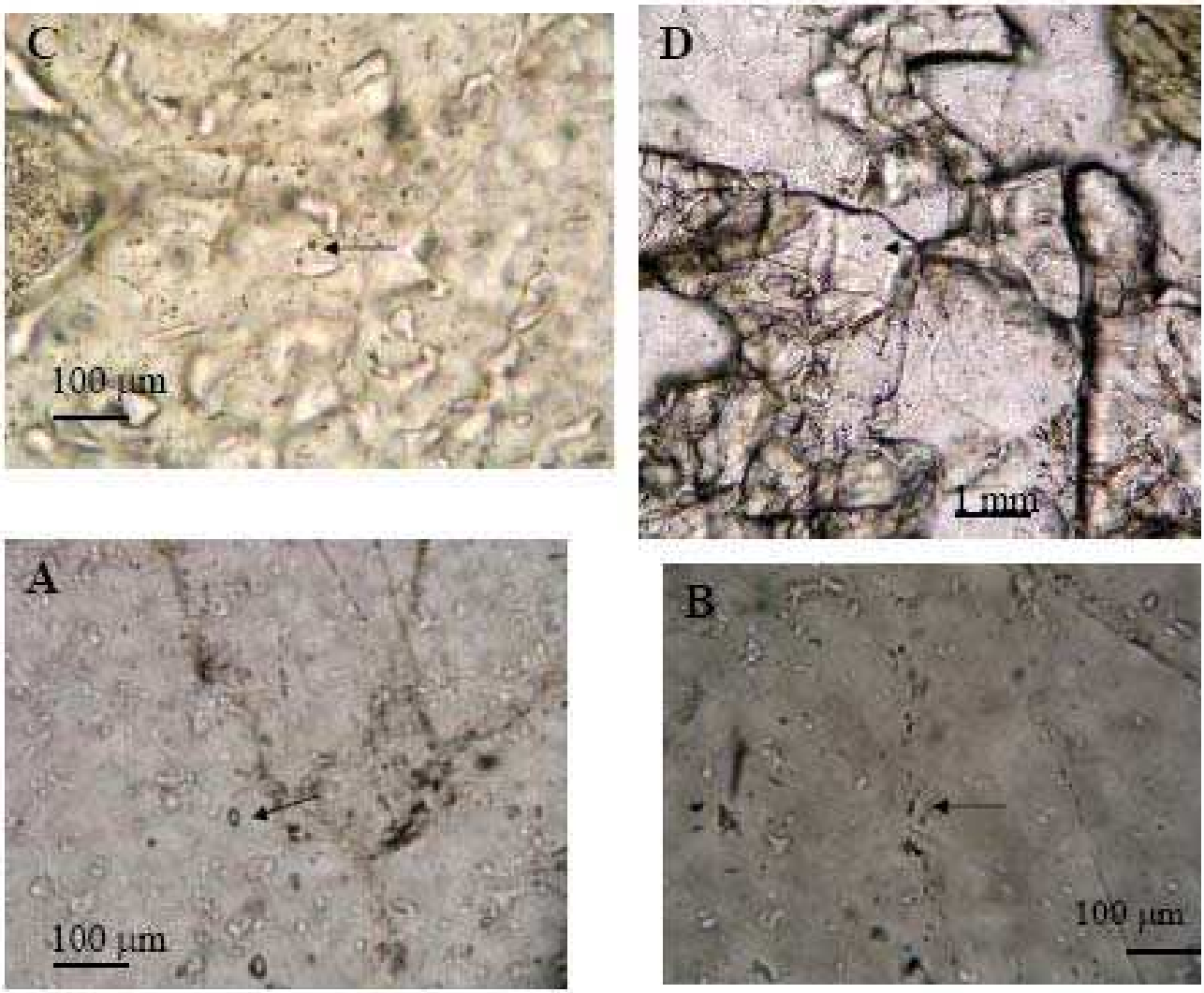

FIG. 5 – Photomicrographs in plane-polarized light illustrating the primary (A) and secondary (B) fluid inclusions in quartz matrix, pyroxene (C) and garnet (D) of the granulite samples.

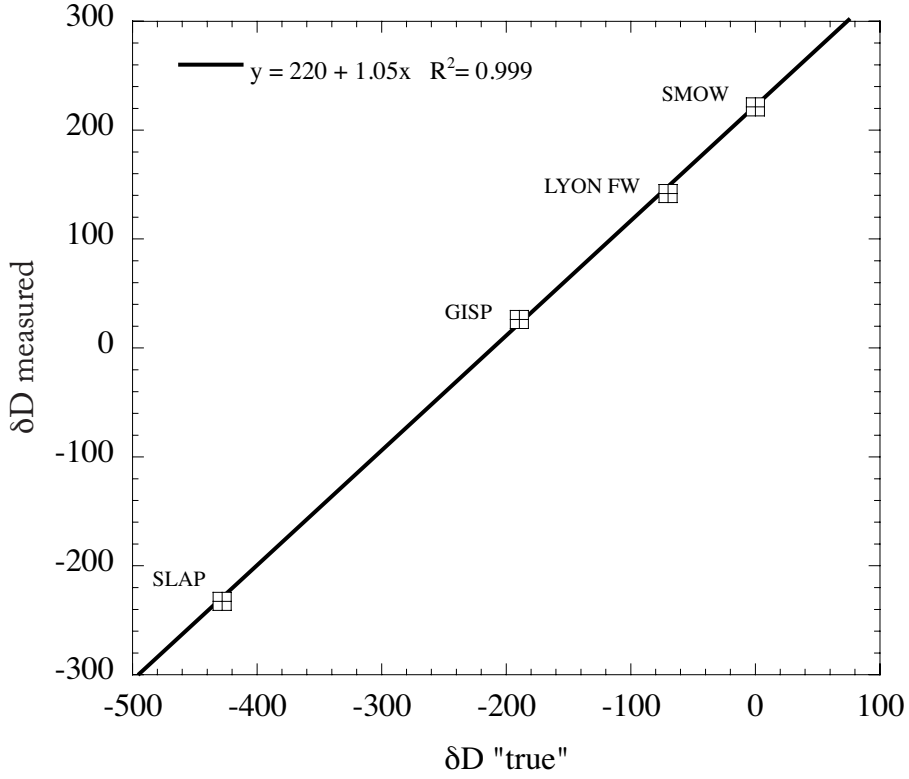

FIG. 6 – Calibration line scaling the measured D/H ratios to the "true" values certified for the international standards of water (SLAP, GISP and SMOW), also including the internal reference water which is a double deionised water derived from Rhône River, France. The equation obtained by a linear regression of data was used to calculate the D/H ratios of both bulk granulites and their water inclusions.

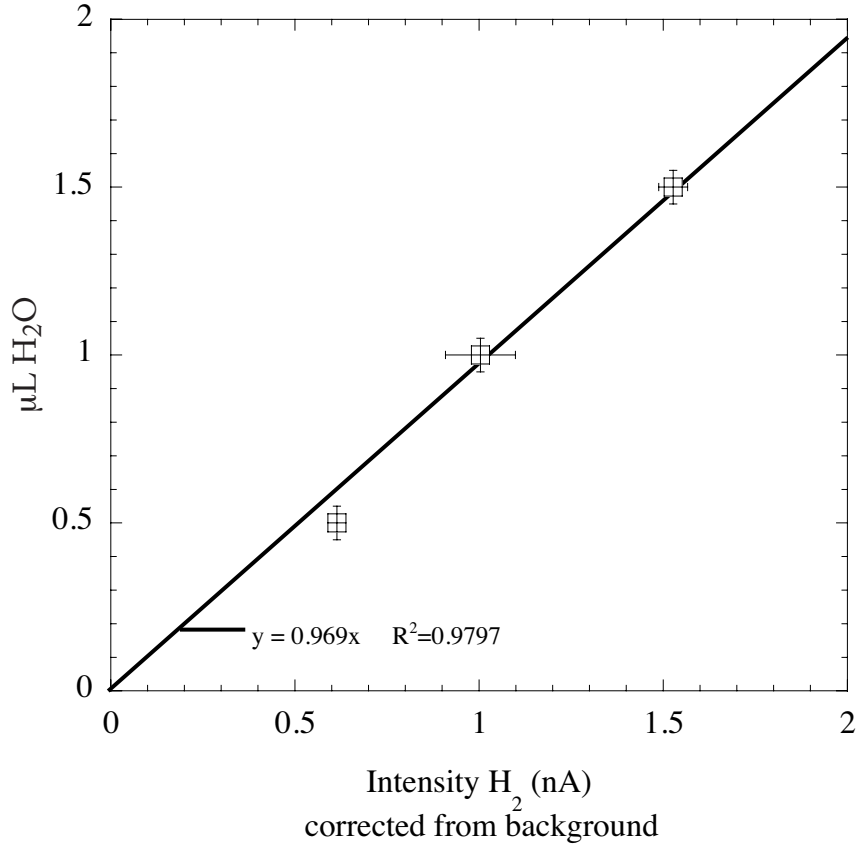

FIG. 7 – Calibration line scaling the measured intensity of mass 2 collector (H_2 gas) to water samples of known weights. The equation obtained by a linear regression of data was used to calculate the amount of water released during the pyrolysis of bulk granulites.

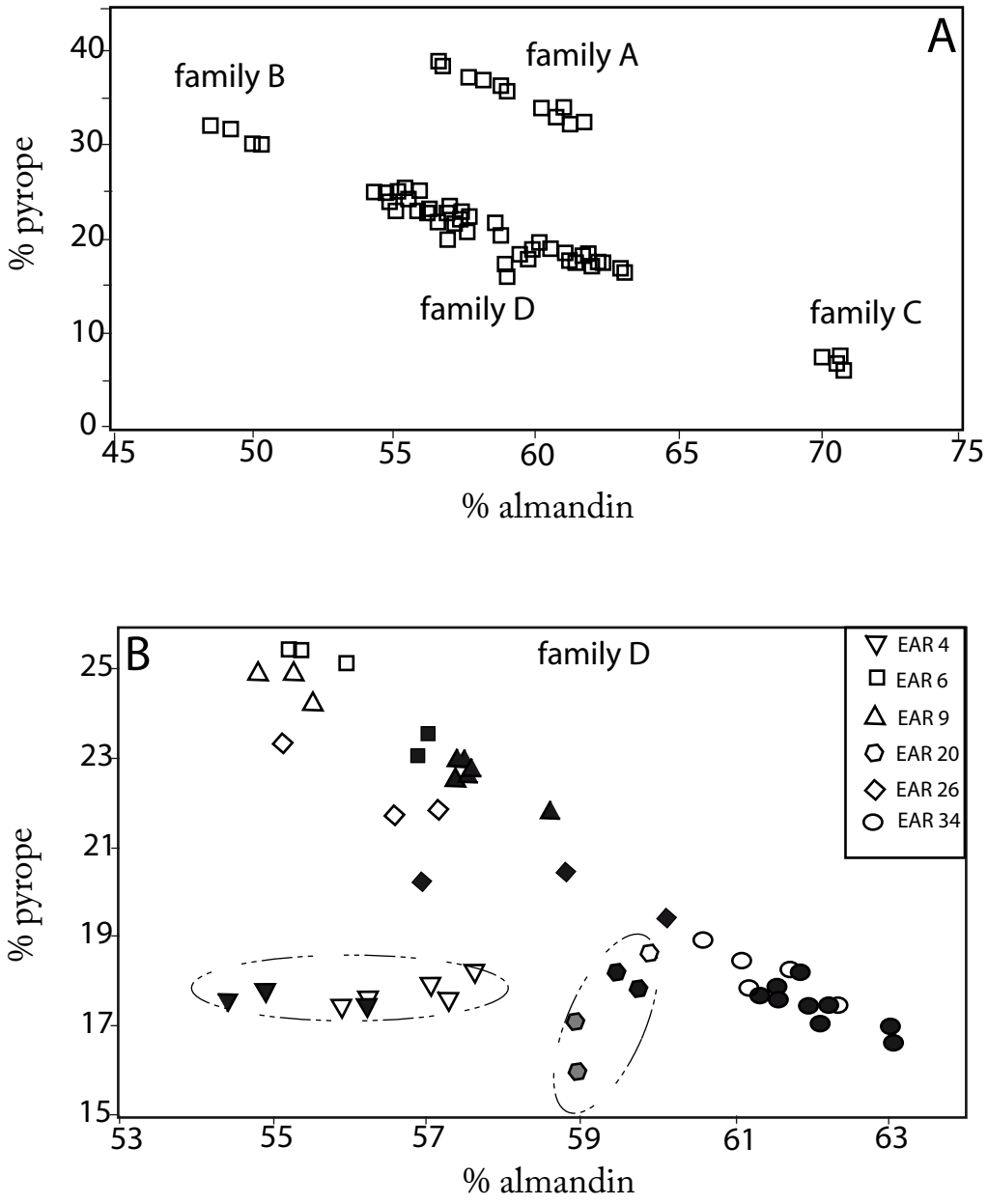

FIG. 8 – A: Chemical compositions of the four garnet families in a plot of %Alm vs % Pyr space. B: Composition of the 3 generations of garnets in the family D. Full symbol represents the first Grt I, open symbol Grt II and grey symbol GrtIII. The general evolution is an increase in the Mg (% pyrope) and a decrease in the Fe (% almandin) content during the growing of Grt I to Grt II. In EAR 4 the Fe content decreases and the Mg content remains constant during the development of second generation of garnet, in EAR 20 the Mg content decreases and the Fe content remains constant during the development of Grt I to Grt III.

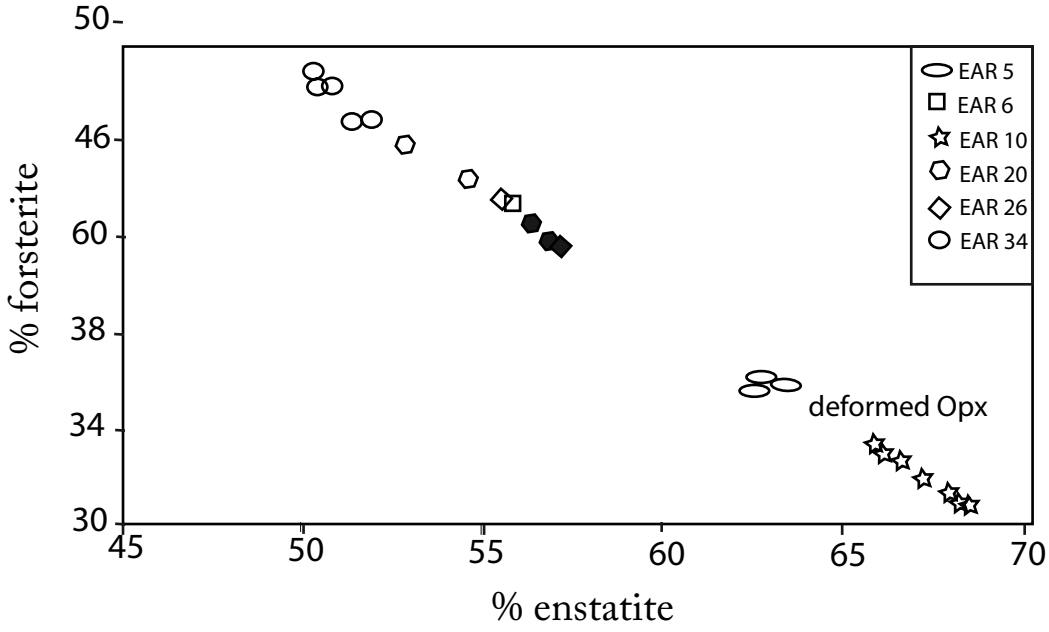

FIG. 9 – Chemical compositions of the first generation of Opx (full symbol) and of the second generation of Opx (open symbol) and of the Opx elongated in the foliation plane.

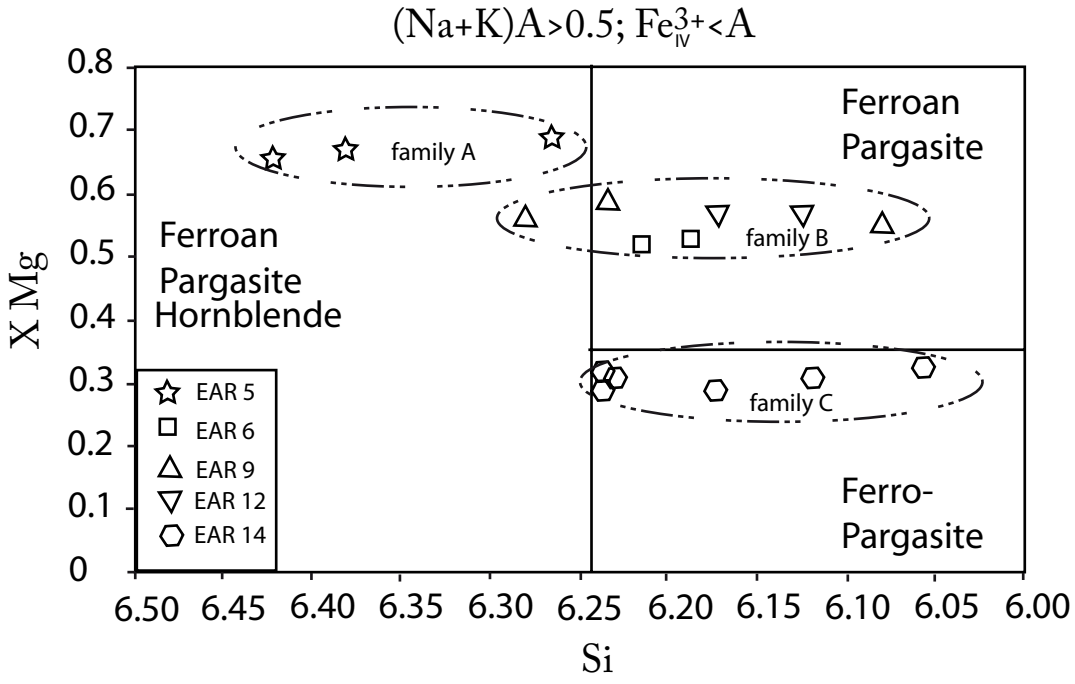

FIG. 10 – Chemical compositions of the 3 families of amphiboles.

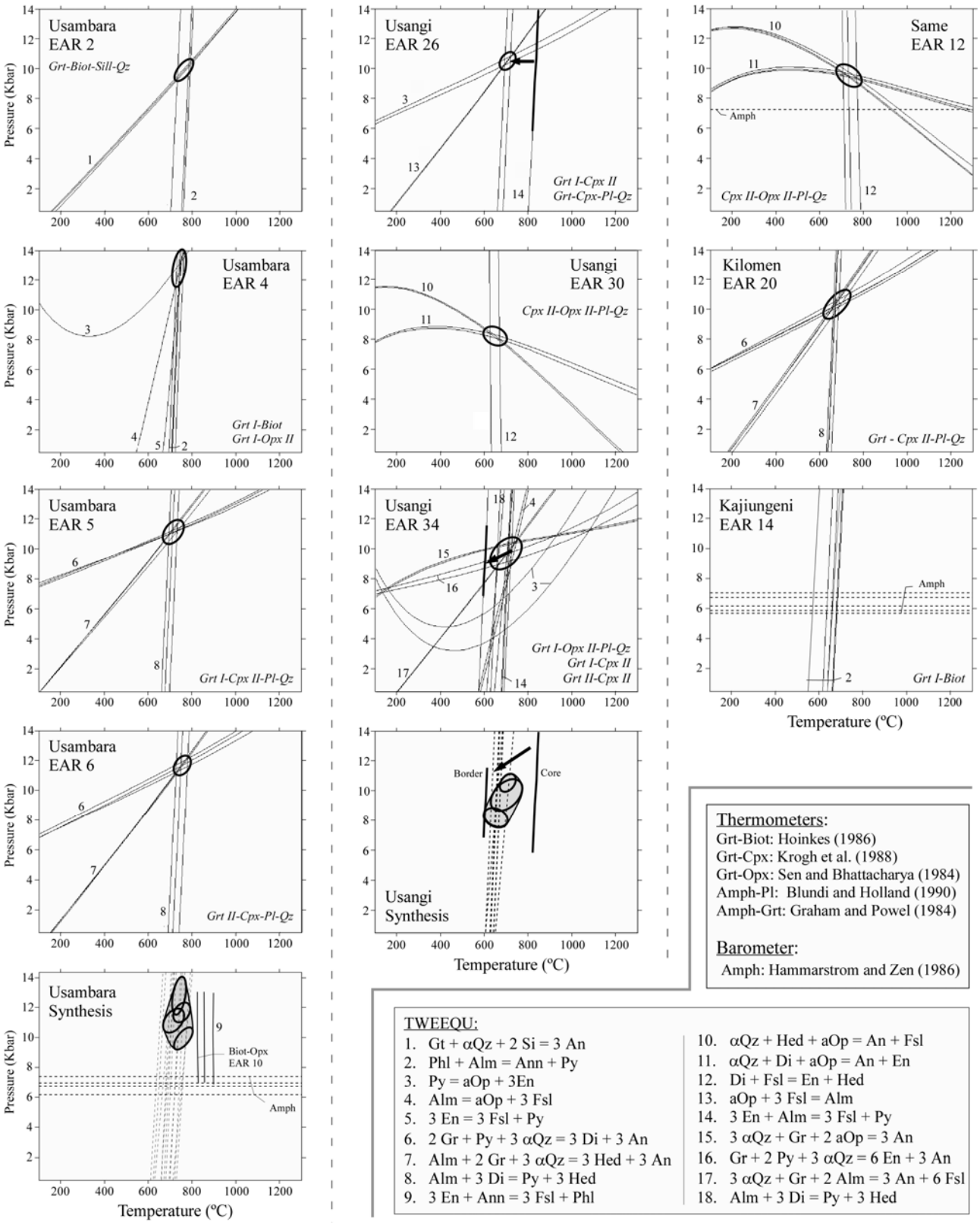

FIG. 11 – Equilibrium P–T conditions calculated with the TWEEQU software (v 2.02). The 18 equilibrium states calculated with the program are listed, as well as the used additional thermometers and barometers (dashed curves on the graphs).

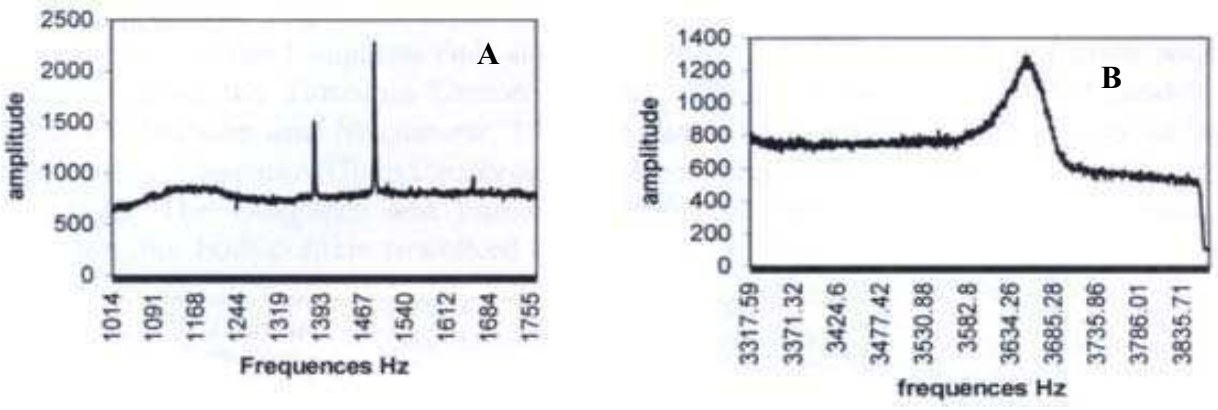

FIG. 12 – Spectrum signatures of the two types of fluid inclusions. A: CO_2 – rich fluid in primary inclusions in quartz, B: H_2O – rich fluid in secondary inclusions in quartz.

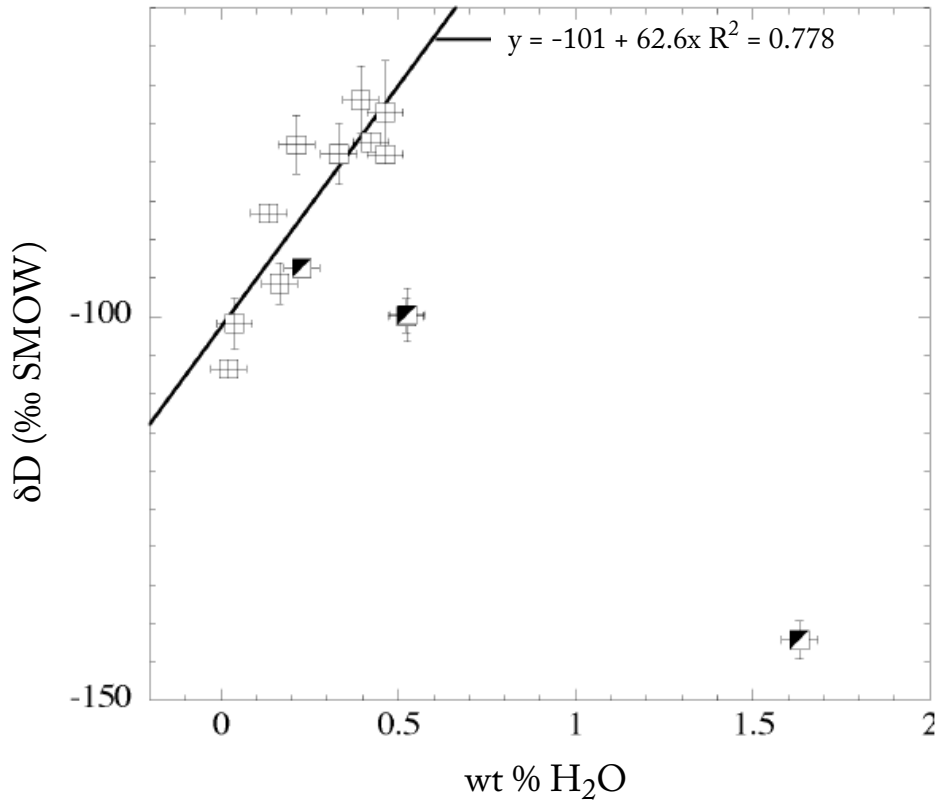

FIG. 13 – δD (‰ SMOW) of bulk Tanzanian (Open Square) and Himalayan (black and white Square) bulk granulites that are reported against the rate of rock hydration (wt% H_2O). Note the significant correlation between the two variables for the Tanzanian granulites (R^2 = 0.778; n = 10).

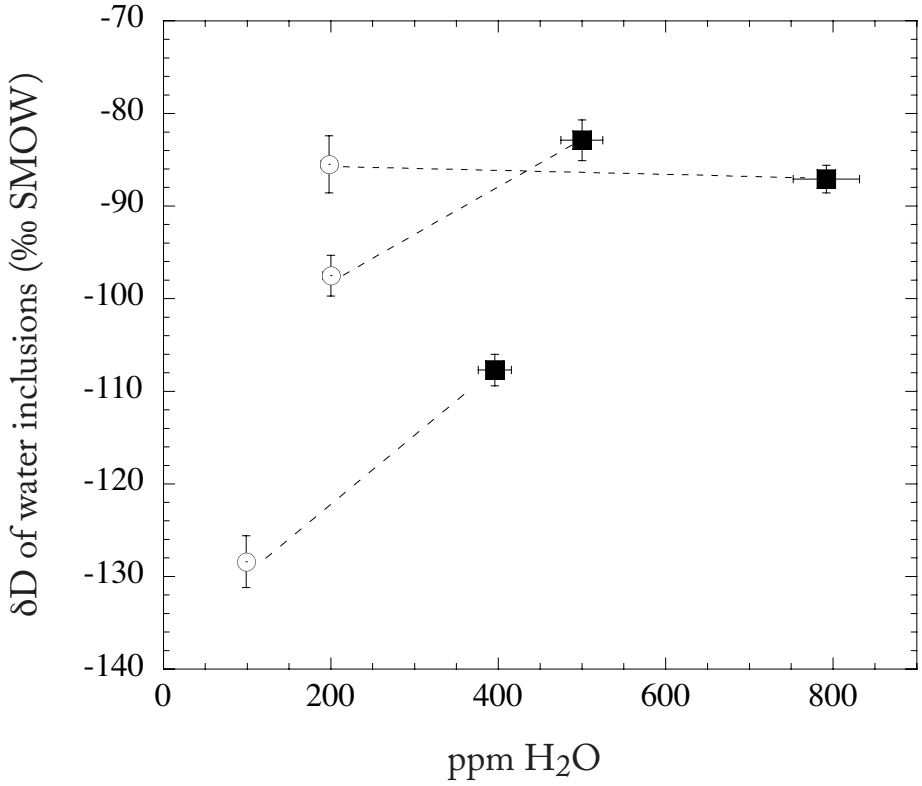

FIG. 14 – Calibration line scaling the measured intensity of mass 2 collector (H_2 gas) to water samples of known weights. The equation obtained by a linear regression of data was used to calculate the amount of water released during the pyrolysis of bulk granulites.

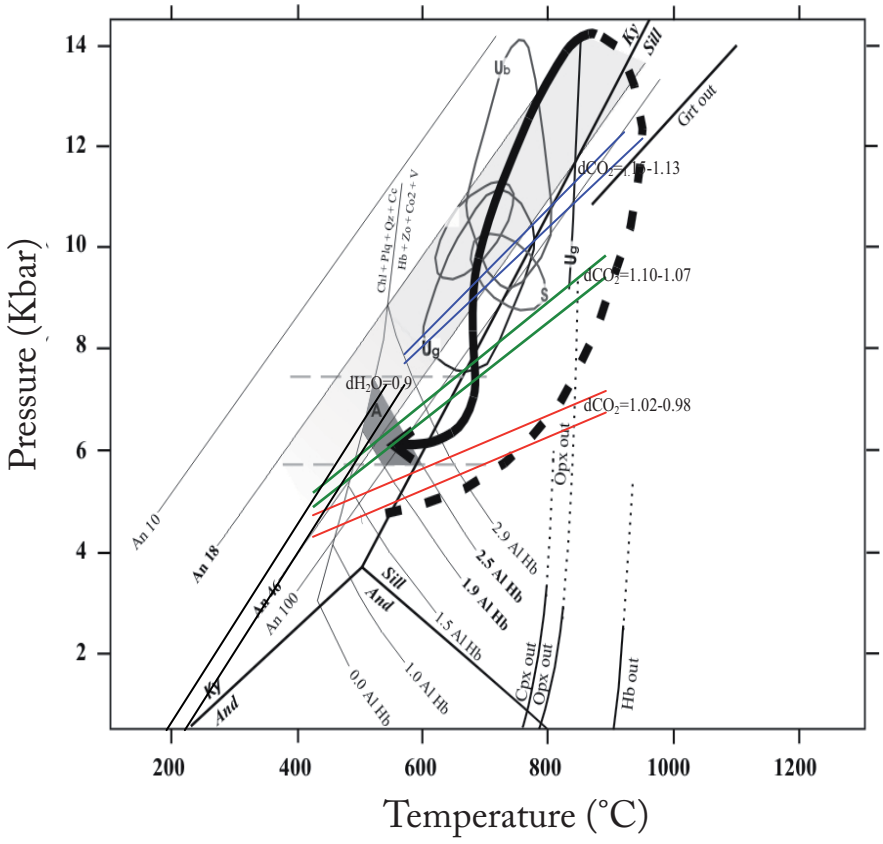

FIG. 15 – Synthesis of the thermo-barometric results for the basic granulites and the possible mean P-T path for the retrograde metamorphism evolution. The equilibrium grids for plagioclases, amphiboles, garnets and aluminium silicates are from Spear (1993). The stippled lines represent the interpolations made for mineral stability conditions. The initial stage of the prograde path is pulled from a survey of Möller (1995, 1998) achieved on metapelites.

Garnets							**Amphiboles**			
Sample	EAR 2	EAR 5	EAR 14	EAR 20	EAR 4	EAR 20	Sample	EAR 5	EAR 9	EAR 14
Family	A	B	C	D	D	D	Name	A	B	C
Garnet type	Grt I	Grt I	Grt I	Grt I	Grt II	Grt III				
Weight %							**Weight %**			
Na2O	0,000	0,038	0,024	0,000	0,015	0,043	Na2O	1,779	1,512	2,095
MgO	9,192	8,854	1,768	4,966	6,085	4,265	MgO	13,502	10,860	6,087
K2O	0,011	0,000	0,000	0,006	0,025	0,000	K2O	0,928	2,082	1,790
CaO	1,770	6,309	7,245	6,456	6,629	6,980	CaO	11,822	11,957	10,695
TiO2	0,000	0,122	0,062	0,103	0,015	0,060	TiO2	2,280	2,702	1,887
FeO	29,134	24,428	32,895	28,441	27,706	27,874	FeO*	12,050	15,534	24,338
MnO	0,624	1,313	1,331	1,892	1,311	2,823	MnO	0,094	0,013	0,046
Cr2O3	0,026	0,120	0,000	0,000	0,000	0,000	Cr2O3	0,129	0,000	0,016
SiO2	38,372	38,661	37,604	38,148	37,465	38,086	SiO2	44,076	41,151	40,225
Al2O3	21,940	21,864	20,610	21,082	21,473	20,784	Al2O3	11,764	13,039	10,690
Total	101,069	101,709	101,539	101,094	100,724	100,915	Total	98,424	98,850	97,869
24 oxygenes							**23 oxygenes - without H2O**			
Site T							Site T			
Si	0,00	5,83	5,96	5,94	5,80	5,96	Si	6,379	6,081	6,227
Al IV	6,00	0,17	0,04	0,06	0,20	0,04	Al iv	1,621	1,919	1,773
Total	6,00	6,00	6,00	6,00	6,00	6,00	sum	8	8	8
Site O							Site C			
Al VI	-6,00	3,71	3,80	3,81	3,72	3,79	Al vi	0,386	0,351	0,178
Cr	0,00	0,01	0,00	0,00	0,00	0,00	Ti	0,248	0,3	0,22
Ti	0,00	0,01	0,01	0,01	0,00	0,01	Cr	0,015	0	0,002
Total	-6,00	3,74	3,81	3,82	3,72	3,80	Fe3+	0	0	0
Site A							Mn	0,012	0,002	0,006
Mg	2,09	1,99	0,42	1,15	1,40	0,99	Mg	2,913	3,392	1,405
Fe	3,72	3,08	4,36	3,70	3,59	3,65	Fe2+	1,427	1,955	3,109
Mn	0,08	0,17	0,18	0,25	0,17	0,37	sum	5	5	5
Ni	0,00	0,00	0,00	0,00	0,00	0,00				
Ca	0,29	1,02	1,23	1,08	1,10	1,17	Site B			
Na	0,00	0,01	0,01	0,00	0,00	0,01	Fe2+	0,194	0,178	0,312
K	0,00	0,00	0,00	0,00	0,00	0,00	Ca	1,833	1,893	1,774
Total	6,19	6,26	6,19	6,18	6,28	6,20	Na	0	0	0
							sum	2,027	2,071	2,086
XCa	0,05	0,16	0,20	0,17	0,18	0,19				
XMg	0,34	0,32	0,07	0,19	0,22	0,16	Site A			
XFe	0,6	0,49	0,70	0,60	0,57	0,59	Na	0,499	0,433	0,629
							K	0,171	0,392	0,353
% Alm	60,18	49,23	70,48	59,90	57,28	58,96	sum	0,67	0,826	0,982
% Gross	4,68	16,29	19,89	17,42	17,56	18,92				
% Pyrop	33,83	31,80	6,75	18,64	22,42	16,08	Mg #	0,641	0,528	0,286
% Spess	1,31	2,68	2,89	4,04	2,75	6,05	Al tot	2,007	2,271	1,95

TAB. 1 – Bulk rock major compositions of the Tanzanian granulite facies rocks.

Biotites			**Cpx**			**Opx**			**Plagioclases**	
sample	EAR 4	EAR 14	Sample	EAR 26	EAR 20	Sample	EAR10	EAR 12	Sample	EAR 20
Family	A		Name	Augite	Diopside	Family	A	B		
						Name	Enstatite	Enstatite		
Weight %			**Weight %**			**Weight %**			**Weight %**	
Na2O	0,011	0,128	Na2O	0,93	1,059	Na2O	0,02	0,03	Na2O	8,055
MgO	15,241	8,662	MgO	12,08	12,296	MgO	24,74	19,60	MgO	0,013
K2O	10,021	9,531	K2O	0,00	0,022	K2O	0,00	0,00	K2O	0,443
CaO	0,024	0,034	CaO	20,17	21,441	CaO	0,25	0,55	CaO	6,224
TiO2	5,783	4,387	TiO2	0,23	0,249	TiO2	0,06	0,05	TiO2	0,000
FeO	13,009	25,274	FeO	12,09	10,568	FeO	20,04	25,70	FeO	0,105
MnO	0,030	0,08	MnO	0,38	0,221	MnO	1,07	1,69	MnO	0,000
Cr203	0,051	0,007	Cr2O3	0,05	0,000	Cr2O3	0,07	0,00	Cr2O3	0,000
SiO2	37,269	35,852	SiO2	50,81	51,737	SiO2	52,30	51,03	SiO2	60,617
Al2O3	14,358	13,048	Al2O3	3,33	2,745	Al2O3	1,90	2,16	Al2O3	24,026
Total	95,746	97,00	Total	100,07	100,316	Total	100,44	100,81	Total	99,483
12 oxygenes			**6 oxygenes**			**6 oxygenes**			**4 oxygenes**	
Si	5,58	5,69	Si	1,919	1,939	Si	1,93	1,929	Site T	
Al tet	2,42	2,31	Al	0,148	0,121	Al	0,08	0,096	Si	2,73
Al octa	0,11	0,13	Ti	0,007	0,007	Ti	0	0,001	Al	1,27
Fe 2+	1,63	3,36	Fe	0,382	0,331	Fe	0,62	0,813	Total	4
Fe 3+	-0,16	-0,34	Mg	0,68	0,687	Mg	1,36	1,105	Site A	
Mg	3,40	2,05	Ca	0,816	0,861	Ca	0,01	0,022	Mg	0
Ti	0,65	0,52	Mn	0,012	0,007	Mn	0,03	0,05	Fe	0
Mn	0,00	0,01	Cr	0,001	0	Cr	0	0,00	Mn	0
Li	0,00	0	Ni	0	0	Ni	0	0,00	Cr	0
Sum Octa	5,63	5,73	Na	0,068	0,077	Na	0	0,00	Ti	0
K	1,91	1,93	Total	4,033	4,031	Total	4,03	4,02	Ni	0
Na	0,00	0,04							Ca	0,3
Cation Proportions			X Fe	0,36	0,33	X Fe	0,31	0,3	Na	0,7
Si	0,43	0,42	AlIV	0,08	0,06	AlIV	0,07	0,1	K	0,003
Al	0,19	0,18	AlVI	0,07	0,06	AlVI	0,01	0,0	Total	1,03
M2+	0,38	0,4								
			% En	36	36,4	% En	67,28	55,4	% Ab	0,68
XMg	5,33	2,32	% Fs	20,8	17,9	% Fs	32,23	43,5	% Or	0,02
			% Wo	43,2	45,6	% Wo	0,49	1,1	% An	0,29

TAB. 1 (suite) – Bulk rock major compositions of the Tanzanian granulite facies rocks.

Site	Sample	T °C	P Kbar	Used assemblage		method
Usambara	EAR 4	710 - 775	11,5 - 14,1	Grt I - Opx II	rim	1
		780		Grt I - Opx II	core	2
		660		Grt I - Opx II	rim	2
	EAR 5	670 - 765	10,2 - 11,8	Grt I - Cpx - Plg - Qzt	rim	1
		660-700		Grt I - Cpx	rim	
	EAR 6	720 - 795	11 - 12,3	Grt II - Cpx - Plg - Qzt	rim	1
		720 - 790		Grt II - Opx	rim	2
Same	EAR 12	680 - 790	8,8 - 10,3		rim	1
Usangi	EAR 26	630 - 720		Grt III - Px II	rim	2
		820 - 850		Grt I - Cpx	core	1
		670 - 745	9,9 - 11,1	Grt I - Cpx - Plg - Qzt	rim	1
	EAR 30	595 - 710	7,6 - 8,9	Cpx - Opx II - Plg - Qzt	rim	1
	EAR 34	630 - 770	8,6 - 10,7	Grt I - Opx II - Plg - Qzt	rim	1
		630 - 720		Grt I - Px II	rim	2
		690 - 705		Grt I - Cpx	core	1
		600 - 610		Grt I - Cpx	rim	1
		706 - 732		Grt II - Cpx	core	1
		645 - 670		Grt II - Cpx	rim	1
Kilomen	EAR 20	620 - 645	9,3 - 11,3	Grt - Cpx - Plg - Qzt	rim	1
		650		Grt III - Cpx	rim	2
Deformation event						
Usambara	EAR 2	720 - 805	9,3 - 10,6	Grt - Bi - Sill - Qzt	rim	1
		640 - 740		Grt - Bi	rim	2
	EAR 4	660 - 780		Grt - Bi	rim	1 + 2
	EAR 10	820 - 900		Bi - Opx	rim	1
Kajiungeni	EAR 14	580 - 730		Grt - Bi	rim	1 + 2
Retromorphic stades						
Usambara	EAR 5	750 - 800	6,1 - 7,4	Al content in Hbl		2
	EAR 6					
Same	EAR 12	750 - 800	7,2	Al content in Hbl		2
Kajiungeni	EAR 14	730 - 820	5,7 - 7,1	Al content in Hbl		2

TAB. 2 – Microprobe analyses of garnet, pyroxene, plagioclase, amphibole and biotite grains from the studied samples. Garnet types correspond to different habits described in the text. Different compositional families are specified. For Amphiboles, Mg # = Mg / (Mg + Fe + Mn), with the number of cations by structural unit.

Primary fluid inclusions

minéral	sample	nature	Tm°C	Th°C	d gr/cm3
Qtz	EAR9	CO2	-58	-30	1.08
Qtz	EAR9	CO2	-56.6	-36	1.1
Qtz	EAR9	CO2	-57.1	-36.1	1.1
grt	EAR26	CO2	-58.4	-43.6	1.13
grt	EAR6	CO2	-57.8	-28.4	0.99
grt	EAR6	CO2	-56.6	-31.4	1.02
plg	EAR6	CO2	-57.1	-35	1.13
plg	EAR34	CO2	-56.8	-26	1.06
OPX	EAR6	CO2	-58.3	-28	1.15
OPX	EAR34	CO2	-56.9	-20	1.13
plg	EAR6	CO2	-57.2	-25	1.14
plg	EAR34	CO2	-58.5	-20	1.03
Qtz	EAR28	CO2	-57.2	-24	1.07
Qtz	EAR28	CO2	-56.8	-20	1.1
Qtz in Grt	EAR14	CO2	-58.6	-13.2	0.98
Qtz in Grt	EAR14	CO2	-56.6	-21.5	1.02
Qtz	EAR13	H2O	-56.6	30.9	0.51

Secondary fluid inclusions			Th°C	d gr/cm3
Qtz	EAR13	H2O	160	0.93
Qtz	EAR13	H2O	270	0.77
Qtz	EAR13	H2O	305	0.7
Qtz	EAR13	H2O	336	0.62
Qtz	EAR13	H2O	284	0.74

TAB. 3 – Thermo-barometric results for studied Tanzanian granulite samples. Mineral assemblages used for calculations are specified. B, C and I refer respectively to mineral border, mineral core, and inclusion. Frames group data obtained from the same mineral grains. Method used for P-T calculations: 1 for TWEEQU software, 2 for other calibrations.

				Whole rock	**Fluid Inclusions**		
Sample	Protolith	P Kb - T°C	Mineralogical association	δD ‰ SMOW	δ13C ‰ PDB	δD ‰ SMOW	
Kenya 625+/-25 Ma						350°C	700°C
EAR 4	andesite	13±1, 740±20	Plg+Qtz+Opx+Grt+*Bi*	-106.8	-6.73		
EAR 5	gabbro	11±0.5, 710±30	Plg+Qtz+Opx+Cpx+Grt+*Bi*+*Hbl*	-77.7	-7.77	-77.1	-110.7
EAR 6	andesitic basalt	11.5±0.5, 750±40	Plg+Qtz+Opx+Cpx+Grt+*Hbl*	100.9	-8.43	***-128.4***	***-107.7***
						-86.1	-100.2
EAR 12	andesite	9.5±0.5, 740±20	Plg+Qtz+Cpx+Opx+*Hbl*	-77.36	-8.49	***-97.5***	***-82.9***
						-89.4	-89.4
EAR 13	dacite		Plg+Qtz+Cpx+Opx+Grt+*Hbl*	-71.9	-7.69	***-85.5***	***-87.1***
						-67.4	-74.9
EAR 14	andesite	680±20	Plg+Qtz+Grt+*Bi*+*Hbl*	-86.6	-7.60		
EAR 20	andesitic basalt	10.5±0.5, 630±10	Plg+Qtz+Cpx+Opx+Grt+*Bi*+*Hbl*	-95.73	-5.37		
EAR 26	andesite	10.7, 810	Plg+Qtz+Cpx+Opx+Grt+*Bi*+*Hbl*	-78.9	-8.86		
EAR 30	andesite	8.25±0.5, 650±50	Plg+Qtz+Cpx+Opx+Grt+*Bi*+*Hbl*	-79	-5.80		
EAR 34	gabbro	9.5±0.5, 700±10	Plg+Qtz+Cpx+Opx+Grt+*Hbl*	-73.5	-6.95		
Namche-Barwa 16+/-2.5 Ma							
NB 25	sediment		Grt+sill+Ky+Bi	-99.95	-2.47		
NB 42	gabbro	~8, ~ 600	Grt+Plg+Hbl	-142.1	-3.95		
NB 48	sediment		Grt+Plg+Qtz+Sill	-93.69	-4.47		
NB 58	sediment	9±1, 740±20	Plg+Grt+Qtz+Sill+Bi	-99.84	-3.47		

TAB. 4 – Results of microthermometry analyses of CO_2-rich fluid trapped in primary inclusions and of H_2O-rich fluid trapped in secondary inclusions in quartz, plagioclase, pyroxene and garnet.

Chapitre 8

Conclusions – Perspectives

Chapitre 8

Conclusions – Perspectives

1. Conclusions

L'objectif de cette thèse était d'aborder certains aspects des interactions entre les enveloppes terrestres du point de vue des cycles géochimiques des fluides. Mon travail est basé sur l'étude des isotopes stables de deux fluides CO_2 et H_2O, dasns des inclusions fluides piégées dans des roches de la croûte terrestre, depuis sa surface jusqu'à l'interface croûte-manteau. Les principaux résultats de ce travail sont :

1.1. Les inclusions fluides dans les matériaux de surface

L'étude du fractionnement isotopique de l'oxygène et des cinétiques d'équilibration entre CO_2 et H_2O en fonction de la salinité a montré que les rapports isotopiques de l'oxygène sont surestimés pour les eaux naturelles très salées ($100 < S < 250$ g.L^{-1}). Il est donc nécessaire d'apporter des corrections aux valeurs isotopiques de l'oxygène lors de l'étude de saumures hydrothermales ou d'eaux salées échantillonnées par exemple dans des lacs hyper–salins ou des lagons. Il a donc fallu tenir compte de ce résultat lors de l'analyse des isotopes stables des eaux libres au cours de l'évaporation d'un volume d'eau puisque les eaux échantillonnées peuvent atteindre une salinité supérieure à 200 g.L^{-1} lors des derniers stades d'évaporation. L'eau piégée dans les inclusions fluides des halites est également une saumure de salinité très élevée. Il est donc nécessaire d'apporter des corrections aux valeurs des compositions isotopiques obtenues sur les inclusions fluides des halites.

La précipitation expérimentale halite en milieu contrôlé a permis de mettre en évidence le potentiel des informations enregistrées dans les inclusions fluides. En effet, les compositions isotopiques de l'hydrogène et de l'oxygène des inclusions aqueuses enregistrent les trajectoires isotopiques d'évaporation de l'eau. Couplées à des analyses microthermométriques, elles peuvent être utilisées pour estimer la température et la vitesse du vent à l'interface eau–air lors

de la croissance des cristaux. L'utilisation des compositions isotopiques des inclusions fluides de halite comme paléo-thermomètre et paléo-anémomètre pour la reconstruction des paléoclimats pour des évènements extraordinaires amenant aux dépôts de sels massifs est d'autant plus importante que les proxys sont peu nombreux dans de tels dépôts. L'application de cette méthode aux dépôts de halite de Sicile d'âge Messinien permet de montrer que la température de l'eau était d'environ 35°C et que le vent avait un impact négligeable sur l'évaporation lors de la formation des évaporites. De plus, les mesures des compositions isotopiques des inclusions fluides ont permis la caractérisation des sources de l'eau évaporée, suggérant que les importants dépôts de sel de Sicile résultent de l'évaporation d'une eau de mer mélangée à une fraction importante d'eau météorique (50 à 75%) provenant en grande partie des fleuves alpins.

1.2. Les inclusions fluides dans les matériaux de la croûte continentale supérieure et intermédiaire

Les isotopes stables des inclusions fluides des matériaux de la croûte profonde (granulites) et intermédiaire (granites) ont été utilisés comme traceurs de sources et de processus (altération, interactions eau–roche, mélanges, contextes de formation).

La distribution avec la profondeur des quantités de CO_2 et des valeurs de $\delta^{13}C$ des inclusions fluides des quartz du granite de Soultz–sous–Forêts (Alsace, France témoignent de processus de mélange dans la croûte entre deux sources distinctes de carbone dérivant pour l'une des carbonates sédimentaires et pour l'autre de la croûte profonde ou du manteau supérieur. La composition isotopique des échantillons de roche totale révèle une troisième source pour le carbone, de moindre importance, qui pourrait résulter de l'oxydation in situ de minéraux carbonés comme le graphite. La distribution des données dans un espace δD–$\delta^{18}O$ montre que l'eau associée au CO_2 dans les inclusions fluides primaires est constituée en grande partie d'eau météorique mélangée à des petites quantités d'eau juvénile. Les inclusions fluides dans le quartz ont donc enregistré les composition isotopiques des paléo–précipitations contemporaines de la cristallisation du granite. Les valeurs de δD et $\delta^{18}O$ obtenues, plus élevées que celles des eaux météoriques actuelles reflètent les températures moyennes de l'air plus élevées (d'environ 6°C). Ces valeurs plus élevées peuvent s'expliquer par la position péri–

équatoriale de la chaîne Varisque quand le granite s'est mis en place. Le mélange d'eau météorique et d'eau juvénile dans les inclusions primaires permet aussi de relier les processus de mélange des eaux au contexte de mise en place du granite.

Les compositions isotopiques du carbone et de l'hydrogène des inclusions fluides primaires des granulites du rift de Pangani montrent que les fluides CO_2 et H_2O circulant à la base de la croûte lors de la formation des granulites sont principalement d'origine mantellique et compatibles avec un contexte de formation de type subduction. Les compositions isotopiques du carbone et de l'hydrogène des inclusions primaires des granulites du Namche–Barwa suggèrent quant à elles une source d'origine crustale pour les fluides piégés lors du pic de métamorphisme, ceci est compatible avec un contexte de formation de type collision continentale. L'origine des fluides des inclusions primaires des granulites peut être reliée au contexte de formation des granulites.

Les compositions isotopiques des inclusions fluides des granulites d'âge Précambrien à Miocène montre que CO_2 et H_2O des inclusions primaires sont principalement d'origine mantellique alors que CO_2 et H_2O des inclusions secondaires sont plutôt d'origine crustale. Les compositions isotopiques de l'hydrogène et du carbone des granulites semblent être reliées aux évolutions isotopiques des cycles globaux de l'eau et du carbone. La relative stabilité des compositions isotopiques du carbone à travers le temps pour le CO_2 des inclusions primaires peut refléter au premier ordre la stabilité de la composition isotopique du carbone du manteau supérieur depuis l'Archéen. En revanche, les valeurs de D/H obtenues sur la roche totale des granulites diminuent d'environ 25 ±5‰ entre l'Archéen et le Miocène, avec un changement rapide qui s'est produit il y a 2 Ga. Elles pourraient refléter l'émergence d'une atmosphère oxydante à la surface de la Terre.

2. Perspectives

Depuis la découverte des évaporites profondes en Méditerranée (Ryan et al., 1973), de gros progrès ont été réalisés dans la compréhension de la Crise de Salinité du Messinien (MSC). Cependant, certains points demeurent obscurs (e.g. la chronologie précise et les environnements de dépôt des évaporites dans le bassin central et la stratification post-évaporitique) et amènent à plusieurs scénarios toujours controversés (voir Butler et al., 1995 ; Clauzon et al., 1996 ; Riding et al., 1998 ; Krijgsman et al, 1999 et Rouchy et Caruso, 2006). En général les auteurs sont d'accord pour considérer la Sicile comme l'un des secteurs clés pour comprendre la MSC. Cela est dû à sa position centrale entre les deux grands bassins Méditerranéens, à l'épaisseur importante de la séquence Messinienne et à la présence de toute la succession évaporitique (gypse, halite et dépôts potassiques ; Decima et Wezel, 1973). Une des questions toujours en suspend est de savoir si la Sicile correspond à un bassin central ou à un bassin marginal. Pour y répondre, je propose d'étudier à la fois les compositions isotopiques des inclusions fluides de la halite de la mine de Racalmuto située à 25 km au Nord-Est de Realmonte à l'intérieur des terres, et de la halite du bassin tunisien échantillonnée au Nord de la Tunisie (entre 1090 et 980 m de profondeur) lors du sondage Carthage 1. Si la Sicile était un bassin central, alors les compositions isotopiques des inclusions fluides des halites de Tunisie, de Realmonte et Racalmuto devraient être similaires (même pente d'évaporation, même intercept avec la droite des eaux météoriques). Si au contraire la Sicile était un bassin marginal, les compositions isotopiques des inclusions fluides des halites de Sicile et du bassin tunisien devraient être différentes (pentes des droites d'évaporation différentes). Dans ce cas, il reste possible que la source de l'eau évaporée soit la même pour le bassin sicilien et le bassin tunisien (même intercept avec la droite des eaux météoriques) et que des mouvements tectoniques aient ensuite isolé le bassin sicilien, en faisant un bassin marginal.

L'étude des compositions isotopiques des inclusions fluides de la halite du Messinien permet la reconstruction de paléoclimats pour des périodes s'étalant sur plusieurs milliers d'années. Il pourrait être intéressant d'appliquer cette étude à des objets plus récents et de taille réduite tels que les lacs salés. La Laguna Mar Chiquita, localisée dans les plaines

subtropicales de la Pampa d'Argentine centrale, est actuellement le plus grand lac salé d'Amérique du Sud (6000 Km^2) Ce lac a fait l'objet de nombreuses études (Harperath, 1887 ; Frank, 1915 ; Bertoldi de Pomar, 1953 ; Martinez 1991) qui ont permis l'obtention d'un enregistrement précis de la salinité de l'eau et de sa température de surface au cours des 200 dernières années. Des campagnes de terrain effectuées en Novembre 1997 (TMC5, 14 et 3) et Juillet 2000 (TMC-00-I et, 00-IIIa) ont prélevé 6 carottes dans les zones les plus profondes du lac. Les travaux effectués sur les carottes montrent que depuis la fin du petit âge glaciaire, le lac à subit des variations hydrologiques importantes reliées à une alternance de périodes sèches et humides (Reati et al. 1996). Du point de vue de la sédimentologie, ces fluctuations induisent soit la précipitation d'évaporites, soit une productivité primaire élevée avec le dépôt de boue riche en matière organique. Le bilan montre des conditions globalement sèches au cours des dernières 240 années, avec des périodes humides de courte durée (fin du $18^{ème}$ siècle, seconde moitié du $19^{ème}$). Cette sécheresse est associée au dépôt d'évaporites dont le plus important est daté à 1767, ce qui correspond à la fin du petit âge glaciaire. Le dernier dépôt d'évaporites est daté à 1969. Depuis cette époque le niveau du lac est au plus haut et la sédimentation se caractérise par le dépôt de boues riches en gastéropodes. En collaboration avec E Piovano et D. Ariztegui je propose d'analyser les inclusions fluides des évaporites carottées dans le lac pour déterminer la température des eaux de surface puis les comparer aux mesures qui ont été effectuées in situ depuis environ 200 ans. Cette étude permettra de mettre en évidence d'une part les basses températures de la fin du petit âge glaciaire et le réchauffement progressif du climat entre 1770 et 1969 et permettra d'autre part de vérifier si les inclusions fluides des évaporites enregistrent les variations climatiques sur de courtes périodes. Si notre étude est concluante nous pourrons l'étendre à l'ensemble de la série sédimentaire du lac qui couvre 14000 ans (des carottes de cette période sont disponibles à l'ETH – Zurich). Ces données seraient uniques pour les régions subtropicales de l'Hémisphère Sud.

Une autre des applications possibles de l'étude des isotopes stables des inclusions fluides piégées dans la halite pourrait être la reconstruction de la chimie des atmosphères anciennes. A l'heure actuelle, les inclusions fluides de gaz atmosphérique dans la glace des glaciers fournissent d'excellents échantillons de la chimie atmosphérique du passé géologique récent

(Raynaud, 1993). Cependant, les échantillons atmosphériques des temps géologiques anciens sont encore difficilement analysables. Les premières tentatives visant à l'analyse de ce type de matériel par l'extraction des bulles de gaz de l'ambre fossile ont été controversées. Il a été suggéré que les bulles dans l'ambre préservent la composition de l'atmosphère au moment où l'ambre est exsudé des arbres (Berner et Landis, 1988). Cependant, d'autres auteurs suggèrent que le contenu en gaz est contrôlé par des réactions de solubilité (Horibe et Craig, 1987), par de la diffusion (Horibe et Craig, 1988) ou par des réactions chimiques entrainant la consommation de l'oxygène (Beck, 1998). Les échantillons de halite formés à l'interface eau–air dans des lacs et des bassins évaporitiques anciens pourraient fournir un échantillonnage non altéré des atmosphères anciennes. De plus, quand les minéraux comme la halite se développent dans des environnements de surface, des micro–organismes et de la matière organique peuvent être piégés à l'intérieur des inclusions fluides. Récemment, des chercheurs ont étudié des micro–organismes qui auraient pu être piégés dans les inclusions fluides de halite datée à 250 Ma (Vreeland et al., 2000). La question du potentiel de préservation et de la durée de piégeage de ces micro–organismes a été posée (Hazen et Roedder, 2001 ; Maughan et al., 2002), mais la possibilité de trouver des organismes viables ou même dégradés dans des inclusions fluides ouvre de nombreuses et passionnantes possibilités pour les études de l'apparition de la vie. L'étude des inclusions fluides est donc susceptible de jouer un rôle important dans l'avenir des reconstructions des paléo–environnements terrestres, qu'il s'agisse de la composition chimique de la mer ou de l'atmosphère ou de l'étude de l'apparition de la vie.

Références

Beck C.W. (1988) Is the air in amber ancient? Technical comments. *Science* **241**, 718–719.

Berner R.A. and Landis G.P. (1988) Gas Bubbles in Fossil Amber as Possible Indicators of the Major Gas Composition of Ancient Air. *Science* **239**, 1406–1409.

Bertoldi de Pomar (1953) Contribucion al Conocimiento del origen de la Laguna Mar Chhiquita de la Provincia de Cordoba. Unpubli. PhD Thesis. Universidad Nacional de Cordoba. Argentina, 149pp.

Butler R.W., Lickorish H., Grasso M., Pedley H.M. and Ramberti L. (1995) Tectonics and sequence stratigraphy in Messinian basins Sicily: constraints on the initiation and termination of the Mediterranean salinity crisis. *Geol. Soc. Am. Bull.* **107**, 425–439.

Clauzon G., Suc J.-P., Gautier F., Berger A. and Loutre M.-F. (1996) Alternate interpretation of the Messinian salinity crisis: Controversy resolved? *Geology* **24**, 363–366.

Decima A. and Wezel F.C. (1973) Late Miocene evaporites of the central Sicilian basin, Italy. In *Leg 13. Initial Reports of the Deep Sea Drilling Project 13* (eds. W.B.F. Ryan and K.J. Hsü), U.S. Government Printing Office, Washington (1973), 1234–1241.

Frank H. (1915) Contribucion al conocimiento de las salinas Grandes y la Mar Chiquita. Provincia de Cordoba. Rev., *Centro. Estud. Ingen.* **3**, 91-107.

Harperath L. (1887) Estudio sobre la composición química de las salinas del interior de la República Argentina. *Bol. Acad. Nac. Cienc. Córdoba* **10**, 427–441.

Hazen R.M. and Roedder E. (2001) How old are the baxteria from the Permian age ? *Nature* **411**, 155.

Horibe, Y. & Craig, H. (1987) Trapped gases in amber; a paleobotanical and geochemical inquiry. *Eos* **68**, 1513.

Horibe Y. and Craig H. (1988) In Reply: Is the Air in Amber Ancient? *Science* **241**, 719–721.

Krijgsman W., Hilgen F.J., Raffi I., Sierro F.J. and Wilson D.S. (1999) Chronology, causes and progression of the Messinian salinity crisis. *Nature* **400**, 652–655.

Martinez D.E. (1991) Caracterizacion Geoquimica de la Lagunas Mar Chiquita, Provincia de Cordoba, Argentina, 274 pp.

Maughan H., Birky C.W., Nicholson W.L., Rosenzweig W.D. and Vreeland R.H. (2002) The Paradox of th « Ancient » Bacterium which contains « Modern » Protein–Coding Genes. *Molecul. Biol. and Evol.* **19**, 1637–1639.

Raynaud D., Jouzel J., Barnola J.M., Chappellaz J., Delmas R.J. and Lorius C. (1993) The ice record of greenhouse gases. *Science* **259**, 926–934.

Reati G. J., Florín M., Fernández G. J. and Montes C. (1996) The Laguna de Mar Chiquita (Córdoba, Argentina): A little known, secularly fluctuating, saline lake. *Biomedical and Life Sciences* **5**, 187–219.

Riding R., Braga J.C., Martín J.M. and Sánchez-Almazo I.M. (1998) Mediterranean Messinian Salinity Crisis: constraints from a coeval marginal basin. Sorbas, SE Spain. *Marine Geology* **146**, 1–20.

Rouchy J.-M. and Caruso A. (2006) The Messinian salinity crisis in the Mediterranean basin: A reassessment of the data and an integrated scenario. *Sedimentary Geology* **188/189**, 35–67.

Vreeland R.H., Rosenzweig W.D. and Powers D.W. (2000) Isolation of 250 million–year–old halotolerant bacterium from a primary salt crystal. *Nature* **407**, 897–900.

Bibliographie

Adams J.M., Faure H., Faure–Denard L., McGlade J. and Woodward F.I. (1990) Increases in terrestrial carbon storage from the last glacial maximum to the present. *Nature* **348**, 711–714.

Adams J.M. and Faure H. (1998) A new estimate of changing carbon storage on land since the last glacial maximum, based on global land ecosystem reconstruction. *Global Planet. Change* **16–17**, 3–24.

Agrinier P., Hékinian R., Bideau D. and Javoy M. (1995) O and H stable isotope compositions of oceanic crust and upper mantle rocks expose in the Hess Deep near the Galapagos Triple Junction. *Earth Planet. Sci. Lett.* **136**, 183-196.

Albarède F. (2009) Volatile accretion history of the terrestrial planets and dynamic implications. *Nature* **461**, 1227–1233.

Alexandrov P., Royer J.J. and Deloule E. (2001) 331 ± 9 Ma emplacement age of the Soultz monzogranite (Rhine Graben basement) by U/Pb ion-probe zircon dating of samples from 5 km depth, *C.R. Acad. Sci. (Paris), Sèrie II* **332**, 747–754.

Alexeev S.V., Alexeeva L.P., Borisov V.N., Shouakar-Stash O., Frape S.K., Chabaux F. and Kononov A.M. (2007) Isotopic composition (H, O, Cl, Sr) of ground brines of the Siberian Platform. *Russian Geol. Geophys.* **48**, 225-236.

Alperin M.J., Reeburgh W.S., Whiticar M.J. and Oremland R.S. (1988) Carbon and hydrogen isotope fractionation resulting from anaerobic methane oxidation. In *Global Biogeochemical Cycles* (ed. J.J. McCarthy). Am. Geophys. Union, Washington DC.

Alt J.C. (1995) Subseafloor processes in mid-ocean ridge hydrothermal systems. In *Seafloor hydrothermal systems; physical, chemical, biological, and geological interactions* (eds. S.E. Humphris, R.A. Zierenberg, L.S. Mullineaux and R.E. Thomson) Geophys. Monograph., Am. Geophys. Union, Washington DC, 85–114.

Alt J.C. and Teagle D.A.H. (1999) The uptake of carbon during alteration of oceanic crust. *Geochim. Cosmochim. Acta* **63**, 1527-1536.

Alt J.C., France-Lanord C., Castillo P. and Galy A. (1992) Low-temperature hydrothermal alteration of Jurassic ocean crust, Site 801. *Proc. O.D.P., Sci. Res.* **129**, 415-427.

Alt J.C., Honnorez J., Laverne C. and Emmemermann R. (1986) Hydrothermal alteration of a 1 km section through the upper oceanic crust, Deep Sea Drilling Project Hole 504B : Mineralogy, chemistry, and evolution of seawater-basalt interactions. *J. Geophys. Res.* **91**, 10309-10335.

Alt J. C., Muehlenbachs K., and Honnorez J. (1986) An oxygen isotopic profile through the upper kilometer of the oceanic crust, DSDP Hole 504B. *Earth Planet. Sci. Lett.* **80**, 217–229.

Alt J.C., Teagle D.A.H., Laverne C., Vanko D.A., Bach W., Honnorez J., Becker K., Ayadi M. and Pezard P.A. (1996) Ridge flank alteration of upper ocen crust in the eastern Pacific: Synthesis of results for volcanic rocks of Holes 504B and 896A. *Proc. O.D.P., Sci. Res.* **148**, 435-450.

Alt J.C., Zuleger E. and Erzinger J. (1995) Mineralogy and stable isotopic composition of the hydrothermally altered lower sheeted dike complex, Hole 504B, Leg 140. *Proc. O.D.P., Sci. Res.* **137**, 155-166.

Andersen T., Austrheim H., Burk, E.A.J. and Elvevold S. (1993) N_2 and CO_2 in deep crustal fluids: evidence from the Caledonides of Norway. *Chem. Geol.* **108**, 113–132.

Andersen T., Whitehouse M.J. and Burke E.A.J. (1997) Fluid inclusions in Scourian granulites from the Lewisian complex of NW Scotland : evidence for CO_2–rich fluid in Late Archaean high–grade metamorphism. *Lithos* **40**, 93–104.

Anderson A.J., Clark A.H., Ma X.P., Palmer G.R., MacArthur J.D. and Roedder E. (1989) Proton–induced X–ray and gamma–ray emission analysis of unopened fluid inclusions. *Econ. Geol.* **84**, 924–939.

Appel P., Möller A. and Schenk V. (1998) High-pressure granulite facies metamorphism in the Pan-African belt of eastern Tanzania: P-T-t evidence against granulite formation by continent collision. *J. Metam. Geol.* **16**, 491–509.

Appel P.W.U., Fedo C.M., Moorbath S. and Myers J.S. (1998) Recognizable primary volcanic and sedimentary features in a low-strain domain of the highly deformed, oldest known (3.7–3.8 Gyr) Greenstone Belt, Isua, West Greenland. *Terra Nova* **10**, 57–62.

Aquilina L., Pauwels H., Genter A. and Fouillac C. (1997) Water–rock interaction processes in the Triassic sandstone and the granitic basement of the Rhine Graben: geochemical investigation of a geothermal reservoir. *Geochim. Cosmochim. Acta* **61**, 4281–4295.

Arthur M.A. (2000) Volcanic contributions to the carbon and sulfur geochemical cycles and global change. In *Encyclopedia of Volcanoes* (eds. H. Sigurdsson, B.F. Houghton, S.R. McNutt, H. Rymer and J. Stix), Academic Press, San Diego, 1045–1056.

Ayora C., Garcia–Veigas J. and Pueyo J.J. (1994) The chemical and hydrological evolution of an ancient potash–forming evaporite basin as constrained by mineral sequence, fluid inclusion composition, and numerical simulation. *Geochim. Cosmochim. Acta* **58**, 3379–3394.

Bach W., Erzinger J., Alt J.C. and Teagle D.A.H. (1996) Chemistry of the lower sheeted dike complex, Hole 504B (Leg 148): Influence of magmatic differentiation and hydrothermal alteration. *Proc. O.D.P., Sci. Res*. **148**, 39-55.

Bach W., Alt J.C., Niu Y., Humphris S.E., Erzinger J., and Dick H.J.B. (2001) The geochemical consequences of late–stage low–grade alteration of lower ocean crust at the SW Indian Ridge: Results from ODP Hole 735B (Leg 176). *Geochim. Cosmochim. Acta* **65**, 3267–3287.

Baker A.J. (1988) Stable isotope evidence for limited fluid infiltration of deep crustal rocks from the Ivrea Zone, Italy. *Geology* **16**, 492–495.

Bakker R.J. and Jansen J.B.H. (1990) Preferential water leakage from fluid inclusions by means of mobile dislocations. *Nature* **345**, 58–60.

Bakker R.J. and Jansen J.B.H. (1994) A mechanism for preferential H_2O leakage from fluid inclusions in quartz based on TEM observations. *Contrib. Mineral. Petrol.* **116**, 7–20.

Barbey P. and Raith M. (1990) The granulit belt of Lapland. In *Granulites and Crustal Evolution*. (eds. D. Vielzeuf and P. Vida), NATO ASI Series, Kluwer, Dordrecht, 111–132.

Bataillé A. (2004) Modélisation de la circulation thermoconvective en milieu fracturé : application à la géothermie des Roches Chaudes et Fracturées à Soultz–sous–Forêts (France). Ph. D. thesis, Université Paul Sabatier, Toulouse.

Bebout G.E. (1996) Volatile Transfer and Recycling at Convergent Margins: Mass-Balance and Insights from High-P/T Metamorphic Rocks. In *Subduction, Top to Bottom* (eds G.E. Bebout, DW Scholl, S.H. Kirby, and J.P. Platt), American Geophysical Union **96**, 179–193.

Beck C.W. (1988) Is the air in amber ancient? Technical comments. *Science* **241**, 718–719.

Bell D.R. and Rossman G.R. (1992) Water in Earth's mantle: the role of nominally anhydrous minerals. *Science* **255**, 1391–1397.

Benison K.C. and Goldstein R.H. (1999) Permian paleoclimate data from fluid inclusions in halite. *Chem. Geol.* **154**, 113–132.

Berman R.G. (1988) Internally-consistent thermodynamic data for stoichiometric minerals in the system Na_2O–K_2O–CaO–MgO–FeO–Fe_2O_3–Al_2O_3–SiO_2–TiO_2–H_2O–CO_2. *J. Petrol.* **29**, 445–522.

Berman R.G. (1990) Mixing properties of Ca–Mg–Fe–Mn garnets. *Am. Mineral.* **75**, 328–344.

Berman R.G. (1991) Thermobarometry using multiequilibrium calculations: a new technique with petrologic applications. *Can. Mineral.* **29**, 833–855.

Berner E.K. and Berner R.A. (1987) *The Global Water Cycle.* Prentice–Hall, Englewood Cliffs.

Berner R.A. (1982) Burial of organic carbon and pyrite sulfur in the modern ocean: its geochemical and environmental significance. *Am. J. Sci.* **282**, 451–473.

Berner R.A., Lasaga A.C. and Garrels R.M. (1983) The carbonate–silicate geochemical cycle and its effect on atmospheric carbon dioxide over the past 100 million years. *Am. J. Sci.* **283**, 641–683.

Berner R.A. and Landis G.P. (1988) Gas Bubbles in Fossil Amber as Possible Indicators of the Major Gas Composition of Ancient Air. *Science* **239**, 1406–1409.

Berner R.A. and Raiswell R. (1983) Burial of organic carbon and pyrite sulfur in sediments over Phanerozoic time: a new theory. *Geochim. Cosmochim. Acta* **47**, 855–862.

Berner R.A., Lasaga A.C. and Garrels R.M. (1983) The carbonate–silicate geochemical cycle and its effect on atmospheric carbon dioxide over the past 100 million years. *Am. J. Sci.* **283**, 641–683.

Bertoldi de Pomar (1953) Contribucion al Conocimiento del origen de la Laguna Mar Chhiquita de la Provincia de Cordoba. Unpubli. PhD Thesis. Universidad Nacional de Cordoba. Argentina, 149pp.

Beukes N.J. and Klein C. (1990) Geochemistry and sedimentology of a facies transition from microbanded to granular iron–formation in the early Proterozoic Transvaal Supergroup, South Africa. *Precamb. Res.* **47**, 99–139.

Biellmann C., Gillet P., Guyot F., Peyronneau J. and Reynard B. (1993). Experimental evidence for carbonate stability in the Earth's lower mantle. *Earth Planet. Sci. Lett.* **118**, 31–41.

Bingen B., Demaiffe D., Hertogen J., Weis D. and Michot J. (1993) K-rich calc-alkaline augen gneisses of Grenvillian age in the SW Norway: migling of mantle-derived and crustal components. *J. Geol.* **101**, 763–778.

Bird M.I., Lloyd J. and Farquhar G.D. (1996) Terrestrial carbon–storage from the last glacial maximum to the present. *Chemosphere* **33**, 1675–1685.

Blanc P.L. (2000) Of sills and straits: a quantitative assessment of the Messinian Salinity Crisis. *Deep-Sea Res.* **47**, 1429–1460.

Blisniuk P.M. and Stern L.A. (2005) Stable isotope paleoaltimetry: A critical review. *Am. J. Sci.* **305**, 1033–1074.

Blundy T.D. and Holland, J.J.B. (1990) Calcic amphibole equilibria and a new amphibole-plagioclase geothermometer. *Contrib. Mineral. Petrol.* **104**, 208–224.

Bodnar R.J. and Bethke P.M. (1984) Systematics of stretching of fluid inclusions 1 : Fluorite and sphalerite at 1 atmosphere confining pressure. *Econ. Geol.* **79**, 141–161.

Bodnar R.J., Reynolds T.J. and Kuehn C.A. (1985) Fluid–inclusion systematics in epithermal systems. In *Society of Economic Geologists, Reviews in Economic Geology, 2, Geology and Geochemistry of Epithermal Systems.* (eds. Berger B. and Bethke R.), 73–97.

Boettcher A.L., O'Neil J.R. (1980) Stable isotope, chemical and petrographic studies of high pressure amphiboles and micas: evidence for metasomatism in the mantle source regions of alkali basalts and kimberlites. *Am. J. Sci.* **280A**, 594–621.

Bohlen S.R. (1991) On the formation of granulites. *J. Geol.* **95**, 617–632.

Boillot G., Agrinier P., Beslier M.O., Cornen G., Froitzheim N., Gardien V., Girardeau J., Gil-Ibarguchi J., Kornprobst J., Moullade M., Schärer U. and Vanney J.R. (1995) A lithospheric syn-rift shear zone at the ocean-continent transition: preliminary results of the Galinaute II cruise (Nautile dives on the Galicia Bank, Spain). *C.R. Acad. Sci. Paris* **321**, 1171–1178.

Boiron M.C., Moisette A., Fabre C., Dubessy J., Banks D and Yardley B. (1997) Ion analysis in individual fluid inclusions by laser ablation-optical emisson spectroscopy : Application to natural inclusions. *ECROFI XIV Abstracts, Nancy,* 44–45.

Bons P.D. (2001) The formation of large quartz veins by rapid ascent of fluids in mobile hydrofractures. *Tectonophysics* **336**, 1–17.

Bortolami G.C., Ricci B., Susella G.F. and Zuppi G.M. (1978) Isotope hydrology of the Val Corsaglia Maritime Alps, Piedmont, Italy. In *Isotopes in Hydrology* International Atomic Energy Agency, Vienna. 327–350.

Bottinga Y. and Craig H. (1969) Oxygen isotope fractionation between CO_2 and water, and the isotopic composition of marine atmospheric CO_2. *Earth Planet. Sci. Lett.* **5**, 285-295.

Bottinga Y. and Javoy M. (1975) Oxygen isotope partitioning among the minerals in igneous and metamorphic rocks. *Rev. Geophys.* **13**, 401–418.

Bottinga Y. and Javoy M. (1990) Mid-ocean ridge basalt degassing: bubble growth and ascent. *Chem. Geol.* **81**, 255–270.

Bourg C., Stievenard M. and Jouzel J. (2001). Hydrogen and oxygen isotopic composition of aqueous salt solutions by gas–water equilibration method. *Chem. Geol.* **173**, 331–337.

Brantley S.L. (1992) The effect of fluid chemistry on quartz microcrack lifetimes. *Earth Planet. Sci. Lett.* **113**, 145–156.

Brenan J.M. and Watson E.B. (1988) Fluids in the Litosphere : 2. Experimental constraints on CO_2 transport in dunite and quartzite at elevated P–T conditions with implications for mantle and crustal decarbonation processes. *Earth Planet. Sci. Lett.* **91**, 141–158.

Brennan S.T. and Goldstein R.H. (1998) Fluid and thermal history of an exhumed petroleum reservoir. *PACROFI program and abstracts,* Las Vegas (unpaginated).

Brennan S.T. and Lowenstein T.K. (2002) The major–ion composition of Silurian seawater. *Geochim. Cosmochim. Acta* **66**, 2683–2700.

Brown P.E. and Hagemann S.G. (1994) MacFlinCor: a computer program for fluid inclusion data reduction and manipulation. In *Fluid Inclusions in Minerals: Method and Applications* (eds B. De Vivo and J.M. Frezzotti), Virginia Tech Press, USA, 231-250.

Brun J.P., Wenzel F. and ECORS-DEKORP team (1991) Crustal scale structure of the southern Rhine graben from ECORS-DEKORP seismic reflection data. *Geology* **19**, 758–762.

Burg J.P., Nievergelt P., Oberli F., Seward D., Davy P., Maurin J.C., Diao Z. and Meier M. (1997) Exhumation during crustal folding in the Namche-Barwa syntaxis. *Terra Nova* **9**, 53–56.

Burg J.P., Davy P., Nievergelt P., Oberli F., Seward D., Diao Z. and Meier M. (1998) The Namche-Barwa syntaxis: evidence for exhumation related to compressional crustal folding. *J. Asian Earth Sci.* **16**, 239–252.

Burke K., Dewey J.F. and Kidd W.S.F. (1977) World distribution of sutures: the sites of former oceans. *Tectonophysics* **40**, 69–99.

Burruss R.C. (1987) Crushing–cell, capillary column gas chromatography of petroleum fluid inclusions : Method and application to petroleum source rocks, reservoirs, and low temperature hydrothermal ores. *American Current Research on Fluid Inclusions Abstracts, Socorro,* (unpaginated).

Butler R.W., Lickorish H., Grasso M., Pedley H.M. and Ramberti L. (1995) Tectonics and sequence stratigraphy in Messinian basins Sicily: constraints on the initiation and termination of the Mediterranean salinity crisis. *Geol. Soc. Am. Bull.* **107**, 425–439.

Canil D. (1999) Vanadium partitioning between orthopyroxene, spinel and silicate melt and the redox states of mantle source regions for primary magmas. *Geochim. Cosmochim. Acta* **63**, 557–572.

Cannat M., Bideau D. and Bougault H. (1992) Serpentinized peridotites and gabbros in the Mid-Atlantic ridge axial valley at 15°37'N and 16°52'N. *Earth Planet. Sci. Lett.* **109**, 87-106.

Cartigny P. (2005) Stable isotopes and the origin of diamond. *Elements* **1**, 79–84.

Cartigny P., Jendrzejewski N., Pineau F., Petit F., and Javoy M. (2001) Volatile (C, N, Ar) variability in MORB, and the respective roles of mantle source heterogeneity and degassing: the case of the Southwest Indian Ridge. *Earth Planet. Sci. Lett.* **194**, 241–257.

Cartigny P., Stachel T., Harris J. F. and Javoy M. (2004) Constraining diamond metasomatic growth using C- and N- stable isotopes: examples from Namibia. *Lithos* **77**, 359–373.

Cendón D.I. (1999) Evolución geoquímica de cuencas evaporíticas Terciarias: Implicaciones en la composición isotópica del sulfato disuelto en el océano durante el Terciario. Ph.D. Dissertation, Universitat de Barcelona, 270 pp.

Cerrai E., Marchetti R., Renzoni R., Roseo L., Silvestri M. and Villani S. (1954) A thermal method for concentrating heavy water. *Chem. Eng. Prog. Symp.* **50**, 271-280.

Chahine M.T. (1992) The hydrological cycle and its influence on climate. *Nature* **359**, 373-380.

Chandler F.W. (1980) Proterozoic redbed sequences of Canada. *Can. Geol. Surv. Bull.* **311**.

Chapman S. and Cowling, T. G. (1951) *Mathematical theory of non-uniform gases (2nd edn)*. Cambridge University Press, **Chapter 10**, 14.

Charou J.L., Fouquet Y., Bougault H., Donval J.P., Etoubleau J., Jean-Baptiste P., Dapoigny A., Appriou P. and Rona P.A. (1998) Intense CH_4 plumes generated by serpentinization of ultramaficrocks at the intersection of the 15°20'N Fracture Zone and the Mid-Atlantic Ridge. *Geochim. Cosmochim. Acta* **62**, 2323–2333.

Chaussidon M., Sheppard S.M.F. and Michard A. (1991) Hydrogen, sulphur and neodymium isotope variations in the mantle beneath the EPR at 12°50'N. In *Stable Isotope Geochemistry: A Tribute to Samuel Epstein.* (eds. H.P.Taylor, J.R. O'Neil and I.R. Kaplan), The Geochemical Society, Special Publication, **vol. 3**, 325–337.

Chen R.-X., Zheng Y.-F., Gong B., Zhao Z.-F., Gao T.-S., Chen B. and Wu Y.-B. (2007) Origin of retrograde fluid in ultrahigh-pressure metamorphic rocks : Constraints from mineral hydrogen isotope and water content changes in eclogite–gneiss transitions in the Sulu orogen. *Geochim. Cosmochim. Acta* **71**, 2299–2325.

Chiodini G., Marini L. and Russo M. (2001) Geochemical evidence for the existence of high-temperature hydrothermal brines at Vesuvio volcano, Italy. *Geochim. Cosmochim. Acta* **65**, 2129–2147.

Church T.M. (1996) An underground route for the water cycle. *Nature* **380**, 579–580.

CIESM (Roveri, M., Krijgsman, W., Suc, J.-P., Lugli, S., Lofi, J., Sierro, F.J., Manzi, V., Flecker, R., and others) (2008) Executive Summary. In *The Messinian Salinity Crisis from mega-deposits to microbiology – A consensus report* (ed. F. Briand), CIESM Workshop Monographs, **33**, 7–28.

Clauzon G., Suc J.-P., Gautier F., Berger A. and Loutre M.-F. (1996) Alternate interpretation of the Messinian salinity crisis: Controversy resolved? *Geology* **24**, 363–366.

Cocherie A., Guerrot C., Fanning M. and Genter A. (2004) Datation U-Pb of two granites types from Soultz (Rhine Graben, France). *C. R. Geosciences* **336**, 775–787.

Cole D.R. and Wesolowski D.J. (1989) Influence of NaCl aqueous solutions on isotopic equilibria and rates of exchange in mineral-fluid systems. *Trans. Geotherm. Res. Council* **13**, 227–234.

Coltice N., Simon L. and Lécuyer C. (2004) Carbon isotope cycle and mantle structure. *Geophys. Res. Lett.* **31**, No. 5, L05603, doi :10.1029/2003GL018873.

Comings B.D. and Cercone K.R. (1986) Experimental contamination of fluid inclusions in calcite. *Soc. Econ. Paleonto. Mineral. Abstr.* **3**, 24.

Coolen J.M. (1980) Chemical petrology of the Furua complex, Southern Tanzania. Ph. D Thesis, Vrije Universiteit, Amsterdam.

Coolen J.M. (1982) Carbonic fluid inclusions in granulites from Tanzania: a comparison of geobarometric methods based on fluid density and mineral chemistry. *Chem. Geol.* **37**, 59–77.

Corliss J.B., Dymond J., Forgon L.I., Edmond J.M., von Herzen R.P., Ballard R.D., Green K., Williams D., Bainbridge A., Crane K. and van Andel T.H. (1979) Submarine thermal springs on the Galápagos Rift. *Science* **203**, 1073–1083.

Craig H. (1961) Isotopic variations in meteoric waters. *Science* **133**, 1702–1703.

Craig H. (1966) Isotopic composition and origin of the Red Sea and Salton Sea geothermal brines. *Science* **54**, 1544–1547.

Craig H. and Gordon L.I. (1965) Deuterium and oxygen-18 variations in the ocean and the marine atmosphere. In *Stable Isotopes in Oceanographic Studies and Paleotemperatures* (ed. E. Tongiorgi.). Lab. Geol. Nucl. 9-130.

Crawford W.A. and Valley J.W. (1990) Origin of graphite in the Pickering Gneiss and the Franklin Marble, Honey Brook Upland, Pennsylvania Piedmont. *Geol. Soc. Am. Bull.* **102**, 807–811.

Criss R.E., Ekren E.B. and Hardyman R.F. (1984) Casto ring zone: A 4,500 km^2 fossil hydrothermal system in the Challis volcanic field, central Idaho. *Geology* **12**, 331–334.

Criss R.E. and Taylor H.P. (1986) Meteoric-hydrothermal systems. In *Stable Isotopes in High Temperature Geological Processes.* (eds. J.W. Valley, H.P. Taylor and J.R. O'Neil), Mineral. Soc. Am., **vol. 16**, 373–424.

Crowley T.J. (1995) Ice age terrestrial carbon changes revisited. *Global Biogeochem. Cycles* **9**, 377–389.

Curry W.B., Duplessy J.C., Labeyrie L.D. and Shackleton N.J. (1988) Changes in the distribution of $\delta^{13}C$ of deep water ΣCO_2 between the last glaciation and the Holocene. *Paleoceanography* **3**, 317–341.

Dai A. (2001) Global precipitation and thunderstorm frequencies. Part I: Seasonal and interannual variations. *J. Climate* **14**, 1092–1111.

Dai A. and Trenberth K.E. (2003) New estimates of continental discharge and oceanic freshwater transport. *Proc. Symp. on Observing and Understanding the Variability of Water in Weather and Climate*, CA, Amer. Meteor. Soc. CD–ROM, JP1.11.

Dai, A., Giorgi F. and Trenberth K.E. (1999) Observed and model-simulated diurnal cycles of precipitation over the contiguous United States. *J. Geophys. Res.* **104**, 6377-6402.

Dai A., Karl T.R., Sun B. and Trenbreth K.E. (2006) Recent trends in cloudiness over the United States: A tale of monitoring inadequacies. *Bull. Amer. Meteor. Soc.* **87**, *597-606.*

Daly J.S., Balagansky V.V., Timmerman M.J., Whitehouse M.J., De Jong K., Guise P., Bogdanova S. Gorbatschev R. and Bridgwater D. (2001) Ion microprobe U-Pb zircon geochronology and

isotopic evidence for trans-crustal suture in the Lapland-Kola Orogen, northern Fennoscandian Shield. *Precamb. Res.* **102**, 289–314.

Dansgaard W. (1964) Stable isotopes in precipitation. *Tellus* **16**, 436-468.

Daux V., Lécuyer C., Adam F., Martineau F. and Vimeux F. (2005) Oxygen isotope composition of human teeth and the record of climate changes in France (Lorraine) during the last 1700 years. *Climatic Change* **70**, 445–464.

Debon F. and Lemmet M. (1999) Evolution of Mg/Fe ratios in late Variscan plutonic rocks from the external crystalline massifs of the Alps. (France, Italy, Switzerland). *J. Petrology* **40**, 1151–1185.

Debussy J., Porty B. and Ramboz C. (1989) Advances in C-O-H-N-S fluid geochemistry based in micro-Raman spectrometry analyses on fluid inclusions. *Eur. J. Mineral.* **1**, 517–534.

Decima A. and Wezel F.C. (1973) Late Miocene evaporites of the Central Sicilian Basin. In *Initial Reports of the Deep Sea Drilling Project, Leg 42 (1)* (eds. W.B.F. Ryan. and K.J. Hsü), Government Printing Office, Washington D.C., U.S., 1234–1240.

Deines P. (1980) The isotopic composition of reduced organic carbon. In *Handbook of Environmental Isotope Geochemistry* (eds. P. Fritz and J.C. Fontes), Elsevier, New York, 329–406.

Deines P., Harris J.W. and Gurney J.J. (1993) Depth–related carbon isotope and nitrogen concentration variability in the mantle below the Orapa kimberlite, Bostwana, Africa. *Geochim. Cosmochim. Acta* **57**, 2781–2796.

Delano J.W. (2001) Redox history of the Earth's interior since 3900 Ma: Implications for prebiotic molecules. *Origins Life Evol. B.* **31**, 311–341.

Deleens E., Ferhi A. and Querioz O. (1983) Carbon isotope fractionation by plants using the C4 pathway. *Physiol. Veg.* **21**, 897–905.

Deloule E., Albarède F. and Sheppard S.M.F. (1991) Hydrogen isotope heterogeneities in the mantle from ion probe analysis of amphiboles from ultramafic rocks. *Earth Planet. Sci. Lett.* **105**, 543–553.

Demeny A. (1995) H isotope fractionation due to hydrogen–zinc reactions and its implications on D/H analysis of water samples. *Chem. Geol.*, **121**, 19–25.

Demouchy S., Jacobsen S.D., Gaillard F. and Stern C.R. (2006) Rapid magma ascent recorded by water diffusion profiles in mantle olivine. *Geology* **34**, 429–432.

Dennis P.F., Rowe P.J. and Atkinson T.C (2001) The recovery and isotopic measurement of water from fluid inclusions in speleothems. *Geochim. Cosmochim. Acta* **65**, 871-884.

Des Marais D.J. (2001) Isotopic evolution of the biogeochemical carbon cycle during the Precambrian. *Rev. Mineral. Geochem.* **43**, 555–578.

Des Marais D.J. and Moore J.G. (1984) Carbon and its isotopes in mid-ocean ridge basaltic glasses. *Earth Planet. Sci. Lett.* **69**, 43–57.

Des Marais D.J., Strauss H., Summons R.E. and Hayes J.M. (1992) Carbon isotope evidence for the stepwise oxidation of the Proterozoic environment. *Nature* **359**, 605–609.

Desmurs L. (1997) Etude pétrologique et géochronologique de la croûte continentale de la marge de Galice. Mémoire de DEA, Université Lyon 1, France.

Dezayes C., Genter A. and Gentier S. (2004) Fracture Network of the EGS geothermal reservoir at Soultz–sous-Forêts (Rhine Graben, France). *Geotherm. Resour. Council Trans.* **28**, 213–218.

Dezes P., Schmid S.M. and Ziegler P.A. (2004) Evolution of the European Cenozoic Rift System: interaction of the Alpine and Pyrenean orogens with their foreland lithosphere. *Tectonophysics* **389**, 1–33.

Dirmeyer P. A., Gao X., Zhao M., Guo Z., Oki T. and Hanasaki N. (2006) The Second Global Soil Wetness Project (GSWP-2): Multi-model analysis and implications for our perception of the land surface. *Bull. Amer. Meteor. Soc.* **87**, 1381–1397.

Dobrovolsky V.V. (1994) *Biogeochemistry of the World's Land.* CRC Press, Boca Raton, Florida.

Doebl F. and Olbrecht W. (1974) An isobath map of the Tertiary base in the Rhine graben. In *Approaches to taphrogenesis* (eds. J.H. Illies and K. Fuchs), Schweizerbart'sche Verlagsbuchhandlung, Stuttargt, 71–72.

Dolomieu C.D. (1792) Sur de l'huile de pétrole dans le cristal de roche et les fluides élastiques tirés du quartz. *Observations sur la physique, l'histoire naturelle et les arts* **42**, 318–319.

Doval M.D. and Hansell D.A. (2000) Organic carbon and apparent oxygen utilization in the Western South Pacific and the central Indian Oceans. *Mar. Chem.* **68**, 249–264.

Drever J.L., Li Y.H. and Maynard J.B. (1988) Geochemical cycles: the continental crust and the oceans. In *Chemical Cycles in the Evolution of the Earth* (eds. C.B. Gregor, R.M. Garrels, F.T. Mackenzie and J.B. Maynard), Wiley, New York, 17–53.

Dubois M. (2000) Inclusions fluides : Approche expérimentale, thermodynamique et applications aux phénomènes hydrothermaux et diagénétiques. Mémoire d'H.D.R., Université des Sciences et Technologies de Lille, 234 pp.

Dubois M., Ayt Ougougdal M., Meere P., Royer J.J., Boiron M-C. and Cathelineau M. (1996) Temperature of paleo-to modern self-sealing within a continental rift basin: the fluid inclusion data (Soultz sous Forets, Rhine graben, France). *Eur. J. Mineral.* **8**, 1065–1080.

Duplessy J.C., Shackleton N.J., Fairbanks R.G., Labeyrie L., Oppo D. and Kallel N. (1988) Deepwater source variations during the last climatic cycle and their impact on the global deepwater circulation. *Paleoceanography* **3**, 343–360.

Dypvik H., Hankel O., Nilsen O., Kaaya C. and Kilembe E. (2001) The lithostratigraphy of the Karoo supergroup in the Kilombero Rift Valley, Tanzania. *J. Afr. Earth Sci.* **32**, 451–470.

Edel J.B., Schulmann K. and Rotstein Y. (2007) The Variscan inheritance of the Upper Rhine Graben: evidence of reactivation in the Lias, Late Eocene-Oligocene up to the recent. *Int. J. Earth Sci.* **96**, 305–325.

El Euch-El Koundi N., Ferry S., Suc J.-P., Clauzon G., Melinte-Dobrinescu M.C., Gorini C., Safra A. and Zargouni F. (2009) Messinian deposits and erosion in northern Tunisia: inferences on Strait of Sicily during the Messinian Salinity Crisis. *Terra Nova* **21**, 41–48.

England G.L., Rasmussen B., Krapez B. and Groves D.I. (2002) Palaeoenvironmental significance of rounded pyrite in siliciclastic sequences of the Late Archaean Witwatersrand Basin: oxygen-deficient atmosphere or hydrothermal alteration? *Sedimentology* **49**, 1133–1156.

Epstein S. and Mayeda T. K. (1953) Variation in ^{18}O content of waters from natural sources. *Geochim. Cosmochim. Acta* **4**, 213–224.

Evans W.C. (1996) A gold mine of methane. *Nature* **381**, 114.

Fabre C., Boiron M.C., Dubessy J., Cathelineau M. and Banks D. (1999) Analysis of fluid inclusions by laser ablation–optical emission spectroscopy, microthermometry and Raman spectroscopy : a reconstitution of the composition and temperature of trapped fluids. *ECROFI XV Abstracts, Potsdam,* 97–99.

Falkowski P., Scholes R.J., Boyle E., Canadell J., Canfield D., Elser J., Gruber N., Hibbard K., Hogberg P., Linder S., Mackenzie F.T., Moore I.B., Pedersen T., Rosenthal Y., Seitzinger S., Smetacek V. and Steffen W. (2000) The global carbon cycle: a test of our knowledge of Earth as a system. *Science* **290**, 291–296.

Farley K.A., Maier-Reimer E., Schlosser P. and Broecker W.S. (1995) Constraints on mantle ^{3}He fluxes and deep-sea circulation from an oceanic general circulation model. *J. Geophys. Res.* **100**, B3, 3829–3839.

Fauquette S., Suc J.-P., Bertini A., Popescu S.-M., Warny S., Bachiri Taoufiq N., Perez Villa M.-J., Chikhi H., Subally D., Feddi N., Clauzon G. and Ferrier J. (2006) How much did climate force the Messinian salinity crisis? Quantified climatic conditions from pollen records in the Mediterranean region. In *Late Miocene to Early Pliocene Environment and Climate Change in the Mediterranean Area*. (eds. J. Agusti, O. Oms and J.E. Meulenkamp) *Palaeogeogr. Palaeoclimatol. Palaeoecol.* **238**, 281–301.

Feder H.M. and Taube H. (1952). Ionic hydration: an isotopic fractionation technique. *J. Chem. Phys.* **20**, 1335–1336.

Fischer T.P., Giggenbach W.F., Sano Y. and Williams S.N. (1998) Fluxes and sources of volatiles discharged from Kudryavy, a subduction zone volcano, Kurile Islands. *Earth Planet. Sci. Lett.* **160**, 81-96.

Flecker R., DeVilliers S. and Ellam R.M. (2002) Modelling the effect of evaporation on the Salinity–$^{87}Sr/^{86}Sr$ relationship in modern and ancient marginal–marine systems : the Mediterranean Messinian Salinity Crisis. *Earth Planet. Sci. Lett.* **3**, 258-266.

Fontaine F.J., Rabinowicz M. and Boulègue J. (2003) Hydrothermal processes at Milos Island (Greek Cyclades) and the mechanisms of compaction–induced phreatic eruptions. *Earth Planet. Sci. Lett.* **210**, 17–33.

Fortier S.M. (1994) An on–line experimental/analytical method for measuring the kinetics of oxygen isotope exchange between CO_2 and saline/hypersaline salt solutions at low (25-50°C) temperatures. *Chem. Geol.* **116**, 155–162.

Fourcade S. and Allègre C.J. (1981) Trace element behavior in granite genesis – a case study: the calc-alkalic plutonism association from the Querigut complex (Pyrénées, France). *Contrib. Mineral. Petrol.* **76**, 177–195.

Francois L.M., Godderis Y., Wamant P., Ramstein G., de Noblet N. and Lorenz S. (1999) Carbon stocks and isotopic budgets of the terrestrial biosphere at mid–Holocene and last glacial maximum times. *Chem. Geol.* **159**, 163–189.

Frank H. (1915) Contribucion al conocimiento de las salinas Grandes y la Mar Chiquita. Provincia de Cordoba. Rev., *Centro. Estud. Ingen.* **3**, 91-107.

Frantz J.D., Mao H.K., Zhang Y., Wu Y., Thompson A.C., Underwood J.H., Glauque R.D. Jones K.W. and Rivers M.L. (1988) Analysis of fluid inclusions by X–ray fluorescence using synchrotron radiation. *Chem. Geol.* **69**, 235–244.

Fritz H., Tenczer V., Hauzenberger C., Wallbrecher E. and Muhongo S. (2009) Hot granulites nappes-Tectonic styles and thermal evolution of the Proterozoic granulite belts in East Africa. *Tectonophysics*, in press.

Frost B.R. and Bucher K. (1994) Is water responsible for geophysical anomalies in the deep continental crust? A petrological perspective. *Tectonophysics*, **231**, 293-309.

Früh-Green G., Plas A., Lécuyer C. (1996) Petrologic and stable isotope constraints on hydrothermal alteration and serpentinization of the EPR shallow mantle at Hess Deep (Site 895). In *Proc. ODP, Sci. Results, 147* (eds. C. Mével, K.M. Gillis, J.F. Allan and P.S. Meyer), College Station, TX (Ocean Drilling Program), 255–291.

Fryer P., Pearce J.A. and Stokking L.B (1990) *Proceedings of the Ocean Drilling Program, Initial Reports, Leg 125*. Ocean Drilling Program.

Fu B., Touret J.L.R. and Zheng Y.-F. (2003) Remnants of premetamorphic fluid and oxygen isotopic signatures in eclogites and garnet clinopyroxenite from the Dabie–Sulu terranes, eastern China. *J. Metam. Geol.* **21**, 561–578.

Furnes H., De Wit M., Staudigel H., Rosing M. and Muehlenbachs K. (2007) A vestige of Earth's oldest ophiolite. *Science* **315**, 1704–1707.

Galimov E.M. (1991) Isotope fractionation related to kimberlite magmatism and diamond formation. *Geochim. Cosmochim. Acta* **55**, 1697–1708.

Gardien V., Arnaud N., Desmurs L. (2000) Petrology and Ar-Ar dating of granulites from the Galicia Bank (Spain) : African craton relics in Western Europe. *Geodinamica Acta* **13**, 103–117.

Gargani J., Moretti I. and Letousey J. (2008) Evaporite accumulation during the Messinian Salinity Crisis: The Suez Rift case. *Geophys. Res. Lett.* **35**, L02401.

Gat J.R. (1981) Lakes. In *Stable Isotope Hydrology; Deuterium and Oxygen-18 in the Water Cycle* (eds. J.R. Gat and R. Gonfiantini). IAEA Techn. Rep. Ser. 210, 203-221.

Gat J.R. and Levy Y. (1978) Isotope hydrology of inland sabkhas in the Bardawil area. *Sinai. Limnol. Oceanog.* **23**, 841-850.

Genda H. and Ikoma M. (2007) Origin of the ocean on the Earth: Early evolution of water D/H in a hydrogen–rich atmosphere. *Icarus* **194**, 42–52.

Genter A. and Traineau H. (1992) Borehole EPS1, Alsace, France: preliminary geological results from granite core analyses for Hot Dry Rock research. *Sci. Drilling* **3**, 205–214.

Genter A., Traineau H., Dezayes C., Elsass P., Ledésert B., Meunier A. and Villemin T. (1995) Fracture analysis and reservoir characterization of the granitic basement in the HDR Soultz project (France). *Geotherm. Sci. Tech.* **4**, 189–214.

Gerard A. and Kappelmeyer O. (1987) The Soultz-sous-Forêts project and its specific characteristics with respect to the present state of experiments with HDR. *Geothermics* **16**, 393–399.

Gerlach T.M. (1991) Present–day CO_2 emissions from volcanoes. *EOS, Trans., AGU* **72**, 249, 254–255.

Gibson J.J. (2002) Short-term evaporation and water budget comparisons in shallowArtic lakes using non-steady isotope mass balance. *J. Hydrol.* **264**, 242-261.

Giggenbach W.F. (1992) Isotopic shifts in waters from geothermal and volcanic systems along convergent plate boundaries and their origin. *Earth Planet. Sci. Lett.* **113**, 495–510.

Giggenbach W.F. (1996) Chemical composition of Volcanic Gases. In *Monitoring and Mitigation of Volcanic Hazards* (eds. R. Scosper and R.I. Tilling), Springer-Verlag, 221-256.

Giletti B.J. (1986) Diffusion effects on oxygen isotope temperatures of slowly cooled igneous and metamorphic rocks. *Earth Planet. Sci. Lett.* **77**, 218–228.

Giletti B.J. and Yund R.A. (1984) Oxygen diffusion in quartz. *J. Geophys. Res.* **89**, 4039–4046.

Gladstone R., Flecker R., Valdes P., Lunt D. and Markwick P. (2007) The Mediterranean hydrologic budget from a Late Miocene global climate simulation. *Palaeogeography, Palaeoclimatology, Palaeoecology* **251**, 254-267.

Glassley W.E. (1983) The role of CO_2 in the chemical modification of deep continental crust. *Geochim. Cosmochim. Acta.* **47**, 597-616.

Goldstein R.H. (1986) Reequilibration of fluid inclusions in low–temperature calcium–carbonate cement. *Geology* **14**, 792–795.

Goldstein R.H. (2001) Fluid inclusions in sedimentary and diagenetic systems. *Lithos* **55**, 159–193.

Goldstein R.H. and Reynolds T.J. (1994) Systematics of fluid inclusions in diagenetic minerals. *SEPM (Society for Sedimentary Geology), Short Course Notes* **31**, 199 pp.

Gomes R., Levison H.F., Tsiganis K. and Morbidelli M. (2005) Origin of the cataclysmic late heavy bombardment period of the terrestrial planets. *Nature* **435**, 466–469.

Gonfiantini R. (1986) Environmental isotopes in lake studies. In *Handbook of Environmental Isotope Geochemistry* (eds. P. Fritz and J.C. Fontes). Vol. 3, Elsevier, 113-168.

Graham C.M., Powel R.P. (1984) A garnet-hornblende geothermometer: Calibration, testing, and application to the Pelona schist, southern California. *J. Metam. Geol.* **2**, 13–31.

Graham C.M., Viglino J.A. and Harmon R.S. (1984) Experimental study of hydrogen-isotope exchange between aluminous chlorite and water and of hydrogen diffusion in chlorite. *Amer. Mineral.* **72**, 566–579.

Graham D. and Sarda P. (1991) Reply to comment by T.M. Gerlach on "Mid-ocean ridge popping rocks: implications for degassing at ridge crests." *Earth Planet. Sci. Lett.* **105**, 568–573.

Grant K.J., Ingrin J., Lorand J.P. and Dumas P. (2007) Water partitioning between mantle minerals from peridotite xenoliths. *Contrib. Mineral. Petrol.* **154**, 15–34.

Graupner T., Brätz H. and Klemd R. (2005) LA–ICP–MS micro–analysis of fluid inclusions in quartz using a commercial Merchantek 266 nm Nd:YAG laser : a pilot study. *Eur. J. Mineral.* **17**, 93–102.

Gregory R.T., Criss R.E. and Taylor H.P. (1989) Oxygen isotope exchange kinetics of mineral pairs in closed and open systems: applications to problems of hydrothermal alteration of igneous rocks and precambrian iron formations. *Chem. Geol.* **75**, 1–42.

Hall C.E. and Parmentier E.M. (2000). Spontaneous melt localization in a deforming solid with viscosity variations due to water weakening. *Geophys. Res. Lett.* **27**, 9–12.

Hall D.L. (1996) Application of fluid inclusions to petroleum exploration : Some recent advances and case studies. *PACOFRI VI Abstracts, Madison*, 59–60.

Hall D.L., Sterner S.M. and Bodnar R.J. (1989) Experimental evidence for hydrogen diffusion into fluid inclusions in quartz. *Geol. Soc. Am. Abstr.* **21**, A358.

Hammarstrom J.M. and Zen E.A. (1986) Aluminium in hornblende: An empirical igneous geobarometer. *Am. Mineral.* **71**, 1297–1313.

Hansell D.A. and Carlson C.A. (1998) Deep–ocean gradients in the concentration of dissolved organic carbon. *Nature* **395**, 263–266.

Harley S.L. (1989) The origin of granulites: a metamorphic perspective. *Geol. Mag.* **126**, 215–247.

Harperath L. (1887) Estudio sobre la composición química de las salinas del interior de la República Argentina. *Bol. Acad. Nac. Cienc. Córdoba* **10**, 427–441.

Hart R.A. (1973) Geochemical and geophysical implications of the reaction between seawater and the oceanic crust. *Nature* **243**, 76-78.

Hart S.R., Blusztajn J., Dick H.J.B., Meyer P.S. and Muehlenbachs K. (1999) The fingerprint of seawater circulation in a 500-meter section of ocean crust gabbros. *Geochim. Cosmochim. Acta* **63**, 4059-4080.

Hauzenberger C., Bauernhofer A., Hoinkes G., Wallbrecher E. and Mathu E. (2004) Pan-African high pressure granulites from SE-Kenya: petrological and geothermobarometric evidence for polyphase evolution in the Mozanbique Belt. *J. Afr. Earth Sci.* **40**, 245–268.

Hauzenberger C., Robl J. and Stüwe W. (2005) Garnet zoning in high P granulite-facies metapelite, Mozambique Belt SE Kenya: constraints on the cooling history. *Europ. J. Mineral.* **17**, 43–55.

Hauzenberger C., Sommer H., Fritz H., Bauernhofer A., Kröner A., Hoinkes G., Wallbrecher E. and Thöni M. (2007) SHRIMP U-Pb zircon Sm-Nd garnet ages from the granulite facies basement of SE Kenya: evidence for Neoproterozoic polycyclic assembly of the Mozambique Belt. *J. Geol. Soc. London* **164**, 189–201.

Hazen R.M. and Roedder E. (2001) How old are the baxteria from the Permian age ? *Nature* **411**, 155.

Hofmann M., Broecker W.S. and Lynch–Stieglitz J. (1999) Influence of a [$CO_{2(aq)}$] dependent biological C–isotope fractionation on glacial $^{13}C/^{12}C$ ratios in the ocean. *Global Biogeochem. Cycles* **13**, 873–883.

Hoinkes G. (1986) Effect of grossular content in garnet on the partitioning of Fe and Mg between garnet and biotite. *Contrib. Mineral. Petrol.* 92, 393–399.

Holland H.D. (1978) *Chemistry of the Atmosphere and Oceans.* Wiley, New York.

Holland H.D. (1984) *The Chemical evolution of the Atmosphere and Oceans.* Princeton University Press.

Holland H.D. (1999) When did the Earth's atmosphere become oxic? A reply. *Geochem. News* **100**, 20–22.

Holland H.D. (2002) Volcanic gases, black smokers, and the Great Oxidation Event. *Geochim. Cosmochim. Acta* **66**, 3811-3826.

Holloway J.R. (1998) Graphite-melt equilibria during mantle melting: constraints on CO_2 in MORB magmas and the carbon content of the mantle. *Chem. Geol.* **147**, 89–97.

Holmden C., Creaser R.A. and Muehlenbachs K. (1997) Paleosalinities in ancient brackish water systems determined by $^{87}SR/^{86}Sr$ ratios in carbonate fossils: A case study from the Western Canada Sedimentary Basin. *Geochim. Cosmochim. Acta* **61**, 2105–2118.

Holmes A. (1951) *The sequence of Pre-Cambrian orogenic belts in south and central Africa.* (eds. K.S. Sandford and F. Blondel), 18th International Geological Congress. Association of African Geological Surveys, London, 254–269.

Holtzman B.K., Groebner N., Zimmerman M., Ginsberg S. and Kohlstedt D. (2003) Stress–driven melt segregation in partially molten rocks. *Geochem. Geophys. Geosyst.* **4**, Art. No. 8607.

Holzer L., Frei R., Barton J.M. and Kramers J.D. (1998) Unraveling the record of successive high grade events in the Central Zone of the Limpopo Belt using Pb single phase dating of metamorphic minerals. *Precamb. Res.* **87**, 87–115.

Hooijkaas G.R., Genter A. and Dezayes C. (2006) Deep seated geology of the granite intrusions at the Soultz EGS site based on 5 km depth boreholes. *Geothermics* **35**, 484–506.

Horibe, Y. & Craig, H. (1987) Trapped gases in amber; a paleobotanical and geochemical inquiry. *Eos* **68**, 1513.

Horibe Y. and Craig H. (1988) In Reply: Is the Air in Amber Ancient? *Science* **241**, 719–721.

Horita J., Cole D.R. and Wesolowski D.J. (1995). The activity-composition relationship of oxygen and hydrogen isotopes in aqueous salt solutions: III. Vapor-liquid water equilibration of NaCl solutions to 350°C. *Geochim. Cosmochim. Acta* **59**, 1139-1151.

Horita J., Ueda A., Mizukami K. and Takatori I. (1989) Automatic δD and $\delta^{18}O$ analyses of multi-water samples using H_2- and CO_2-water equilibration methods with a common equilibration set-up. *Apl. Radiat. Isot.* **40**, 801–805.

Horita J. and Wesolowski D.J. (1994) Liquid-vapor fractionation of oxygen and hydrogen isotopes of water from the freezing to the critical temperature. *Geochim. Cosmochim. Acta* **58**, 3425–3437.

Horita J., Zimmermann H. and Holland H.D. (2002) Chemical evolution of seawter during the Phanerozoic : Implications from the record of marine evaporites. *Geochim. Cosmochim. Acta* **66**, 3733–3756.

Houghton R.A (2003) The Contemporary Carbon Cycle. In *Treatise on Geochemistry, Volume 8* (eds. H.D. Holland and K.K. Turekian), Elsevier, New York, 473–513.

Hsü K.J., Ryan W.B.F. and Cita M.B. (1973) Late Miocene desiccation of the Mediterranean. *Nature* **242**, 240–244.

Humphris S.E. and Thompson G. (1978) Hydrothermal alteration of oceanic basalts by seawater. *Geochim. Cosmochim. Acta* **42**, 107–125.

Hunten D.M., Pepin R.O. and Walker, J.C.G. (1987) Mass fractionation in hydrodynamic escape. *Icarus* **69**, 532–549.

Ikoma M. and Genda H. (2006) Constraints on the mass of a habitable planet with water of nebular origin. *Astrophys. J.* **648**, 696–706.

Ito E. and Clayton R. N. (1983) Submarine metamorphism of gabbros from the Mid-Cayman Rise: An oxygen isotopic study. *Geochim. Cosmochim. Acta* **47,** 535–546.

Ito E., Harris D.M. and Anderson A.T. (1983) Alteration of oceanic crust and geologic cycling of chlorine and water. *Geochim. Cosmochim. Acta* **47**, 1613–1624.

Ittekot V. (1988) Global trends in the nature of organic matter in river suspensions. *Nature* **332**, 436–438.

Jacquemont B. (2002) Etude des interactions eau–roche dans le granite de Soultz–sous–Forêts. Quantification et modélisation des transferts de matière par les fluides. Ph. D. thesis, Université Louis Pasteur, Strasbourg.

Jambon A. (1994) Earth degassing and large-scale geochemical cycling of volatile elements. In *Volatiles in magmas* (eds. M.R. Caroll and J.R. Holloway), Reviews in Mineralogy, Mineral Soc. Am., Washington, DC, **30**, 479–517.

Javoy M. (1980) $^{18}O/^{16}O$ and D/H ratios in high temperature peridotites. *C.N.R.S. Colloques internationaux* **272**, 279-287.

Javoy M. and Pineau F. (1991) The volatiles record of a "popping" rock from the Mid-Atlantic Ridge at 14°N: chemical and isotopic composition of gas trapped in the vesicles. *Earth Planet. Sci. Lett.* **107**, 598–611.

Javoy M., Pineau F. and Delorme H. (1986) Carbon and nitrogen isotopes in the mantle. *Chem. Geol.* **57**, 41-62.

Johnson W.J. and Goldstein R.H. (1993) Cambrian seawater preserved as inclusions in marine low–magnesium calcite cement. *Nature* **362**, 335–337.

Kakuichi M. and Matsuo S. (1985) Fractionation of hydrogen and oxygen isotopes between hydrated and free water molecules in aqueous urea solution. *J. Phys. Chem*. **89**, 4627-4632.

Kappelmeyer O. and Gérard A. (1989) The European project at Soultz-sous-Forets. In: *Proc. 4th Intl. Seminar on the Results of EC Geothermal Energy Research and Demonstration Florence* 27–30 April, Kluwer, 283–334.

Karato S. (1990) The role of hydrogen in the electrical conductivity of the upper mantle. *Nature* **347**, 272–273.

Karhu J. and Holland H.D. (1996) Carbon isotopes and the rise of atmospheric oxygen. *Geology* **24**, 867–870.

Karlsen D.G., Nedkvitne T. and Larter S.R. (1993) Hydrocarbon composition of authigenic inclusions : Application to elucidation of petroleum reservoir filling history. *Geochim. Cosmochim. Acta* **57**, 3641–3659.

Kasting J.F., Eggler D.H. and Raeburn S.P. (1993) Mantle redox evolution and the oxidation state of Archean atmosphere. *J. Geol.* **101**, 245-257.

Kastner M., Elderfield H., Martin J.B., Suess E., Kvenvolden K.A. and Garrison R.E. (1990) Diagenesis and interstitial-water chemistry at the Peruvian continental margin-Major constituents and strontium isotopes. *Proc. O.D.P., Sci. Res.* **112**, 413-440.

Kastner M., Elderfield H., Jenkins W.J., Gieskes J.M. and Gamo T. (1993) Geochemical and isotopic evidence for fluid flow in the Western Nankai Subduction Zone, Japan. *Proc. O.D.P., Sci. Res.* **131**, 397-413.

Katz R.F., Spiegelman M. and Holtzman B. (2006). The dynamics of melt and shear localization in partially molten aggregates. *Nature* **442**, 676–679.

Kazahaya K. (1986). Chemical and isotopic studies on hydrothermal solutions. Ph.D. dissertation, Tokyo Inst. Techn., pp. 185.

Kelemen P.B., Hirth G., Shimizu N., Spiegelman M. and Dick H.J.B. (1997). A review of melt migration processes in the adiabatically upwelling mantle beneath oceanic spreading ridges. *Philosophical Transactions of the Royal Society of London, series A- Mathematical physical and engineering sciences* **355**, 283–318.

Kelley D.S. (1996) Methane-rich fluids in the oceanic crust. *J. Geophys. Res.* **101**, 2943–2962.

Kennedy W.Q. (1964) The structural differentiation of Africa in the Pan-African (± 500 my) tectonic episode. *Univ. Leeds, Res. Inst. African Geol., Annu. Rep.* **8**, 48–49.

Keppler H. and Smyth J.R. (2006) Water in Nominally Anhydrous Minerals. *Mineral. Soc. Am.* **62**,Washington D.C. 478 pp.

Kerrick D.M. (2001) Present and past nonanthropogenic CO_2 degassing from the solid earth. *Rev. Geophys.* **39**, 565–585.

Kerrick D.M., McKibben M.A., Seward T.M. and Caldeira K. (1995) Convective hydrothermal CO_2 emission from high heat flow regions. *Chem. Geol.* **121**, 285–293.

King D.S.H., Zimmerman M.E. and Kohlstedt D.L. (2009). Stress–driven melt segregation in partially molten olivine-rich rocks deformed in Torsion. *J. Petrol.*, 10.1093/petrology/egp062.

Kishima N. and Sakai H. (1980) O-18 and deuterium determination on a single water sample of a few milligrams. *Anal. Chem.* **52**, 356-358.

Kloppmann W., Girard J.P. and Négrel Ph. (2002) Exotic stable isotope compositions of saline waters and brines from the crystalline basement. *Chem. Geol.* **184**, 49-70.

Kohlstedt D.L., Zimmerman M.E. and Mackwell S.J. (2009) Stress-driven melt segregation in partially molten feldspathic rocks. *J. Petrol.,* doi:10.1093/petrology/egp043

Korzun V.I. (1978) *World Water Balance and Water Resources of the Earth. Studies and Reports in Hydrology*, **Vol 25**, UNESCO, 587 pp.

Kovalevich V.M. (1975) Thermometric studies of inclusions in artificial crystals of halite. *Fluid Inclusion Res.* **8**, 96.

Kovalevich V.M. (1976) Halite of the salt deposits of Miocene age from the Forecarpathians. *Fluid Inclusion Res.* **9**, 72.

Kovalevich V.M., Peryt T.M. and Petrichenko O.I. (1998) Secular variation in seawater chemistry during the Phanerozoic as indicated by brine inclusions in halite. *J. Geol.* **106**, 695–712.

Kovalevych V.M., Marshall T., Peryt T.M., Petrychenko O.Y. and Zhukova S.A. (2006) Chemical composition of seawater in Neoproterozoic: Results of fluid inclusion study of halite from Salt Range (Pakistan) and Amadeus Basin (Australia). *Precamb. Res.* **144**, 39–51.

Krijgsman W., Hiigeni F.J, Raffi I., Sierro F.J. and Wilson D.S. (1999) Chronology, causes and progression of the Messinian salinity crisis. *Nature* **400**, 652–655.

Krogh E.J. (1988) The garnet, clinopyroxene Fe–Mg geothermometer, a reinterpretation of existing experimental data. *Contrib. Mineral. Petrol.* **99**, 44–48.

Kröner A., Jaeckel P., Brandl G., Nemchin A.A. and Pidgeon R.T. (1999) Single zircon ages for granitoid gneisses in the Central Zone of the Limpopo Belt, Southern Africa and geodynamic significance. *Precamb. Res.* **93**, 299–337.

Kröner A., Wendt J.I., Milisenda C., Compston W. and Maphala R. (1993) Zircon geochronology and Nd systematics of the Ancient Gneiss Complex, Swaziland, and implications for crustal evolution. *Bulletin of the Swaziland Geological Survey and Mines Department* **11**, 15–37.

Ku T.L. and Luo S. (1992) Carbon isotopic variations on glacial–to–interglacial time scales in the ocean: modeling and implications. *Paleoceanography* **7**, 543–562.

Kump L.R. and Seyfried W.E. (2005) Hydrothermal Fe fluxes during the Precambrian: effect of low oceanic sulfate concentrations and low hydrostatic pressure on the composition of black smokers. *Earth Planet. Sci. Lett.* **235**, 654–662.

Kuroda Y., Suzuoki T. and Matsuo S. (1977) D/H ratios of the coexisting phlogopite and richterite from mica nodules and a peridotite in South African kimberlites. *Contrib. Mineral. Petrol.* **52**, 315–318.

Kuski T.M., Stern R.J. and Tucker R.D. (2003) Evolution of the East African and related orogens, and the assembly of Gondwana. *Precamb. Res.* **123**, 81–85.

Kyser T.K. (1986) Stable isotope variations in the mantle. In *Stable isotopes in high temperature geological processes.* (eds. J.W. Valley, H.P. Taylor and J.R. O'Neil), Review in Mineralogy **16**, Mineralogical Society of America. 141–164.

Kyser T.K. and O'Neil J.R. (1984) Hydrogen isotope systematics of submarine basalts. *Geochim. Cosmochim. Acta* **48**, 2123–2133.

Ladouche B. and Weng Ph. (2005). Hydrochemical assessment of the Rochefort marsh: Role of surface and groundwater in the hydrological functioning of the wetland. *J. Hydrol.* **314**, 22–42.

Lamb W. and Valley J.W. (1984) Metamorphism of reduced granulites in low CO_2 vapour–free environnement. *Nature* **312**, 56–58.

Lawrence J.R. and Taylor H.P. (1971) Deuterium and oxygen-18 correlation: clay minerals and hydroxides in quaternary soils compared to meteoric waters. *Geochim. Cosmochim. Acta* **35**, 993–1003.

Leake B.E. (1978) Nomenclature of amphibole. *Can. Mineral.* **16**, 105–124.

Le Cloarec M.F. and Marty B. (1991) Volatile fluxes from volcanoes. *Terra Nova* **3**, 17-27.

Lécuyer C., Gardien V., Rigaudier T., Martineau F., Fourel F. and Cros A. (2009) Oxygen isotope fractionation and equilibration kinetics between CO_2 and H_2O as a function of salinity of aqueous solutions. *Chem. Geol.* **264**, 221–233.

Lécuyer C., Gillet Ph. and Robert F. (1998) Hydrogen isotope composition of seawater and the global water cycle. *Chem. Geol.* **145**, 253–265.

Lécuyer C., Dubois M., Marignac Ch., Gruau G., Fouquet, Y. and Ramboz C. (1999) Phase separation and fluid mixing in subseafloor back arc hydrothermal systems : A microthermometric and oxygen isotope study of fluid inclusions in the barite-sulfide chimneys of the Lau basin. *J. Geophys. Res.* **104**, 17911-17927.

Ledésert B., Berger G., Meunier A., Genter A. and Bouchet A. (1999) Diagenetic-type reactions related to hydrothermal alteration in the Soultz-sous-Forêts granite, France. *Eur. J. Miner.* **11**, 731–741.

Lein A.Y. (1984) Anaerobic consumption of organic matter in modern marine sediments. *Nature* **312**, 148–150.

Leuenberger M., Siegenthaler U. and Langway C.C. (1992) Carbon isotope composition of atmospheric CO_2 during the last ice age from an Antarctic ice core. *Nature* **357**, 450–488.

Li Y.H. (2000) *A compendium of geochemistry: from solar nebula to the human brain.* Princeton University Press, Princeton.

Lowenstein T.K., Li J. and Brown C.N. (1998) Paleotemperatures from fluid inclusions in halite : method verification and a 100,00 year paleotemperature record, Death Valley, CA. *Chem. Geol.* **150**, 223–245.

Lowenstein T.K., Timofeeff M.N., Brennan S.T., Hardie L.A. and Demicco R.V. (2001) Oscillations in Phanerozoic Seawater Chemistry : Evidence from Fluid Inclusions. *Science* **294**, 1086–1088.

Lugli S., Schreiber B.C. and Triberti B. (1999) Giant Polygons in the Realmonte salt (Agrigento, Sicily). *J. Sed. Res.* **69**, 764–771.

Maboko, M.A.H., 1997. P-T conditions of metamorphism in the Wami River granulite complex, central coastal Tanzania: implications for Pan-African geotectonics in the Mozambique Belt of eastern Africa. *J. Afr. Earth Sci.* **24**, 51–64.

Majoube M. (1971) Oxygen-18 and deuterium fractionation between water and steam. *J. Chem. Phys.* **68**, 1423–1436.

Maridet O., Escarguel G., Costeur L., Mein P., Hugueney M. and Legendre S. (2007) Small mammals (rodents and lagomorphs) European biogeography from the Late Oligocene to the mid Pliocene. *Global Ecol. Biogeogr.* **16**, 529–544.

Martinez D.E. (1991) Caracterizacion Geoquimica de la Lagunas Mar Chiquita, Provincia de Cordoba, Argentina, 274 pp.

Martinez I., Agrinier P., Schärer U. and Javoy M. (1994) A SEM–ATEM and stable isotope study of carbonates from the Haughton impact crater. Canada. *Earth Planet. Sci. Lett.* **121**, 559–574.

Marty B. and Jambon A. (1987) C/3He in volatile fluxes from the solid Earth: Implications for carbon geodynamics. *Earth Planet. Sci. Lett.* **83**, 16–26.

Marty B. and Tolstikhin I.N. (1998) CO_2 fluxes from mid-ocean ridges, arcs and plumes. *Chem. Geol.* **145**, 233–248.

Marty B. and Zimmermann L. (1999) Volatiles (He, C, N, Ar) in mid-ocean ridge basalts : assessment of shallow-level fractionation and characterization of source composition. *Geochim. Cosmochim. Acta* **63**, 3619–3633.

Maslin M.A. and Thomas E. (2003) Balancing the deglacial global carbon budget: the hydrate factor. *Quat. Sci. Rev.* **22**, 1729–1736.

Matthews A., Ayalon A and Bar-Matthews M. (2000). D/H ratios of fluid inclusions of Soreq cave (Israel) speleothems as a guide to the Eastern Mediterranean Meteoric Line relationships in the last 120 ky. *Chem. Geol.* **166**, 183–191.

Maughan H., Birky C.W., Nicholson W.L., Rosenzweig W.D. and Vreeland R.H. (2002) The Paradox of the « Ancient » Bacterium which contains « Modern » Protein–Coding Genes. *Molecul. Biol. and Evol.* **19**, 1637–1639.

McCarthy K.T., Pichler T. and Price R.E. (2005). Geochemistry of Champagne Hot Springs shallow hydrothermal vent field and associated sediments, Dominica, Lesser Antilles. *Chem. Geol.* **224**, 55-68.

McConnel R.B. (1972) Geological Development of the Rift System of Eastern Africa. *Geol. Soc. Am. Bull.* **83**, 2549–2572.

McLimans R.K. (1987) The application of fluid inclusions to migration of oil and diagenesis in petroleum reservoirs. *Appl. Geochem.* **2**, 585–603.

Meert J.G. (2003) A synopsis of events related to the assembly of eastern Gondwana. *Tectonophysics* **362**, 1–40.

Meert J.G. and Van der Voo R. (1996) Paleomagnetic and $^{40}Ar/^{39}Ar$ study of the Sinay dolerite, Kenya, Implications for Gondwana assembly. *J. Geol.* **104**, 131–142.

Meert J.G., Van der Voo R. and Ayub S. (1995) Paleomagnetic investigation of the Neoproterozoic Gagwe lavas and Mbozi complex, Tanzania and the assembly of Gondwana. *Precamb. Res.* **74**, 225–244.

Melzer M. (2001) Pan-African granulites in the Precambrian basement of eastern Tanzania: a geochemical, fluid inclusions and P-T history, DEA de l'Université de Clermont-Ferrand II.

Ménot R.P., Pêcher A., Rolland Y., Peucat J.J., Pelletier A., Duclaux G. and Guillot S. (2005) Structural setting on the Neoarchean terrains in the Commonwealth Bay Area (143-145°E), Terre Adélie Craton, East Antarctica. *Gondwana Res.* **8**, 1-9.

Merlivat L. (1978) Molecular diffusivity of H216O, HD16O and H218O in gases. *J. Chem. Phys.* **69**, 2864–2871.

Mével C. (2003) Serpentinization of abyssal peridotites at mid-ocean ridges. *C. R. Geoscience* **335**, 825–852.

Meybeck M. (1981) River transport of organic carbon to the ocean. In *Flux of Organic Carbon by Rivers to the Oceans.* Carbon Dioxide Effects Research and Assessment Program (eds. G.E. Likens and F.T. Mackenzie), US DOE, Washington, DC, 219–269.

Meybeck M. (1987) Global chemical weathering of surficial rocks estimated from river dissolved loads. *Am. J. Sci.* **288**, 401–428.

Meybeck M. (1988) How to establish and use world budgets of riverine materials. In *Physical and Chemical Weathering in Geochemical Cycles* (eds. A. Leman and M. Meybeck), Kluwer Academic, Dordrecht, 247–272.

Miller D.H. (1965) The heat and water budget of the Earth's surface. *Adv. Geophys.* **11**, 175–302.

Millero F., Huang F., Graham T. and Pierrot D. (2007) The dissociation of carbonic acid in NaCl solutions as a function of concentration and temperature. *Geochim. Cosmochim. Acta* **71**, 46-55.

Milliman J.D. (1993) Production and accumulation of calcium carbonate in the ocean: budget of a nonsteady state. *Global Biogeochem. Cycles* **7**, 927–957.

Milliman J.D., Quinchun X. and Zuosheng Y. (1984) Transfer of particulate organic carbon and nitrogen from the Changjiang River to the ocean. *Am. J. Sci.* **284**, 824–834.

Moecher D.P., Valley J.W. and Essene E.J. (1994) Extraction and carbon isotope analysis of CO2 from scapolite in deep crustal granulites and xenoliths. *Geochim. Cosmochim. Acta* **58**, 959–967.

Moissette A., Shepherd T.J. and Chenery S.R. (1996) Calibration strategies for the elemental analysis of individual aqueous fluid inclusions by laser ablation–ICP–MS. *J. Anal. Atom. Spec.* **11**, 177–186.

Möller A. (1995) Pan-African granulites and early Proterozoic eclogites in the Precambrian basement of eastern Tanzania: P-T-t history and crustal evolution of the complex Mozambique Belt, PhD Thesis Christian-Albrechts-Universität Kiel, 206pp.

Möller A., Mezger K. and Scenk, V. (2000) U-Pb dating of metamorphism and prolonged slow cooling of high pressure granulites in Tanzania, East Africa. *Precamb. Res.* **104**, 123–146.

Moomaw W.R., Moreira J.R., Blok K., Greene D.L., Gregory K., Jaszay T., Kashiwagi T., Levine M., McFarland M., Prasad N.S., Price L., Rogner H.H., Sims R., Zhou F. and Zhou P. (2001) Technological and economic potential of greenhouse gas emissions reduction. In *Climate Change 2001: Mitigation. Contribution of Working Group III to the Third Assessment Report of the Intergovernmental Panel on Climate Change* (eds. B. Metz, O. Davidson, R. Swart and J. Pan), Cambridge University Press, New York, 171–299.

Moore J.G. (1970) Water content of basalt erupted on the ocean floor. *Contrib. Miner. Petrol.* **28**, 272-279.

Moore J.C. and Vrolijk P. (1992) Fluids in accretionary prisms. *Rev. Geophys.* **30**, 113-135.

Morbidelli A., Chambers J., Lunine J.I., Petit J.M., Robert F., Valsecchi G.B. and Cyr K.E. (2000) Source regions and time scales for the delivery of water to Earth. *Meteorit. Planet. Sci.* **35**, 1309–1320.

Morgan G.B., Chou I.M., Pasteris J.D. and Olsen S.N. (1993) Re–equilibration of CO_2 fluid inclusions at controlled hydrogen fugacities. *J. Metam. Geol.* **11**, 155–164.

Morimoto M. (1988) Nomenclature of pyroxenes. *Am. Mineral.* **73**, 1123–1133.

Morner N.A. and Etiope G. (2002) Carbon degassing from the lithosphere. *Global Planet. Change* **33**, 185–203.

Morrison J., Brockwell T., Merren T., Fourel F. and Phillips A.M. (2001) Online high–precision stable hydrogen isotopic analysis on nanoliter water samples. *Anal. Chem.* **73**, 3570–3575.

Mosbrugger V., Utescher T. and Dilcher D.L. (2005) Cenozoic continental climatic evolution of Central Europe. *PNAS* **102**, 14964–14969.

Muehlenbachs K. (1998) The oxygen isotope composition of the oceans, sediments and the seafloor. *Chem. Geol.* **145**, 263-273.

Muhongo S. and Tuisku P. (1996) Pan-African high pressure isobaric cooling: evidence from the mineralogy and thermobarometry of the granulite-facies rocks from the Uluguru Mountains, eastern Tanzania. *J. Afr. Earth Sci.* **23**, 443–463.

Muhongo S., Tuisku P. and Mtoni Y. (1999) Pan-African pressure-temperature evolution of the Merelani area in the Mozambique Belt in northeast Tanzania. *J. Afr. Earth Sci.* **29**, 353–365.

Muhongo S., Kröner A. and Nemchin A.A. (2001) Zircon ages from granulites facies rocks in the Mozambique Belt of Tanzania and implications for Gondwana assembly. *J. Geol.* **109**, 171–189.

Mulch A. and Chamberlain C.P. (2007) Paleoaltimetry: geochemical and thermodynamic approaches. *Rev. Min. Geochim.* **66**, 89-118.

Nakicenovic N., Grubler A. and McDona A. (1998) *Global Energy Perspectives.* Cambridge University Press, New York.

Nagaseki H., Hayashi K. and Iida A. (2006) Quantitative analysis of fluid inclusions by synchrotron X–ray fluorecence. *Eur. J. Mineral.* **18**, 309–318.

Newton R.C. (1986) Fluids of granulite facies metamorphism. In *Fluid–rock interactions during metamorphism* (eds. J.V. Walther and B.J. Wood). Springer–Verlag, New–York, 36–59.

Newton R.C., Smith J.V. and Windley B.F. (1980) Carbonic metamorphism, granulites and crustal growth. *Nature* **288**, 45-50.

Norton D. and Knight J. (1977) Transport phenomena in hydrothermal systems: cooling plutons. *Am. J. Earth Sci.* **277**, 937–981.

Norton D. and Taylor H.P.J. (1979) Quantitative simulation of the hydrothermal systems of crystallizing magmas on the basis of transport and oxygen isotopic data: an analysis of the Skaergaard intrusion. *J. Petrol.* **20**, 421–448.

Ohmoto H., Yamaguchi K.E. and Ono S. (2001). Questions regarding Precambrian sulfur isotope fractionation. *Science* **292**, 1959.

Oki T. (1999) The global water cycle. In *Global Energy and Water Cycles* (eds. K.A. Brownig and R.J. Gurney), Cambridge University Press, 10-29.

Oki T. and Kanae S. (2006) Global hydrological cycles and world water resources. *Science* **313**, 1068-1072.

O'Leary M.H. (1988) Carbon isotopes in photosynthesis. *BioScience* **38**, 328–335.

O'Neil J.R. and Adami L.H. (1969) The oxygen isotope partition function ratio of water and the structure of liquid water. *J. Phys. Chem.* **73**, 1553-1558.

O'Neil J.R. and Truesdell A.H. (1991) Oxygen isotope fractionation studies of solute-water interactions. In: *Stable Isotope Geochemistry: A Tribute to Samuel Epstein*, H.P. Taylor, J.R. O'Neil and I.R. Kaplan (Eds), The Geochemical Society, Special Publication **n° 3**, pp. 17-25.

Otto D., Rasse D., Kaplan J., Wamant P. and Francois L. (2002) Biospheric carbon stocks reconstructed at the last glacial maximum: comparison between general circulation models using prescribed and computed sea surface temperatures. *Global Planet. Change* **33**, 117–138.

Parmentier E.M. (1981) Numerical experiments on O18 depletion in igneous intrusion cooling by ground water convection. *J. Geophys. Res.* **86**, 7131–7144.

Pasteris J.D. (1987) Fluid inclusions in mantle xenoliths. In *Mantle Xenoliths* (ed. P.H. Nixon). Wiley, Chichester, 691–707.

Pauwels H., Fouillac C. and Fouillac A.M. (1993) Chemistry and isotopes of deep geothermal saline fluids in the Upper Rhine Graben: Origin of compounds and water–rock interactions. *Geochim. Cosmochim. Acta* **57**, 2737–2749.

Pavlov A.A. and Kasting J.F. (2002) Mass-independent fractionation of sulfur isotopes in Archean sediments: strong evidence for an anoxic Archean atmosphere. *Astrobiology* **2**, 27-41.

Peacock M. (1990) Fluid processes in subduction zones. *Science* **248**, 329-337.

Peslier A.H. and Luhr J.F. (2006) Hydrogen loss from olivines in mantle xenoliths from Simcoe (USA) and Mexico: mafic alkalic magma ascent rates and water budget of the sub-continental lithosphere. *Earth Planet. Sci. Lett.* **242**, 302–319.

Petrychenko O.Y., Peryt T.M. and Chechel E.I. (2005) Early Cambrian seawater chemistry from fluid inclusion in halite from Siberian evaporites. *Chem. Geol.* **219**, 149–161.

Peucat J.J., Ménot R.P., Monnier O. and Fanning C.M. (1999) The Terre Adélie basement in the East-Antarctica Shield: geological and isotopic evidence for a major 1,7 Ga thermal event ; comparison with the Gawler Craton in South Australia. *Precamb. Res.* **94**, 205-224.

Pierre C., Vergnaud-Grazzini C., Thunron D. and Saliege J.F. (1986) Compositions isotopiques de l'oxygene et du carbone des masses d'eau en Mediterranee. *Mem. Soc. Geol. It. Al.* **36**, 165-174.

Pierret M.C., Clauer N., Bosch D., Blanc G. and France-Lanord C. (2001). Chemical and isotopic ($^{87}Sr/^{86}Sr$, $\delta^{18}O$, δD) constraints to the formation processes of Red-Sea brines. *Geochim. Cosmochim. Acta* **65**, 1259–1275.

Pili E. (1997) Distribution et transfert des fluides à l'échelle de la lithosphère continentale. Investigations géochimique et géophysique des granulites de Madagascar. Thèse de doctorat, Univ. Lyon 1, France, 252 pp.

Pili E., Sheppard S.M.F., Lardeaux J.-M., Martelat J.-E. and Nicollet C. (1997) Fluid flow vs. Scale of shear zones in the lower continental crust and the granulite paradox. *Geology* **25**, 15-18.

Planck T. and Langmuir C.H. (1998) The chemical composition of subducting sediment and its consequences for the crust and mantle. *Chem. Geol.* **145**, 325-394.

Popescu S.-M., Dalesme F., Jouannic G., Escarguel G., Head M.J., Melinte-Dobrinescu M.C., Sütő-Szentai M., Bakrac K., Clauzon G. and Suc J.-P. (2009) *Galeacysta etrusca* complex, dinoflagellate cyst marker of Paratethyan influxes into the Mediterranean Sea before and after the peak of the Messinian Salinity Crisis. *Palynology*, in press.

Pottorf R.J., Gray G.G., Kozar M.G., Flitchen W.M. and Richardson M. (1997) Paleothermometry techniques applied to burial history and hydrocarbon migration analyses, Tampico–Misantla Basin, Mexico. *American Association of Petroleum Geologists Abstracts with Programs,* p. A94.

Poty B. and Weisbrod A. (1976) Les inclusions fluides comme guide pour la prospection des gîtes métallifères. *Ann. Mines,* 1–6.

Powell R. (1983) Processes in granulite-facies metamorphism. In *Migmatites, Melting and Metamorphism*. (eds. M.P. Atherton, C.D. Gribble), Nantwich, Shiva, 127-139.

Prentice K.C. and Fung I.Y. (1990) The sensitivity of terrestrial carbon storage to climate change. *Nature* **346**, 48–51.

Prentice K.C., Sykes M., Lautenschlager M., Harrison S., Denissenko O. and Bartlein P. (1993) Modelling global vegetation patterns and terrestrial carbon storage at the last glacial maximum. *Global Ecol. Biogeogr. Lett.* **3**, 67–76.

Prezbindowski D.R. and Tapp J.B. (1991) Dynamics of fluid inclusion alteration in sedimentary rocks : a review and discussion. *Org. Geochem.* **17**, 131–142.

Prodehl C., Mueller St., Glahn A., Gutscher M. and Haak V. (1992) Lithospheric cross section of the European Cenozoic Rift System (ECRIS). In *Geodynamic of rifting* (ed. P.A. Ziegler) *Tectonophysics* **208**, 113-138.

Proskurowski G., Lilley M.D. and Olson E.J. (2008) Stable isotopic evidence in support of active microbial methane cycling in low-temperature diffuse flow vents at 9°50'N East Pacific Rise. *Geochim. Cosmochim. Acta* **72**, 2005-2023.

Qian T., Dai A., Trenberth K.E. and Oleson K.W. (2006) Simulation of global land surface conditions from 1948 to 2004: Part I: Forcing data and evaluations. *J. Hydrometeo.* **7**, 953-975.

Rabinowicz M., Dandurand J.L., Jakubowski M. Schott J. and Cassan J.P. (1985) Convection in a North Sea oil reservoir; inferences on diagenesis and hydrocarbon mitigation. *Earth Planet. Sci. Lett.* **74**, 387–404.

Rabinowicz M. and Toplis M.J. (2009) Melt segregation in the lower part of the partially molten mantle zone beneath an oceanic spreading center: numerical modelling of the combined effects of shear segregation and compaction. *J. Petrol.* **50**, 1071–1106.

Rabinowicz M. and Vigneresse J.L. (2004) Melt segregation under compaction and shear channeling: application to granitic magma segregation in a continental crust. *J. Geophys. Res.* **109**, doi:10.1029/2002JB002372.

Ranero C.R., Phipps Morgan J., McIntosh K.D. and Reichert C. (2003) Bending, faulting, and mantle serpentinization at the Middle America trench. *Nature* **425**, 367–373.

Rassmussen B. and Buick R. (1999) Redox state of the Archean atmosphere; evidence from detrital heavy minerals in ca. 3250-2750 Ma sandstones from the Pilbara Craton, Australia. *Geology* **27**, 115–118.

Raymond S.N., Quinn T. and Lunine J.I. (2004) Making other Earths: Dynamical simulations of terrestrial planet formation and water delivery. *Icarus* **168**, 1–17.

Raymond S.N., Quinn T. and Lunine J.I. (2005) Terrestrial planet formation in disks with varying surface density profiles. *Astrophys. J.* **632**, 670–676.

Raynaud D., Jouzel J., Barnola J.M., Chappellaz J., Delmas R.J. and Lorius C. (1993) The ice record of greenhouse gases. *Science* **259**, 926–934.

Reati G. J., Florín M., Fernández G. J. and Montes C. (1996) The Laguna de Mar Chiquita (Córdoba, Argentina): A little known, secularly fluctuating, saline lake. *Biomedical and Life Sciences* **5**, 187–219.

Reinfelder J.R., Kraepiel A.M. and Morel F.M.M. (2000) Unicellular C_4 photosynthesis in marine diatom. *Nature* **407**, 996–999.

Richardson C.N. (1998) Melt flow in a variable viscosity matrix. *Geophys. Res. Lett.* **277**, 937–981.

Riding R., Braga J.C., Martín J.M. and Sánchez-Almazo I.M. (1998) Mediterranean Messinian Salinity Crisis: constraints from a coeval marginal basin. Sorbas, SE Spain. *Marine Geology* **146**, 1–20.

Risacher F., Alonso H. and Salazar C. (2003). The origin of brines and salts in Chilean salars: a hydrochemical review. *Earth Sci. Rev.* **63**, 249–293.

Robert, F., Gautier, D., Dubrulle, B. (2000) The Solar System D/H: Observations and theories. *Space Sci. Rev.* **92**, 201–224.

Roberts S.M. and Spencer R.J. (1995) Paleotemperatures preserved in fluid inclusions in halite. *Geochim. Cosmochim. Acta* **59**, 3929–3942.

Robinson P.T., Dick H.J.B. and Von Herzen R. (1991) Metamorphism and alteration in oceanic layer 3: Hole 735B. *Proc. O.D.P., Sci. Res.* **118**, 541–549.

Roedder E. (1962) Studies of fluid inclusion I : Low temperature application of a dual–purpose freezing and heating stage. *Econ. Geol.* **57**, 1045–1061.

Roedder E. (1963) Studies of fluid inclusion II : Freezing data and their interpretation. *Econ. Geol.* **58**, 167–211.

Roedder E. (1965) Liquid CO_2 inclusions in olivine–bearing nodules and phenocrysts from basalts. *Am. Mineral.* **50**, 1746–1782.

Roedder E. (1984) Fluid Inclusions. *Mineralogical Society of America, Reviews in Mineralogy* **12**, Washington D.C., 644 pp.

Roedder E. (1984b) The fluids in salt. *Am. Mineral.* **69**, 413–419.

Roedder E. (1994) Fluid inclusion evidence of mantle fluids. In *Minerals: Methods and Applications* (eds. B. DeVivo and M.L. Frezzotti). Virginia Polytechnic Institute and State University, Blacksburg, 283–296.

Roedder E. and Skinner B.J. (1968) Experimental evidence that fluid inclusions do not leak. *Econ. Geol.* **63**, 715–730.

Rouchy J.-M. and Caruso A. (2006) The Messinian salinity crisis in the Mediterranean basin: A reassessment of the data and an integrated scenario. *Sedimentary Geology* **188/189**, 35–67.

Roveri M., Lugli S., Manzi V. and Schreiber B.C. (2008a) The Messinian Sicilian stratigraphy revisited: new insights for the Messinian salinity crisis. *Terra Nova* **20**, 483–488.

Roveri M., Manzi V., Gennari R., Iaccarino S.M. and Lugli S. (2008b) Recent advancements in the Messinian stratigraphy of Italy and their Mediterranean-scale implications. *Bolletino della Società Paleontologica Italiana* **47**, 71-85.

Rummel F. (1991) Physical properties of the rock in the granitic section of borehole GPK-1, Soultz-sous-Forêts. *Geotherm. Sci. Tech.* **3**, 199–216.

Rye R. and Holland H.D. (1998) Paleosols and the evolution of atmospheric oxygen: a critical review. *Am. J. Sci.* **298**, 621–672.

Saal A.E., Hauri E.H., Langmuir C.H. and Perfit M.R. (2002) Vapour undersaturation in primitive mid-ocean-ridge basalt and the volatile content of Earth's upper mantle. *Nature* **419**, 451-455.

Sano Y. and Marty B. (1995) Origin of carbon in fumarolic gas from island arcs. *Chem. Geol.* **119**, 265–274.

Sano Y. and Williams S.N. (1996) Fluxes of mantle and subducted carbon along convergent plate boundaries. *Geophys. Res. Lett.* **23**, 2749–2752.

Santosh M. and Tsunogae T. (2003) Extremely high density pure CO_2 fluid inclusions in a garnet granulite from southern India. *J. Geol.* **111**, 1–16.

Sarda P. and Graham D. (1990) Mid-ocean ridge popping rocks: implications for degassing at ridge crests. *Earth Planet. Sci. Lett.* **97**, 268–289.

Sarmiento J.L. and Gruber N. (2002) Sinks for anthropogenic carbon. *Phys. Today* **5**, 30–36.

Sarnthein M., Winn K., Duplessy J.C. and Fontugne M.R. (1988) Global variations of surface ocean productivity in low and mid latitudes: influence on CO_2 reservoirs of the deep ocean and atmosphere during the last 21,000 years. *Paleoceanography* **3**, 361–399.

Sasaki S. (1990) The primary solar-type atmosphere surrounding the accreting Earth: H2O-induced high surface temperature. In *Origin of the Earth* (eds. H.E. Newsom and J.H. Jones), Oxford Univ. Press, New York, 195–209.

Satterfield C.L., Lowenstein T.K., Vreeland R.H. and Rosenzweig W.D. (2005) Paleobrine temperatures, chemistries, and paleoenvironments of Silurian salina formation F–1 Salt, Michigan Basin, U.S.A., from petrography and fluid inclusions in halite. *J. Sedim. Res.* **75**, 534–546.

Schaller M., Steiner O., Studer I., Holzer L., Herweg M. and Kramers J.D. (1999) Exhumation of Limpopo Central Zone granulites and dextral continent-scale transcurrent movement at 2000 Maalong the Palala Shear Zone, Northern Province, South Africa. *Precamb. Res.* **96**, 263–288.

Schidlowski M. (1987) Application of stable isotopes to early biochemical evolution on Earth. *Ann. Rev. Earth. Planet. Sci.* **15**, 47–72.

Schidlowski M. (2001) Carbon isotopes as biogeochemical recorders of life over 3.8 Ga of Earth history: evolution of a concept. *Precamb. Res.* **106**, 117–134.

Schilling J.G., Bergeron M.B. and Evans R. (1980) Halogens in the mantle beneath the North Atlantic. *Phil. Trans. R. Soc. Lond.* **297**, 147-178.

Schlesinger W.H. (1997) *Biogeochemistry: An Analysis of Global Change.* Academic Press, New York.

Schlesinger W.H. and Melack J.M. (1981) Transport of organic carbon in the world's rivers. *Tellus* **33B**, 172–187.

Schmidt M.W. and Poli S. (1998) Experimentally based water budgets for dehydrating slabs and consequences for arc magma generation. *Earth Planet. Sci. Lett.* **163**, 361–379.

Schmincke H.U. (2000) *Vulkanismus.* Wissenschaftliche Buchgesellschaft.

Schnaebele R. (1948) Monographie géologique du champ pétrolifère de Péchelbronn. *Mem. Serv. Carte Géol. Alsace Lorraine* **7**, p. 254.

Schubert G. and Reymer A.P.S. (1985) Continental volume and freeboard through geological time. *Nature* **316**, 336-339.

Schumacher M.E. (2002) Upper Rhine Graben: role of pre-existing structures during rift evolution. *Tectonics* **21**, 10.1029/2001TC900022.

Schwarcz H.P., Harmon R.S., Thompson P. and Ford D.C. (1976) Stable isotope studies of fluid inclusions in speleothems and their paleoclimatic significance. *Geochim. Cosmochim. Acta* **40**, 657-665.

Scott T. and Kohlstedt D.L. (2006) The effect of large melt fraction on the deformation behaviour of peridotite. *Earth Planet. Sci. Lett.* **246**, 177–187.

Sen S.K. and Bhattacharya A. (1984) An orthopyroxene-garnet thermometer and its application to the Madras charnockites. *Contrib. Mineral. Petrol.* **88**, 64–71.

Seyfried W.F. and Dibble W.E.Jr. (1980) Seawater-peridotite interaction at 300°C and 500 bars: implications for the origin of oceanic serpentinites. *Geochim. Cosmochim. Acta* **44**, 309–321.

Shackleton R. (1993) Tectonics of the lower crust: a view from the Usambara Mountains, NE Tanzania. *J. Struct. Geol.* **15**, 663–671.

Shakleton N.J. (1977) Carbon–13 in Uvigerina: tropical rainforest history and the equatorial Pacific carbonate dissolution cycles. In *The Fate of Fossil Fuel CO_2 in the Oceans.* (eds. N.R. Andersen and A. Malahoff), Plenum, New York, 401–427.

Sharp J.H. (1997) Marine dissolved organic carbon: are the older values correct? *Mar. Chem.* **56**, 265–277.

Sharp Z.D., Papike J.J., Durakiewicz T. (2003) The effect of thermal decarbonation on stable isotope compositions of carbonates. *Amer. Mineral.* **88**, 87–92.

Sheppard S.M.F., Epstein S. (1970) D/H and $^{18}O/^{16}O$ ratios of minerals of possible mantle or lower crustal origin. *Earth Planet. Sci. Lett.* **9**, 232–239.

Shepherd T.J. and Chenery S.R. (1995) Laser ablation ICP–MS elemental analysis of individual fluid inclusions : An evaluation study. *Geochim. Cosmochim. Acta* **59**, 3997–4007.

Shiklomanov I.A. (Ed.) (1997) *Assessment of water resource and water availability in the world*, World Meteorological organization, Stockholm Environment Institute, Geneva, Switzerland.

Simon L. (2003) Quelques exemples de modélisations géochimiques des interactions entre les enveloppes terrestres. Ph. D. thesis, Ecole Normale Supérieure de Lyon.

Smith H.J., Fischer H., Wahlen M., Mastroianni D. and Deck B. (1999) Dual modes of the carbon cycle since the last glacial maximum. *Nature* **400**, 248–250.

Smith M.P. (1997) Fluid inclusion well logs : Petroleum migration, seals, and proximity to pay. *ECROFI XIV Abstracts, Nancy*, p. 310.

Snow J.E. and Dick H.J.B. (1995) Pervasive magnesium loss by marine weathering of peridotite. *Geochim. Cosmochim. Acta* **59**, 4219–4235.

Sobolev A.V. and Chaussidon M. (1996) H_2O concentrations in primary melts from supra-subduction zones and mid-ocean ridges : Implications for H_2O storage and recycling in the mantle. *Earth Planet. Sci. Lett.* **137**, 45-55.

Sofer Z. and Gat J.R. (1972). Activities and concentrations of oxygen-18 in concentrated aqueous salt solutions: analytical and geophysical implications. *Earth Planet. Sci. Lett.* **15**, 232–238.

Sommer H., Kröner A., Hauzenberger C. and Muhongo S. (2003) Metamorphic petrology and zircon geochronology of high-grade rocks from the CMB of Tanzani: crustal recycling of Archean and Paleoproterozoic material during the Pan-African orogeny. *J. Metam. Geol.* **21**, 915–934.

Sommer H., Hauzenberger C., Fröner A. and Muhongo S. (2008) Isothermal decompression history in the "Western granulites" terrain, central Tanzania: Evidence from reaction textures and trapped fluids in metapleites. *J. Afr. Earth Sci.* **51**, 123–144.

Sorby H.C. (1858) On the microscopical structure of crystals indicating the origin of rocks and minerals. *Quater. J. Geol. Soc. London* **14**, 453–500.

Spear F.S. (1993) Metamorphic phase equilibria and pressure–temperature–time paths. *Mineral. Soc. Am. Monograph*, 799 pp.

Spitzy A. and Leenheer J. (1991) Dissolved organic carbon in rivers. In *SCOPE 42: Biogeochemistry of Major World Rivers* (eds. E.T. Degens, S. Kempe and J.E. Richey), Wiley, New York, 213–232.

Stakes D., Mével C., Cannat M. and Chaput T. (1991) Metamorphic stratigraphy of hole 735B. *Proc. O.D.P., Sci. Res.* **118**, 153-180.

Staudigel H., Hart S.R and Richardson S.H. (1981) Alteration of the oceanic crust : Processes and timing. *Earth Planet. Sci. Lett.* **52**, 311–327.

Staudigel H.R., Hart S., Schmincke H.U. and Smith B.M. (1990) Cretaceous ocean crust at DSDP Sites 417 and 418: Carbon uptake from weathering versus loss by magmatic outgassing. *Geochim. Cosmochim. Acta* **53**, 3091–3094.

Staudigel H., Davies G.R., Hart S.R., Marchant K.M. and Smith B.M. (1995) Large scale isotopic Sr, Nd and O isotopic Anatomy of altered oceanic crust: DSDP/ODP sites 417/418. *Earth Planet. Sci. Lett.* **130**, 169–180.

Staudigel H., Plank T., White B. and Schmincke H.U. (1996) Geochemical Fluxes During Seafloor Alteration of the Basaltic Upper Oceanic Crust: DSDP sites 417 and 418. In *Subduction Top to Bottom* (eds. G.E. Bebout, D.W. Scholl, S.H. Kirby, and J.P. Platt), **Vol. 96**, AGU, pp 19-38.

Stern R.J. (1994) Arc assembly and continental collision in the Neoproterozoic East Africa Orogen: implications of consolidation of Gondwanaland. *Ann. Rev. Earth Planet. Sci.* **22**, 319–351.

Stevenson D.J. (1989) Spontaneous small scale melt segregation in partial melts undergoing deformation. *Geophys. Res. Lett.* **16**, 1067–1070.

Stussi J., Cheilletz A., Royer J. Chevremont P. and Feraud G. (2002) The hidden monzogranite of Soultz-sous-Forêts (Rhine Graben, France). Mineralogy, petrology and genesis. *Géologie de la France* **1**, 45–64.

Sundquist E.T. (1985) Geological perspectives on carbon dioxide and the carbon cycle. In *The Carbon Cycle and Atmospheric CO_2: Natural Variations Archean to Present: Geophysical Monograph 32* (eds. E.T. Sundquist and W.S. Broecker), American Geophysical Union, Washington, DC, 5–60.

Sundquist E.T. (1993) The global carbon dioxide budget. *Science* **259**, 934–941.

Sundquist E.T. and Plummer L.N. (1981) Carbon dioxide in the ocean surface layer: some modeling considerations. In *Carbon Cycle Modelling* (ed. B. Bolin), Wiley, New York, 259–270.

Sundquist E.T. and Visser K. (2003) The Geologic History of the Carbon Cycle. In *Treatise on Geochemistry, Volume 8* (eds. H.D. Holland and K.K. Turekian), Elsevier, New York, 425–472.

Suzuoki T. and Epstein S. (1976) Hydrogen isotope fractionation between OH–bearing minerals and water. *Geochim. Cosmochim. Acta* **40**, 1229–1240.

Swanenberg H.C. (1980) Fluid inclusions in high grade metamorphic rocks from SW *Norway. Geol. Ultraiectina* **25**, 1–147.

Szabo C. and Bodnar R.J. (1995) Chemistry and origin of mantle sulfides in spinel peridotite xenoliths from alkaline basaltic lavas, Norgrad–Gömör Volcanic Field, northern Hungary and southern Slovakia. *Geochim. Cosmochim. Acta* **59**, 3917–3927.

Tajika E. and T. Matsui (1993) Evolution of seafloor spreading rate based on ^{40}Ar degassing history. *Geophys. Res. Lett.* **20**, 851–854.

Tatsumi Y. (1989) Migration of fluid phases and genesis of basalt magmas in subduction zones. *J. Geophys. Res.* **94**, 4697-4707.

Taube H. (1954) Use of oxygen isotope effects in the study of hydrated ions. *J. Chem. Phys.* **58**, 523–528.

Taylor H.P. (1968) The oxygen isotope geochemistry of igneous rocks. *Contrib. Mineral. Petrol.* **19**, 1–71.

Taylor H.P. (1977) Water/rock interactions and the origin of H2O in granitic batholiths. *J. Geol. Soc. London*. **133**, 509–558.

Taylor H.P. (1988) Oxygen, hydrogen, and strontium isotope constraints on the origin of granites. *Trans. Royal Soc. Edinburgh* **79**, 317–338.

Taylor H.P. and Sheppard S.M.F. (1986) Igneous rocks: I. Processes of isotopic fractionation and isotope systematics. In *Stable Isotopes in High Temperature Geological Processes.* (eds. J.W. Valley, H.P. Taylor and J.R. O'Neil). *Mineral. Soc. Am.* **16**, 227–271.

Taylor S.R. and McLennan S.M. (1995) The geochemical evolution of the continental crust. *Rev. Geophys.* **33**, 241–265.

Tenczer V., Hauzenberger C., Fritz CA., Whitehouse M., Mogessie A., Wallbrecher E., Muhongo S. and Hoinkes G. (2006) Anorthosites in the Eastern Granulites of Tanzania- new SIMS zircon U-Pb ages data, petrography and geochemistry. *Precam. Res.* **148**, 85–114.

Tenzer H., Mastin L. and Heinemann B. (1991) Detremination of planar discontinuities and borehole geometry in the crystalline rocks of the borehole GPK1 at Soultz-sous Forets. *Geotherm. Sci. Tech.* **3**, 31-67.

Thompson A.B. (1992) Water in the Earth's upper mantle. *Nature* **358**, 295-302.

Timofeeff M.N., Lowenstein T.K., Brennan S.T., Demicco R.V., Zimmermann H., Horita J. and Von Borstel L.E. (2001) Evaluating seawater chemistry from fluid inclusions in halite : Examples from modern marine and nonmarine environments. *Geochim. Cosmochim. Acta* **65**, 2293–2300.

Torsvik T.H. (1998) Palaeozoic palaeogeography: a north Atlantic viewpoint. *Geol. Soc. Sweden (G.F.F)* **120**, 109–118.

Touray J.C., Beny C. and Dubessy J. (1985) Micro-characterization of fluid inclusions in minerals by Raman microprobe. *Scanning Electron Microscop.* **1**, 103–118.

Touret J. (1971) Le faciès granulitique en Norvège Méridionale II : Les inclusions fluides. *Lithos* **4**, 423–436.

Touret J. (1977) The significance of fluid inclusions in metamorphic rocks. In *Thermodynamics in Geology* (ed. D.G. Fraser). NATO ASI Series, C. 35, Reidell Pub., Dordrecht, 113–168.

Touret J. (1981) Fluid inclusions in high grade metamorphic rocks. In *Short Course in Fluid Inlusions: Application to Petrology* (eds. L.S. Hollister and M.L. Craford). Min. Assoc. Canada, Calgary, 182–308.

Touret J. (1995) Fluid regile in southern Norway, the record of fluid inclusions. In *The deep Proterozoic crust in the North Antlantic Provinces*. (eds. A.C. Tobi and J.L.R. Touret), NATO ASI Ser. C. Reidel Publishing Company. 517–549.

Touret J. (2001) Fluids in metamorphic rocks. *Lithos* **55**, 1–25.

Touret J. and Dietvorst P. (1983) Fluid onclusions in migmatites. In *Migmatites* (ed. J.R. Ashworth), Blackie, Glassgow, 265-288.

Traineau H., Genter A., Cautru J., Fabriol H. and Chevremont P. (1991) Petrography of the granite massif from drill cutting analysis and well log interpretation in the geothermal HDR borehole GPK1 (Soultz, Alsace, France). *Geotherm. Sci. Tech.* **3**, 1–29.

Trenberth K.E. (1998) Atmospheric moisture residence times and cycling Implications for rainfall rates with climate change. *Climatic Change* **39**, 667-694

Trenberth K.E. and Stepaniak D.P. (2003) Co-variability of components of poleward atmospheric energy transports on seasonal and interannual timescales. *J. Climate* **16**, 3691-3705.

Trenberth K.E, Dai A., Rasmussen R.M. and Parsons D.B. (2003) The changing character of precipitation. *Bull. Amer. Meteor. Soc*. **84**, 1205-1217.

Trenberth K.E, Fasullo J. and Smith L. (2005) Trends and variability in column integrated atmospheric water vapor. *Climate Dynamics* **24**, 741-758.

Trenberth K.E, Smith L., Qian T., Dai A. and Fasullo J. (2007) Estimates of the Global Water Budget and its Annual Cycle Using Observational and Model Data. *J. Hydrometeo. Special Section* **8**, 758–769.

Truesdell A.H. (1974). Oxygen isotope activities and concentrations in aqueous salt solutions at elevated temperatures: consequences for isotope geochemistry. *Earth Planet. Sci. Lett.* **23**, 387–396.

Tsunogae T., Santosh M., Osanai Y., Owada M., Toyoshima T. and Hokada T. (2002) Very high-density carbonic fluid inclusions in sapphirine-bearing granulites fromTonagh island in theArcheanNapier complex, eastAntarctica: implications for CO_2 infiltration during ultrahigh-temperature (T>1100°C) metamorphism. *Contrib. Mineral. Petrol.* **143**, 279–299.

Turner M.G. (1989) The outgassing history of the Earth's atmosphere. *J. Geol. Soc. London* **146**, 147–154.

Utescher T., Mosbrugger V., Ivanov D. and Dilcher D.L. (2009) Present–day climatic equivalents of European Cenozoic climates. *Earth Planet. Sci. Lett.* **284**, 544–552.

Valentine D.L., Chidthaisong A., Rice A., Reeburgh W.S. and Tyler S.C. (2004) Carbon and hydrogen isotope fractionation by moderately thermophilic methanogens. *Geochim. Cosmochim. Acta* **68**, 1571–1590.

Van Campo E., Guiot J. and Peng C. (1993) A data–based reappraisal of the terretrial carbon budget at the last glacial maximum. *Global Planet. Change* **8**, 189–201.

Van den Kerkhof A.M. and Hein U.F. (2001) Fluid inclusion petrography. *Lithos* **55**, 27–47.

Vanko D.A. and Stakes D.S. (1991) Fluids in oceanic layer 3: Evidence from veined rocks; Hole 735B, southwest Indian Ridge. *Proc. O.D.P., Sci. Res.* **118**, 181-215.

Varekamp J.C., Kreulen R., Poorter R.P.E. and Van Bergen M.J. (1992) Carbon source in arc volcanism, with implications for the carbon cycle. *Terra Nova* **4**, 363-373.

Veizer J. and Jansen S.L. (1979) Basement and sedimentary recycling and continental evolution. *J. Geology* **87**, 341-370.

Vennemann T.W. and O'Neil J.R. (1993) A simple inexpensive method of hydrogen isotope and water analysis of minerals and rocks based on zinc reagent. *Chem. Geol.* **103**, 227–234.

Villemin T., Alvarez F. and Angelier J. (1986) The Rhine graben : extension, subsidence and uplift. *Tectonophysics* **128**, 45–59.

Volfinger M., Ramboz C., Aissa M. and Choï C.G. (1997) Some practical aspects of the quantitative analysis of fluid inclusions by the PIXE method. *ECROFI XIV Abstracts, Nancy*, 344–345.

Von Huene R. and Scholl D.W. (1991) Observations at convergent margins concerning sediment subduction, subduction erosion, and the growth of continental crust. *Rev. Geophys.* **29**, 279-316.

Von Grafenstein U., Erlenkeuser H., Müller J., Trimborn P. and Alefs J. (1996) A 200 year mid-European air temperature record preserved in lake sediments : An extension of the $d^{18}O$-air temperature relation in the past. *Geochim. Cosmochim. Acta* **60**, 4025–4036.

Vreeland R.H., Rosenzweig W.D. and Powers D.W. (2000) Isolation of 250 million–year–old halotolerant bacterium from a primary salt crystal. *Nature* **407**, 897–900.

Vry J., Brown P.E., Valley J.W. and Morrison J. (1988) Constraints on granulite genesis from carbon isotope compositions of cordierite and graphite. *Nature* **332**, 66–68.

Wallmann K. (2001) The geological water cycle and the evolution of marine $\delta^{18}O$ values. *Geochim. Cosmochim. Acta* **65**, 2469-2485.

Watson E.B. and Brenan J.M. (1987) Fluids in the lithosphere : 1. Experimentally-determined wetting characteristics of CO_2–H_2O fluids and their implications for fluid transport, host-rock physical properties, and fluid inclusion formation. *Earth Planet. Sci. Lett.* **85**, 497–515.

Wernicke B. (1985) Uniform-sense normal simple shear of the continental lithosphere. *Can. J. Earth. Sci.* **22**, 108–125.

Wickham S.M. and Taylor H.P. (1987) Stable isotope constraints on the origin and depth of penetration of hydrothermal fluids associated with Hercynian low-pressure regional and crustal anatexis in the Pyrenées. *Contrib. Mineral. Petrol.* **95**, 255–268.

Wilcox W.R. (1968) Removing inclusions from crystals by gradient techniques. *Industr. Engin. Chemistry* **60**, 12–23.

Windley B.F. (1977) Timing of continental growth and emergence. *Nature* **270**, 426-428.

Wollast R. (1994) The relative importance of biomineralization and dissolution of $CaCO_3$ in the global carbon cycle. In *Past and Present Biomineralization Processes* (ed. F. Doumenge). Musée Océanographie, Monaco, 13–35.

Wood B.J., Brynzia L.T. and Johnson K.E. (1990) Mantle oxidation state and its Relationship to tectonic environment and fluid speciation. *Science* **248**, 337-345.

Wyllie P.J. (1982) Subduction products according to experimental prediction. *Geol. Soc. Am. Bull.* **93**, 468–476.

Xia Q.K., Yang X.Z., Deloule E., Sheng Y.M. and Hao Y.T. (2006) Water in the lower crustal granulite xenoliths from Nushan, eastern China. *J. Geophys. Res.* **111,** 10.1029/2006JB004296.

Yardley B.W.D., Meere A., Cathelineau M. and Valley J. (1995) Are quartz veins forming under Strasbourg today? A stable isotope study of veins quartz from Soult-sous-Forêts. *Terra Nova abstr.* **7**, 185.

Yardley B.W.D. and Valley J.W. (1994) How wet is the Earth's crust ? *Nature* **371**, 205-206.

Zachos J.C., Pagani M., Sloan L., Thomas E. and Billups K. (2001) Trends, rhythms, and aberrations in global climate, 65 Ma to present. *Science* **292**, 686–693.

Zeyen H., Volker F., Wehrle V., Fuchs K., Sobolev SV. and Altherr R. (1997) Styles of continental rifting: crust-mantle detachment and mantle plumes. *Tectonophysics* **278**, 329–352.

Zimmermann H. (2000) Tertiary seawater chemistry; implications from primary fluid inclusions in marine halite. *Am. J. Sci.* **300**, 723–767.